HOLOCENE SEDIMENTATION ON THE VIETNAMESE SHELF: FROM SOURCE TO SINK

Dissertation

zur Erlangung des Doktorgrades

der Mathematisch-Naturwissenschaftlichen Fakultät

der Christian-Albrechts-Universität

zu Kiel

vorgelegt von

Alexander Schimanski

Kiel

2002

Abstract

Worldwide, the shelf regions were intensively affected by the last deglacial sea-level rise. The Vietnamese Shelf (South China Sea) provides the opportunity to study the effects of a rising sea-level on shelf regions of different width. With its wide and gently inclining shelves in the North and South, both hosting two major world rivers (Red River, Mekong), and numerous small mountainous rivers draining onto a narrow, steep shelf in the central part with a high rising hinterland, the coastal area of Vietnam represents a region with contrasting general conditions.

25 sediment cores from modern water depths between 21 m and 169 m and two river samples from the Mekong and Red River have been investigated in order to characterize sedimentary processes, stratigraphy, provenance, distribution and sediment budget during the Late Pleistocene and Holocene in the study area. Geophysical, sedimentological, micropaleontological, and geochemical methods were applied in this first detailed and comprehensive characterization of deposits from the Vietnamese Shelf with a stratigraphy based on 45 AMS ^{14}C dates. The sediments of the cores could be assigned to 3 areas, the *Northern Shelf* (southern Gulf of Tonkin), the *Central Shelf*, and the *Southern Shelf* (paleo-Mekong). These three areas are characterzied by different sedimentological conditions resulting in varying sedimentation and mass accumulation rates. On the wide *Northern Shelf* the sedimentation rates are low with ca. 10 cm/kyr due to sediment starvation, except of the prograding Red River delta as primary sediment sink. The narrow *Central Shelf* shows high sedimentation rates of 50 - 100 cm/kyr on the average, caused by sediments delivered by the small mountainous rivers of central Vietnam. Here, very high sedimentation rates of 500 - 1000 cm/kyr were observed for early Holocene sediments. On the wide *Southern Shelf* sedimentation is limited to 5 - 10 cm/kyr (25 - 40 cm/kyr in sheltered areas) also due to sediment starvation, except of the prograding Mekong delta. On the *Northern* and *Southern Shelves* equilibrium between deposition and erosion could not be established yet, whereas the depositional equilibrium on the *Central Shelf* was quickly established due to high terrigenous input from the small mountainous rivers.

Comparison of tentative sea-level data, derived from dating of suitable paleo-facies, with the sea-level curve of Hanebuth et al. (2000) suggests subsidence on the *Central Shelf*, possibly due to high mass accumulation rates, and uplift for the *Northern Shelf*, possibly due to tectonic activity in this region.

Investigations of major- and trace element as well as Sr- and Nd-isotopic composition of shelf and river sediments showed that the Red River, the Mekong and small mountainous rivers draining the Annamite chain of Central Vietnam act as endmembers for the shelf deposits. The sediments on the Vietnamese Shelf are mainly delivered by the small mountainous rivers and the Mekong. The influence of the Red River on the sedimentation in

the study area is low. Furthermore, sediments from a core covering the Holocene time interval, from the shelf in the paleo-Mekong area reflect variation of sources, with increased amounts of Annamite sediment during the early Holocene. This is probably caused by strengthened SW-monsoon in the Annamite region.

Together with denudation data taken from the literature a conceptual sediment buget was calculated for the Vietnamese Shelf. It shows that the major part ($144 \pm 36 \times 10^6$ t/yr) of the sediment transported by the Mekong (160×10^6 t/yr) is deposited in the Mekong Delta and only 9 - 18 x 10^6 t/yr are deposited on the *Southern Shelf*. On the *Central Shelf*, the sediment delivered by the small mountainous rivers is with 40 - 100 x 10^6 t/yr about half of the amount transported by the Mekong. The *Central Shelf* stores 20 - 40 x 10^6 t/yr of sediment. The remaining part bypasses the shelf or is transported towards the deeper parts of the South China Sea by slumps from the steep shelf. The Red River, transporting 130×10^6 t/yr of sediment, deposits the major part of his load in the Red River Delta. Only ca. 20×10^6 t/yr are stored on the *Northern Shelf*.

Kurzfassung

Weltweit wurden die Schelfregionen vom Meeresspiegelanstieg nach dem letzten Glazial intensiv beeinflusst. Der Vietnamesische Schelf (Südchinesisches Meer) bietet die Möglichkeit, Auswirkungen des Meeresspiegelanstiegs auf Schelfregionen unterschiedlicher Breite zu studieren. Mit breiten, flach geneigten Schelfgebieten im Norden und Süden, die beide das Mündungsgebiet großer Flüsse umfassen (Mekong, Red River), und andererseits zahlreichen kleinen Bergflüssen, die auf den schmalen, steil abfallenden Schelf vor Zentral-Vietnam entwässern, bieten die Küsten Vietnams eine Region gegensätzlicher Rahmenbedingungen.

25 Sedimentkerne aus modernen Wassertiefen zwischen 21 m und 169 m sowie zwei Sedimentproben vom Mekong und vom Red River wurden untersucht, um Sedimentations-prozesse, Stratigraphie, Herkunft und Sedimentverteilung während des späten Pleistozäns und des Holozäns zu charakterisieren und zu bilanzieren. Geophysikalische, sedimentologische, mikropaläontologische und geochemische Methoden wurden in dieser ersten umfassenden Studie zur Charakterisierung von Schelfsedimenten in Vietnam angewandt und ein stratigraphisches Gerüst, basierend auf 45 AMS ^{14}C Datierungen, erstellt. Die untersuchten Sedimente sind drei unterschiedlichen Regionen zugeordnet: dem *nördlichen Schelf* (südlicher Golf von Tonking), dem *zentralen Schelf* (Mittel-Vietnam) und dem *südlichen Schelf* (paleo-Mekong). Diese drei Regionen zeichnen sich durch unterschiedliche sedimentologische Bedingungen aus, die unterschiedliche Sedimentations- und Akkumulationsraten zur Folge haben. Auf dem breiten *nördlichen Schelf* sind die

Sedimentationsraten mit ca. 10 cm/kyr aufgrund von reduziertem terrigenen Eintrag, außer im progradierenden Red River Deltasystem, gering. Aufgrund von Sedimentzufuhr durch die kleinen Bergflüssen Zentral-Vietnams zeigt der schmale *zentrale Schelf* hohe Sedimentationsraten von durchschnittlich 50 - 100 cm/kyr. Hier traten auch sehr hohe Sedimentationsraten von 500 - 1000 cm/kyr während des frühen Holozäns auf. Auf dem breiten *südlichen Schelf* liegen die Sedimentationsraten aufgrund von reduziertem terrigenen Eintrag, außer im progradierenden Mekong Deltasystem, zwischen 5 und 10 cm/kyr (25 - 40 cm/kyr in geschützten Gebieten). Auf dem *nördlichen* und *südlichen Schelf* konnte sich ein Gleichgewicht zwischen Sedimentation und Erosion bisher nicht einstellen, wohingegen es sich auf dem *zentralen Schelf* aufgrund hohen terrigenen Eintrags von den kleinen Bergflüssen schnell eingestellt hat.

Ein Vergleich von vorläufigen Meeresspiegeldaten, die durch die Datierung von geeigneten Paläofazies ermittelt wurden, mit der Meerespiegelkurve von Hanebuth et al. (2000), deutet auf Subsidenz des *zentralen Schelfs* hin. Ursache hierfür sind möglicherweise hohe Akkumulationsraten. Vorläufige Meeresspiegeldaten für den *nördlichen Schelf* sprechen für Hebung, möglicherweise aufgrund tektonischer Aktivität in dieser Region.

Untersuchungen von Haupt- und Spurenelementen sowie der Zusammensetzung von Sr- und Nd-Isotopen von Schelf- und Flußsedimenten zeigen, daß der Red River, der Mekong und die kleinen Bergflüsse, die die Annamite-Gebirgskette Zentral-Vietnams entwässern, als Endglieder für die Schelfsedimente fungieren. Die Sedimente auf dem Vietnamesischen Schelf werden vornehmlich von den kleine Bergflüssen und dem Mekong geschüttet. Der Einfluß des Red Rivers auf das Sedimentationsgeschehen im Untersuchungsgebiet ist gering. Weiterhin zeigen die Ablagerungen eines Kerns vom *südlichen Schelf* (paleo-Mekong), der das Holozän umfasst, Veränderungen der Sedimentquellen, die auf erhöhte Anteile von Annamite Sediment während des frühen Holozäns hindeuten. Dies wurde möglicherweise durch verstärkten SW-Monsun in der Annamite Region hervorgerufen.

Zusammen mit Denudationsraten, die der Literatur entnommen wurden, und im Rahmen dieser Arbeit bestimmter Akkumulationsraten wurde eine konzeptionelle Sedimentbilanz für den Vietnamesischen Schelf erstellt. Es zeigt sich, daß der Großteil ($144 \pm 36 \times 10^6$ t/yr) der vom Mekong transportierten Sedimentfracht (160×10^6 t/yr) im Mekong Delta abgelagert wird und nur 9 - 18 x 10^6 t/yr auf dem *südlichen Schelf* sedimentiert werden. Auf dem *zentralen Schelf* macht das von den kleinen Bergflüssen geschüttete Sediment mit 40 - 100 x 10^6 t/yr etwa die Hälfte der vom Mekong geschütteten Menge aus. Hier werden 20 - 40 x 10^6 t/yr auf dem Schelf abgelagert. Der übrige Teil passiert den Schelf oder wird über Rutschungen vom relativ steilen Schelf in tiefere Bereiche des Südchinesischen Meeres transportiert. Der Red River liefert eine Sedimentmenge von ca. 130 x 10^6 t/yr und lagert den größten Teil seiner Fracht im Red River Delta ab. Nur ca. 20 x 10^6 t/yr werden auf dem nördlichen Schelf sedimentiert.

Danksagung
An erster Stelle danke ich meinem Doktorvater Prof. Dr. Karl Stattegger für die Vergabe und die Betreuung dieser Arbeit, sowie viele Diskussionen und Anregungen. Auch die zahlreichen Expeditionen und Forschungsreisen in ferne Länder waren toll. Danke!
Meinem zweiten Betreuer Priv. Doz. Dr. Karsten Haase danke ich für die Einführung in die Geheimnisse der Geochemie und seine weitreichenden Anregungen und Diskussionsbereitschaft.
Zu meinem Freund und Kollegen Dr. "tilli_san" Till Hanebuth (AIST Tsukuba) bestand, vor allem in den letzten Monaten, eine Internet-Standleitung nach Japan. Danke für deine große Einsatzfreude und wertvolle Tipps und Anregungen. Deine Sundaschelf Erfahrung war mir ein Wegbereiter von unschätzbarem Wert.
Mein Freund und Kollege Dr. Germain "Charles Gauthier" Bayon (SOC Southampton) war mir ein hervorragender Mentor in Sachen Sr- und Nd-Isotopengeochemie. Merci mon cher pote!
Prof. Dr. Bob Nesbitt (SOC Southampton) danke ich für seine Gastfreundschaft die ich im Rahmen eines Socfac-Grants 2 Monate lang am SOC genießen durfte. Dr. Rex Taylor, Dr. Andy Milton und Posy Boella betreuten mich in den Labors. Thanks to you all!
Prof. Dr. Pieter Grootes, Dr. Frank Bruhn und die gesamte Mannschaft vom Leibniz-Labor der Universität Kiel führten die zahlreichen AMS-Datierungen durch und haben mit fruchtbaren Diskussionen zum Gelingen der Arbeit beigetragen. Die Sauerstoffisotopenmessungen nahmen Dr. Helmut Erlenkeuser und sein Team vor.
Besonderer Dank geht an die Sunda- und Südchinasee-Familie: Markus Kienast (UBC Vancouver) hat die Hauptelemente gemessen, Dr. Ludvig "Bärchen" Löwemark half bei der Interpretation der Radiographien und Dr. Stephan "Puschi" Steinke, Witold Szczucínski und Hiroshi "Klaus" Kawamura hatten für Fragen und Diskussionen immer ein offenes Ohr.
Dr. Jan Scholten und Petra Fiedler leisteten bei der Aufbereitung und Messung der Tonmineralpräparate hervorragende Arbeit. Dr. Thomas "Plätzchen" Pletsch stand bei der Vorbereitung und Interpretation mit gutem Rat zur Seite. Dr. Dieter Garbe-Schönberg sei für die Einführung in das ICP-MS gedankt
Großer Dank gebührt auch Inge Dold für die Durchführung von zahllosen Kohlenstoffmessungen. Des Weiteren bedanke ich mich bei Wilma Rehder, Sigrid Mülhan und Bärbel Burmeister für die Hilfe beim Anfertigen der Radiographien sowei bei Wolfgang Reimers für Kernlager-Schließdienste.
Uschi Faber hatte bei Bedarf an Beprobungsmaterial immer ein offenes Ohr, und daß sie mir den Radiographiepräparate-Schneider vermacht hat vergesse ich ihr nie.
Prof. Dr. Wolfgang Kuhnt, Dres. Renata Szarek, Sylvia Hess, Mara Weinelt und Thorsten "Cheffchen" Kiefer halfen bei mikropaläontologischen Fragestellungen.
Ohne meine HiWis Ronja Düffel, Witold Szczucínski, Cornelia Gai, Alexander Beck und allen voran Daniel "bester HiWi der Welt" Unverricht wären die unverzichtbaren Datenmengen nicht entstanden.
Dres. Martin Wiesner (Uni Hamburg), Yoshiki Saito (AIST Tsukuba) und Gert van den Bergh (NIOZ Texel) stellten Proben von Mekong und Red River Delta zur Verfügung. Bei Kapitän und Mannschaft von FS SONNE bedanke ich mich herzlich für den Einsatz zur Probennahme während der SONNE 140 Ausfahrt.
Meinen Weggefährten im Graduiertenkolleg danke ich für die gemeinsame Zeit, unzählige Kaffeepausen sowie etliche Grillsessions und GK Stammtische: Volker "mein Freund Botzi" Karpen, Zimmerkollege Dr. Stefan "der Lottodoktor" Purkl, Alexander "der Hacker" Heuser, Dr. Mischa Abratis, Barbara Teichert, Béatrice Cailleau, Dr. Thomas Walter, Britta Lissina, Dr. Angelika Schmidt, Sandra Bollwerk, Jenny Kandiano, Nico "Geomar" Urbanski, Axel Mohr und Dr. Ralf Schmidt waren immer wieder gute Hilfen und Informationsquellen in diversen Belangen.
Ein lautes "Thanx brah'!" geht an Max Cremer (SOEST Hawaii) der half die groben Falten aus dem Englischen zu bügeln, sowie an Caroline und Nils Steinmeyer nach London.
Meinen Eltern und Schwiegereltern danke ich für Unterstützung, Interesse und immerwährenden Zuspruch.
Zuletzt, aber mit größter Inbrunst, danke ich meiner lieben Frau Chrissi und meiner süßen Tochter Greta. Danke für eure Liebe und Geduld und daß ihr immer da seid und mir uneingeschränkt entgegenkommt!

Euch allen herzlichen Dank!

Diese Arbeit wurde im Rahmen des Graduiertenkollegs "Dynamik globaler Kreisläufe im System Erde" von der Deutschen Forschungsgemeinschaft gefördert. Die SONNE 140 Ausfahrt wurde vom BMBF finanziert.

TABLE OF CONTENTS

1 Introduction

The world's continental shelves, comprising appoximately 7.5 % of the total ocean area, are the gate keepers between the continents and the oceans. Terrigenous sediments delivered from the continents are deposited on the shelf or, depending on grain size and hydrographic conditions, pass over it into the deep sea. In contrast to the deeper parts of the world's oceans, the shelves are directly affected by sea-level fluctuations, leaving clear indications of sea-level lowstands in the form of terrestrially influenced paleofacies or unconformities within the sediments. The deposits formed at the dynamic land-sea interface provide unique records of environmental change. Both terrestrial and marine conditions can be unraveled by studying the sedimentary composition and the distribution of those deposits.

Continental shelves play an important role as a bypassing area for fine-grained sediment as well as an important depocenter itself. Budgets of shelf sediment yield important information about denudation and climate in the hinterland.

Due to the deglacial sea-level rise the *autochtonous* character of some parts of the shelves still plays an important role in sediments of Holocene age, whereas other shelf areas of the same age show *allochthonous* sedimentation.

Ancient shelf deposits, with their high amount of land-derived organic matter, bear a high potential for fossil fuel, making the shelves an economically important resource area.

Finally, a significant percentage (ca. 25 %) of the world's population lives on the coast and most of the largest urban concentrations are located in coastal areas (FAO, 1998), making it important to understand causes and consequences of sea-level rise.

1.1 Geological Setting

Southeast Asia is regarded as an amalgamation of several allochthonous continental blocks. The majority of Vietnam is part of the ancient Indochina (Indosinian) block (Fontaine and Workman, 1997). From north to south several tectonic zones can be distiguished. The most important faults separating those tectonic regions from each other are the Song Hong (Ailao Shan-Red River), Song Ma and Song Ca faults, all located in northern Vietnam and responsible for Neogene tectonics in this area. Here, Oligocene - Miocene extensional domes, linked to extension of the continental margin and back-arc spreading in the South China Sea (SCS), have been identified (Tapponnier et al.; 1982; Leloup et al., 1995; Lepvrier et al., 1997; Jolivet et al., 1999; Nagy et al., 2000). The Ailao Shan-Red River shear zone, resulting from collision-extrusion of the Indochina block in the course of the Himalayan orogeny, is one of the major discontinuities in Southeast Asia. It is still active and subject of

numerous investigations (Wang et al., 1998; Zhang and Schärer, 1999; Bodet and Schärer, 2000).

The central and southern part of Vietnam, bearing the Kontum Massif with an Archean-Proterozoic basement, is regarded as relatively stable. Also the often reported 110°-fault does not seem to be active at recent times (Hall, 1996). The southern part of Vietnam has undergone intensive intrusion activity in the Mesozoic and Cenozoic (Fontaine and Workman, 1997) and is largely covered with basalts of Neogene-Quaternary age (Nguyen et al., 1996; Nagy et al., 2001). The most recent volcanic activity occurred in the Ile des Cendres complex (Catwick Islands) off southern Vietnam in 1923.

Morphologically, the Kontum Massif is part of the north - south trending Annamite chain with elevations up to 2600 m, and it approaches the coast in the area of central Vietnam. It is host to many small mountainous rivers draining into the South China Sea (Fig. 2).

1.1.1 Monsoon Climate and Implications

The Asian Monsoon system, consisting of the Indian Monsoon, the East Asian Monsoon and the Plateau Monsoon (An et al. 2000), is the generator for oceanic surface circulation in the South China Sea (Fig. 1). For the western part of the SCS the general direction of the oceanic currents is from north to south in winter and south to north in summer at both, recent and Last Glacial Maximum (LGM) -times (Wang et al., 1995). The East Asian Monsoon is the most important climate factor for the SCS. The winter monsoon (northern hemisphere winter) is characterized by cold air from high latitudes flowing along the eastern margin of the Tibetan Plateau towards the SCS, resulting in a north-easterly wind direction. During the summer monsoon, warm and humid air from the low latitudes of the Indian Ocean is flowing towards the northeast over the SCS onto the East Asian continent which results in a south-westerly wind direction.

Due to the East Asian Monsoon cool, dry winters and warm, humid summers characterize the climate in the study area. The partly very high precipitation and riverine input affects the sea surface salinity in the study area, resulting in lower values (~1 psu) in front of the Mekong and Red River and along the Vietnamese Coast (Wyrtki, 1961).

With only small passages, like the Strait of Malacca in the east and the Karimata and Bashi Strait in the west, connecting the SCS to the Pacific and Indian Ocean, the exchange of water masses is limited and was even lower during LGM-times, when the SCS was a semi-enclosed basin due to a lowered sea-level.

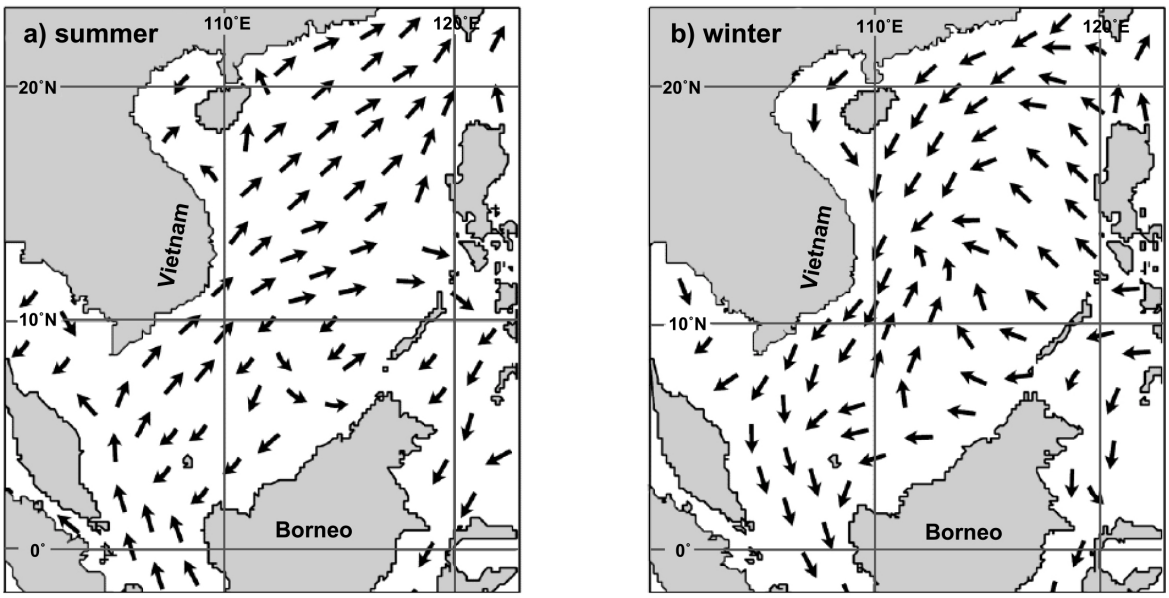

Fig. 1: *Seasonal sea-surface circulation patterns in the South China Sea (after Wang et al., 1995, modified) a) summer, b) winter*

1.1.2 The Vietnamese Shelf

The shelf off the Vietnamese Coast has extensions of varying dimensions, from very wide to very narrow. In the vicinity of the Mekong River and where the Vietnamese Shelf merges with the Sunda Shelf it expands to more than 500 km. The central part of the Vietnamese Shelf is very narrow with lateral extensions as low as 20 km between 13°N and 15°N. In the North, in the area of the Gulf of Tonkin the shelf expands again to hundreds of kilometers.

Even though the South China Sea is an intensively studied part of the world's oceans (Broecker et al., 1988; Wang and Wang, 1990; Wang et al., 1995; Wang, 1999; Hanebuth, 2000; Bühring, 2001; Steinke, 2001; Szarek, 2001), little effort has been made to investigate and understand its western marginal part in the area off the Vietnamese Coast. Early studies (Niino and Emery, 1961; Emery, 1968) characterize some of the deposits on the Vietnamese Shelf as *relict sediments* not related to the modern depositional environment. Those deposits are the remainders of sediments deposited subaerially or in lacustrine or marshy environments during sea-level lowstand that were continuously reworked by bioturbation and other authigenic processes. The rapid deglacial sea-level rise (Hanebuth et al. 2000) left the seafloor in disequilibrium where the depositional environment could not respond to the quick oceanographic and hydrographic changes, leaving a blanket of *relict sediments*. Few internationally published studies focussed on sea-level rise and shelf sedimentation during the Quaternary in Vietnam (e.g. Fontaine and Delibrias, 1974).

The French-Vietnamese Ponaga-cruise and related studies focussed on rifting processes and Cenozoic tectonic events off Vietnam (PONAGA, 1993; Rangin et al., 1995; Roques et al.,

1997). Most recent investigations on shelf sedimentation revealed thick sediment wedges and propose modern sedimentation rates of ca. 0.35 cm/year (Wiesner et al., 1999; Schimanski and Stattegger, 2001; Szczucínski and Stattegger, 2001).

1.1.3 The Vietnamese Hinterland

Detrital sediments supplied by rivers draining into the South China Sea account for the major part of the deposits on the Vietnamese Shelf. The Mekong in the South and the Red River in the North are among the ten largest rivers in the world in terms of sediment discharge (Milliman and Meade, 1983). Both rivers are draining large basins with predominantly post-Paloezoic sediments and are forming extensive deltas. The central part of Vietnam is characterized by hundreds of small mountainous rivers draining the Annamite chain and also probably contributing large amounts of detritus to the Vietnamese Shelf (Milliman and Syvitski, 1992; Schimanski et al., 2001). Here, as a part of the Kontum Massif, rocks of partly Precambrian age are cropping out (Fontaine and Workman, 1997; Lan et al., 2000; Nagy et al. 2001) which stands in contrast to the age of sediments delivered by the Mekong and the Red River. This difference will be used later in this work to determine sediment provenances for the deposits from the Vietnamese Shelf.

1.1.4 Influence of Deglacial Sea-Level Rise

Wide parts of the Vietnamese Shelf were exposed during times of sea-level lowstand. Especially the areas of wide shelf extent experienced far reaching flooding with the subsequent sea-level rise. This dynamic process influenced the sedimentary environment strongly. The depositional system was reorganized and morphological structures inundated. Facies associations and depocenters shifted with rising sea-level from shelf break to more nearshore shelf regions. The exposed surface was eroded during transgression, leaving an inundated surface which is recorded in the sediment as a hiatus.

With rising sea-level the high mountains of the vietnamese hinterland reached a more proximal position in relation to potential depocenters, although this effect is weakenend by the narrowness of the shelf in this area. Nevertheless, the sedimentary compositon of nearshore deposits is affected strongly by the enormous amounts of sediment eroded from those mountains and changes in the sedimentological and geochemical composition yield key-information on change of sources and/or climate.

1.2 Study Area

The study area extends from north to south along the Vietnamese Coast (Fig. 2) from 16:44.40° N; 108:27.77° E (northernmost sediment station 18426) to 7:00.20° N; 107:54.87° E (southernmost sediment station 18375). The investigated sediment cores are from modern water depths between 21 m and 169 m and the sediment recovery was up to 8 m.

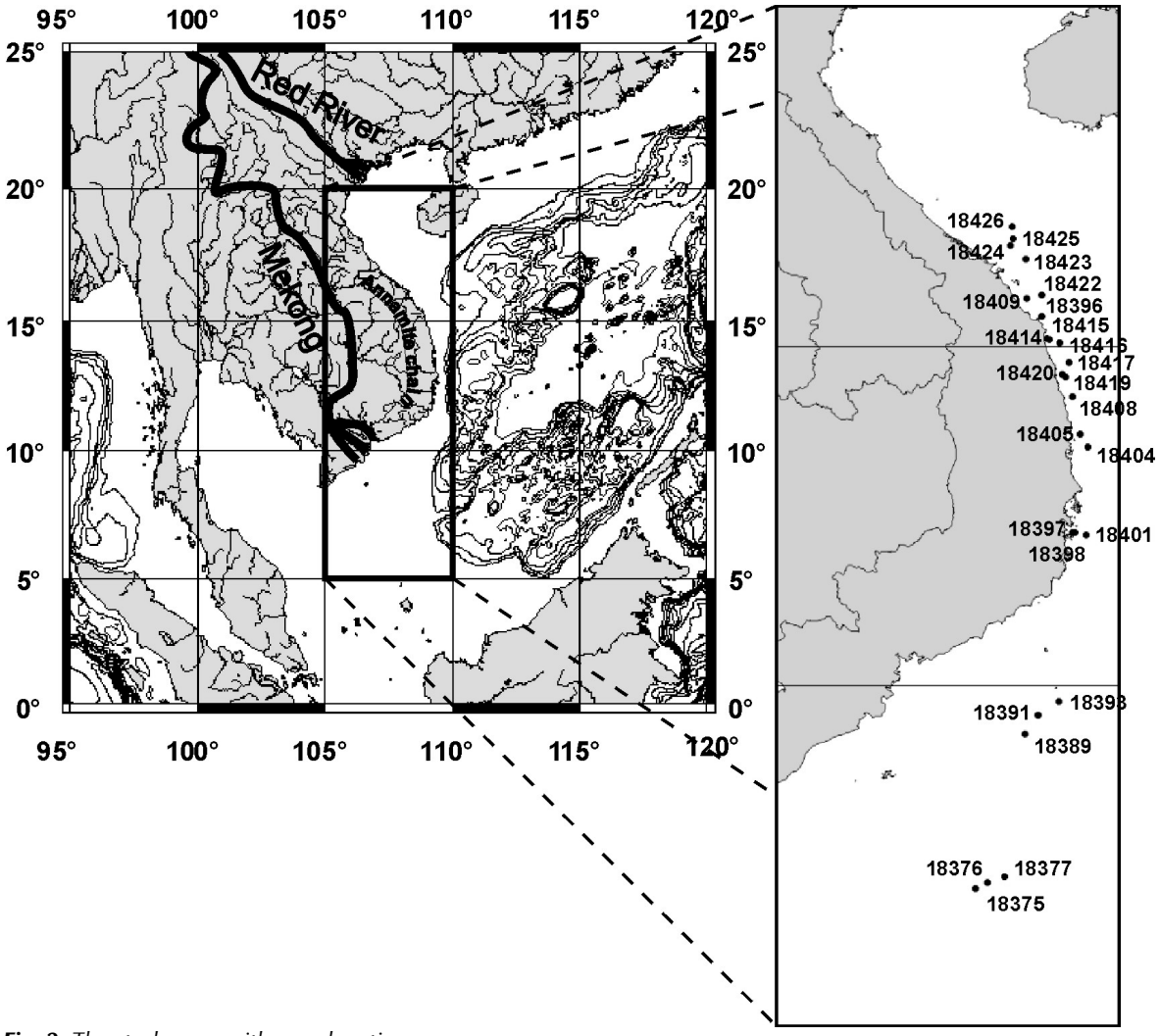

Fig. 2: *The study area with core locations*

1.3 Objective of this Study

The goal of this study is to characterize sedimentation processes on the Vietnamese Shelf and to reconstruct changes in sedimentary processes from source to sink during the last 20 kyr with special focus on the Holocene. In order to reach those goals knowledge of yet unknown information is necessary. Since almost no sedimentological, geochemical and geophysical information from the Vietnamese Shelf exists or is accessible for western scientists, a general

database had to be developed at first hand. With the help of this database the following sub-projects were realized:

- Sedimentological and geochemical characterization of the sediment deposited in the study area
- Development of a stratigraphic framework based on AMS-^{14}C dates
- Understanding processes controlling sedimentation and erosion
- Identification of the provenance of the terrigenous sediments (detritus)
- Identification of possible climatic changes in the hinterland reflected by the geochemical composition of sediment
- Development of a sediment budget for the detrital sediments delivered by the Mekong, the Red River and small mountainous rivers.
- Contribution to the general understanding of the dynamics at the land-sea interface

Results are presented in 3 separated chapters. The first, dealing with the Holocene Sedimentation on the Vietnamese Shelf, is a comprehensive description of the sedimentary processes in the study area and presents a detailed AMS-^{14}C stratigraphy. In the second chapter light is thrown on the provenance of detrital sediments on the Vietnamese Shelf. Major element-, trace element- and isotope geochemistry were used to distinguish between sediments and possible endmembers delivered by the numerous rivers draining into the SCS. The third part of this work provides a sediment budget for the rivers along the Vietnamese Coast promoting the importance of the usually underestimated small mountainous rivers.

2 Materials and Methods

Numerous methods have been used to characterize the material. An overview of samples taken and methods employed is illustrated in a flow chart in Fig. 3.

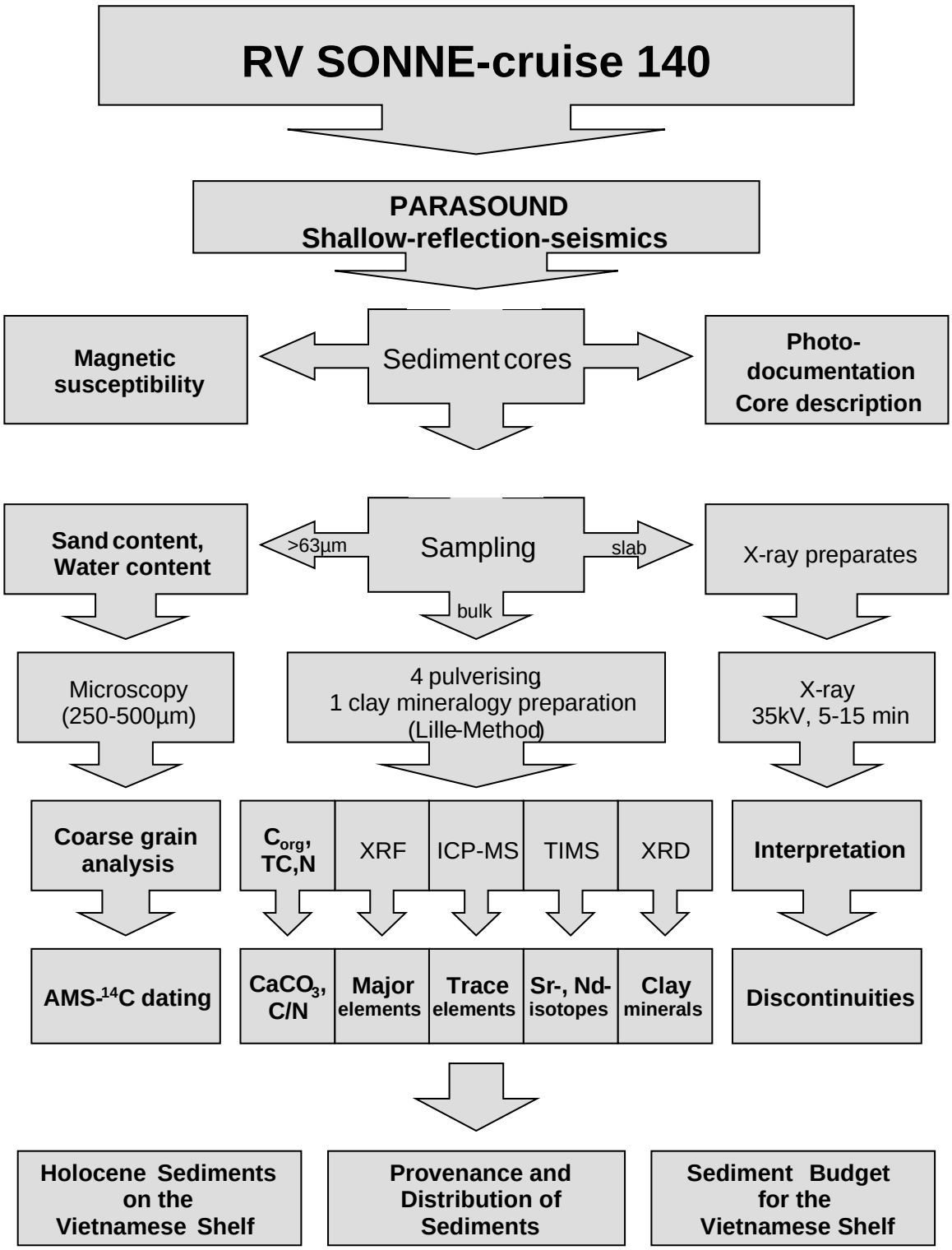

Fig. 3: *Flow chart illustrating sampling and methodological procedures. Work steps contributing to the results are* ***bold***

2.1 Materials

The sediments were cored during cruise 140 with R/V SONNE (SÜDMEER III) to the South China Sea in April 1999 (Wiesner et al. 1999).

58 sediment stations were cored during the cruise, of which 25 cores were selected for further analysis relevant in this study (Tab. 1). All cores, except vibracores 18375-2 18376-2 and 18377-2, were cored with a gravity corer. The sediment cores are from water depths between 21 m and 169 m.

Tab. 1: *Station list of the sediment cores with sediment recovery*

Core No	Coring device	Latitude [°] N	Longitude [°] E	Water depth[m]	Recovery [cm]
18375 -2	VC	7:00.20	107:54.87	87	369
18376 -2	VC	7:05.27	108:06.42	89	477
18377 -2	VC	7:10.71	108:20.28	98	357
18389 -3	GC-3	9:16.45	108:39.09	109	271
18391 -2	GC-6	9:33.91	108:49.60	115	478
18393 -3	GC-6	9:45.61	109:07.95	155	540
18396 -3	GC-6	15:25.51	108:53.27	61	499
18397 -2	GC-6	12:14.71	109:19.91	45	532
18398 -3	GC-18	12:14.23	109:22.81	59	719
18401 -3	GC-12	12:12.90	109:32.09	134	707
18404 -3	GC-6	13:30.13	109:33.67	169	385
18405 -3	GC-6	13:41.10	109:27.02	130	547
18408 -3	GC-12	14:14.34	109:19.05	108	754
18409 -3	GC-12	15:41.21	108:40.79	40	577
18414 -3	GC-6	15:05.83	108:57.78	21	448
18415 -2	GC-6	15:04.98	109:00.03	38	559
18416 -2	GC-6	15:02.23	109:08.97	66	506
18417 -3	GC-12	14:44.81	109:17.61	97	798
18419 -3	GC-12	14:32.23	109:14.09	82	641
18420 -2	GC-6	14:34.13	109:11.36	62	557
18422 -3	GC-6	15:44.92	108:53.46	84	568
18423 -2	GC-6	16:16.62	108:39.59	97	548
18424 -2	GC-6	16:28.61	108:26.15	90	575
18425 -2	GC-6	16:34.53	108:28.31	95	556
18426 -2	GC-6	16:44.42	108:27.80	92	513

2.2 Sedimentological Methods

2.2.1 Core Description

Onboard R/V Sonne the sediment cores were split and photographed. The macroscopic description of the sediment was carried out immediately after opening of the cores due to possible evaporation and oxidation of the fresh sediment surfaces. The sediment color was described using the GSA Rock Color Chart. Since shelf sediment shows a high variation in macroscopic composition, the sedimentary characteristics concerning grain size (sand, silt, mud), content of marine organisms (foraminifera, shells, sea urchins), and sedimentary

structures like burrows, erosional surfaces and transitions were recorded in detail and can be found in the cruise report (Wiesner et al., 1999).

2.2.2 Coarse Grain Analysis

The sand content has been determined on all cores at 20 cm to 100 cm intervals. Variation in the granulometry can be an important facies indicator since changes in erosion of the hinterland and river discharge influence the amount and sedimentary composition on the detrital sediment. The abundance of marine organisms like foraminifera or shell fragments which are usually part of the sand fraction, is also facies indicative. The marine character of a shelf sediment can be expressed via its carbonate content.

The two most important sources for sand on the Vietnamese Shelf are siliciclastics delivered by the rivers on the one hand and marine microorganisms (mostly foraminifera) and shell fragments on the other.

All cores were investigated for the composition of the coarse grain fraction. Samples were taken every 50 cm to 100 cm, freeze-dried, washed over a 63 μm sieve and sieved into fractions. The fraction from 250 μm to 500 μm was split with an Otto-microsplitter until at least 300 grains were left for counting, which ensures the representativity of the sample (Plas and Tobi, 1965). In the coarse grain analysis the following groups were considered:

- Planktonic foraminifera
- Benthic foraminifera
- Shell fragments
- Lithoclasts
- Plant fragments
- Glaucony

The coarse grain analysis is a useful tool in environments with a high facies variability as shown in previous studies by Schimanski (1999) and Hanebuth (2000).

Transitions from more terrestrially influenced to more marine influenced environments, as they are implicated by sea-level rise, are recorded in the composition of the coarse fraction, which allows, together with other proxies, a precise facies interpretation.

2.2.3 X-ray Radiography

Most internal sedimentary structures are not visible for the naked eye. Shelf sediments are exposed to various physical influences from burrowing by organisms over erosion due to

currents or slumps to cross bedding. These story-telling structures are important indicators for the paleo-environment. Additionally, discontinuities caused by changing hydrographic conditions are detectable by X-ray radiography.

The archive halves of the freshly opened cores have been sampled for sediment slabs approximately 1 cm thick and exposed to X-ray radiation at 35 kV. The exposure time lay between 5 min and 15 min, depending on sediment type and thickness of the slab.

Ca. 90 m of X-ray radiographies were analyzed over a light table and graphically illustrated in a special profile (X-ray Log) taking into account grain size, sediment structure and degree of bioturbation (Fig. 4). A special focus lay in the identification of discontinuities within the deposits.

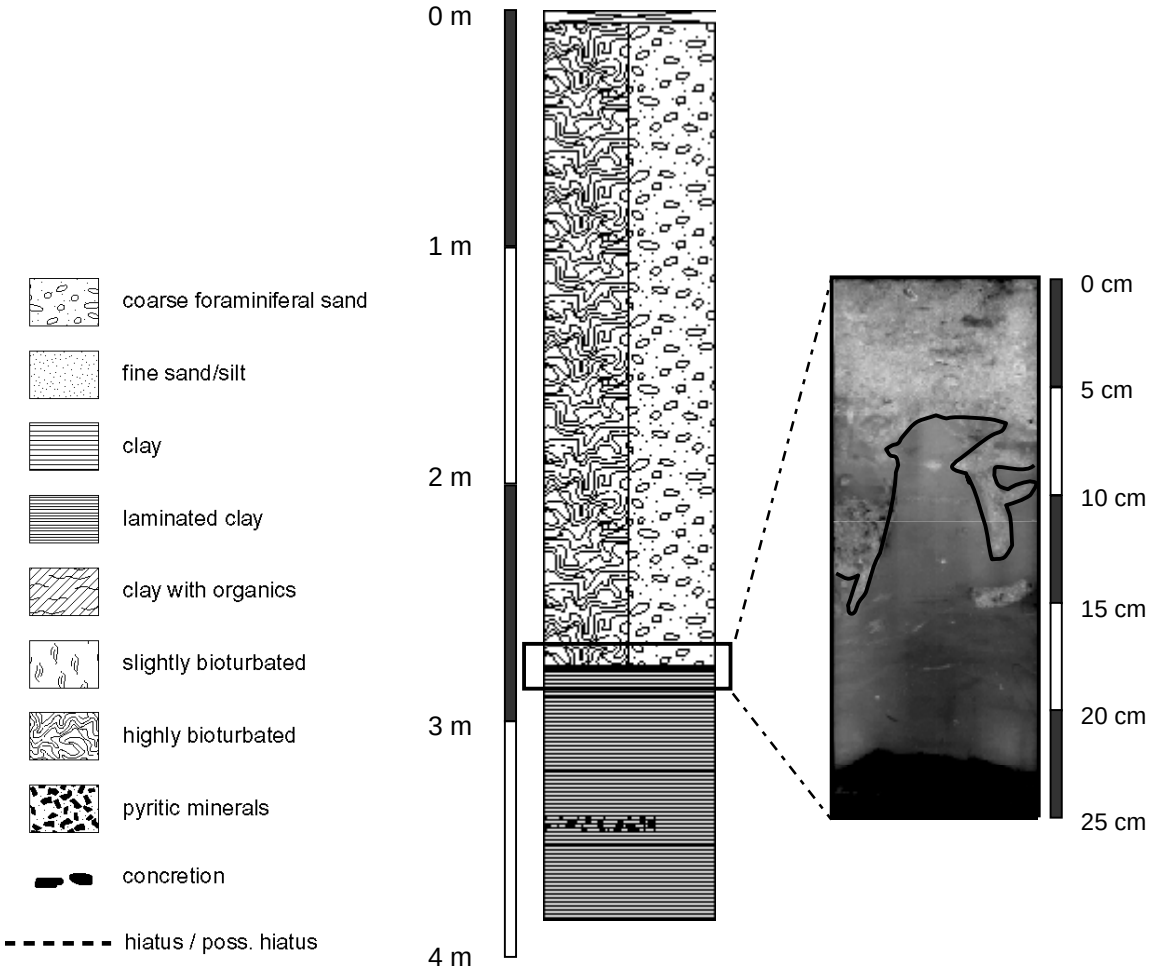

Fig. 4: *X-ray Log depicting sediment structure, grade of bioturbation and discontinuities. Right: sediment slab with discontinuity (highlighted)*

Furthermore, discontinuities on the shelf are often caused by the transgressing water masses flooding the shelf in the course of a sea-level rise. This kind of discontinuity can be used to determine the time of transgression if the sediment below and above the discontinuity is dated and the hiatus only covers a short time interval.

2.2.4 Clay Mineralogy

The four most abundant clay minerals smectite, illite, chlorite and kaolinite show certain assemblages in dependence of the composition of the source rocks and transport media (Gingele et al., 2001). Clay minerals in the study area are mainly delivered by rivers, but also via aoelian transport a significant amount of dust is contributed to the sediment column (Duce et al. 1991). To determine variations in source and, to a lesser extent, in climate, recent samples and samples of early Holocene age have been investigated for their clay mineral distribution.

Preparation procedures generally followed the method of Holtzapffel (1985). The bulk sediment sample was suspended in demineralized water on a stirring plate and decarbonated by adding 0.2 N HCl. The pH value was continuously controlled during this process. Acid residue was washed out and an aliquot of the $< 2\mu$m fraction was separated by settling method according to Stoke's law (transformed after Hotzapffel, 1985):

$$t = 190 \times X/d^2$$

Where t = settling time [min], X = depth of settling particles [cm] and d = diameter of settling particles [μm]

The filter transfer method (Moore and Reynolds, 1989) was used to generate oriented samples by sucking an aliquot through cellulose nitrate filters (0.2 μm pore width). After drying at 50°C the sample was transferred on an aluminium slide and measured on a Philips PW 1710 X-ray diffractometer with Cu-Kα radiation and automatic divergence slit. XRD scans were performed with a step width of 0.01° 2Θ/s in a range of 2 - 40° 2Θ on both, untreated and glycolated (overnight at 60°C) samples.

Peak areas were calculated after manual baseline correction using the MacDiff software, version 4.2.5 (Petschik, 2000) after the techniques of Biscaye (1964, 1965).

2.2.5 Magnetic Susceptibility

The magnetic susceptibility (MagSus) was measured onboard using a Multi Sensor Core Logger (MSCL/016) designed and built by GEOTEC, Haslemere, UK. The magnetic susceptibility, which is bound to the amount of magnetizable minerals within the sediment, was measured on unsplit core sections of 12 cm in diameter at 100 cm core sections with a resolution of 1 cm. Variations in MagSus can be attributed to changing concentration of

magnetizable minerals which are steered by change of sources, erosion and reworking of the sediment as well as hydrographic conditions influencing grain size.

2.3 AMS-^{14}C Dating

Since a classical paleoceanographical stratigraphy using oxygen isotopes of foraminiferal tests is neither suitable for the Holocene time interval nor for shallow marine conditions, the stratigraphy can rely on precise AMS-radiocarbon dating of the sediment.

Because undisturbed, continuous sediment records were not necessarily expected, the first focus lay on the dating of discontinuities detected with the help of X-ray radiography and other methods described above. Wood fragments and other organic material bearing no reservoir effect were only found in two cores (18389-3 and 18415-2). To circumvent the problem of elapsed time between death of a marine organisms and final deposition in addition to the generally uncertain reservoir effect, only "fresh" and intact carbonates were selected. Sea urchins with their fragile ambulacrae, bivalve shells with two shells still attached to each other via the ligament, intact pteropods with a very fine shell or foraminifera (*Rotalia sp*.) from unfragmented sediment where chosen to ensure reliable datings (cp. photo-plate, appendix). In some cases where no intact material was detectable, shell fragments were dated and in one case bulk sediment.

The preparational procedure started with separation from the sediment, followed by drying, washing, drying again and washing in demineralized water in an ultrasonic bath. Further preparations prior to the measurements and the measurements themselves were carried out at the Leibniz-Laboratory for Radiometric Dating and Isotope Research, Kiel. AMS-^{14}C ages were measured on a 3 MV Tandentron 4130 AMS system from High Voltage Engineering Europe. The analytical precision for counting and machine statistics is 0.25 to 0.3 % for modern samples (Nadeau, 1997; Nadeau,1998).

The calibration program CALIB (HTML version 4.3) was used to calibrate AMS-^{14}C years to calender years BP (Stuiver and Reimer, 1993). A calibration of the measured AMS-^{14}C ages is necessary since the activity of ^{14}C in the atmosphere was not constant at all times. Fluctuations in the rate of production of ^{14}C results in ^{14}C-plateaus where the same ^{14}C age covers a wide span of real time. Other dating methods such as U/Th-dating, varve chronology and tree-ring chronology are used to verify the true age of samples. The currently used calibration curve is the INTCAL98 curve (Stuiver et al., 1998).

The standard reservoir age of 400 yrs for marine samples is probably not appropriate for shallow water sediments from the SCS. Southon et al. (in press) found significantly lower

reservoir ages for modern shallow water carbonate samples from the SCS, whereas Wang et al. (1999) report higher reservoir ages for water masses at 400 m depth.

2.4 Geochemical Methods

All samples for geochemical analysis were freeze-dried, aliquots were ground in an agate mortar and dried again overnight. All cores have been investigated for organic and total carbon, whereas major elements as well as trace elements and Sr- and Nd-isotopes have been determined on 16 samples being representative for recent and early Holocene deposits along the Vietnamese Shelf from north to south.

2.4.1 Organic Carbon, Total Carbon, Total Nitrogen (C_{org}, TC, N_{tot}, $CaCO_3$) and Carbonate Content

The carbon and nitrogen content of the dried and fine ground bulk sediment (20 - 40 mg) was measured using a CHN-O Elemental Analyser of Carlo Erba Instruments. C_{org} samples were weighed into silver cartridges and 10 % HCl was added to the sample to dissolve the carbonaceous fraction of the sediment. The sediment was then burned at 1021°C and the generated CO_2-gas measured in a thermal conductivity detection unit. Acetanilid was used as a standard.

In a second procedure using tin cartridges, sediment (without HCl being added) was analysed for the content of total carbon (TC) and total nitrogen.

The carbonate content can then be calculated, assuming that all of the carbonate is present as calcite or aragonite:

$$CaCO_3\ [\%] = (TC - C_{org}) \times 8.33$$

Further the C/N-ratio was calculated. It is given by C_{org}/N_{tot} and can help to estimate the influence of terrestrial sediment on the study area, but has to be used with caution. Tyson (1995) reports C/N-rations for coastal plain and modern shelf sediments hardly exceeding values >30. Greater values possibly reflect a higher influence of particulate organic matter like wood fragments and leaf tissue.

2.4.2 Major Elements

The major elements were analyzed on powdered samples in the Department of Marine Biogeochemistry and Paloeoceanography at the University of British Columbia (Vancouver) using XRF techniques on glass beads. The glass beads are cast from a mixture of 0.4 g of

sample material and a flux by heating to 1100° C for 15 min. The analyses were carried out on a Philips PW 1400 wavelength-dispersive sequential automatic spectrometer. The complete procedure is described in detail by Calvert et al. (1985).
Results were corrected for sea salt assuming a salinity of 35 psu with an average concentration of dissolved salt.

2.4.3 Trace Elements and Sr- and Nd-Isotopes

The geochemical composition of detrital sediments reflects the geochemistry of the source rocks. To determine provenance and distribution of detrital sediments on the Vietnamese Shelf, 16 samples were analyzed for the concentration of Trace Elements and Sr- and Nd-isotopic composition. Seven surface samples of bulk sediment, reflecting the recent conditions and nine bulk samples dated with the AMS-^{14}C technique to early Holocene age have been investigated to detect change of sources due to modified sedimentological conditions including oceanograpy, hydrography and climate.
Trace element and isotopic analyses were carried out during two visits to Socfac (Southampton Oceanography Centre, Large Scale Analytical Facility) at the Southamptom Oceanography Centre.
Sample preparation generally followed the work of Bayon et al. (2002). They showed that exchangeable and carbonate fractions as well as Fe-Mn oxy-hydroxides have a great effect on the REE and isotopic signal. The removal of those fractions via sequential leaching led to a detrital fraction of pure continental origin.
Approximately 200 mg of the sediment were weighed into glass beakers with 10 % (v/v) acetic acid to remove the carbonate and exchangeable fractions. After four hours in an ultrasonic bath, the suspension was rinsed and centrifuged.
10 ml of a mixture of 1M hydroxylamine hydrochloride solution in 25 % (v/v) acetic acid (HH) was added to the residue in PTFE beakers to extract iron and manganese oxides. After three hours on a hotplate at 90° C the solution was centrifuged again.
The organic fraction was removed from the residue by adding 10 ml of 5 % H_2O_2 which was left on a shaker overnight. The remaining detrital fraction was treated with 2 ml of aqua regia to remove possible non-detrital remnants. Finally, the detritus was digested on a hotplate at 170°C for 48 hours by adding a HF-$HClO_4$ (3 ml/2 ml) mixture and subsequently evaporated to dryness. To avoid the formation of fluorides further 1.5 ml of $HClO_4$ were added. After evaporation the sample was taken up in 6 ml of 6M HCl and the "mother" solutions were ready for further processing, i. e. ICP-MS analyses and chemical separation prior to isotope analyses. Sr was isolated from the mother solution using columns filled with Sr resin (Sr spec, EiChrom Industries Inc. Illinois, USA). Prior to the separation of Nd, the REE were isolated

from the major elements by cation exchange. Nd was separated from the REE using HDEHP-coated teflon powder columns.

Sr and Nd isotopes were measured with a seven-collector VG-Micromass Sector 54 thermal ionization mass spectrometer with an external precision of +/-14ppm (2 s.d.) for $^{86}Sr/^{88}Sr$ and +/- 8ppm (2 s.d.) for $^{143}Nd/^{144}Nd$. Isotope ratios were normalized to $^{86}Sr/^{88}Sr = 0.1194$ and $^{146}Nd/^{144}Nd = 0.7219$. The analysis of the standards NBS SRM 987 and JNdi returned a $^{87}Sr/^{86}Sr$ of 0.710243 ± 8 and a $^{143}Nd/^{144}Nd$ of 0.512109 ± 14, respectively.

Analyses of the REE were performed by inductively coupled plasma mass spectrometry (ICP-MS) using a VG Elemental PlasmaQuad 2+ (external accuracy 5% (2 s.d.), internal precision better than 3% (2 s.d.) (Barrat and Nesbitt, 1996).

2.4.4 Oxygen Isotopes of Foraminiferal Shells

Three cores have been investigated for variations in $\delta^{18}O$ and $\delta^{13}C$ of foraminiferal tests. The only species with a continuous and sufficient abundance throughout the cores were the benthic foraminifera *Elphidium advenum* (CUSHMAN, 1922) and *Nonion subturgitum* (CUSHMAN, 1924), respectively. The signal of the stable oxygen isotopes largely depends on the conditions of the ambient waters (temperature, salinity) (Shackleton, 1977; 1987).

Where available, 20 specimen were selected from the dry-sieved 250 - 500 μm fraction, cracked and washed three times with ethanol for 20 seconds in an ultrasonic bath to remove detritus and carbonate fragments. Finally, the samples were dried at 40°C overnight.

The stable isotopes were measured at the Leibniz-Laboratory for Radiometric Dating and Isotope Research, Kiel with a Finnigan MAT 251 to a precision of 0.08 ‰ for $\delta^{18}O$ and 0.04 ‰ for $\delta^{13}C$ relative to the PeeDee River Belemnite (PDB) standard.

2.5 Further Methods

2.5.1 Parasound

Prior to coring operations, the sea-floor of the study area was investigated with the shipboard Parasound-system (STN Atlas Elektronik GmbH, Bremen) which uses the parametric effect. Here, two different frequencies (18 kHz and 20.5 - 23.5 kHz, respectively) are emitted, generating a working frequency of 2.5 - 5.5 kHz which results in narrow beam characteristics returning precise signals of the sea-floor and its subsurface reflectors. Correlation of sedimentary strata (investigated on the sediment cores) with similar physical characteristics is thus simplified and the lateral extent of sediment bodies traceable. Together with the ground-

truthing of sedimentological and geochemical investigations the abundance and distribution of sedimentary strata on the shelf can be estimated.

2.5.2 Cross Correlation

Several methods were employed to characterize the deposits from the study area. Nevertheless, each single method employed in this work yields only limited information about present and past sedimentological conditions. Only the integration of all results to a mosaic can lead to a clear image of the depositional history.

Tab. 2 shows an overview over the different methods employed on each core to investigate the sampled material.

Tab. 2: *Methods employed on each core*

Core No	Sample frequency (every cm)	Number of AMS-^{14}C datings	X-ray radio-graphies	Coarse gr. analysis	$CaCO_3$, C_{org}, TC, N_{tot}	$\delta^{18}O$	Major element geochem.	Trace element geochem.	Sr-/ Nd-Isotopes	Clay mineral.
18375-2	50	-	x	x	x					
18376-2	50	2	x	x	x					
18377-2	60	-	x	x	x					
18389-3	40	3	x	x	x					
18391-2	20	5		x	x		x	x	x	x
18393-3	50	3	x	x	x					
18396-3	100	1	x	x	x					
18397-2	20	2	x	x	x					
18398-3	50	-	x	x	x					
18401-3	20	2	x	x	x		x	x	x	x
18404-3	20	3	x	x	x					x
18405-3	20	-	x	n.a.	x					
18408-3	20	3	x	x	x					
18409-3	100	3	x	x	x		x	x	x	x
18414-3	20	1		x	x	x	x	x	x	x
18415-2	50	4	x	x	x		x	x	x	
18416-2	20	2		x	x	x	x	x	x	x
18417-3	100	2		x	x					
18419-3	100	2		x	x					
18420-2	100	2		x	x					
18422-3	20	1		x	x					
18423-2	20	2	x	x	x		x	x	x	x
18424-2	100	-		x	x					
18425-2	100	1		x	x					
18426-2	20	2	x	x	x					x

3 Principal Database

3.1 AMS-^{14}C Dating

45 samples were dated with the AMS-^{14}C method. All results were calibrated to calendar years BP (cp. chapter 4). While most samples date back to late Pleistocene or early Holocene times the youngest date is 665 AMS-^{14}C years BP and the oldest is >49220 AMS-^{14}C years BP. Tab. 3 gives an overview over the results of the AMS-^{14}C dating campaign.
For easy comparison of cores and respective ^{14}C-dates Fig. 5 shows an overview over all cores (X-ray Log or core description) from south to north with water depths and all AMS-^{14}C dates.

3.1.1 Reservoir Age for Marine Carbonate Samples from the Vietnamese Shelf

Shortly published reservoir ages for sediments from the South China Sea by Southon et al. (in press) vary between 244 ± 60 and 540 ± 60 years BP. A calculated reservoir age, derived from unaltered wood and carbonate shell fragments, respectively, from core 18415-2 returns a possible reservoir age of 210 ± 65 years BP which is in accordance with Southon's data from Singapore and Saigon. Generally, reservoir ages in the SCS seem to match with the globally assumed 400 years (Southon et al., in press), although the reservoir age may differ notably from the globally assumed value (Grootes, pers. comm.) due to the influence meteoric water, especially in the coastal area. However, to ensure comparability with previous studies from the SCS, dates measured on carbonate shells were corrected for a reservoir effect of 400 yrs.

3.2 Sedimentology

The principal sedimentological results of the 25 sediment cores including $CaCO_3$, C_{org} and C/N are outlined in Tab. 4. Contents of sand, $CaCO_3$, C_{org}, and results of C/N, MagSus, component analysis and the X-ray log can be found as profile plots in the appendix. An example is depicted in Fig. 6. Other results like content of water, total carbon and nitrogen can be found in the data spreadsheet in the appendix.

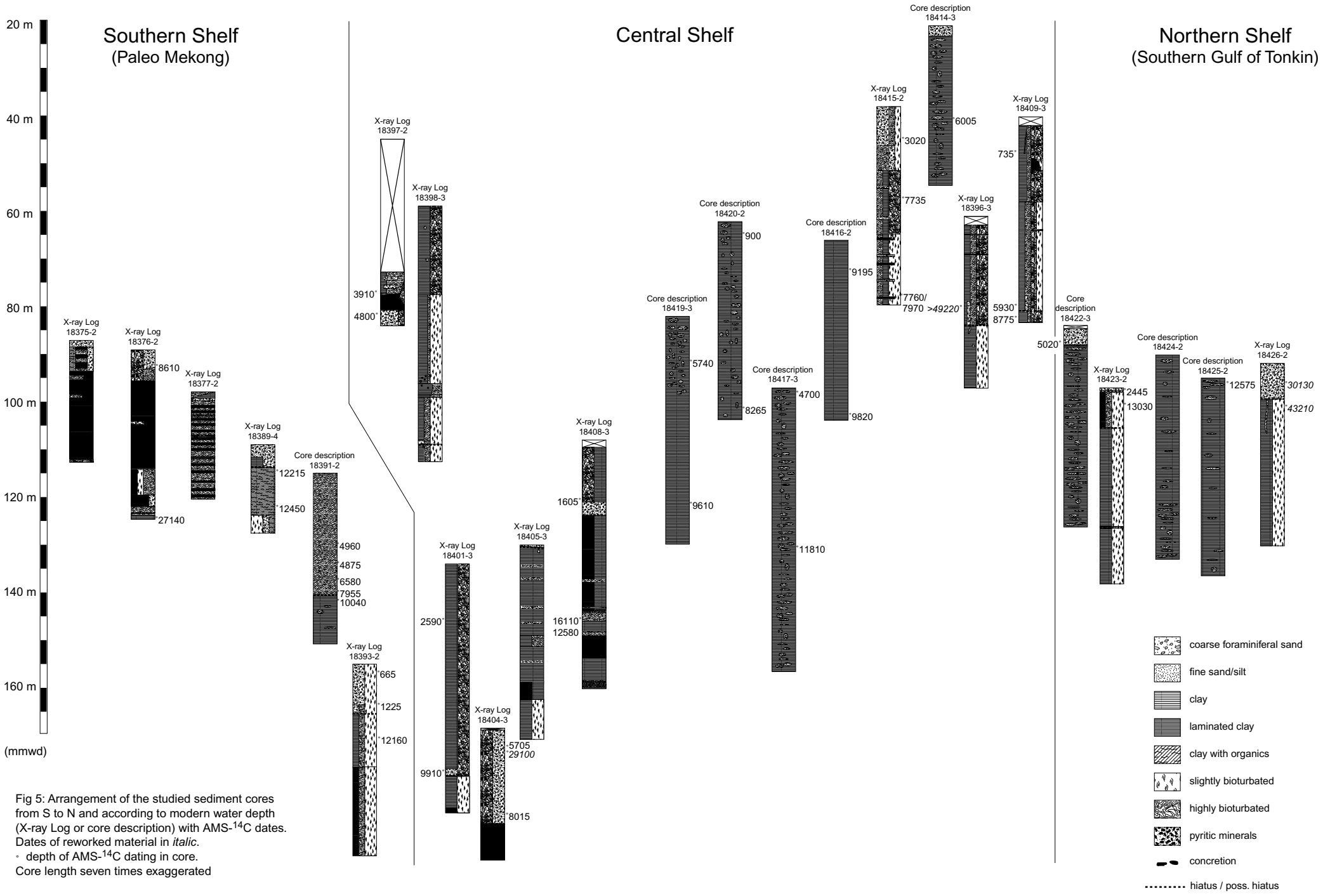

Fig 5: Arrangement of the studied sediment cores from S to N and according to modern water depth (X-ray Log or core description) with AMS-^{14}C dates. Dates of reworked material in *italic*.
◦ depth of AMS-^{14}C dating in core.
Core length seven times exaggerated

Tab. 3: *Results of the AMS-^{14}C dating campaign*

Core number	Water depth [m]	Sample depth [cm]	Sample material	mg C	AMS-^{14}C age [years BP]	Deviation +	Deviation -	δ^{13}C [‰]	Deviation ±
18376-2	89	40	bivalve shell (*Arca sp.?*)	2.1	**8610**	45	45	0.42	0.08
18376-2	89	472	crustacean arm	0.7	**27140**	210	200	-4.11	0.25
18389-4	109	99	wood, insoluble	4.7	**12215**	50	50	-27.98	0.12
18389-4	109	99	wood, humic acids	1.1	**12160**	70	70	-28.01	0.07
18389-4	109	186	wood, insoluble	5.1	**12450**	70	70	-27.47	0.06
18391-2	115	207	selected shell fragments	1.5	**4960**	35	35	0.61	0.06
18391-2	115	255	gastropod fragment	2.0	**4875**	35	35	0.41	0.22
18391-2	115	295	pteropods	1.3	**6580**	45	45	-0.37	0.14
18391-2	115	332	sea urchin (sand dollar)	1.6	**7955**	40	40	0.27	0.14
18391-2	115	360	*Rotalia sp.*	1.4	**10040**	60	60	0.03	0.23
18393-3	156	25 - 32	bivalve shell (*Arca sp.*)	0.8	**665**	25	25	-0.56	0.17
18393-3	156	102 - 107	bivalve shell (*Paphia sp.*)	1.3	**1225**	25	25	-1.22	0.14
18393-3	156	207	selected shell fragments	0.4	**12160**	60	60	-4.11	0.12
18393-3	156	207	selected shell fragments	1.1	**24330**	170	170	1.43	0.05
18396-3	61	250	*Rotalia sp.*	2.0	**>49220**			0.31	0.09
18397-2	45	413	small gastropod	2.0	**3910**	35	35	0.18	0.09
18397-2	45	488	gastropod	0.8	**4800**	35	35	-2.74	0.25
18401-3	134	226	gastropod	0.9	**2590**	40	40	0.69	0.16
18401-3	134	590	*Rotalia sp.*	1.1	**9910**	50	50	-0.68	0.35
18404-3	169	49-57	pteropods	1.3	**5705**	35	35	5.86	0.31
18404-3	169	60	*Rotalia sp.*	0.8	**29100**	390	370	-1.09	0.14
18404-3	169	225	gastropod	1.3	**8015**	50	50	4.27	0.09
18408-3	108	152	pteropods	1.6	**1605**	30	30	-0.38	0.05
18408-3	108	265	bulk sediment, lauge	1.0	**16110**	120	120	-23.03	0.11
18408-3	108	265	bulk sediment, humic acid	0.2	**12580**	310	290	-23.80	0.42
18409-3	40	90 - 93	selected shell fragments	1.0	**735**	30	30	-0.54	0.16
18409-3	40	525	sea urchin (sand dollar)	1.5	**5930**	35	35	0.99	0.13
18409-3	40	559	sea urchin	1.4	**8775**	50	50	0.11	0.27
18414-3	21	267	bivalve shell *(Glycimeris sp./Cardium sp.)*	1.0	**6005**	35	35	-0.02	0.05
18415-2	38	106 - 109	gastropod (*Phasianella solida*)	2.2	**3020**	30	30	-0.36	0.09
18415-2	38	250	pteropods	1.3	**7735**	40	40	-3.21	0.30
18415-2	38	526	fresh carbonate fragments	1.4	**7970**	50	45	0.39	0.13
18415-2	38	526	wood	3.5	**7760**	45	45	-29.28	0.06
18416-2	66	97-99	bivalve shell (*Paphia sp.*)	1.4	**9195**	45	45	-2.1	0.13
18416-2	66	491-492	bivalve shell (*Paphia sp.*)	1.2	**9820**	50	50	0.16	0.13
18417-3	97	9-17	gastropod (*Cymatium sp.*)	0.8	**4700**	45	45	0.48	0.26
18417-3	97	450	*Rotalia sp.*	1.4	**11810**	60	60	-2.66	0.32
18419-3	82	130	*Rotalia sp.*	1.3	**5740**	60	60	1.83	0.09
18419-3	82	525	sea urchin fragment	0.74	**9610**	60	60	-2.33	0.21
18420-2	62	40-43	pteropods	0.9	**900**	25	25	-0.73	0.18
18420-2	62	511	sea urchin fragments	1.5	**8265**	50	50	0.87	0.13
18422-3	84	51	gastropod	1.2	**5020**	30	30	0.78	0.08
18423-2	97	2	selected shell fragments with periostracum	1.6	**2445**	30	30	0.75	0.05
18423-2	97	46.5	sea urchin	1.3	**13030**	60	60	-1.75	0.20
18425-2	95	29	bivalve shell (*Barbatia amygdalumtostum)*	0.8	**12575**	60	60	-0.38	0.12
18426-2	92	55	bivalve shell (*Isognomon sp.)*	1.4	**30130**	320	300	3.47	0.04
18426-2	92	133	*Rotalia sp.*	1.3	**43210**	2630	1980	-0.21	0.17

Tab. 4: *Important sedimentological features of the investigated cores. Percentage of components referring to the 250 - 500 µm fraction*

Core No water depth	Short description
18375-2 87 m	high sand content in the upper part; low $CaCO_3$ except at the top
18376-2 89 m	discontinuity in the lower part; sand content highly variable; lowest part dominated by shell fragments and lithoclasts, middle part lithoclasts and plant fragments, upper part foraminifers, shell fragments and lithoclasts;
18377-2 98 m	high sand content in lower part; nearly 100 % lithoclasts in lower part passing over to 50 % plant fragments in upper part
18389-3 109 m	
18391-2 115 m	low sand content in lowest part passing over to a high sand content in upper part; high C_{org} content in lowest part passing over to low C_{org} in upper part; mainly foraminifers and shell fragments
18393-3 156 m	high sand and $CaCO_3$ content in upper part; discontinuity between 100 cm and 200 cm
18396-3 61 m	discontinuity around 300 cm; low sand content with maximum of 36 %, mainly plant fragments in the lower part changing to shell fragments and lithoclasts in the upper part; sediment partly reworked
18397-2 45 m	two discontinuities in lower part; low sand content, not much variation throughout the core except one outlier in the lower part, low C_{org} in lowest part
18398-3 59 m	discontinuity in lower part; low sand content, generally low variability
18401-3 134 m	discontinuity around 600 cm; about 15 % of sand, not much variation throughout the core; mainly foraminifers and shell fragments
18404-3 169 m	discontinuity around 250 cm, sand content 0 - 80 %, high $CaCO_3$ of up to 36 % in the middle part , in the lowest part mainly plant fragments and lithoclasts, otherwise shell fragments and lithoclasts (partly reworked)
18405-3 130 m	poss. discontinuity at the top, low sand content, no variation throughout the core
18408-3 108 m	discontinuity at 212 cm; very low sand content in lower part, up to 30 % in the upper part; lower part dominated by plant fragments and lithoclasts, upper part dominated by shell fragments; partly reworked
18409-3 40 m	discontinuity around 540 cm, low sand content except below discontinuity;
18414-3 21 m	sand content around 50 %; low $CaCO_3$, higher C/N than previous cores; core dominated by lithoclasts and shell fragments but shell and plant fragments in lowest part
18415-2 38 m	no obvious discontinuities, but numerous slumps in lower and middle part; sand content ca. 60 % in upper ,30 % in lower part; low $CaCO_3$ except upper in part; lower part mainly shell and plant fragments, middle part shell fragments, upper part lithoclasts;
18416-2 66 m	low sand content in lower part, up to 20 % in upper part, low variation in other proxies; mainly shell and plant fragments, uppermost part mainly shell fragments and lithoclasts
18417-3 97 m	decreasing sand content with depth, low variation in other proxies; lower part dominated by shell and plant fragments upper part shell fragments with some lithoclasts
18419-3 82 m	very low sand content in lower part, up to 50 % in upper part, $CaCO_3$ around 10 %; shell fragments and lithoclasts in lower part, shell fragments and foraminifers in upper part
18420-2 62 m	sand content around 50 % except lowest part (5 %), $CaCO_3$ around 10 %; mainly shell fragments, lowest part with benthic foraminifers and plant fragments
18422-3 84 m	decreasing sand content with depth, $CaCO_3$ generally low except uppermost sample

18423-2 97 m	two discontinuities in the upper part; sand content generally low except one outlier (26 %) in upper part
18424-2 90 m	low sand content, generally low variability
18425-2 95 m	decreasing sand content with depth, low variability; mainly plant fragments with increasing amounts of shell fragments upcore
18426-2 92 m	discontinuity around 100 cm; sand content low in lower part but high in upper part; lower part dominated by plant fragments, upper part bylithoclasts and glaucony → reworked

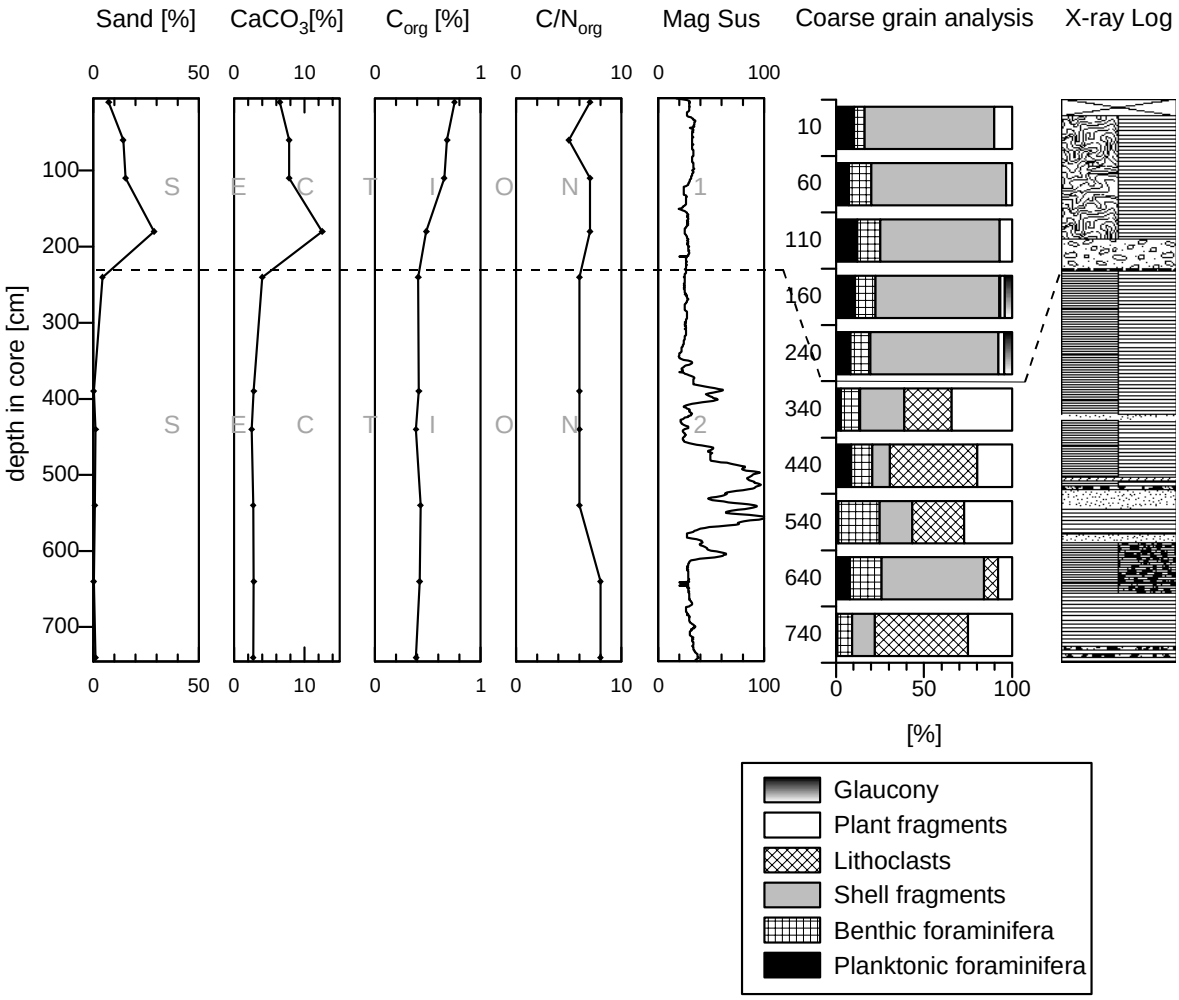

Fig. 6: *Example of basic sedimentological data obtained from each sediment core. Percentage of components referring to the 250 - 500 µm fraction, core 18408-3. For X-ray Log legend see* ***Fig. 4*** *or* ***Fig. 13***

The sediments from the Vietnamese Shelf are generally gray to olive clays with considerable amounts of silt and sand. In the area of the paleo-Mekong the sediments are more brownish due to the influence of the Mekong. Here, the sediments have partly very high sand contents, sometimes exceeding 90 %. Further offshore, sand content typically diminishes due to decreasing influence of the Mekong. The central part of the study area is characterized by high sand contents due to the proximity of the hinterland. Sediments from deeper cores (< 90 m) partly show high sand contents due to a high abundance of marine

microorganisms. In the northern part of the study area the sand content is generally low. Only the uppermost centimeters of the deposits show sand contents exceeding 10 %. This higher sand content is attributable to reworking processes which is confirmed by glaucony and anomalous ages of tests of *Rotalia sp*. and bivalve shells.

The carbonate content is primarily controlled by the amount of marine microorganisms or fragments thereof and shows highest values in the cores from deeper water depths (> 90 m) where the marine influence is highest compared to the other coring sites investigated in this study. Cores from shallower water depths, which are not in the direct influence of rivers show also partly high carbonate content.

In contrast to Hanebuth (2000) who found a broad variety of paleo-facies that were deposited during different stages of sea-level on the Sunda Shelf, the variability of paleo-facies on the Vietnamese Shelf is surprisingly low. One possible reason may be the selection of sampling locations which on the Sunda Shelf were mostly drowned paleo-valleys, but on the Vietnamese Shelf had to be local depressions, due to the rare abundance of paleo-valleys (cp. Wiesner et al. 1999). Another reason, especially on the narrow central part of the Vietnamese Shelf, may be the high gradient of the shelf, which left the old terrestrial surface exposed to intensive erosion in the course of sea-level rise. Previous investigations on sediments from the paleo-Mekong delta on the Vietnamese Shelf (Richter, 1998) revealed terrestrial facies which, however, were limited to a range of 900 AMS-^{14}C years between 11 ^{14}C kyr BP and 10 ^{14}C kyr BP within a core from 62 m of modern water depth. Similar results from core 18389-3 (12213, 12448 ^{14}C years BP, this study) support the assumption, that facies- and moreover, sea-level reconstructions with lacking paleo-facies or age variability in the paleo-Mekong area of the Vietnames Shelf are difficult.

3.2.1 Discontinuities

The discontinuities discovered in the X-ray radiographies are mostly to be interpreted as erosional hiatuses caused in the course of the deglacial sea-level rise. Where suitable material was found, the sediment core was dated above and below the discontinuity to determine a minimum and maximum age for the formation of the discontinuity. Only three discontinuities from those cores are possibly unconformities in the sense of the sequence stratigraphic concept, which are surfaces with evidence of subaerial exposure (van Wagoner et al., 1988), since they are the only deposits that bear remarkable amounts of terrestrial material where deposition in a nearshore environment was followed by deposition in a marine facies after the formation of the discontinuity. If compared with the actual sea-level curve for the SCS (Hanebuth et al. 2000) the dated materials (and therefore the discontinuities) from sediment stations 18376-2, 18389-3 and 18426-2 show matching ^{14}C ages.

All other discontinuities show a contact of marine facies on marine facies, making the discontinuities almost useless for paleo sea-level investigations.
The datings of the other discontinuities show a hiatus of several thousand years indicating that a significant time span of non deposition or erosion took place.

3.2.2 Sedimentation Rates

Sedimentation rates have been calculated on the basis of continuous core sections as linear sedimentation rates (LSR). With the sedimentological methods described above continuous, hiatus-free core sections were selected for AMS-^{14}C dating. The age of the core tops was considered to be of recent age so that a minimum sedimentation rate for all dated cores is calculable. The sedimentation rates for the Vietnamese Shelf vary widely for the different coring sites. They roughly range between 5 cm/kyr and 100 cm/kyr, but also extremely high sedimentation rates of 500 - 1000 cm/kyr are observed for short time intervals during the early Holocene. Evaluation and comparison of sedimentation rates on the Vietnamese Shelf will be more precisely be dealt with in chapter 4.

3.2.3 Mass Accumulation Rates

The determination of the mass accumulation rate (MAR) occurred on the basis of the following equation:

$$\text{MAR [g/cm}^2 \text{ x kyr}^1\text{]} = \text{linear sedimentation rate [cm/kyr]} \quad \text{x} \quad \text{dry bulk density [g/cm}^3\text{]}$$

The mass accumulation rates range from 6 to 1200 g/cm^{2}kyr which stands in contrast to average Holocene MARs for the western margin of the SCS published by Wang (1999) who quotes an average rate of 4.86 g/cm²kyr.
In chapter 6 MAR will be used to calculate sediment budgets for the detrital sediments on the Vietnamese Shelf in consideration of the provenance studies from chapter 5 and denudation in the source areas from the literature.

3.2.4 Clay Mineral Assemblage

The composition of clay minerals shows variations from north to south with illite as tho most abundant clay mineral in all samples. The northernmost sample from the Red River delta shows with 75 % the highest illite content compared to other samples with 40 to 50 % illite. One sample from a sediment station in front of the Annamite chain shows with 20 % higher smectite content than other cores which show 0 - 10 % smectite. Kaolinite and chlorite values are in the range of 20 - 30 %.

3.3 Geochemistry

3.3.1 Organic Carbon, Carbonate Content and C/N

The content of organic carbon of the investigated sediment varies between 0.06 and 2.08 %. C_{org} is highest in sediments which are directly influenced by terrestrial material, like core 18391-2 which lay in the direct influence of the Mekong during the early Holocene. Deposits from nearshore positions or in front of rivers show higher C_{org} values than those from further offshore. Generally the content of organic carbon lies between 0 an 0.5 %.

Contrarily, the carbonate content is highest in cores which are under a strong marine influence. Therefore the lowest carbonate content was measured in core 18376-2, which in parts shows no marine influence and the highest carbonate content in core 18404-3 from 169 m water depth with 36.6 %. The average $CaCO_3$ values vary around 5 %.

The C/N, as another indicator for terrigenous influenced sedimentation, shows values between 5 and 23, being highest in core 18414-3, which is with 21 m of water depth the shallowest and most proximal of the investigated cores. The general C/N of the other cores from the study area ranges around 8.

3.3.2 Major Elements, Trace Elements and Sr- and Nd-isotopes

Recent (surface) and early Holocene sediments have been analyzed to monitor provenance and change of sources and/or climate during the past 10 kyr.

Detrital sediments on the Vietnamese Shelf are delivered by rivers draining into the SCS. Having different source areas the composition of the sediments transported by the rivers reflects the composition of the source area. Mekong sediment, Red River sediment and sediment from the small mountainous rivers from central Vietnam have been presumed as possible endmembers. The analysis of the possible endmember sediments returned clearly distinguishable values. The shelf sediments yield results between the endmembers results. Sediment core 18391-2 off the Mekong River has been analyzed downcore and comprises the complete Holocene time interval, showing clear trends for source and/or climatic changes in the hinterland (Schimanski et al. 2001).

The sediment geochemistry and provenance and distribution of the sediments will be treated in chapter 5.

3.3.3 Oxygen Isotopes of Foraminiferal Shells

Two cores from the Central Shelf have been investigated for oxygen isotopic composition of foraminiferal shells. In core 18414-3 a trend towards lighter values upcore is observed. This trend lies in the range of 0.5 ‰ measured on both, *Nonion subturgitum* (CUSHMAN, 1924)

and *Elphidium advenum* (CUSHMAN, 1922) from 267 cm core depth, dated to 6005 ^{14}C years BP on a bivalve shell, to the top of the core.

Measurements on the same species from core 18416-2 dated to 9820 ^{14}C years BP in 491.5 cm core depth and 9195 ^{14}C years BP in 98 cm core depth show inconsistent oxygen isotopic data . Partly, single measurements from the same core depth reveal differences in $\delta^{18}O$ of 1.5 ‰.

3.4 Parasound shallow Seismics

More than 1000 miles of seismic profiling have been carried out during SONNE cruise 140 (Wiesner et al., 1999). The sediment cores presented here have also been selected with the help of the seismic profiles. Sediment cores bearing prominent subsurface reflectors that possibly represent discontinuities, ideally the Pleistocene land surface, were prefentially selected. Tab. 5 shortly describes the seismic survey at the coring sites. Only those reflectors are mentioned that have been penetrated with the coring device. Seismic records are presented in chapter 4.

Tab. 5: *Seismic profiles from the coring sites. Note that only those reflectors are mentioned that were penetrated by the coring device. For seismic records refer to chapter 4. mbsf = meters below sea floor*

Core No	Seismic facies characterization
18375-2	cored close to incised valley fill
18376-2	cored close to incised valley fill, penetrated several strong reflectors
18377-2	strong reflectors in incised valley, inhomogeneously layered
18389-3	unclear, stratification inhomogeneous
18391-2	prominent reflector at 3 to 4 mbsf
18393-3	sediment wedge at shelf edge with no correspondance to neighbouring cores except uppermost part
18396-3	prominent subsurface reflector at 2 to 3 mbsf uppermost part possibly corresponding to 18409-3
18397-2	proximal beginning of huge sediment wedge, weakening of reflectors at ca. 4 mbsf corresponding to upper part of 18398-3
18398-3	weakening of reflectors at ca. 5 mbsf corresponding to 18397-2, thickening of sediment wedge
18401-3	upper part possibly corresponding to uppermost part of 18398-3
18404-3	slight subsurface reflector
18405-3	unclear, stratification inhomogeneous
18408-3	prominent subsurface reflector at ca. 3 mbsf
18409-3	only weak subsurface reflectors, upper part corresponding to 18396-3
18414-3	no prominent reflectors
18415-2	upper meters corresponding to 18414-3; numerous prominent reflectors (slumps?) inside "sequence" below 2 to 3 meters wedging out seaward
18416-2	slight seaward dipping reflectors, lower part is not corresponding to 18415-2 or 18417-3
18417-3	upper two meters with weak reflection signal; stronger reflectors in ca. 2 mbsf dipping seaward

18419-3	no prominent subsurface reflectors
18420-2	no prominent subsurface reflectors, corresponding to 18419-3 with thickened "sequence"
18422-3	strong reflection of upper 10 meters
18423-2	prominent reflector at 1 to 2 mbsf in small depression, Pleistocene surface possibly penetrated
18424-2	prominent subsurface reflector at 4 to 5 mbsf in gentle paleo-valley
18425-2	paleo-valley incised ca. 40 m deep
18426-2	at least one prominent reflectors in upper 5 mbsf

Direct correspondence is recognizable at cores 18397-2 and 18398-3, 18396-3 and 18409-3, 18414-2 and 18415-3 as well as 18416-2 and 18417-3. Those cores are directly correlatable with each other, which was corroborated by AMS-^{14}C datings as well as by coarse grain analysis.

The prominent subsurface reflectors identified in the seismic record generally match with discontinuities revealed in the X-ray radiographies. This permits a straightforward correlation of subsurface reflectors over longer distances.

3.5 Depositional Environment and Facies Assignment

With rising sea-level the depositional environment changed and facies transitions occurred. The 25 sediment cores are composed of sediments which are attributable to five different facies types. To assign the facies sections into genetically coherent facies types, a facies classification in accordance with Hanebuth (2000), Hanebuth and Stattegger (2002) and Hanebuth et al. (submitted, cp. appendix) has been developed. The facies are described from distal to proximal to the coastline.

Open Shelf facies

This facies type was deposited under fully marine conditions. It is characterized by olive gray to dark greenish gray, sandy foraminiferal mud. The sand fraction, generally ranging between 15 and 50 % is dominated by shell fragments (bivalve shells, echinoderms, gastropods) and the sediment is completely bioturbated. The material shows a relatively high carbonate content with values up to 36 %. C_{org} content ranges around 0.5 %. At the base of this facies, a discontinuity separates the deposits from the underlying sediment. The upper part of core 18404-3 shows the typical characteristics of this facies type (Fig. 7).

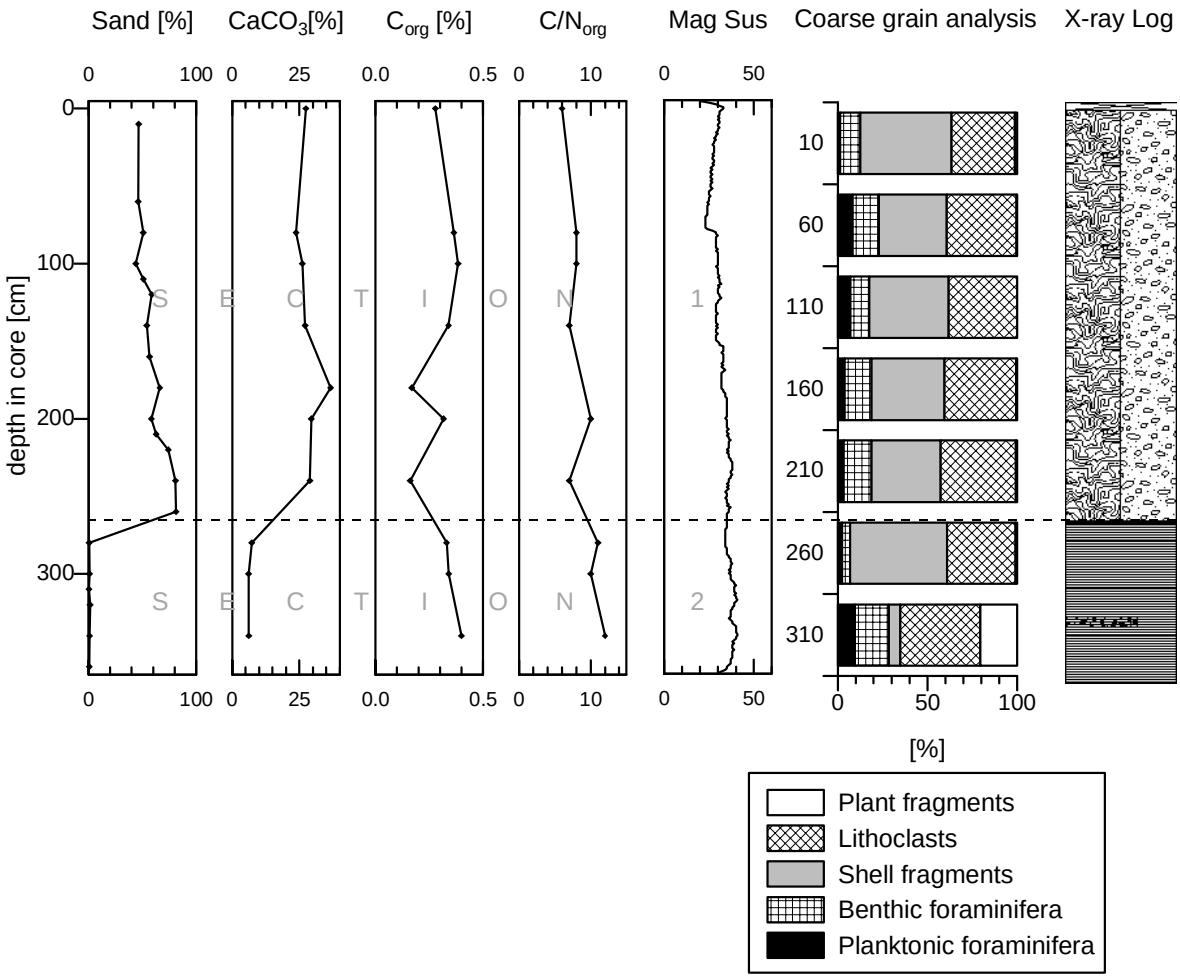

Fig. 7: *Open Shelf facies, basic sedimentological data of core 18404-3 (section 1)*

Inner Shelf facies

This facies differs from the *open shelf* facies by a more proximal position of deposition. It is typically made up of olive gray silty clay with shell fragments deposited under marine conditions. The sand content is generally lower than 10 % and is dominated by shell fragments (50 - 90 %). Terrigenous influence is mostly restricted to the silt and clay fraction, but plant fragments occur sporadically. The carbonate content does not exceed 5 %, except in surface samples and the C_{org} ranges between 0.2 and 1 %. The sediment is generally strongly bioturbated. Core 18409-3 (section 1) is representative for this kind of facies (Fig. 8).

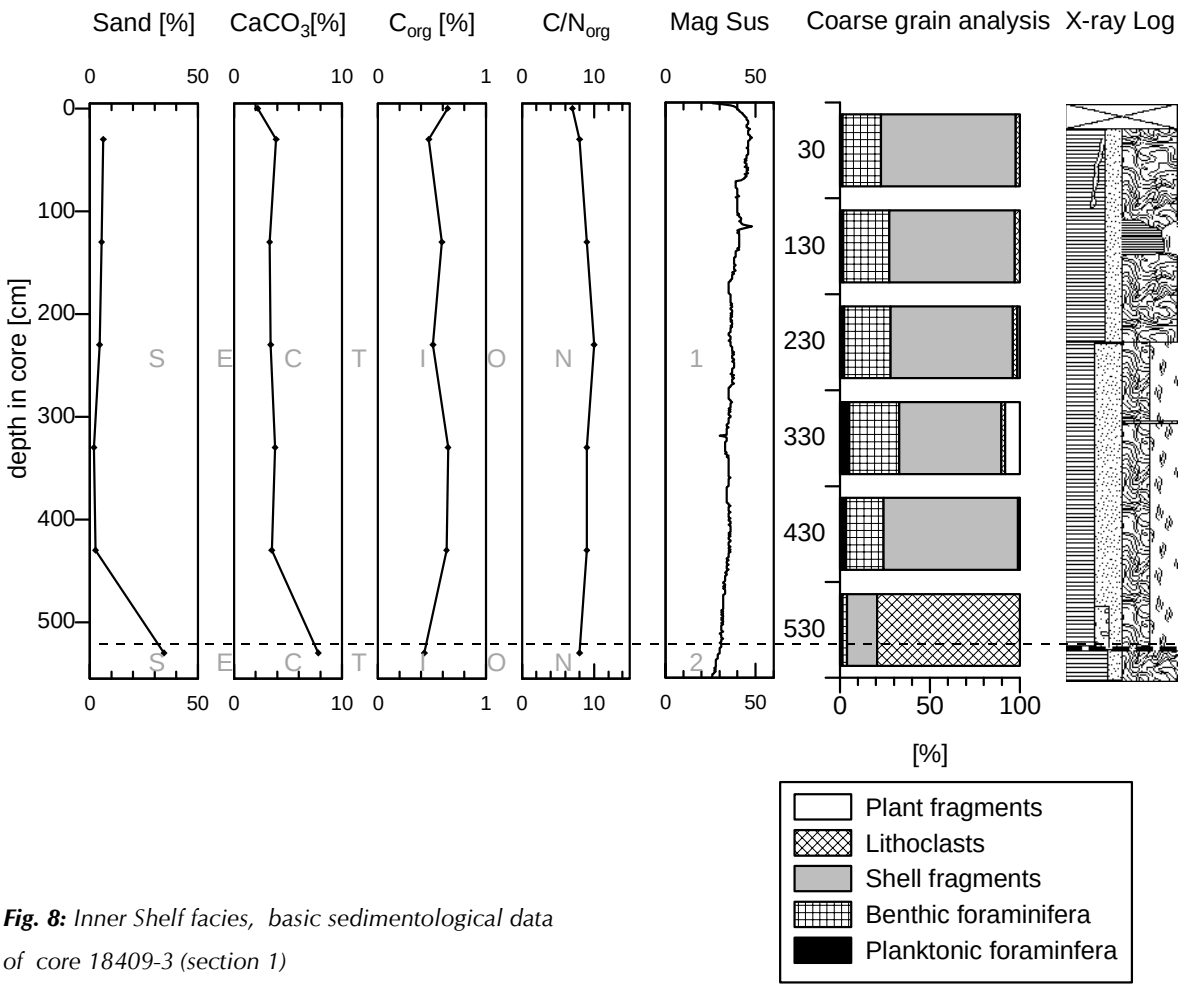

Fig. 8: *Inner Shelf facies, basic sedimentological data of core 18409-3 (section 1)*

Siliciclastic Inner Shelf facies

The *siliciclastic inner shelf* facies is characterized by a strong terrigenous influence indicated by extremely high amounts of lithoclast (50 - 90 %) in the sand fraction. The sand fraction accounts for ca. 50 % of the sediment for this facies type. The sandy clay with silty patches is olive gray in color. Carbonate content is generally lower than 4 %, while C_{org} ranges around 0.4 %. C/N ratios are partly higher than in other facies with values reaching 20, indicating terrigenous influence. The sediment is only slightly bioturbated which indicates relatively high sedimentation rates. The deposition of this facies type occurred under marine conditions with a high terrigenous influence due to the proximity of rivers. Core 18414-3 shows the typical characteristics of this facies type (Fig. 9).

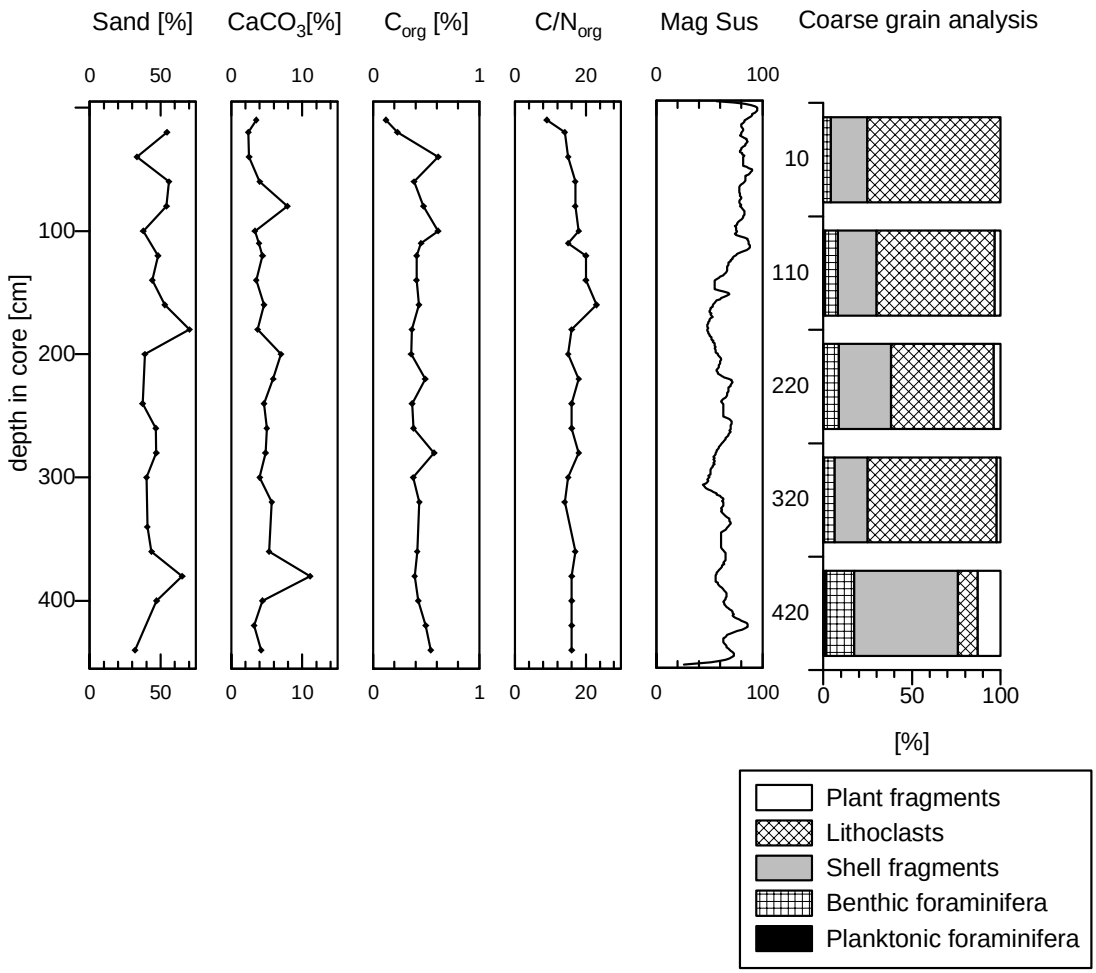

Fig. 9: *Siliciclastic Inner Shelf facies, basic sedimentological data of core 18414-3*

Delta Front and Mouth facies

Deposits accumulated in the *Delta Front and Mouth* facies are generally fine grained with ca. 5 % of sand and intercalations of sand occur frequently. The sand fraction is dominated by lithoclasts but also plant fragments are abundant. The sediment color is brownish gray to olive gray. The sediment is rarely bioturbated and lamination occurs frequently. Furthermore cross- and flaserbedding is common. An extremely low carbonate content of <1 %, C_{org} values around 0.5 % an C/N ratios $>$ 10 characterize this facies type. The depositional conditions were strongly influenced by the large river systems, indicated by a high amount of terrigenous material and depositional structures indicating cross bedding. Section 2 of core 18376-2 is made up of this facies type (Fig. 10).

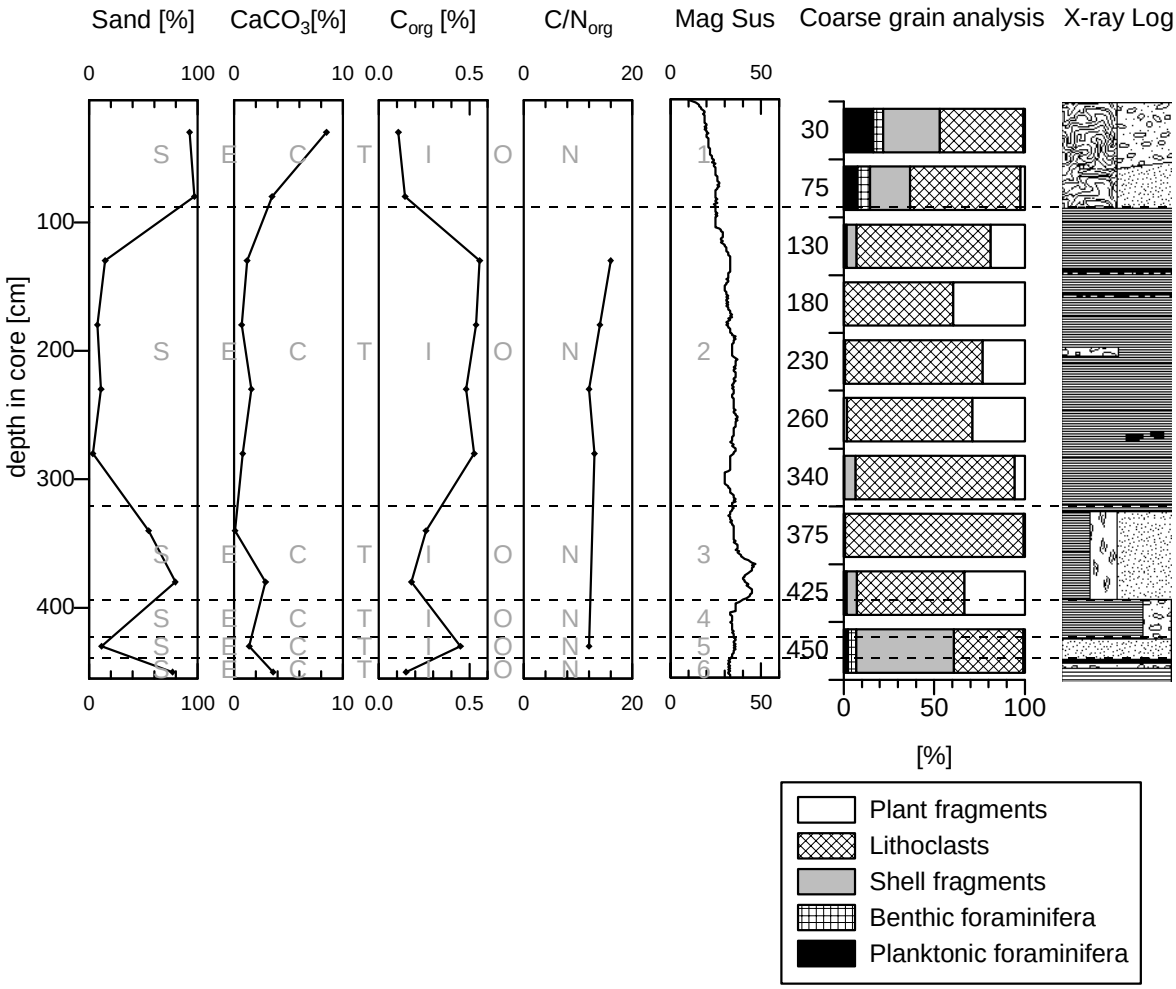

Fig. 10: *Delta Front and Mouth facies, basic sedimentological data of in core 18376-2 (section 2)*

Tidal Flat facies

This facies is free of bioturbation and shows fine laminations of alternating layers of sand and mud indicating rhythmic deposition in a tidally influenced environment. The sand content of this facies is highly variable, depending on sampling of a sand- or mud layer, and ranges between 4 and 89 %. The sand fraction is dominantly composed of lithoclasts. Plant fragments and sporadically shell fragments occur as well. The carbonate content is very low, showing values around 1 %. The C/N ratio is higher than in other facies exceeding values of 20, indicating nearshore terrigenous influence. Core 18377-2 contains the *Tidal Flat* facies (Fig. 11).

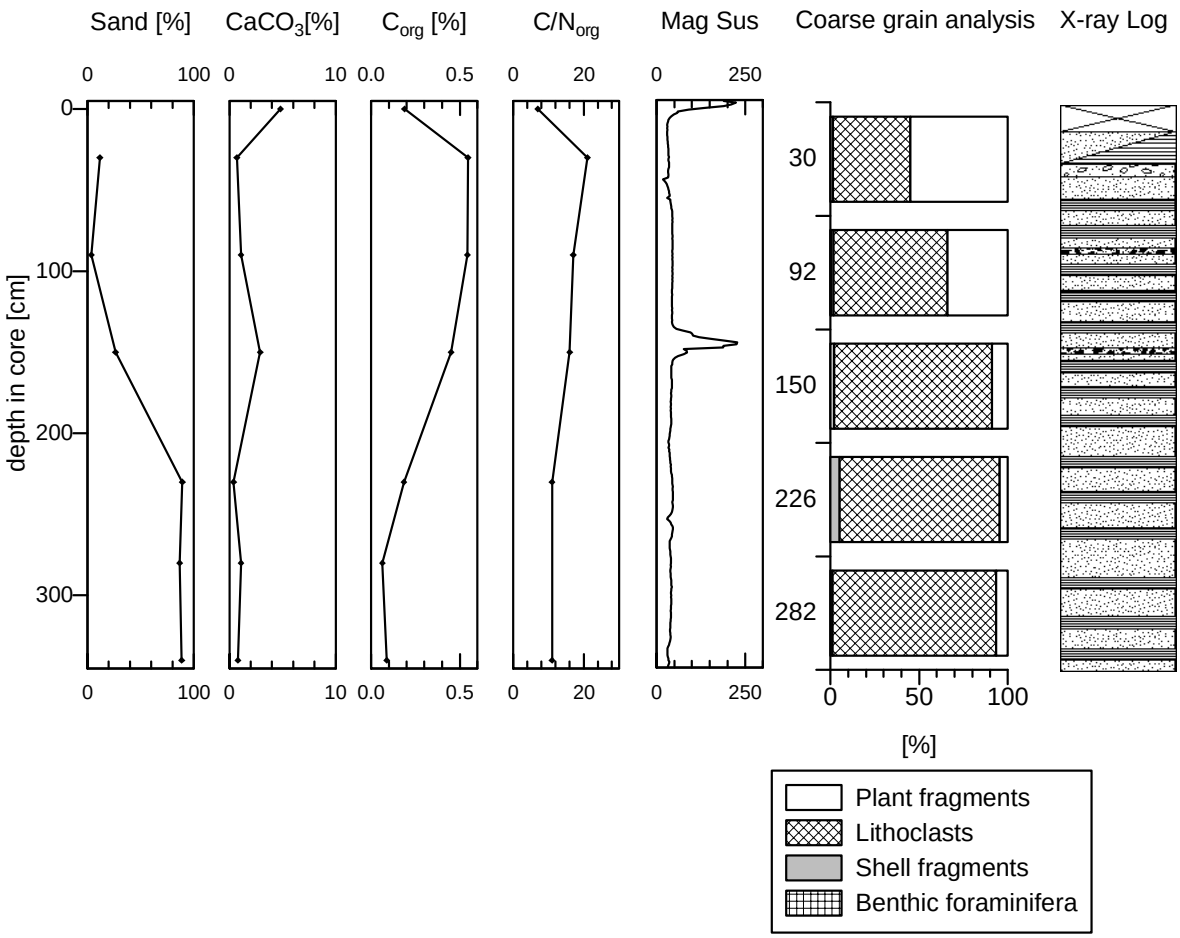

Fig. 11: *Tidal Flat facies, basic sedimentological data of core 18376-2*

4 Holocene and late Pleistocene Sediments on the Vietnamese Shelf: Distribution, Stratigraphy, and Relation to Sea-Level Changes

4.1 Introduction

The Vietnamese Shelf, the western margin of the South China Sea (SCS), with a total area of 700 000 km^2, was widely exposed during the last sea level lowstand (Fig. 12). The sea-level rise following the Last Glacial Maximum (LGM) of approximately 120 m (Fairbanks, 1989; Hanebuth et al., 2000) resulted in flooding of those exposed areas. Especially the northern (Gulf of Tonkin) and the southern part (Sunda Shelf) of the Vietnamese Shelf experienced flooding over large areas due to the wide extension and resulting low gradient of the shelf in this area. Here the shoreline migrated over hundreds of kilometers with rising sea level. In contrast, the shelf off central Vietnam is with partly only 20 km of width very narrow and shoreline migration was restricted to some tens of kilometers. Nevertheless the changing oceanographic conditions resulted in a reorganisation of the depositional system. The watermasses inundated morphological structures and a marine type of sedimentation set in. The equilibrium of deposition and erosion was disordered severely. Sediments were reworked on a large scale and in some parts the sea floor still is in disequilibrium indicated by relict sediments (Emery 1968). This paper targets the evolution of Holocene sedimentation on the Vietnamese Shelf and focuses on the distribution and stratigraphy of sediments based on AMS-^{14}C dating, seismic records, X-ray radiography and a number of sedimentological methods with special focus on the Holocene sea-level rise.

4.1.1 Sources of Detrital Sediment

The sources for detrital sediments on the Vietnamese Shelf are the rivers draining into the SCS along the Vietnamese Coast. In the south of the study area the Mekong forms an extensive delta. In the north, the Red River (Song Hong) forms as well a delta and drains sediment into the Gulf of Tonkin. Both rivers, with an average sediment discharge of 160 x 10^6 t/yr and 130 x 10^6 t/yr, respectively, range under the ten largest rivers of the world in terms of sediment discharge (Milliman and Meade, 1983). The Mekong and the Red River drain mountainous regions and have their sources in the eastern Himalaya and the Tibetan Plateau, respectively. Furthermore, hundreds of small mountainous rivers drain into the SCS along the central part of the Vietnamese coast between the two major rivers. Their total sediment discharge is not known, but the sediment yield of small mountainous rivers is generally underestimated (Milliman and Syvitski, 1992). Especially the small Vietnamese rivers, contributing their load to the central part of the Vietnamese Shelf, may yield large

amounts of sediment since the central part of Vietnam is characterized by a high rising hinterland with elevations up to 1000 m only some kilometers from the coast and a total elevevation of up to 2600 m.

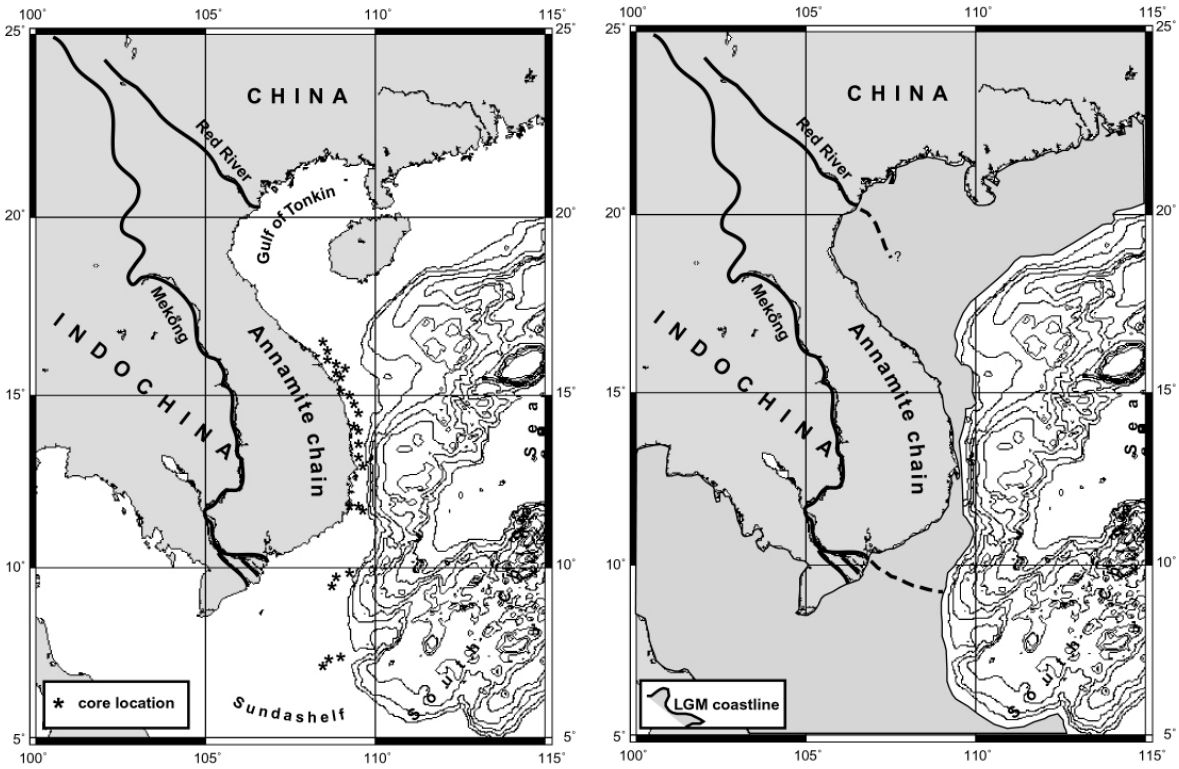

Fig. 12: *The Vietnamese Shelf today (with core locations) and at the time of the LGM*

4.2 Material and Methods

25 sediment cores from water depths between 21 and 169 mmwd (meters of modern water depth) which were taken on the Vietnamese Shelf during a research cruise with R\V SONNE in April 1999 have been investigated in this study (

Tab. **6**). The deposits are generally clays with considerable amounts of silt and sand. The study area lies in south-north elongation along the Vietnamese Coast from 7°N to 17°N (Fig. 12). In the South and in the North several incised valley fills were cored which were cut into the Pleistocene land surface and subsequently filled by the paleo-Mekong River and paleo-rivers in the North, respectively. The coring sites on the central part of the Vietnamese Shelf were restricted to seaward trending wedge-like sediment bodies and downlap structures.

Tab. 6: *List of sediment cores*

Core No.	Coring device	Latitude [°] N	Longitude [°] E	Water depth [m]	Recovery [cm]
18375 -2	VC	7:00.20	107:54.87	87	369
18376 -2	VC	7:05.27	108:06.42	89	47
18377 -2	VC	7:10.71	108:20.28	98	357
18389 -3	GC-3	9:16.45	108:39.09	109	276
18391 -2	GC-6	9:33.91	108:49.60	115	478
18393 -3	GC-6	9:45.61	109:07.95	155	540
18396 -3	GC-6	15:25.51	108:53.27	61	499
18397 -2	GC-6	12:14.71	109:19.91	45	532
18398 -3	GC-18	12:14.23	109:22.81	59	719
18401 -3	GC-12	12:12.90	109:32.09	134	707
18404 -3	GC-6	13:30.13	109:33.67	169	385
18405 -3	GC-6	13:41.10	109:27.02	130	547
18408 -3	GC-12	14:14.34	109:19.05	108	754
18409 -3	GC-12	15:41.21	108:40.79	40	577
18414 -3	GC-6	15:05.83	108:57.78	21	448
18415 -2	GC-6	15:04.98	109:00.03	38	559
18416 -2	GC-6	15:02.23	109:08.97	66	506
18417 -3	GC-12	14:44.81	109:17.61	97	798
18419 -3	GC-12	14:32.23	109:14.09	82	641
18420 -2	GC-6	14:34.13	109:11.36	62	557
18422 -3	GC-6	15:44.92	108:53.46	84	568
18423 -2	GC-6	16:16.62	108:39.59	97	548
18424 -2	GC-6	16:28.61	108:26.15	90	575
18425 -2	GC-6	16:34.53	108:28.31	95	556
18426 -2	GC-6	16:44.42	108:27.80	92	513

4.2.1 Sedimentological Characterization of Deposits

The sediments from the study area have been investigated with several methods previously described like granulometry, geochemistry, coarse grain analysis and X-ray radiography. The combination of those proxies provides an overview over recent conditions and allows to draw conclusions on the paleo-environment. A sudden change of the results of the investigated proxies can mostly be attributed to a change in facies (Hanebuth, 2000; Hanebuth et al., submitted)

4.2.2 Seismic Survey

The sea floor of the Vietnamese Shelf was surveyed using the shipboard Parasound system to characterize sea-floor morphology and geometry of subsurface seismic reflectors as well as to ensure coring at suitable locations. The Parasound system with its narrow beam characteristics generates a well resolved record of the subsurface reflectors with a penetration of the sea floor up to 150 m, depending on bottom characteristics (Spieß, 1993).

4.2.3 AMS-^{14}C Dating

Precise AMS-radiocarbon dating provides the basis for the stratigraphic framework. AMS-^{14}C ages were determined with a 3 MV Tandentron 4130 AMS system at the Leibniz-Laboratory for Radiometric Dating and Isotope Research to a precision of 0.3 % (counting and machine statistics) for modern samples (Nadeau, 1997; Nadeau, 1998). The ^{14}C-ages have been calibrated to calendar years BP using the latest version of the calibration program CALIB 4.3 (Stuiver and Reimer, 1993; Stuiver et al., 1998). All ages measured on marine carbonate samples were corrected for a reservoir effect of 400 years.

4.2.4 X-ray Radiographies

Internal sedimentary structures, sometimes not visible on the first glance, are detectable by X-ray radiography. The catastrophic effect of the deglacial sea-level rise on the depositional environment resulted in discontinuities in the sedimentary record, which can be identified with the help of X-ray radiographies. Also small scale variations like bioturbation, lamination and cross-bedding are recorded in the sediment and are visible in the X-ray radiographies.

4.3 Results and Interpretation

4.3.1 AMS-^{14}C Framework

The stratigraphy is based on 45 AMS-^{14}C dates (Tab. 7). Carbonate shells of marine organisms in *in situ* position were preferentially used to obtain reliable dates. Intact sea urchins, bivalve shells with both shells still connected via the ligament, gastropods and fragile but intact pteropod shells were used to exclude former reworking of the dated sample material. Hanebuth (2000) showed that macro-wood fragments return reliable ages as well. Wood samples were dated in two cases. When the above mentioned material was not available, benthic foraminifera (*Rotalia sp.*), shell fragments and in one case bulk sediment were dated.

4.3.2 X-ray Radiographies and Core Descriptions

The investigated sediments were directly influenced by sea-level rise and most cores contain discontinuities caused by flooding of the shelf and subsequent erosion (Fig. 13). These discontinuities represent hiatuses sometimes comprising several thousand years. The sediment was dated shortly below and above the discontinuity with sufficient distance to the discontinuity to prevent dating of material possibly bioturbated across the boundary. Core 18393-2 from the southern part of the study area and cores 18423-2 and 18426-2 from the north show hiatuses of more than 10 kyr. In contrast, hiatuses in cores from the central part are of shorter duration with a maximum of 3 kyr in core 18409-3.

Tab. 7: *AMS-^{14}C ages and sedimentation rates*

	Lab code	Core No	Water depth [m]	Sample depth [cm]	Sample material	mg C	^{14}C age [years BP]	Deviation +	Deviation -	δ^{13}C [‰]	Deviation +-	Sedimentation rate [cm/kyr]
Paleo Mekong	KIA16060	**18376-2**	89	40	bivalve shell (*Arca sp.?*)	2.1	**8610**	45	45	0.42	0.08	4.6
	KIA16061	**18376-2**	89	472	crustacean arm	0.7	**27140**	210	200	-4.11	0.25	
	KIA9870	**18389-4**	109	99	wood, insoluble	4.7	**12215**	50	50	-27.98	0.12	8.1
		18389-4	109	99	wood, humic acids	1.1	**12160**	70	70	-28.01	0.07	
	KIA9871	**18389-4**	109	186	wood, insoluble	5.1	**12450**	70	70	-27.47	0.06	386
	KIA16052	**18391-2**	115	207	selected shell fragments	1.5	**4960**	35	35	0.61	0.06	41.7
	KIA16053	**18391-2**	115	255	gastropod fragment	2.0	**4875**	35	35	0.41	0.22	
	KIA14656	**18391-2**	115	295	pteropods	1.3	**6580**	45	45	-0.37	0.14	23.4
	KIA12328	**18391-2**	115	332	sea urchin (sand dollar)	1.6	**7955**	40	40	0.27	0.14	26.9
	KIA14159	**18391-2**	115	360	*Rotalia sp.*	1.4	**10040**	60	60	0.03	0.23	13.4 (hiatus?)
	KIA16054	**18393-3**	156	25 - 32	bivalve shell (*Arca sp.*)	0.8	**665**	25	25	-0.56	0.17	42.8
	KIA16055	**18393-3**	156	102 - 107	bivalve shell (*Paphia sp.*)	1.3	**1225**	25	25	-1.22	0.14	135.7
	KIA16056	**18393-3**	156	207	selected shell fragments	0.4	**12160**	60	60	-4.11	0.12	hiatus+reworked
		18393-3	156	207	selected shell fragments	1.1	**24330**	170	170	1.43	0.05	hiatus+reworked
Central Shelf	KIA14161	**18396-3**	61	250	*Rotalia sp.*	2.0	**>49220**			0.31	0.09	5 (reworked)
	KIA16058	**18397-2**	45	413	small gastropod	2.0	**3910**	35	35	0.18	0.09	105.6
	KIA13285	**18397-2**	45	488	gastropod	0.8	**4800**	35	35	-2.74	0.25	84.2 (hiatus)
	KIA14162	**18401-3**	134	226	gastropod	0.9	**2590**	40	40	0.69	0.16	87.3
	KIA12326	**18401-3**	134	590	*Rotalia sp.*	1.1	**9910**	50	50	-0.68	0.35	49.7
	KIA15645	**18404-3**	169	49-57	pteropods	1.3	**5705**	35	35	5.86	0.31	9.2
	KIA14160	**18404-3**	169	60	*Rotalia sp.*	0.8	**29100**	390	370	-1.09	0.14	reworked
	KIA12329	**18404-3**	169	225	gastropod	1.3	**8015**	50	50	4.27	0.09	74.4
	KIA16057	**18408-3**	108	152	pteropods	1.6	**1605**	30	30	-0.38	0.05	94.7
	KIA12331	**18408-3**	108	265	bulk sediment, lauge	1.0	**16110**	120	120	-23.03	0.11	
		18408-3	108	265	bulk sediment, humic acid	0.2	**12580**	310	290	-23.80	0.42	1.02 (hiatus)
	KIA16062	**18409-3**	40	90 - 93	selected shell fragments	1.0	**735**	30	30	-0.54	0.16	124.5
	KIA14655	**18409-3**	40	525	sea urchin (sand dollar)	1.5	**5930**	35	35	0.99	0.13	83.4
	KIA13286	**18409-3**	40	559	sea urchin	1.4	**8775**	50	50	0.11	0.27	11.9 (hiatus)
	KIA10594	**18414-3**	21	267	bivalve shell *(Glycimeris sp./Cardium sp.)*	1.0	**6005**	35	35	-0.02	0.05	44.5
	KIA16059	**18415-2**	38	106 - 109	gastropod (*Phasianella solida*)	2.2	**3020**	30	30	-0.36	0.09	35.6
	KIA13146	**18415-2**	38	250	pteropods	1.3	**7735**	40	40	-3.21	0.30	30.2
	KIA16066	**18415-2**	38	526	fresh carbonate fragments	1.4	**7970**	50	45	0.39	0.13	1175
	KIA16067	**18415-2**	38	526	wood	3.5	**7760**	45	45	-29.28	0.06	
	KIA9198	**18416-2**	66	97-99	bivalve shell (*Paphia sp.*)	1.4	**9195**	45	45	-2.1	0.13	10.6 (erosion)
	KIA9199	**18416-2**	66	491-492	bivalve shell (*Paphia sp.*)	1.2	**9820**	50	50	0.16	0.13	542.7
	KIA15642	**18417-3**	97	9-17	gastropod (*Cymatium sp.*)	0.8	**4700**	45	45	0.48	0.26	2.7 (erosion)
	KIA13147	**18417-3**	97	450	*Rotalia sp.*	1.4	**11810**	60	60	-2.66	0.32	61.4
	KIA14158	**18419-3**	82	130	*Rotalia sp.*	1.3	**5740**	60	60	1.83	0.09	22.6
	KIA16063	**18419-3**	82	525	sea urchin fragment	0.74	**9610**	60	60	-2.33	0.21	102.0
	KIA15644	**18420-2**	62	40-43	pteropods	0.9	**900**	25	25	-0.73	0.18	46.1
	KIA16064	**18420-2**	62	511	sea urchin fragments	1.5	**8265**	50	50	0.87	0.13	63.7
southern Gulf of Tonkin	KIA12330	**18422-3**	84	51	gastropod	1.2	**5020**	30	30	0.78	0.08	10.1
	KIA16065	**18423-2**	97	2	selected shell fragments with periostracum	1.6	**2445**	30	30	0.75	0.05	0.82
	KIA10595	**18423-2**	97	46.5	sea urchin	1.3	**13030**	60	60	-1.75	0.20	4.2 (hiatus)
	KIA15641	**18425-2**	95	29	bivalve shell (*Barbatia amygdalumtostum)*	0.8	**12575**	60	60	-0.38	0.12	2.3 (hiatus?)
	KIA15643	**18426-2**	92	55	bivalve shell (*Isognomon sp.)*	1.4	**30130**	320	300	3.47	0.04	1.8 (reworked)
	KIA12327	**18426-2**	92	133	*Rotalia sp.*	1.3	**43210**	2630	1980	-0.21	0.17	5.9 (reworked)

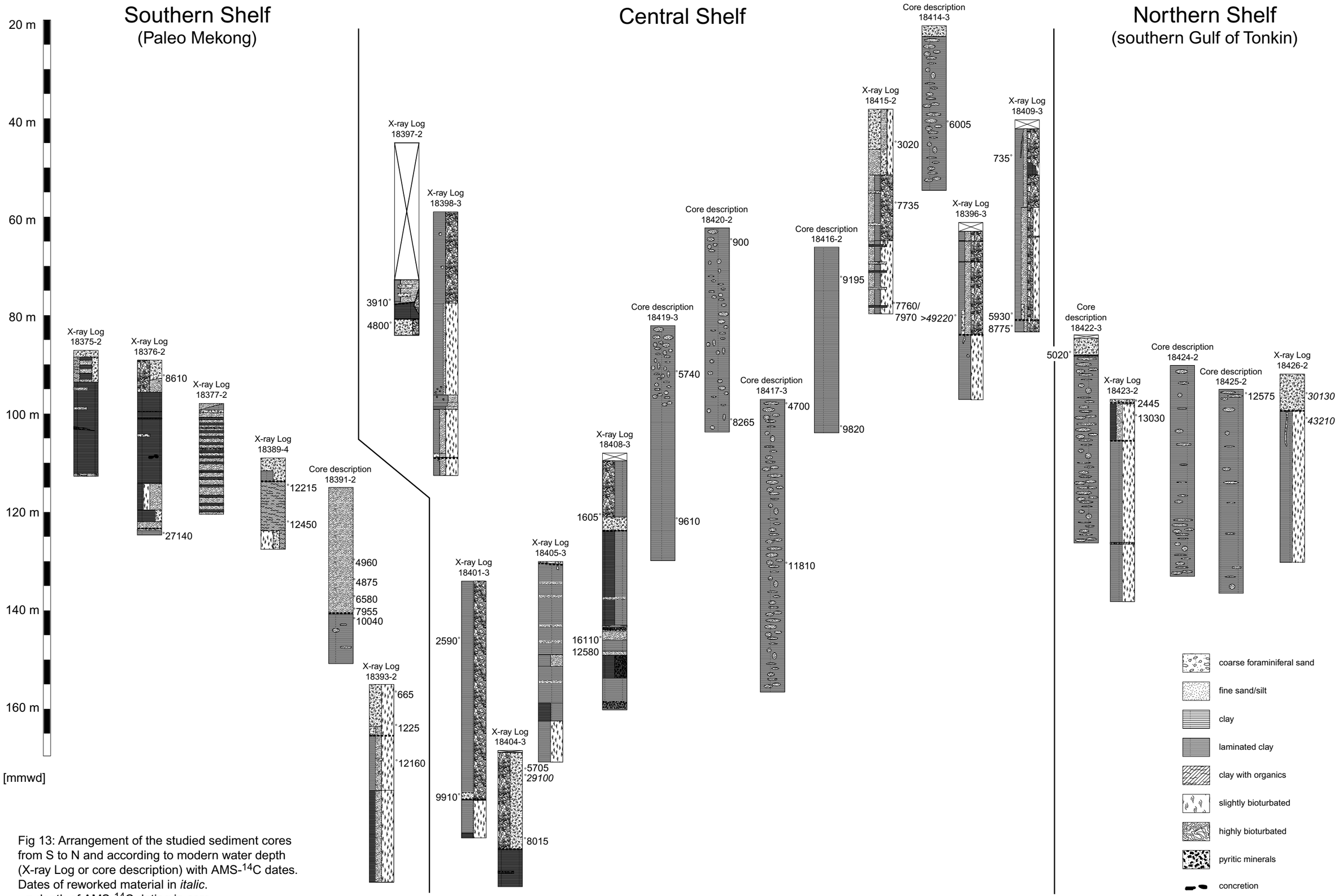

Fig 13: Arrangement of the studied sediment cores from S to N and according to modern water depth (X-ray Log or core description) with AMS-^{14}C dates. Dates of reworked material in *italic*.
◦ = depth of AMS-^{14}C dating in core.
Core length seven times exaggerated

4.3.3 South-North trending Sedimentological Features on the Vietnamese Shelf

The deposits identified in the sediment cores can be generally assigned to three different regions which show typical sedimentological characteristics. In the southern part of the study area a *Southern Shelf* area (Paleo-Mekong) was identified, further north a *Central Shelf* area can be recognized and in the north a *Northern Shelf* area (southern Gulf of Tonkin) can be distinguished. For analytical results (sand-, carbonate-, organic carbon content and coarse grain analysis) of the cores refer to appendix.

4.3.3.1 Southern Shelf, Paleo-Mekong

Sediment cores 18375-2, 18376-2, 18377-2, 18389-2, 18391-2 and 18393-2 belong to the *Southern Shelf* area (Fig. 12, Fig. 13).

With exception of core 18391-2 they all show only a thin Holocene sediment cover with usually high sand and carbonate contents in the upper part of the cores. The carbonate content of the Holocene sand blanket generally increases with water depth as a result of stronger marine influence and thus higher amounts of marine microorganisms. In contrast, C_{org} content is higher in the shallower cores, reflecting terrigenous input from the Mekong River. The composition of the 250 - 500 μm-fraction of the sand cover is dominated by lithoclasts, shell fragments and benthic and planktonic foraminifera.

Core 18376-2 is presented exemplarily in detail (Fig. 14). It is the only core containing more than three different sections. The uppermost core section (*section 1*) represents the thin sand cover of Holocene age. In this core it was dated to 8610 ^{14}C years BP. Downcore (*section 2*) the sediment consists mainly of laminated clay. $CaCO_3$ is lower and C_{org} higher than in the sandy upper part. The coarse grain analyses reveal lithoclasts and plant fragments as dominating components for the investigated fraction. *Section 3* shows again high sand content with slight bioturbation, slightly higher $CaCO_3$ and lower C_{org} compared to section 2 and furthermore exclusively lithoclasts as components of the coarse grain analysis. *Section 4* shows the similar results as *section 2* with a slightly higher sand content. In *section 5* sand content is high and the coarse grain analysis dominated by shell fragments and lithoclasts, whereas $CaCO_3$ is slightly higher and C_{org} lower than in the above section. Further downcore *section 5* and 6 are separated by a discontinuity below which section 6 shows lower sand content and has been dated by AMS radiocarbon dating to 27140 ^{14}C years BP.

The seismic record shows that the coring site lies in a broad incised valley probably originating from the ancient drainage system of the Mekong River. The geometry of the sequences is unclear due to a poor seismic signal, but shows numerous prominent subsurface

reflectors (Fig. 15) which probably match with the boundaries of the core sections (cp. Wiesner et al. 1999).

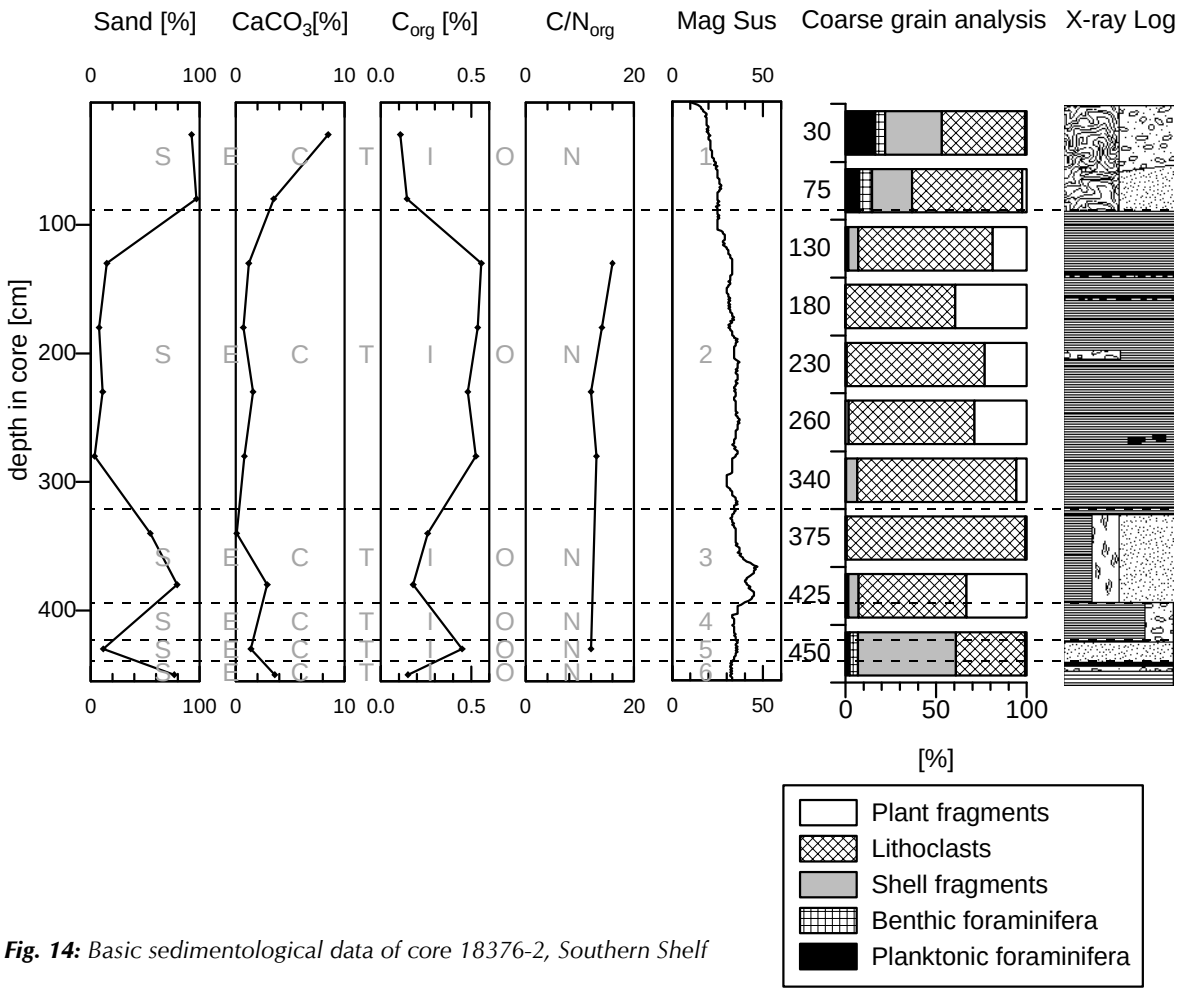

Fig. 14: *Basic sedimentological data of core 18376-2, Southern Shelf*

Incised valley systems (Fig. 15) favour the deposition and preservation of facies successions deposited in the course of rising sea level. Hanebuth and Stattegger (2002) studied incised valley fills on the Sunda Shelf and discovered numerous facies types deposited in relation to the last transgression. They found that facies successions of incised valley fills are extremely heterogeneous. With huge (paleo)-river systems, like the paleo-North Sunda River and the paleo-Mekong, as sediment feeders, short, event-like periods of high sedimentation stand in contrast to continuous sedimentation due to high sediment input and lateral shifting of distributaries as well as seasonal pulses of sediment discharge. These deposits are intermitted by long lasting periods of non-deposition and erosion. Richter (1999) found similar conditions in a sediment core from the paleo-Mekong delta from 56 mmwd.

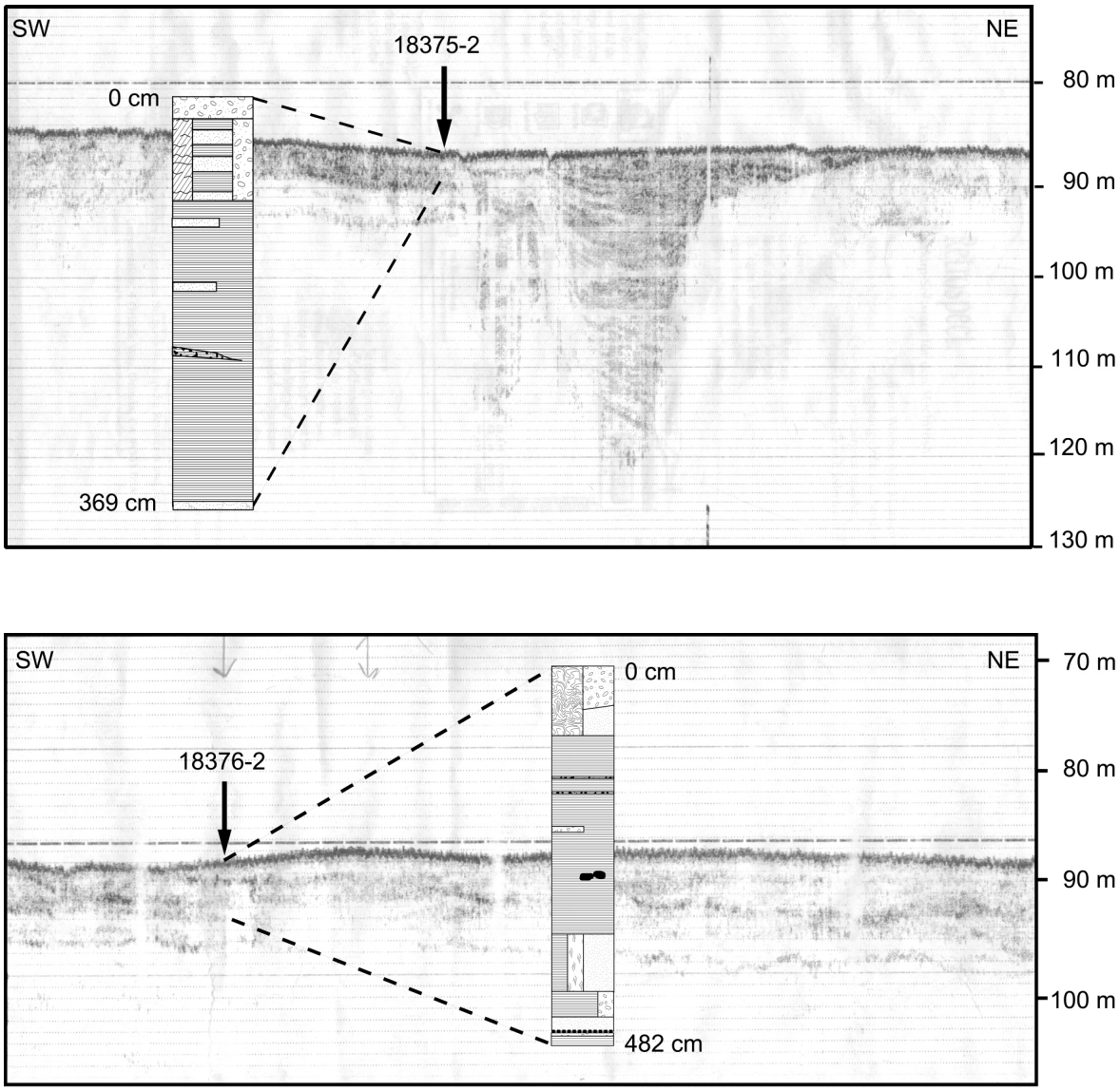

Fig. 15: *Shallow seismic* Parasound *records showing incised valley structures of stations 18375-2 and 18376-2. Profile length ca. 6.0 and 4.9 km, respectively*

Other cores from the *Paleo-Mekong* area also contain the thin sand cover of Holocene age as topmost section. An exception makes core 18377-2 of which the top 15 cm were lost during coring. The lower section of **core 18375-2** consists of laminated clay with neglible amounts of sand and $CaCO_3$ and slightly higher C_{org} than in the upper part. The 250 - 500 μm fraction is dominated by plant fragments and lithoclasts. This section probably correlates with *section 2* of core 18376-2. Station 18375-2 lies as well in an incised valley system (Fig. 15). Here, fewer "facies" were penetrated than at station 18376-2.

Core 18377-2 is mainly composed of lithoclasts and plant fragments. The cored section probably correlates to section 2 of core 18376-2, although sand intercalations are present

throughout the core, which resulted in extremely varying sand and carbonate contents. It was as well cored in a valley fill.

The deposits underlying the Holocene sediment cover in **core 18389-3** have as well been accumulated in an event-like style. The clayey sediment contains high amounts of organic material and the coarse grain analyses reveal plant fragments as dominating component with small amounts of lithoclasts and foraminifera. The core has been dated on wood fragments to 12215 ± 50 and 12450 ± 70 ^{14}C years BP, respectively. Here, the wood sample was fractionated into humic acids and acid-alkaline residuals. Due to their immobility, acid-alkaline residuals provide more reliable ages than the mobile humic acids which was also shown by Hanebuth (2000), although in the case presented here, the bias in age of 55 ^{14}C years (Tab. 7) between alkaline residuals and humic acids is neglectable and certifies the autochthonous character of the sediment.

Like for the previously presented cores from the *Southern Shelf* area the seismic record shows incised valley fills.

Cores 18391-2 and 18393-3 were cored in an area where the seismic records show horizontal stratification for the upper 10 - 20 m and yield a thicker layer of Holocene sediment. Sediment **core 18391-2** was cored in the proximal part of a seaward thickening sediment "wedge" (Fig. 16) that seems to be of post-glacial age. Five AMS-^{14}C dates have been carried out for this core of which four returned ^{14}C-ages of 4960, 4875, 6580 and 7955 years BP, respectively, for the Holocene cover and 10040 ^{14}C years BP for the underlying deposits. Inversion of the upper two dates has to be attributed to dating of *selected shell fragments* for the uppermost sample, which probably contains reworked material. In the landward direction of station 18391-2 a prominent morphological structure, probably the basement is cropping out. It eventually sheltered the wedge-like sedimentary structure from erosion and made a preservation possible.

Below the distal part of the sediment wedge downlapping structures are present. They were probably formed in the paleo-delta of the Mekong River which is supported by the low grade of bioturbation, high sand content and low carbonate content of the sediments of the lower part of **core 18393-3** from 156 mmwd which reached and penetrated the downlapping surfaces. Here the coarse grain analyses of the 250 -500 μm fraction are less representative since the biggest part of the sediment belongs to the 63 - 125 μm fraction which consists mainly of siliciclastics. The Holocene cover sediments were dated to 1225 and 665 ^{14}C years BP and the downlapping structures to 12160 ^{14}C years BP.

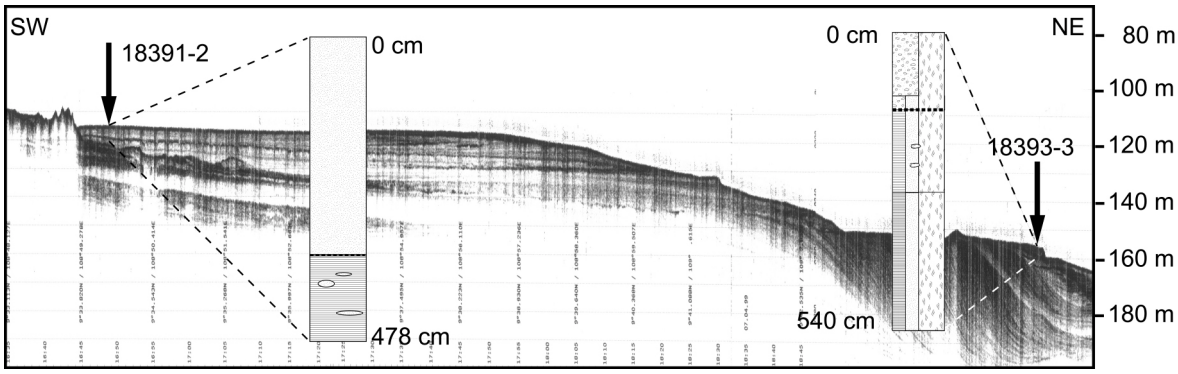

Fig. 16: *Shallow seismic profiles at station 18391 (a) and 18393 (b). Profile length ca. 46 km*

Resumée and Interpretation for the *Southern Shelf* area

The shallow-seismic records of *Southern Shelf* cores 18375-2, 18376-2, 18377-2 and 18389-3 show incised valley structures or the edge of an incised valley, respectively. Incised valleys structures have been studied intensively by Hanebuth and Stattegger (2002) on the central part of the Sunda Shelf. They found similar sedimentation patterns with only thin Holocene mud blankets covering transgressive deposits and interpret those as starved of terrigenous material which is exposed to reworking processes. Niino and Emery (1961) and Emery (1968) found similar conditions on the Vietnamese Shelf and characterized the deposits as *relict sediments*. Here equilibrium between deposition and erosion following the deglacial sea-level rise could not be established yet. Additionally turbulent conditions, reflected by the high sand content are probably responsible for intermittent non-deposition or erosion of Holocene material. An exception is observable for core 18391-2 which shows 340 cm of Holocene sediment, probably due to its sheltered position. Sedimentation rates for the Holocene cover sediments are generally in the range of 5 to 10 cm/kyr but are exceeded by far of those derived from core 18391-2 and 18393-3 which are in the range of 25 to 40 cm/kyr with peak sedimentation rates of 135 cm/kyr from core 18393-3.

The sediments underlying the Holocene cover of core 18375-2, 18376-2 and 18377-2 were deposited in the direct influence of the Mekong River, i.e., in the former Mekong Delta. The sediments of the cores 18375-2 and 18376-2 correspond to the *Delta Front* to *Delta Mouth* facies, while core 18377-2 was probably deposited in *Tidal Flat* facies. (For facies classification refer to chapter 3.5). Hanebuth and Stattegger (2002) found similar deposits in cores from the drowned delta of the North Sunda River which were accumulated in corresponding depositional environments.

Deposits preceeding the Holocene cover sediments in core 18389-3 were probably accumulated in a tidally influenced *Delta Front* environment. Lamination and flaser bedding

of mud and plant fragments as well as lenticular structures together with low bioturbation correspond to the *Delta Front* facies of Hanebuth and Stattegger (2002).
The sedimentation rate determined for this section nearly reaches 400 cm/kyr but is restricted to a very short time interval.

4.3.3.2 Central Shelf

The narrow *Central Shelf* area is represented by sediment cores 18397-2, 18398-3, 18401-3, 18404-3, 18405-3, 18408-3, 18419-3, 18420-2, 18417-3, 18416-2, 18415-2, 18414-3, 18396-3 and 18409-3 from south to north (Fig. 12, Fig. 13). All cores contain the Holocene cover, dated by AMS-^{14}C, as topmost layer. Some of the cores are completely composed of Holocene sediment. In contrast to the *Southern Shelf* area, the Holocene cover sediments of the narrow *Central Shelf* area can generally be divided into three types of sediments:

Type (1) represents sediments with a very high sand content, low carbonate content and a dominance of lithoclasts in the coarse grain fraction (**18396-3, 18414-3, 18415-2, 18417-3** (upper part)). Type 1 Holocene cover sediments were found in cores from shallow water depths (21 m - 61 m) and in the discharge area of small rivers (97 m of water depth at station 18417). Fig. 17a shows the results of core 18414-3 as a representative example for this kind of deposits.

Type (2) comprises sediments with a low sand content, low carbonate content and shell fragments as major constituents of the coarse grain fraction (**18397-2, 18398-3, 18405-3, 18409-3, 18416-2, 18417-3** (lower part), **18419-3** (lower part)). Type 2 Holocene cover deposits were identified in cores from shallow to intermediate water depths (40 m - 97 m). They are closely related to type 1 sediments whereas their position is less proximal to small rivers. Core 18409-3 contains typical deposits of this kind and is displayed in Fig. 17b.

Type (3) is described by sediment with high sand content, high carbonate content and shell fragments and foraminifera prevailing in the coarse grain analyses (**18401-3, 18404-3, 18408-3, 18419-3** (upper part), **18420-2**). This sediment was preferentially found in cores from greater water depth (62 m - 169 m) where the influence of rivers is low. These kind of deposits are described by the results of core 18408-3 in Fig. 17c.

Cores 18397-2, 18409-3, 18414-3, 18415-2, 18416-2, 18419-3 and 18420-2 are completely made up of Holocene deposits of the various types. The other cores of the *Central Shelf* area contain clayey sediments with low sand content and a generally lower carbonate content below the Holocene cover (Fig. 17c, section 2). Lithoclasts and plant fragments become a prominent part of the coarse grain fraction with increasing core depth. This is also the case in cores which are entirely of Holocene age.

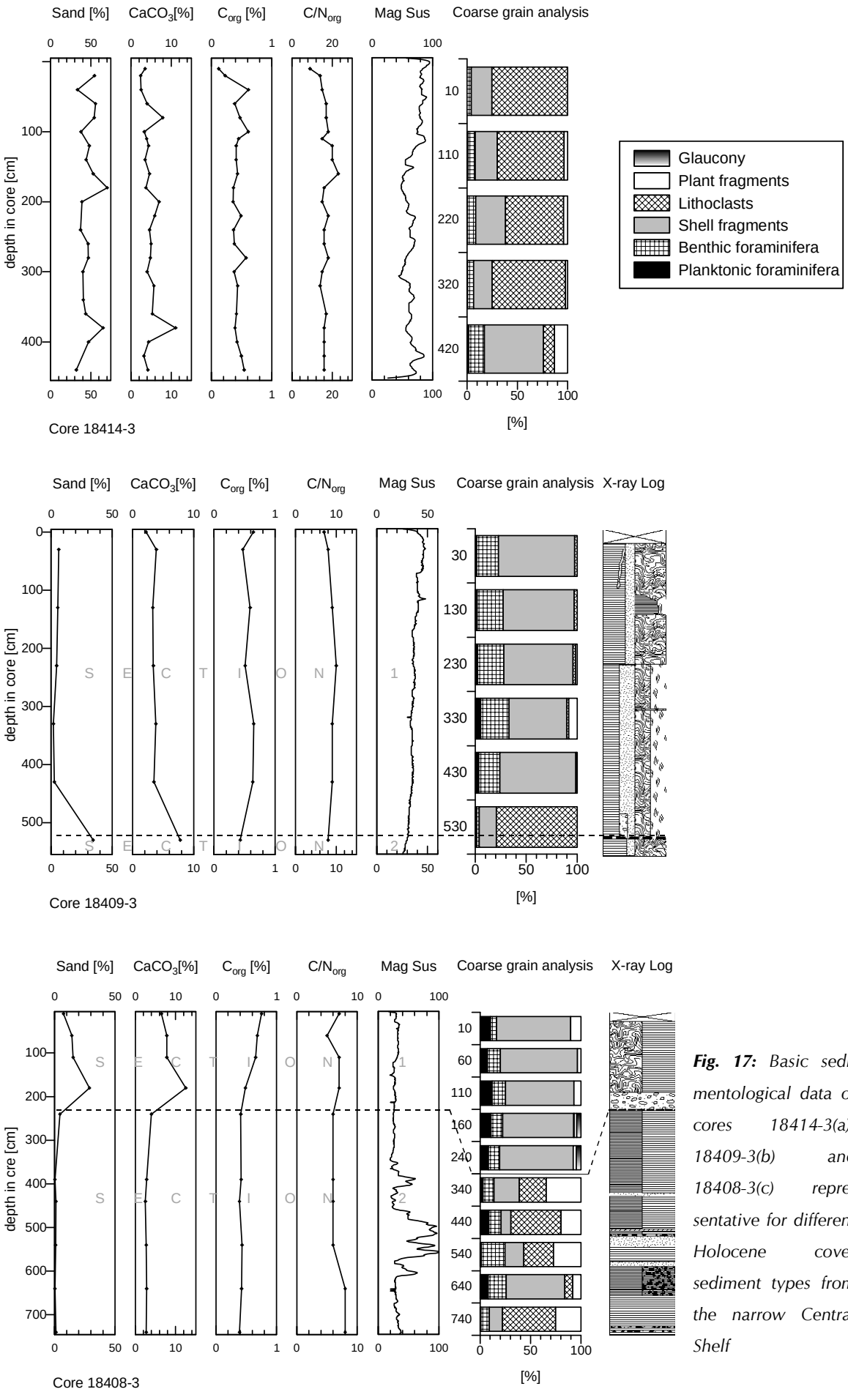

Fig. 17: *Basic sedimentological data of cores 18414-3(a), 18409-3(b) and 18408-3(c) representative for different Holocene cover sediment types from the narrow Central Shelf*

The Holocene cover sediment and the underlying clayey deposits are usually separated by a discontinuity which was discovered in the X-ray radiographies (Fig. 13). Erosion of the underlying deposits resulted in a sharp contact which is sometimes blurred by bioturbation.

In contrast to the *Southern Shelf* area, the seismic record of the *Central Shelf* area shows, that only minor incised valley structures exist in this region. Stacks of deposits up to 50 m thick were penetrated by the signal of the Parasound system. The discontinuities discovered in the sediment cores are mostly traceable as subsurface seismic reflectors (18397-2, 18398-3, 18401-3 (Fig. 19a) (cp. Szczucínski and Statteger (2001)), 18404-3, 18408-3 (Fig. 19b), 18409-3 (Fig. 19c), 18415-2, 18396-3 (Fig. 19d). They occur as a more or less abrupt change in signal intensity in the seismic record.

Benthic foraminifera of cores 18414-3 and 18416-2 have been analyzed for oxygen isotopic composition. While the data of core 18414-3 shows a trend towards lighter values upcore, core 18416-2 shows inconsistent $\delta^{18}O$ values (Fig. 18). The trend in core 18414-3 lies in the range of 0.5 ‰ on both, *Nonion subturgitum* and *Elphidium advenum*, between 267 cm core depth, dated to 6005 ^{14}C years BP and the core top. Oxygen isotopes of the same species of core 18416-2, dated to 9820 ^{14}C years BP in 491.5 cm core depth and 9195 ^{14}C years BP in 98 cm core depth, show inconsistent $\delta^{18}O$ values. Here, differences of 1.5 ‰ are observed for single measurementsof the same core depth and oxygen isotopic composition varies largely throughout the core.

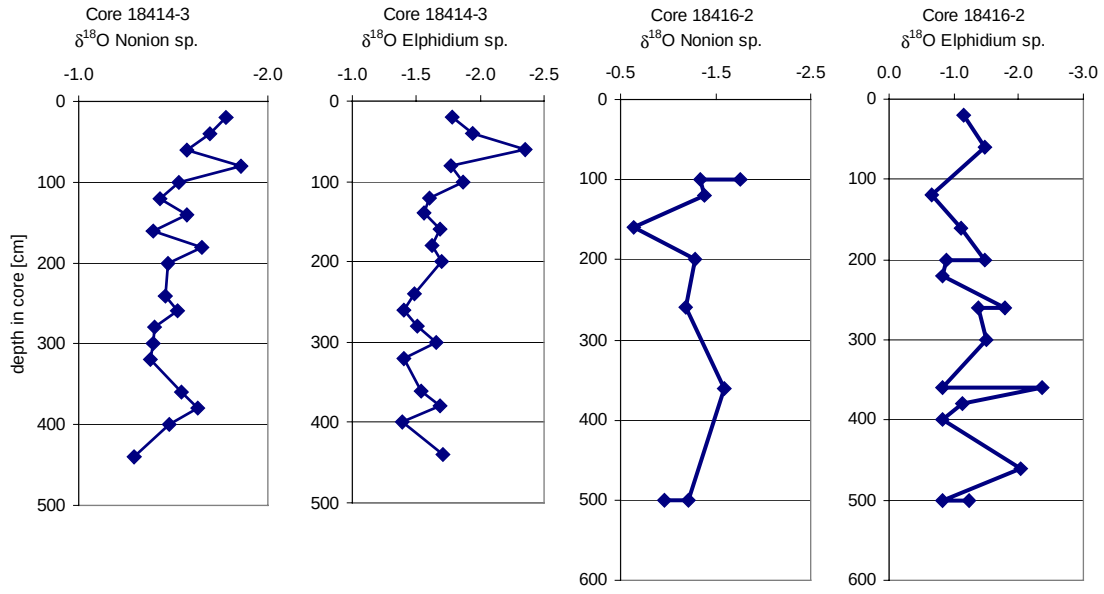

Fig. 18: *Oxygen isotopic composition of benthic foraminifera of cores 18414-3 (left) and 18416-2 (right)*

Resumée and Interpretation for *Central Shelf*

Type 1 Holocene cover sediments with high sand content and low $CaCO_3$ content were deposited under high terrigenous influence due to shallow water depth and/or proximity to rivers. This is supported by a high content in lithoclasts in the coarse grain fraction. The material was deposited in an environment corresponding to *Siliciclastic Inner Shelf* facies which looks similar to *Delta Front* and *Delta Mouth* facies. The numerous small mountainous rivers probably compensate for large deltas which are not existing along this section of the Vietnamese Coast. Furthermore, the proximity of the source area would also explain the granulometric composition of the deposits, since siliciclastics belonging to the sand fraction constitute the major part of the deposits.

Type 2 Holocene cover sediments formed in an area more distal from direct river input. Here the low sand content indicates less energetic conditions apart the direct influence of rivers or below the wave base. The major part of the sediment belongs to the silt and clay fraction and is probably constitutet of siliciclastic material since the carbonate content is low. The domination of shell fragments in the coarse grain fraction gives evidence for an increased marine type of sedimentation compared to type 1 Holocene cover sediments. These deposits belong to the *Inner Shelf* facies.

Type 3 Holocene cover sediments formed in areas with low terrigenous input in water depths generally deeper than 100 m and outside the influence of submarine fans related to small rivers. Here, a marine type of sedimentation prevails which is reflected by high sand and carbonate contents due to large amounts of carbonate shells. A marine type of sedimentation is also indicated by shell fragments and foraminifera as major components of the coarse grain fraction. These sediments were deposited in *Open Shelf* facies.

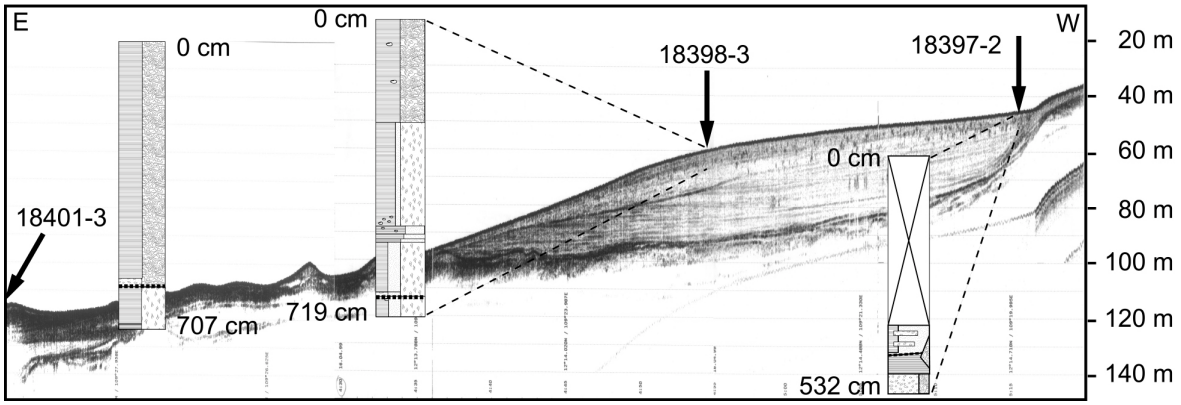

a)

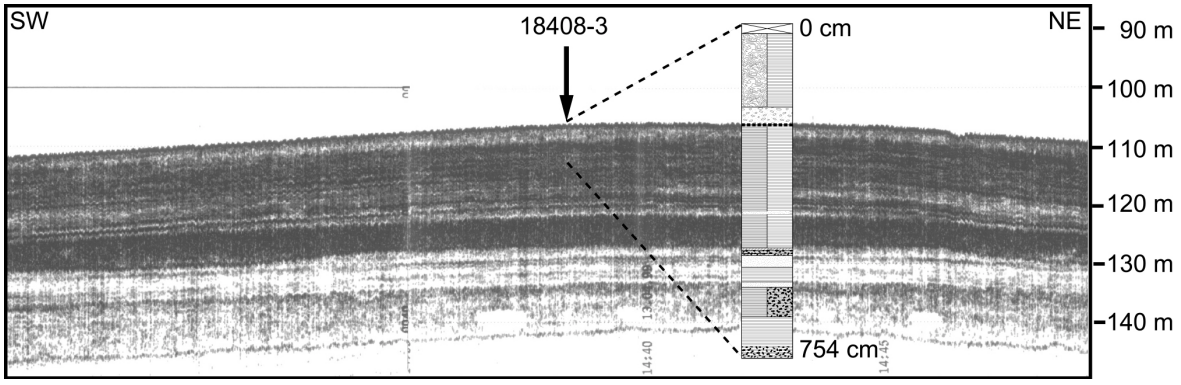

b)

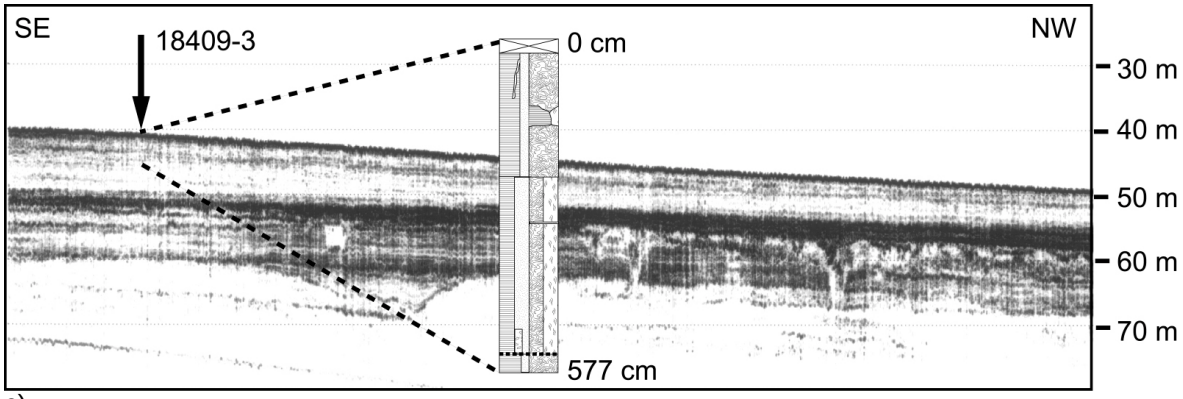

c)

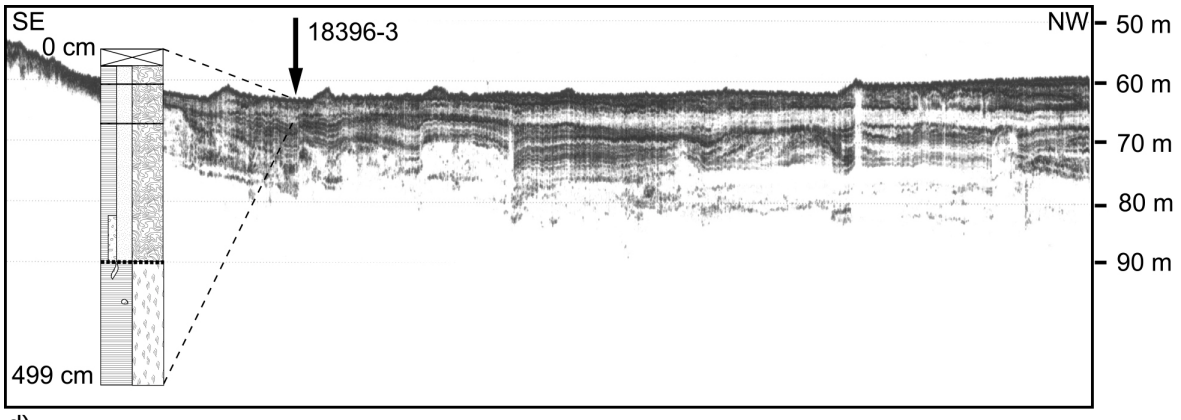

d)

Fig. 19: *Seismic record with subsurface reflectors and x-ray log of cores 18397-2, 18398-3 and 18401-3 (a), core 18408-3 (b), core 18409-3 (c) and core 18396-3 (d). Profile length ca. 17.1 km, 7.9 km, 5.0 km and 6.3 km, respectively*

The fine grained sediments underlying the Holocene cover were deposited during lower sea level. They generally occur in cores from more distal positions to the coastline. Their low carbonate content and high content in plant fragments in the coarse grain fraction indicates increased terrigenous influence. The low grade of bioturbation in comparison to the Holocene cover sediments (Fig. 13) is a sign for reduced activivity of sediment-dwelling organisms or a high sedimentation rate. The depositional facies corresponds to *Siliciclastic Inner Shelf* to *Inner Shelf* facies. Here, compared to *Holocene cover type 1*, fine-grained sediment was deposited due to increased distance between the source area and the core location during times of lower sea level.

The sedimentation rates of Holocene cover sediments in the *Central Shelf* area are in the range of 50 to 100 cm/kyr (Tab. 7). Single, significantly lower, sedimentation rates are attributable to sediment bypassing or dating of eventually reworked material.

Two cores from the transect 18414-3, 18415-2, 18416-2, 18417-3 show extremely high sedimentation rates. Cores 18414-3 and 18415-2 contain type 1 Holocene sediments with large amounts of lithoclasts which were probably delivered by small rivers (Song Vê, Song Trà Khúc, Song Lai Giang) which drain the highly elevated hinterland (up to 2600 m) close to the coastline. Extensive dunes fields and sandbars along the coastline (Defense Mapping Agency, 1972) attest a high availabilty of sand/lithoclasts. In the lower part of cores 18415-2 and 18416-2, representing early Holocene sediments, the sedimentation rates exceed 1000 and 500 cm/kyr, respectively. X-ray radiographies of core 18415-2 (Fig. 13) show layers of silt and sand in the lower part of the core which could be the result of episodic slumps due to high sedimentation rate or episodically high sediment discharge from rivers. A single chaotical slump for the lower part of core 18415-2 can be ruled out since ^{14}C age-control certifies a reasonable age profile (Tab. 7). Additionally, such a structure would be visible in the seismic record.

Core 18417-3 has been dated to 4700 ^{14}C years BP on an interval from 9 - 17 cm core depth which indicates that there is no recent accumulation of material. Since the deposits of some cores clearly lack linear sedimentation rates, bypassing of sediment to deeper parts of the SCS must be assumed. Bypassing of sediment has also been described by Szczucínski and Stattegger (2001) for recent sediments from a transect in Nha Trang Bay, southern Vietnam.

4.3.3.3 Southern Gulf of Tonkin, Northern Shelf

Sediment cores **18422-3, 18423-2, 18424-2, 18425-2** and **18426-2** represent the *Northern Shelf* area (Fig. 12, Fig. 13). Here, the thickness of the Holocene sediment cover is restricted to a few decimeters. In core 18424-2 and 18425-2 it is limited to the topmost centimeters.

Like in the sediment cores from the *Southern Shelf* area the Holocene cover sediments are characterized by generally high sand and carbonate contents and by foraminifera and shell fragments as major components of the coarse grain fraction. Core 18426-2 contains a reasonable percentage of glaucony.

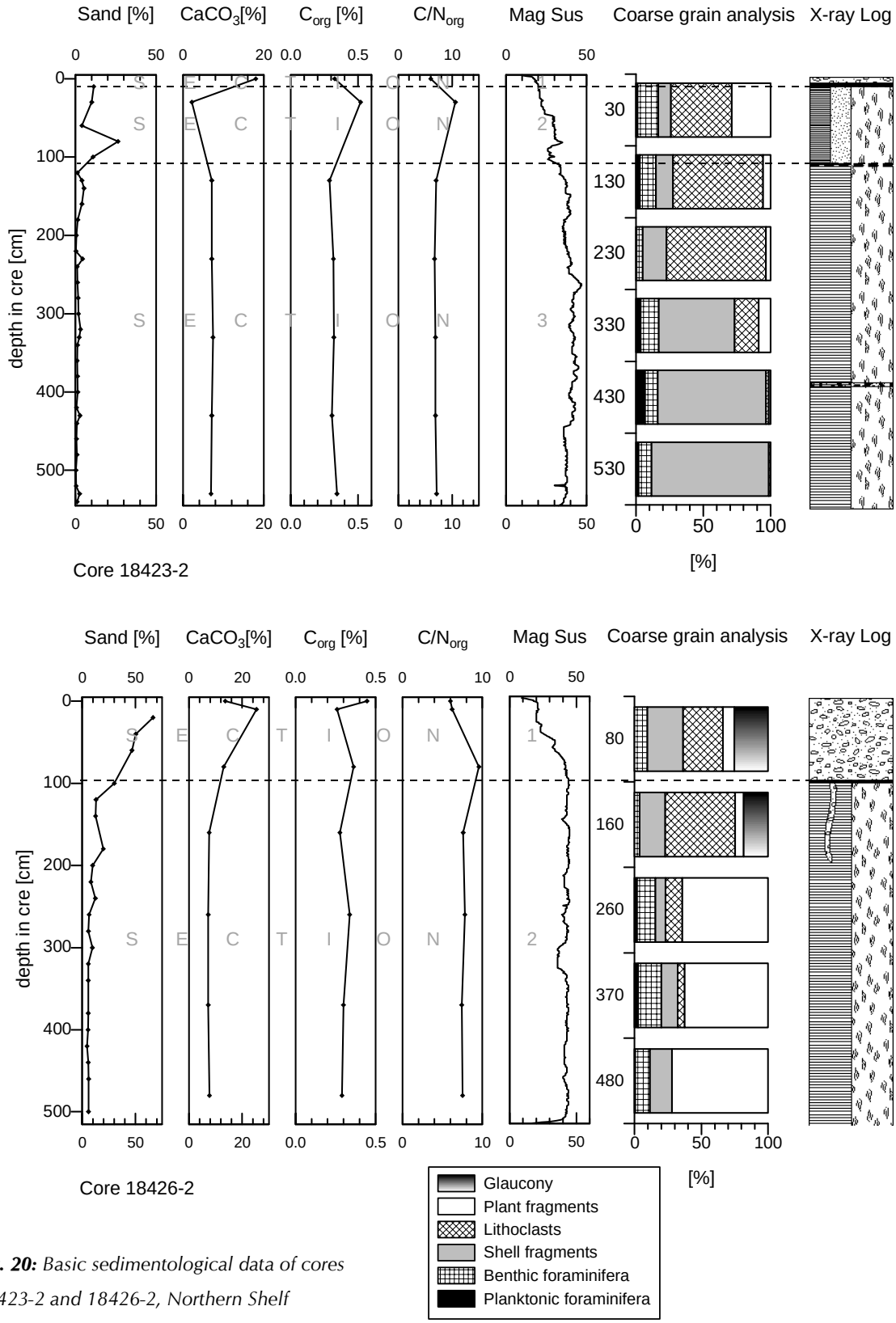

Fig. 20: *Basic sedimentological data of cores 18423-2 and 18426-2, Northern Shelf*

Cores 18422-3, 18423-2 and 18426-2 show a discontinuity, separating the Holocene cover sediments from the underlying deposits, whereas core 18423-2 contains a third section below a second discontinuity (Fig. 13). On those cores, the Holocene cover sediments have been dated to 5020, 2445 and 30130 ^{14}C years BP, respectively, whereas the age of core 18426-2 (30130 ^{14}C years BP) was measured on a probably reworked bivalve shell.

The sections directly underlying the Holocene sediments are generally fine grained with a low sand content smaller than 10 % and a low carbonate content of < 2 %. Section 3 of core 18423-2 shows a higher carbonate content. In core 18426-2 the section underlying the Holocene cover has a higher carbonate content ranging around 8 %. This section has been dated on benthic foraminifera (*Rotalia sp.*) to 43210 ^{14}C years BP. From the seismic record a seaward dipping of the sediments is evident (Fig. 21c).

The coarse grain analyses of the deposits underlying the Holocene cover reveal plant fragments and lithoclasts as major constituents whereas section 3 of core 18423-2 shows a decrease in shell fragments upcore. AMS dating of the deposits from core 18423-2 and core 18425-2 return ages of 13030 and 12575 ^{14}C years BP, respectively.

The seismic records show incised valley structures for cores 18423-2 (Fig. 21a), 18424-2 and 18425-2 (Fig. 21b), whereas cores 18422-3 and 18426-2 (Fig. 21c) were cored at sites with continuous stratification.

Resumée and Interpretation for *Northern Shelf*

Core 18422-3 and 18426-2 show the thickest Holocene sediment covers with 55 cm and 100 cm, respectively, whereas the deposits from core 18426-2 contain reworked material, indicated by a relatively high percentage of glaucony and well rounded, partly corroded tests of foraminifera (*Rotalia sp.*) which withstands transportation and reworking processes relatively unhurt. The glaucony is of autochthonous origin, since a big share of it evolved from foraminiferal tests whose remains and sutures are still noticeable. Additionally the glaucony seems to be highly mature since the grains are dark green.

Autochthonous glaucony of high maturity, accounted as an indicator for the condensed section/maximum flooding surface (Vail et al., 1984; Loutit et al., 1988; Saito, 1991; Amorosi, 1995), occurs in the sediments shortly above and below the discontinuity of core 18426-2 and was probably dispersed by bioturbational processes. The discontinuity thus probably represents the marine flooding surface.

A reliable value for Holocene sedimentation rates can only be calculated from core 18422-3, where it is around 10 cm/kyr. All other cores do not possess a representative Holocene sediment cover due to their location in incised valleys or due to ages measured on reworked material.

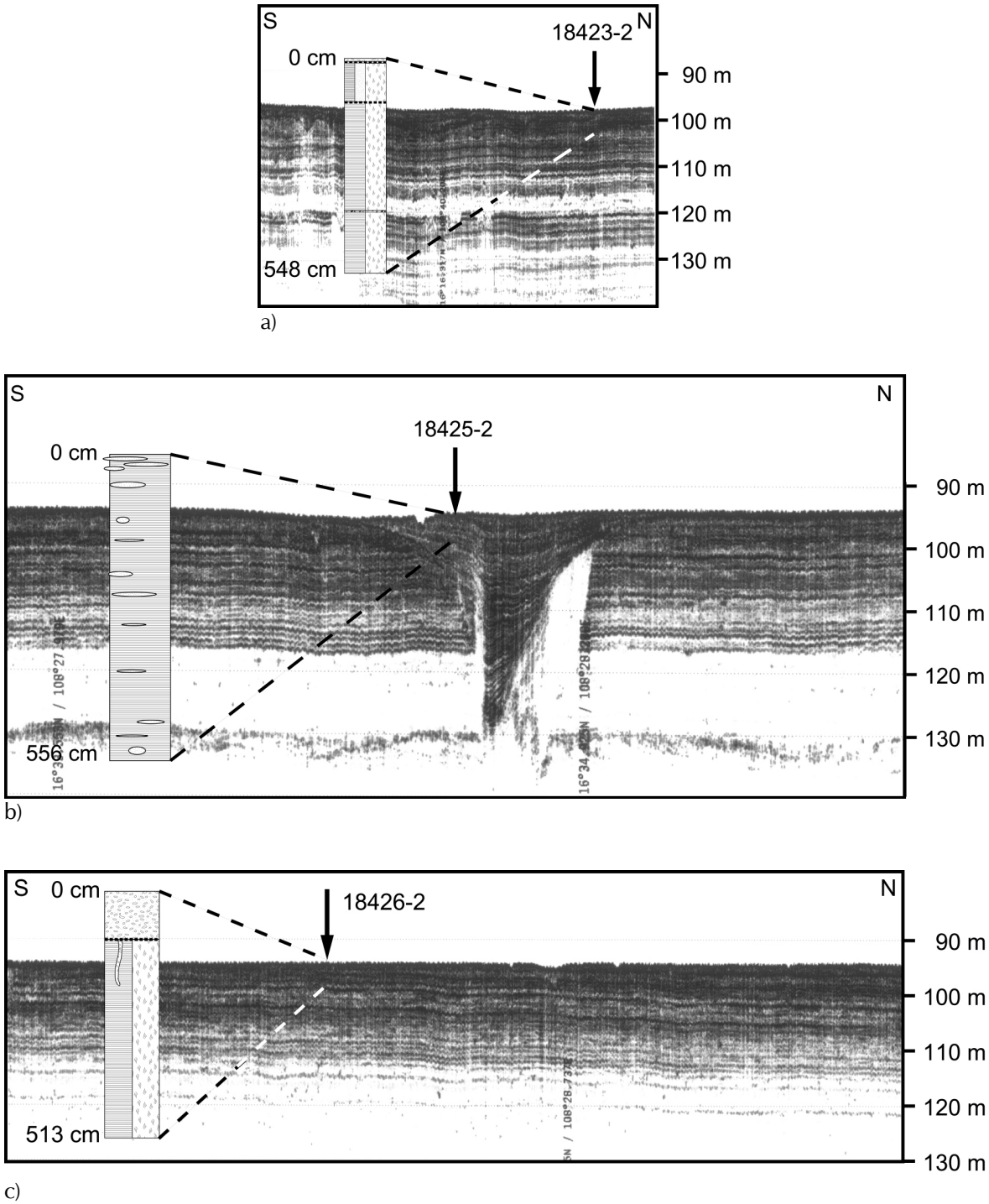

Fig. 21: *Seismic record of cores 18423-2 (a), 18425-2 (b) and 18426-2 (c). Profile lengths ca. 3.7 km, 4.5 km and 5.8 km, respectively*

The underlying deposits of core 18426-2 with an age of 43 210 ^{14}C years BP in 133 cm core depth were probably deposited during a regressional phase, suggested by seaward dipping reflectors in the seismic record (Fig. 21c). The sea level at that time of ca. -80 m (Hanebuth et al. 2000) would also explain the high content of plant fragments in the coarse grain fraction.

The deposits underlying the Holocene sediment cover in the remaining cores from the *Northern Shelf* show various sediments with high amounts of plant fragments and lithoclasts

(up to 96 %) in the coarse grain fraction (see appendix), typical for incised valley fills (cp. Hanebuth, 2000). Both cores indicate a high terrigenous influence due to river supply and deposition in shallow water depths down to -20 m corresponding to the *Delta Mouth* facies (cp. Hanebuth, 2000; Hanebuth and Stattegger, 2002). The incised valleys were probably cut into the Pleistocene land surface by branches of paleo-rivers draining into the SCS.

4.4 Discussion

4.4.1 Sedimentology

As shown above the deposits from the Vietnamese Shelf can be grouped into three genetic areas: a *Southern Shelf area*, a *Central Shelf* area and a *Northern Shelf* area. Holocene deposits from the *Southern Shelf* and *Northern Shelf* equal in many aspects due to similar sedimentological conditions on a wide shelf in the former influence of large river systems. The Holocene sedimentation rates in the *Southern Shelf* area are with 5 - 10 cm/kyr and with 25 - 40 cm/kyr in sheltered locations nearly equal to those in the *Northern Shelf* with ca. 10 cm/kyr. The partly higher sedimentation rate on the *Southern Shelf* reflects the position still in the influence of the Mekong River, whereas *Northern Shelf* locations nowadays are detached of direct riverine influence. Sediment starvation, following the sequence stratigraphic concept (Vail et al., 1991), is observed in both areas as a consequence of rising sea level in the late Pleistocene and early Holocene. On the *Northern Shelf* a condensed section is preserved. In both areas, with the rapidly rising sea level, sediment supply was reduced drastically due to an increased distance to large sediment suppliers. The terrigenous type of sedimentation was replaced by a marine type and reworking processes subsequently homogenized the Holocene deposits which is reflected by chronologically inconsistent ^{14}C dates and glaucony formed in the condensed section. Therefore the Holocene cover sediments must be regarded as relict sediments.

In either area drowned incised valley structures are observed underlying the Holocene cover sediments. During transgression, the valleys were filled with probably estuarine or delta deposits with a low carbonate content and a high content in lithoclasts and plant fragments.

The Holocene deposits of the *Central Shelf* differ from those of the previously discussed regions. Depending on recent sedimentological conditions and intensity of terrigenous influence the Holocene sediments on the *Central Shelf* can be sorted into three groups. The sedimentation rate is high with values from 50 to 100 cm/kyr due to the proximity of mountainous rivers draining directly into the SCS nearby. Peak sedimentation rates of 500

and 1 000 cm/kyr are observed in core sections from locations with a very high availability of siliciclastic material which is probably delivered by those mountainous rivers. These high sedimentation rates occurred during early Holocene times and are probably correlatable with strengthened SW-monsoon in the Annamite region (cp. Maxwell, 2001).

The effect of sediment starvation accompanying the rapid sea-level rise was neutralized due to the narrowness of the shelf in the *Central Shelf* area, keeping a nearshore position. Instead, the steady supply of terrigenous sediments to the depocenters allowed the accumulation of thick Holocene deposits. The model of non-deposition and sediment starvation during sea-level rise is not applicable for this area.

The transparency of the seismic reflectors due to high sedimentation rates in this region together with a comparison of sedimentological as well as geochemical proxies and ^{14}C dates permits the correlation of sediment cores:

A direct correspondance of sediment cores can be detected in the core pairs 18397-2 and 18398-3, 18398-3 and 18401-3, 18414-3 and 18415-2, 18419-3 and 18420-2 (Fig. 22), whereas the types of deposits from the *Southern Shelf* and the *Northern Shelf* are too manifold for direct correlation. Cores 18397-2, 18398-3 and 18401-3 from a profile perpendicular to the coast in Nha Trang Bay can be correlated from both, the seismic record (Fig. 19) and sedimentological results (appendix). In core 18397-2 two discontinuities revealed by X-ray radiographies and strongly supported by variations in sand-, carbonate-, C_{org}-content and coarse grain analyses, are present. Here, a section of clayey, unbioturbated deposits occurs. It shows a high percentage of lithoclasts in the coarse grain fraction and probably accumulated in an event-like manner since the deposits below and above this section have been dated to 4800 and 3910 ^{14}C years BP, respectively. The sediments above and below this 'slump' correlate with the deposits of the cores 18398-3 and 18401-3. Szczucínski and Stattegger (2001) interpreted the unconformity in this profile as the transgressive surface. The age profile of core 18397-2 stands in contrast to the findings of Szczucínski and Stattegger (2001), and is clearly indicating a Holocene age of the lower unit (Fig. 13).

Further north in the study area the seismic records of cores 18419-3 and 18420-2 confirm landward thickening sequences (Fig. 22) which certifies a strong influence of terrigenous sediments. In combination with the sedimentological results the upper 450 cm of core 18420-2 seem to match with the uppermost 150 cm or so of core 18419-3 (appendix). The age profile of both cores supports this assumption (Fig. 13).

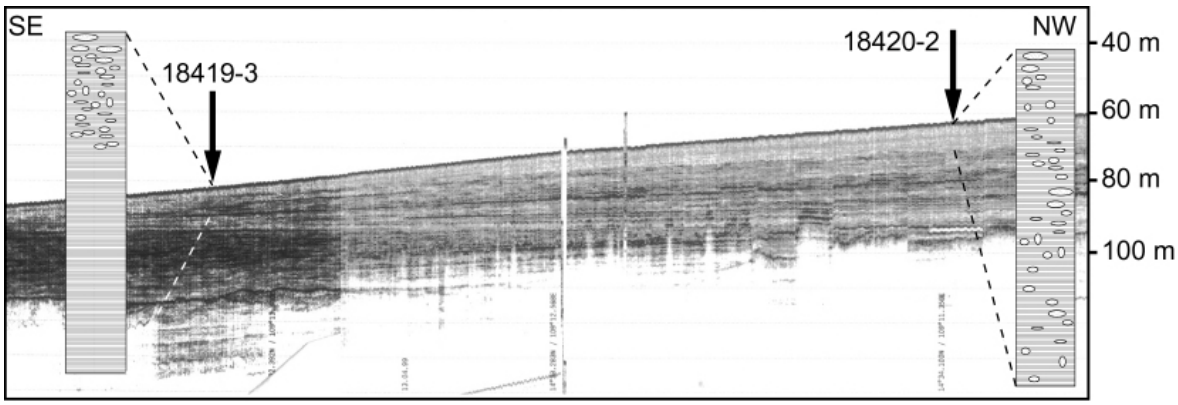

Fig. 22:*Thickening landward sequence cored at station 18419-3 and 18420-2. Profile length ca. 9 km*

4.4.2 Sedimentation Rates/Accumulation Rates

Sedimentation rates for the *Central Shelf* are one to two orders of magnitude higher than those from the *Southern Shelf* and the *Northern Shelf,* respectively. This strengthens the assumption that small mountainous rivers contribute a large share of sediments to the SCS and the worlds oceans in general (Milliman and Syvitski,1992). For modern sediments from the profile of Nha Trang Bay in the *Central Shelf* area, Szczucínski and Stattegger (2001) determined modern sedimentation rates based on the ^{210}Pb method ranging between 100 and 400 cm/kyr. These results coincide with our findings although determination of sedimentation rates based on radiocarbon dating is much more reliable than by ^{210}Pb which is assumed to overestimate the real values. (Carpenter et al., 1982; Carpenter et al., 1985).

The sparseness of data concerning Holocene MAR on the shelves of the SCS does not allow a detailed intercomparison of MAR. Gao (cited in Wang, 1999) determined an accumulation rate of 2.24 g/cm^{2}kyr on deposits from 180 mmwd in the northern part of the SCS off Hainan. Min (cited in Wang, 1999) calculated a MAR of 29.46 g/cm^{2}kyr in a core from 124 mmwd from the northeastern part of the SCS (Fig. 23). Comparison of their sedimentation rates with the sedimentation rates from this study certifies comparatively very high sedimentation rates on the *Central Shelf*. Following the sedimentation rates, the deposits from this study, with dry bulk densities of ca. 1.15 g/cm^3 on the average (max. 0.8, min. 1.3 g/cm^3), show mass accumulation rates (MAR) of 6 to 12 g/cm^{2}kyr (30 to 45 g/cm^{2}kyr in sheltered areas) for the *Southern Shelf* and ca. 12 g/cm^{2}kyr for the *Northern Shelf*, respectively (Fig. 23). MAR in the *Central Shelf* area outrange this values with 60 - 120 g/cm^{2}kyr on the average and 600 - 1200 g/cm^{2}kyr in areas with a high avalability of siliciclastic material (Fig. 23). Thus, the findings of Gai and Min (cited in Wang, 1999) are exceeded at least by a factor of two to four by MAR in the *Central Shelf* area, whereas regions with peak sedimentation outrange their values by a factor ranging between 20 and 40.

For the deeper parts of the SCS, Schönfeld and Kudrass (1993) found a modern MAR of 0.51 g/cm²kyr for the shallowest core in their study from 220 mmwd. Wang (1999) proposes average MAR of 4.86 g/cm²kyr for the western marginal part of the SCS. However, a comparison of shelf sediments versus shelf break, slope and deep sea sediments is not reasonable since the deglacial sea-level rise resulted in a shifting of depocenters from the shelf break and slope to more proximal regions (Schönfeld and Kudrass, 1993; Hanebuth, 2000).

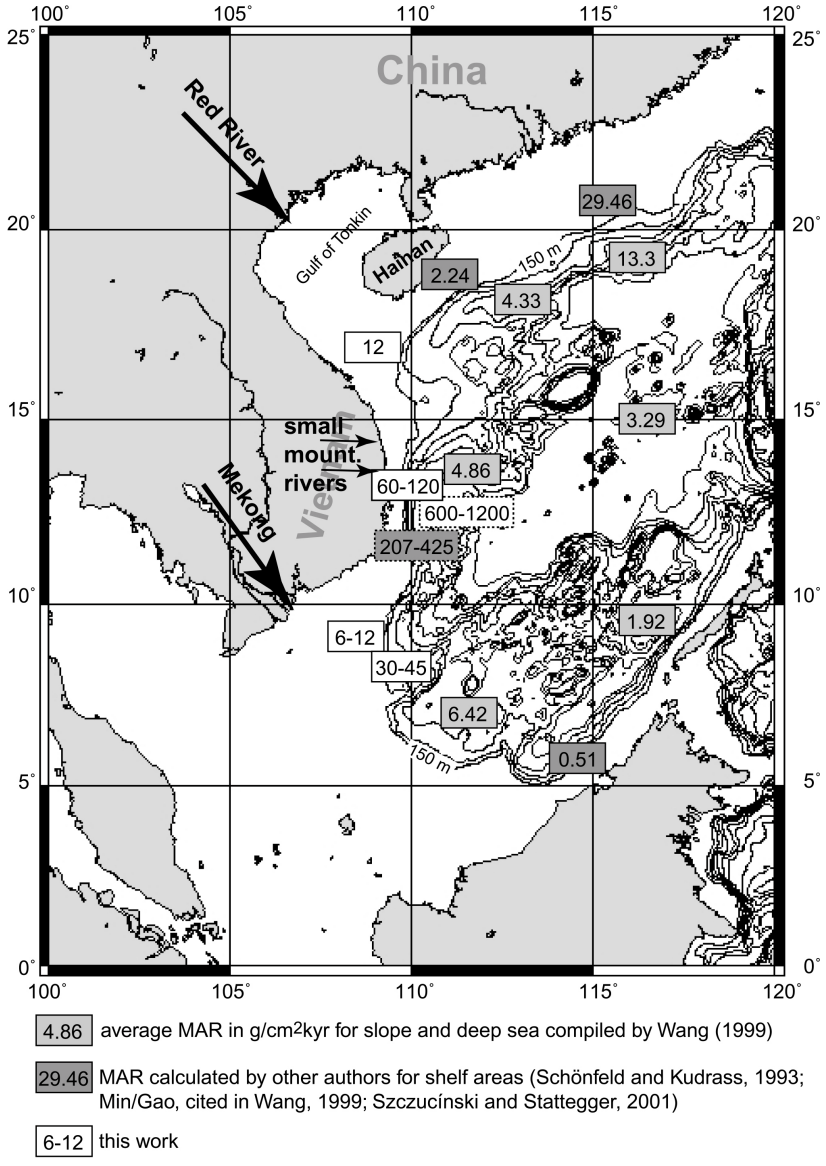

Fig. 23: *Mass accumulation rates in the Southern Shelf area, the Central Shelf area and the Northern Shelf area*

4.4.3 Oxygen Isotopes

The trend in core 18414-3 from 21 mmwd in $\delta^{18}O$ towards lighter values between 6005 ^{14}C years BP and probably recent time can be interpreted as increased influence of meteoric waters. This increased influence could either be caused by shoreline progradation following the slight sea level lowering after the last highstand at approximately 5500 years BP or by more humid climatic conditions.

Double measurements from core 18416-2 show differences in oxygen isotopic composition of up to 1.5 ‰. This variation could be attributed to heterogeneous and variable sedimentological conditions on the shallow shelf, influenced by changes of riverine input as well as reworking processes. Furthermore slumps, which are observed at sediment station 18415-2, probably affected the site of core 18416-2 as well, which is supported by the age profile of this core with 9820 ^{14}C years BP in 491.5 cm core depth and 9195 ^{14}C years BP in 98 cm core depth. Due to enormous sedimentological variations on the shelf, oxygen isotopes can generally not be regarded as a promising tool in this environment.

4.4.4 Reservoir Age

Radiocarbon (^{14}C) is produced in the upper atmosphere by cosmic rays. Its mixing with carbon in the oceans in the form of CO_2 is slower than mixing with carbon in the atmosphere. Furthermore upwelling of deep ocean water also brings ancient, less radioactive carbon to the ocean surface. This results in depletion of marine organisms (tissue and carbonate tests) in ^{14}C compared to organisms which draw their ^{14}C directly from the atmosphere (e.g. plants). Therefore marine samples can yield apparent ages several hundred years older than land-derived samples. This discrepancy is called the reservoir effect.

Generally, the reservoir effect was considered to be 400 years in all the oceans. Today it is known that the effect varies geographically as well as through time. Known marine reservoir ages range from 190 $\pm$ 40 ^{14}C years in front of coastal Peru and Chile (Southon et al., 1995) over ca. 580 ^{14}C years for parts of the eastern Pacific (Shackleton et al., 1988) to 788 $\pm$ 33 ^{14}C years for the northeastern Pacific (Southon et al., 1992). Furthermore the magnitude of the reservoir effect in the Iceland and Norwegian Seas may have varied by as much as 1600 ^{14}C years over the last 50 ka. (Voelker et al., 1998). Wang et al. (1999) assume a reservoir age of up to 1500 years for the SCS at the time of the last glacial maximum.

Therefore every regional study that employs radiocarbon dating on marine organisms should establish the correct reservoir correction for that region. Many previous studies in the South China Sea used a standard reservoir correction of 400 years. Especially in coastal areas with high terrigenous runoff an influence of non marine ^{14}C has to be considered (cp. Willkomm,

1986). The coastal waters of Vietnam receive large amounts of fluvial input from the southeast Asian continent, which is enriched in ^{14}C compared to marine waters. Those meteoric waters bias the isotopic signal of seawater towards the atmospheric signal. Southon et al. (in press) calculated reservoir ages between 540 ± 60 and 244 ± 60 ^{14}C years for marine carbonate samples (corals, gastropods, bivalve shells) from the coastal SCS, which support the use of the standard reservoir correction of 400 years.

In the course of this study a possible reservoir age has been determined on core 18415-2 from unaltered shell fragments and wood fragments, respectively. Respective materials from 526 cm core depth were dated to 7970 ± 50 and 7760 ± 45 ^{14}C years BP, which results in a reservoir age of 210 ± 65 years (Grootes, pers. comm.).

However, since core 18415-2 shows some coarse layers in the X -ray radiographs (Fig. 13) which are interpreted as slump-like structures, the reliability of this reservoir age is debatable since there may occur a time-lag between the ^{14}C age and the final deposition of the wood fragments. Additionally, dating of shell fragments bears an uncertainty concerning freshness of the dated material due to possible transport and reworking of the material prior to deposition. Therefore, and to ensure comparability with previous studies (Hanebuth et al. 2000), marine carbonate samples of this study have been corrected for the standard reservoir age of 400 years.

4.4.5 Paleo-Facies and Sea level

The dated sediments were deposited in paleo-environments of certain water depths of which some are relevant for sea level reconstruction. Particular sections of the cores 18376-2, 18389-3, 18423-2, 18425-2 and 18426-2 were deposited as *Delta Mouth* or *Delta Front* facies with corresponding water depths of 5 - 20 m. Those deposits generally correspond to *Delta Mouth* and *Front* facies on the Sunda Shelf and the recent Mekong Delta (Hanebuth, pers. comm., Ta et al., in press). Deposits of core 18389-3 accumulated as *Delta Front* facies with tidally induced intercalations of organic patches and sandy layers and also probably formed in water depths between 5 and 20 m. Sections of the cores 18408-3, 18409-3, 18414-3, 18415-2, and 18417-3 include sediments matching with the characteristics of *Siliciclastic Inner Shelf* facies. Here paleo-water-depths of 5 - 30 m are assumed.

After corrections for paleo-water-depth, sample depth in core and the mean of the paleo-water-depth a range for paleo sea-level was determined together with calibration to calendar years BP (Tab. 8). Most of the data coincide with the sea level curve of Hanebuth et al. (2000) (Fig. 21). Colored markers indicate data that have been corrected for paleo-water-depth from the *Northern Shelf* (red), the *Central Shelf* (blue) and the *Southern Shelf* (green), respectively.

Other dates from samples which do not represent paleo-environments suitable for sea-level reconstruction have been plotted for completeness. Note that the 1 sigma range has not been plotted.

The calibrated dates from the *Southern Shelf* of core 18389-3 (14.14 kyr BP in 99 cm core depth and 14.92, 14.88, 14.36 kyr BP in 186 cm core depth) group in the area of melt water pulse (MWP) 1A (Fig. 24). Hanebuth et al. (2000) dated a major rise in sea level of 16 m in the SCS between 14.6 and 14.3 kyr BP. The dates of core 18389-3 do not necessarily show a rapid sea-level rise for the time of MWP 1A. However, a slight change in the depositional environment occurred in core 18389-3 between 186 cm core depth and 99 cm core depth (see appendix), showing an increase in carbonate content, which is probably attributable to increasing marine conditions due to a rise in sea-level. Furthermore, the range in water depth for the depositional facies (width of error bars) does not exclude a rapid sea-level rise.

Tab. 8: *Possible paleo-water-depths and calibrated radiometric ages*

Core No	Water depth [m]	Sample depth [cm]	Paleo facies	Range of paleo water depth [m]	Possible paleo sea-level [-m]	AMS-^{14}C age [yrs] BP	Deviation +/-	Calibrated ages [kyr] BP
18376-2	89	40	-			**8610**	45	9.02
18376-2	89	472	Delta Front/Mouth	5-20	**-81.22**	**27140**	210	
18389-3	109	99	Delta Front/Mouth	5-20	**-97.49**	**12215**	50	14.14
18389-3	109	99	Delta Front/Mouth	5-20	**-97.49**	**12160humic**	70	14.12
18389-3	109	186	Delta Front/Mouth	5-20	**-98.36**	**12450**	70	14.92, 14.88, 14.36
18391-2	115	207	-			**4960**	35	5.30
18391-2	115	255	-			**4875**	35	5.23
18391-2	115	295	-			**6580**	45	7.13
18391-2	115	332	-			**7955**	40	8.39
18391-2	115	360	-			**10040**	60	11.06, 10.98, 10.83
18393-3	156	28	-			**665**	25	0.30
18393-3	156	104	-			**1225**	25	0.75
18393-3	156	207	-			**12160**	60	13.79, 13.70, 13.52
18393-3	156	207	-			**24330**	170	
18396-3	61	250	-			**>49220**		
18397-2	45	413	-			**3910**	35	3.87
18397-2	45	488	-			**4800**	35	5.04
18401-3	134	226	-			**2590**	40	2.29
18401-3	134	590	-			**9910**	50	10.78, 10.71, 10.65
18404-3	169	53	-			**5705**	35	6.15, 6.12
18404-3	169	60	-			**29100**	390	
18404-3	169	225	-			**8015**	50	8.44
18408-3	108	152	-			**1605**	30	1.17
18408-3	108	265	Siliciclastic Inner Shelf	5-30	**-93.15**	**16110**	120	
18408-3	108	265	Siliciclastic Inner Shelf	5-30	**-93.15**	**12580**	310	15.15, 14.68, 14.41
18409-3	40	91	-			**735**	30	0.40
18409-3	40	525	-			**5930**	35	6.32
18409-3	40	559	Siliciclastic Inner Shelf	5-30	**-28.09**	**8775**	50	9.39, 9.23, 9.11
18414-3	21	267	Siliciclastic Inner Shelf		**-23.67**	**6005**	35	6.41
18415-2	38	107	-			**3020**	30	2.77
18415-2	38	250	Siliciclastic Inner Shelf	5-30	**-23.00**	**7735**	40	8.18
18415-2	38	526	Siliciclastic Inner Shelf	5-30	**-25.76**	**7970**	50	8.40
18415-2	38	526	Siliciclastic Inner Shelf	5-30	**-25.76**	**7760**	45	8.54, 8.53, 8.52
18416-2	66	98	-			**9195**	45	9.83
18416-2	66	491	-			**9820**	50	10.59, 10.44, 10.37
18417-3	97	13	-			**4700**	45	4.89
18417-3	97	450	Siliciclastic Inner Shelf	5-30	**-84.00**	**11810**	60	13.18
18419-3	82	130	-			**5740**	60	6.17
18419-3	82	525	-			**9610**	60	10.30
18420-2	62	41	-			**900**	25	0.51
18420-2	62	511	-			**8265**	50	8.80
18422-3	84	51	-			**5020**	30	5.33
18423-2	97	2	-			**2445**	30	1.85
18423-2	97	46.5	Delta Front/Mouth	5-20	**-84.97**	**13030**	60	15.14, 14.69, 14.40
18425-2	95	29	Delta Front/Mouth	5-20	**-82.79**	**12575**	60	14.09
18426-2	92	55	-			**30130**	320	
18426-2	92	133	Delta Front/Mouth	5-20	**-80.83**	**43210**	2630	

Calculation of possible paleo sea-levels occurred after the following formula:
Modern water depth + sample depth in core - mean of paleo-water-depth for respective paleo facies = paleo sea-level
(Example calculation for core 18389-3, 186 cm: 109 m + 1.86 m - 12.5 m = 98.36 m)

Sea level indications in the *Central Shelf* area are a bit speculative due to an uncertain range of water depth of the *Siliciclastic Inner Shelf* paleo facies. Nevertheless, some of the data points are situated below the reference curve of Hanebuth et al. (2000), which could be caused by subsidence due to the extremely high sediment input shown above (Fig. 24).
In contrast, data points of *Northern Shelf* deposits plot above the sea-level curve of Hanebuth et al. (2000) (Fig. 24, Fig. 25). Active tectonics off North Vietnam could be attributable for this. An uplift of some meters could have caused such a shift, although too little is known about tectonic activity in this region.

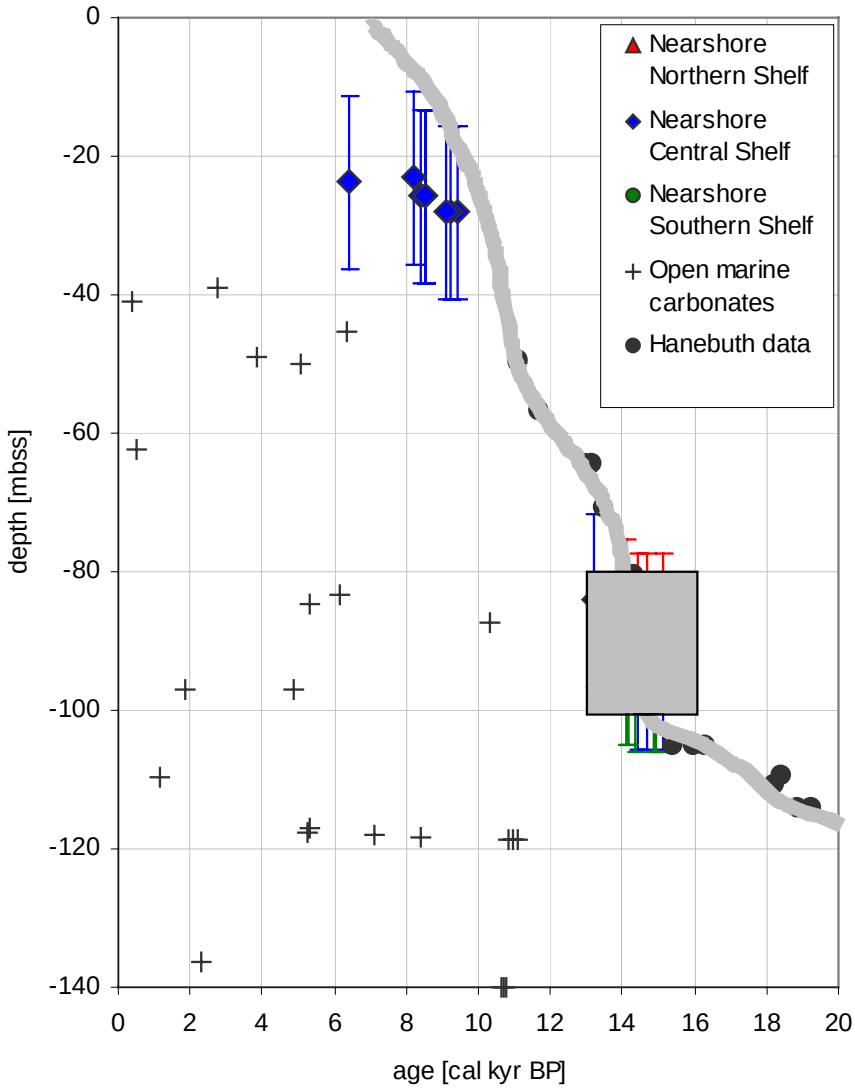

Fig. 24: *Comparison of tentative sea level data from Vietnamese Shelf deposits with the sea level curve of Hanebuth et al. (2000). Despite the wide error bar due to uncertainty in facies assignment* Southern Shelf *cores plot within the sea level curve of Hanebuth et al., whereas* Central Shelf *deposits plot below and* Northern Shelf *deposits above the curve. Calibrated ages from samples without possible sea-level indication are plotted for completeness. Note that the 1 sigma range of AMS dates has not been incorporated. Shaded area of meltwater pulse 1A is zoomed in* ***Fig. 25***

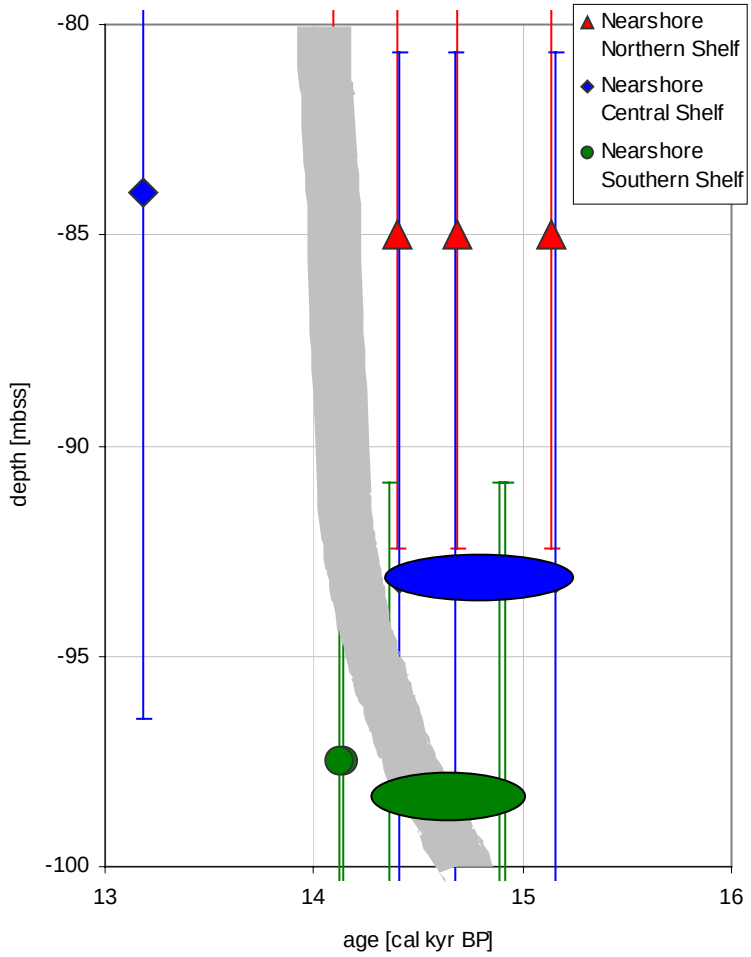

Fig. 25: *Tentative sea-level data from the Vietnamese Shelf during meltwater pulse 1A*

4.4.6 Discontinuities

The discontinuities within the sediment cores represent hiatuses with a duration in the range of ca. 2500 years, calculated from cores 18391-2 and 18409-3. Generally, the ^{14}C dates below the discontinuities match with the rising sea level, i. e. discontinuities from deeper water depths were generated earlier than those from shallower water depths. The same can be stated for the sediments which were deposited directly above the discontinuities. Therefore, the discontinuities are interpreted to be caused by erosion due to hydrographic changes in the course of the rising sea level. A comparison of the data (Tab. 9) with the sea level curve of Hanebuth et al. (2000) shows that from the calculations in core 18409-3 a minimum water depth of ca. 18 m was given when the underlying deposits have been accumulated. Thereafter sea level rose and a time of erosion or non-deposition led to the formation of a hiatus. After a certain rise in sea level a new type of sedimentation set in. The minimum water cover for sedimentation to set in was ca. 35 m in core 18409-3. In most

other cores the hiatuses only formed under a higher water cover (i.e. at a stage of higher sea level) and renewed sedimentation began under a higher water cover than in core 18409-3. Especially cores from the *Southern Shelf* (18389-3, 18391-2, 18393-2) show relatively high sea level before and after hiatus formation. Eventually, subsidence is responsible for this increased water depth.

In contrast, core 18423-2 from the *Northern Shelf* indicates an emergence of 3 m above sea level employing the Hanebuth-curve, although marine(!) sediment has been found and dated, here. Since reworking of the dated sediment is very unlikely (sea urchin, cp. photo plate, appendix), regional uplift, as proposed before in the sea level discussion, seems to be a probable explanation.

Tab. 9: *Duration of hiatuses, with sea level and water cover below and above hiatuses at time of hiatus formation (erosion). Sea-level data from Hanebuth et al. (2000)*

Core No	Water depth [m]	Cal. age below hiatus [years] BP	Cal. age above hiatus [years] BP	Min. duration hiatus [years]	Sea level below hiatus [m]	Sea level above hiatus [m]	Water cover below hiatus [m]	Water cover above hiatus [m]
18409-3	40	**9390-9110**	**6320**	2790	-22	-5	18	35
18423-2	97	**15140-14400**			-100		-3	
18408-3	108	**15150-14410**			-100		8	
18389-3	109	**14140**			-80		29	
18391-2	115	**11060-10830**	**8390**	2440	-50	-30	65	85
18401-3	134		**10780-10650**			-40		94
18393-2	156	**13790-13520**			-70		86	
18404-3	169		**8440**			-10		159

4.5 Conclusions

The deposits of the Vietnamese Shelf are multifaceted, with changing depositional environments, which were strongly influenced by the deglacial sea-level rise. Concerning depositional processes the shelf can be divided into three different areas: the *Northern Shelf* in the southern Gulf of Tonkin, the narrow *Central Shelf* in front of the high-rising Annamite chain and the *Southern Shelf* in the area of the paleo-Mekong.

The following conclusions can be drawn:

- Sedimentation rates are highly variable. (i) On the *Southern Shelf*, a low sedimentation rate of 5 – 10 cm/kyr (25 – 40 cm/kyr in sheltered areas) is observed. (ii) The *Central shelf* shows a very high sedimentation rate of 50 – 100 cm/kyr (500 – 1000 cm/kyr for short periods) and (iii) *Northern Shelf* is characterized by a low sedimentation rate around 10 cm/kyr.

- Small mountainous rivers along the coast of central Vietnam deliver huge quantities of sediment. Here, with 60 - 120 g/cm²yr (occasionally 600 - 1200 g/cm²yr), the highest mass accumulation rates in the SCS have been observed so far. These values exceed mass accumulation rates of other shelves from the SCS at least by a factor of 2 to 4.
- The high mass accumulation rates of 600 - 1200 g/cm²yr occurred in early Holocene times and are probably caused by enhanced erosion in the Annamite mountains due to intensified SW-monsoon.
- On the *Southern Shelf,* the highest facies variability was found due to the abundance of incised valley systems.
- The Central Shelf shows low facies variability due to lack of incised valleys.
- A condensed section/marine flooding surface indicated by the abundance of glaucony, occurs on the Northern Shelf.
- Relict sediments are only observable in areas of low sedimentation rate, i.e. *Southern Shelf* and *Northern Shelf*. Here, the equilibrium between deposition and erosion could not be established, yet.
- Due to the high terrigenous input from the small mountainous rivers the depositional equilibrium was established quickly on the *Central Shelf*.
- Comparison of sea-level indications with the sea level curve of Hanebuth et al. (2000) shows agreement for *Southern Shelf* deposits. Data points from *Central Shelf* deposits below the Hanebuth-curve may be caused by subsidence due to high sediment input. In contrast, data points from the *Northern Shelf* above the Hanebuth-curve are probably caused by tectonic uplift in this region.

5 Provenance and Distribution of Sediments on the Vietnamese Shelf: Indications from Trace Elements and Sr and Nd-Isotopes

5.1 Introduction

Detrital sediments of the Vietnamese Shelf are delivered by two of the major SE-Asian rivers draining into the South China Sea (SCS), the Mekong in the South and the Red River in the North as well as by numerous small mountainous rivers which drain into the SCS along the narrow central part of the Vietnamese Coast (Fig. 26). Concerning sediment discharge, both rivers are among the 10 largest rivers of the world, contributing 160 x 10^6 (Mekong) and 130 x 10^6 (Red River) tons per year of detrital sediment respectively (Milliman and Meade, 1983). Sediment discharge has never been estimated for the small mountainous rivers along the Vietnamese Coast but Milliman and Meade (1992) stated that sediment delivery to the worlds' oceans by small mountainous rivers is probably highly underestimated.

With the two large rivers draining into the SCS nearby one would expect mass accumulation rates (MAR) to be highest on the shelf in front of the river mouths. In contrast, a shallow seismic survey on the Vietnamese Shelf and sedimentological investigations of core material revealed thicker stacks of Holocene sediments on the narrow *Central Shelf* than in front of the river mouths. Together with precise AMS-^{14}C age control, sedimentation rates as well as MAR have been determined for the Vietnamese Shelf (cp. chapter 4). MAR are extremely high on the narrow central part of the Vietnamese Shelf with an average of 60 - 120 g/cm^{2}yr and 600 - 1200 g/cm^{2}yr during peak accumulation and exceed MAR from other areas (Min, cited in Wang, 1999) of the South China Sea (SCS) by a factor of 2 to 30. MAR in the southern part of the Vietnamese Shelf in the area off the Mekong River and in the northern part of the Vietnamese Shelf in the Gulf of Tonkin (southern part) are lower with an average of ca. 12 g/cm^{2}yr.

This chapter focuses on provenance studies based on chemical (major and trace elements) and isotopic composition (Sr and Nd isotopes) of Holocene sediments on the Vietnamese Shelf. In earlier investigations, the decay systematics of Sm-Nd and Rb-Sr isotope systems have been successfully applied to marine sediments (Grousset et al., 1988, 1998; Nakai, 1993; Hemming et al., 1998; Asahara et al., 1999; Walter et al. 2000)

5.1.1 Possible Sources of Terrigenous Sediment

Draining different source rocks, the geochemical composition of the detrital sediment deposited on the Vietnamese Shelf should reflect the composition of the source area.

The Mekong arises in the eastern Tibetan Plateau while the source of the Red River lies in the Yunnan mountains of southwestern China. The small rivers of central Vietnam drain the Annamite chain which stretches in north south elongation closely along the coast (Fig. 26, Fig. 27).

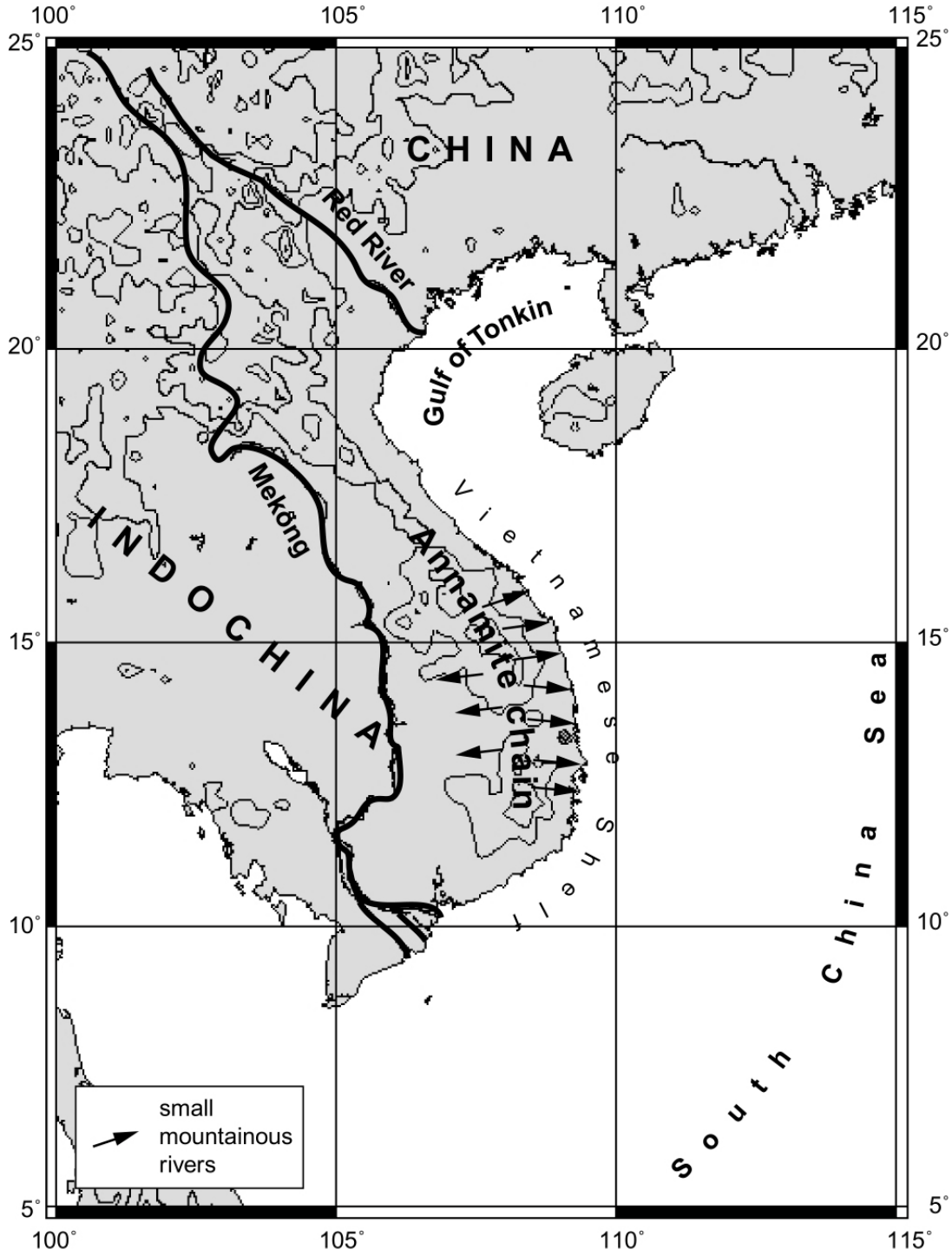

Fig. 26: *Geographical features of the study area*

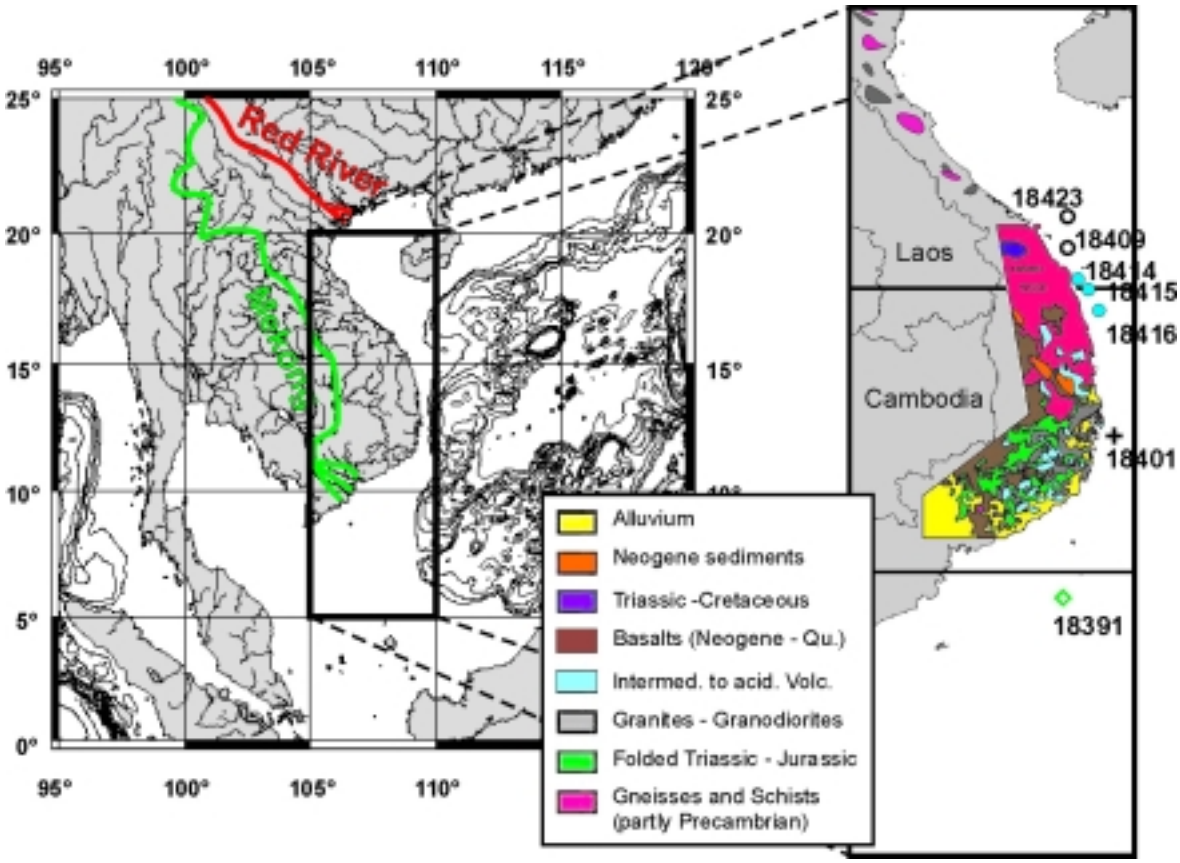

Fig. 27: *Study area with schematic geological map of Vietman and sampling locations*

While the two large rivers predominantly drain young rocks that formed in relation to the Himalayan orogeny, the Annamite chain with the Kontum Massif as a part of it bears continental crust of Precambrian age (Fig. 27). This implies a different isotopic composition of Sr and Nd of the rocks from the source area, which are eroded by weathering processes and are transported as suspended sediment via rivers. Aeolian transport of fine grained weathering products from other regions may provide sediment as well. Thus the isotopic composition of sediments provides information on the geographical provenance as well as its transport mechanisms (Grousset et al., 1988, 1998; Nakai, 1993; Hemming et al., 1998; Asahara et al., 1999). For the western part of the SCS the general direction of the oceanic circulation patterns is from north to south in winter and south to north in summer (Fig. 28).

5.2 Samples

Sediment samples were selected in order to obtain a representative dataset along the Vietnamese coast (Fig. 27). Red River sediment, Mekong sediment and surface sediment from station 18414-3 from 21 m of water depth, considered to be composed of detritus from the Annamite chain, were selected as possible endmember samples. On the shelf, sediment

stations were selected in front of the Mekong River (18391-2), along the Vietnamese Coast in front of the Annamite chain (18401-3, 18415-2, 18416-2, 18409-3) and in the southern part of the Gulf of Tonkin (18423-2) probably receiving sediment from the Red River. Water depths of the sampling locations vary between 38 and 134 m (Tab. 10). In the following the sediment cores will be grouped and referred to as *northern cores* (18409-3, 18423-2), *central cores* (18415-2, 18416-2), *southern core* (18401-3) and *Mekong fan core* (18391-2).

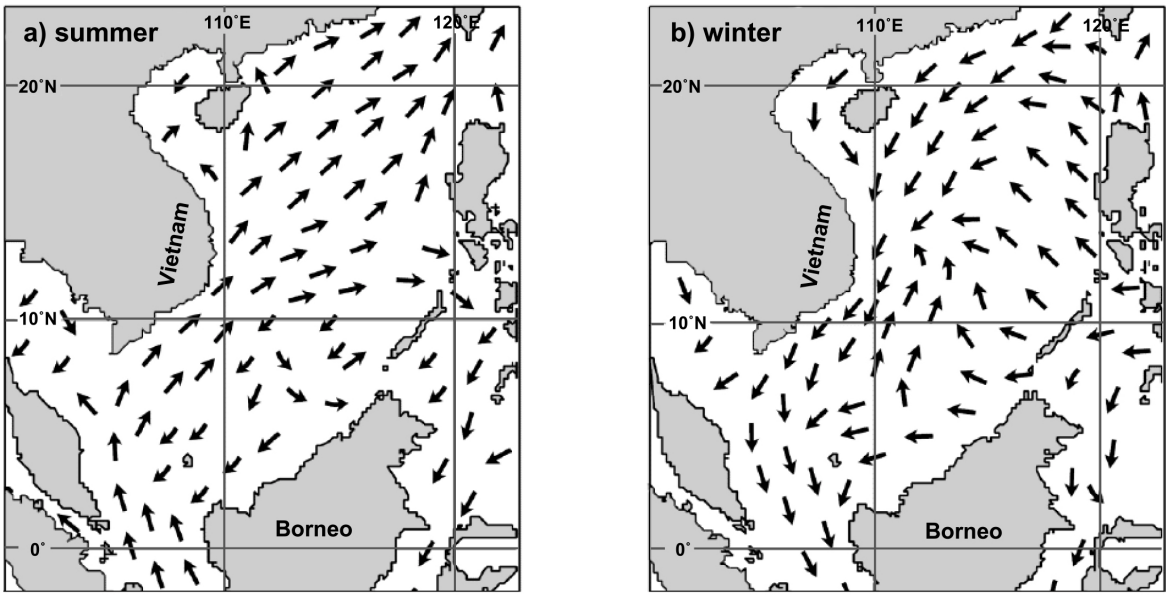

Fig. 28: *Sea-surface circulation patterns in the South China Sea. a) summer, b) winter*

Surface sediment was taken from box cores from the same stations as the sediment cores. The surface sediment is assumed to be of recent age. The cores were sampled for sediments which have been AMS-^{14}C dated previously in order to investigate deposits of late Pleistocene to early Holocene age.

Although the distribution of Sr isotopes is known to be grain size dependent (Dasch, 1969; Eisenhauer, 1999; Walter et al., 2000) bulk sediment was selected for analyses. For Nd isotopic composition this effect has not been observed and Nd isotopes can be used to constrain source regions (Walter et al., 2000). Due to a large difference in length of transport paths, especially for the possible endmember sediments, a difference in grain size results as a logical consequence. Sediments transported all the way down the Red River and the Mekong are very fine grained, while the weathering products of the Annamite chain, with extremely short transport ways and a high gradient of the rivers draining into the SCS, are extremely coarse. The investigated sediment cores are clayey to silty muds with varying percentages of terrigenous material between 63 and 99 %.

Tab. 10: *Sampling locations with Sr and Nd isotopic data of bulk sediment samples*

Core No	Latitude [°]	Longitude [°]	Water depth [m]	Depth in core [cm]	age [^{14}C years BP]	Sr [ppm]	$^{87}Sr/^{86}Sr$	Nd [ppm]	$^{143}Nd/^{144}Nd$	$\varepsilon_{Nd}(0)$
Mekong sediment	9:42.00 N	106:09.00 E		surface	recent*	79.39	0.722530	27.7	0.512090	-10.7
18414-3 (Annamite sediment)	15:05.83 N	108:57.78 E	21	surface	recent*	113.79	0.722832	26.5	0.511968	-13.1
Red River sediment	20:04.00 N	106:28.00 E		surface	recent*	80.94	0.720417	30.9	0.512058	-11.3
18391-2	9:33.91 N	108:49.60 E	115	surface	recent*	73.74	0.723252	24.7	0.512097	-10.5
18391-2				220	4900	79.36	0.720606	21.5	0.512036	-11.8
18391-2				290	6500	79.48	0.720295	22.9	0.512013	-12.2
18391-2				332	7955	82.97	0.720770	21.8	0.512047	-11.5
18391-2				360	10040	84.35	0.722979	23.9	0.512017	-12.1
18401-3	12:12.90 N	109:32.09 E	134	surface	recent*	77.88	0.727038	28.2	0.512021	-12.0
18401-3				591	9910	76.99	0.722732	22.5	0.512028	-11.9
18415-2	15:04.98 N	109: 00.03 E	38	250	7735	58.93	0.724564	16.2	0.512016	-12.1
18416-2	15:02.23 N	109:08.97 E	66	surface	recent*	46.45	0.723097	5.3	0.512029	-11.9
18416-2				490	9820	92.50	0.721481	23.8	0.512012	-12.2
18409-3	15:41.21 N	108:40.79 E	40	surface	recent*	65.90	0.730552	30.5	0.512009	-12.3
18409-3				560	8775	67.02	0.725076	26.9	0.511995	-12.5
18423-2	16:16.62 N	108:39.59 E	97	46.5	13030	71.19	0.728150	25.4	0.512019	-12.1

* surface sediments are considered to be of recent age
$\varepsilon_{Nd}(0) = [^{143}Nd/^{144}Nd_{meas}/0.512638 - 1] \times 10000$ using the CHUR value of Jacobsen and Wasserburg (1980)

5.3 Analytical Methods

5.3.1 Major Elements

Major elements were analysed on powdered samples in the Department of Marine Biogeochemistry and Paloeoceanography at the University of British Columbia (Vancouver) using XRF techniques on glass beads. The glass beads are cast from a mixture of 0.4 g of sample material and a flux (Spectroflux 105, composed of $Li_2B_4O_7$, $LiCO_3$ and La_2O_3) by heating to 1100° C for 15 min. The analyses were carried out on a Philips PW 1400 wavelength-dispersive sequential automatic spectrometer. The complete procedure is described in detail by Calvert et al. (1985).

Results were corrected for sea salt presuming a salinity of 35 psu with an average concentration of dissolved salt.

5.3.2 Sr and Nd Isotopes and Trace Elements

In this study 16 samples of bulk sediment have been investigated to detect change of sources due to modified sedimentological conditions including oceanograpy, hydrography and climate. Seven samples are from the sediment surface, reflecting recent conditions and nine samples from deeper core sections, dated to late Pleistocene to early Holocenene age, using the AMS-^{14}C technique.

Trace element and isotopic analyses were carried out during two visits at Socfac (Southampton Oceanography Centre, Large Scale Analytical Facility) at the Southampton Oceanography Centre.

Sample preparation generally followed the work of Bayon et al. (in press). They showed that exchangeable and carbonate fractions as well as Fe-Mn oxy-hydroxides have a great effect on the rare earth elements (REE) and isotopic signal. The removal of these fractions via sequential leaching led to a detrital fraction of pure continental origin.

Approximately 200 mg of the sediment were weighed into glass beakers with 10 % (v/v) acetic acid to remove the carbonate and exchangeable fractions. After four hours in an ultrasonic bath, the suspension was rinsed and centrifuged.

10 ml of a mixture of 1M hydroxylamine hydrochloride solution in 25 % (v/v) acetic acid (HH) were added to the residue in PTFE beakers to extract iron and manganese oxides. After three hours on a hotplate at 90° C the solution was centrifuged again.

The organic fraction was removed from the residue by adding 10 ml of 5 % H_2O_2 which was left on a shaker overnight. The remaining "detrital fraction" was treated with 2 ml of aqua regia to remove possible non-detrital remnants. Finally the detritus was digested on a hotplate at 170°C for 48 hours by adding a HF-$HClO_4$ (3 ml/2 ml) mixture and subsequently evaporated to dryness. To avoid the formation of fluorides further 1.5 ml of $HClO_4$ were added. After evaporation the sample was taken up in 6 ml of 6M HCl and the 'mother' solutions were ready for further processing, i. e. ICP-MS analyses and chemical separation prior to isotope analyses.

Sr was isolated from the 'mother' solution using columns filled with Sr resin (Sr spec, EiChrom Industries Inc. Illinois, USA). Prior to the separation of Nd, the REE were isolated from the major elements by cation exchange, using cation exchange resin Dowex 50W-X8 (200-400) mesh, H+ form (supplied by Merck Ltd) loaded onto small polypropylene columns. Nd was separated from the REE using HDEHP-coated teflon powder columns.

Sr and Nd isotopes were measured with a seven-collector VG-Micromass Sector 54 thermal ionization mass spectrometer with an external precision of +/-14ppm (2 s.d.) for ^{86}Sr/^{88}Sr and +/- 8ppm (2 s.d.) for ^{143}Nd/^{144}Nd. The resulting ε_{Nd} error is in the range of 0.1 units.

Isotope ratios were normalised to $^{86}Sr/^{88}Sr = 0.1194$ and $^{146}Nd/^{144}Nd = 0.7219$. The analysis of the standards NBS SRM 987 and JNdi returned a $^{87}Sr/^{86}Sr$ of 0.710243 ± 7 (2 s.d.) and a $^{143}Nd/^{144}Nd$ of 0.512109 ± 5 (2 s.d.), respectively.

Analyses of the REE were performed by inductively coupled plasma mass spectrometry (ICP-MS) using a VG Elemental PlasmaQuad 2+ (external accuracy 5% (2 s.d.), internal precision better than 3% (2 s.d.) (Barrat and Nesbitt, 1996).

5.3.3 Clay Minerals

Clay minerals show certain assemblages in dependence of the composition of the source rocks and transport media (Gingele et al., 2001). Smectite, illite, chlorite and kaolinite in the study area are mainly delivered by rivers, while aoelian transport contributes a less significant amount of dust to the sediment column (Duce et al. 1991). Variations in source and, to a lesser extent, in climate, can be obtained by the investigation of recent and early Holocene samples for their clay mineral distribution. The relative abundance of clay minerals is a function of their source rocks and transport processes. While the weathering processes of the volcanic island arc of Indonesia is likely to produce smectite (Gingele et al. 2001), the main product of physical weathering in the Himalayas are illite and chlorite (Colin et al. 1999). Colin et al. (1999) have used the smectite/(Illite+chlorite) ratio as a proxy of the intensity of chemical weathering in SW Asia.

Preparation procedures generally followed the methods of Holtzapffel (1985). The bulk sediment sample was suspended in demineralised water on a stirring plate and decarbonated by adding 0.2N HCl. The pH was continuously controlled during this process. Acid residue was washed out and an aliquot of the $<2\mu$m fraction was separated by settling method according to Stoke's law (transformed after Hotzapffel, 1985):

$$t = 190 \times X/d^2$$

Whereas t = settling time [min], X = depth of settling particles [cm] and d = diameter of settling particles [μm]

The filter transfer method (Moore and Reynolds, 1989) was used to generate oriented samples by sucking an aliquot through cellulose nitrate filters (0.2 μm pore width). After drying at 50°C the sample was transferred on an aluminium slide and measured on a Philips PW 1710 X-ray diffractometer with Cu-Kα radiation and automatic divergence slit. XRD scans were performed with a step width of 0.01° 2Θ/s in a range of 2 - 40° 2 Θ on both, untreated and glycolated (overnight at 60°C) samples.

Peak areas were calculated after manual baseline correction using the MacDiff software, version 4.2.5 (Petschik, 2000) after the techniques of Biscaye (1964, 1965).

5.4 Sedimentological Framework

Fig. 29 shows the sand and silt + clay distribution, AMS-^{14}C age and terrigenous mass accumulation rate (MAR) of cores 18391-2, 18401-3, 18416-2 and 18409-3, of which surface and downcore samples have been analyzed. The sand and silt + clay content of endmember samples and samples 18415-2 and 18423-2 with AMS-^{14}C age are as well depicted in Fig. 29. The stratigraphy of Mekong fan core 18391-2 is based on five AMS radiocarbon datings. It shows a high sand content in the range of 70 % in the upper part and a MAR around 40 g/cm²kyr slightly increasing upcore.

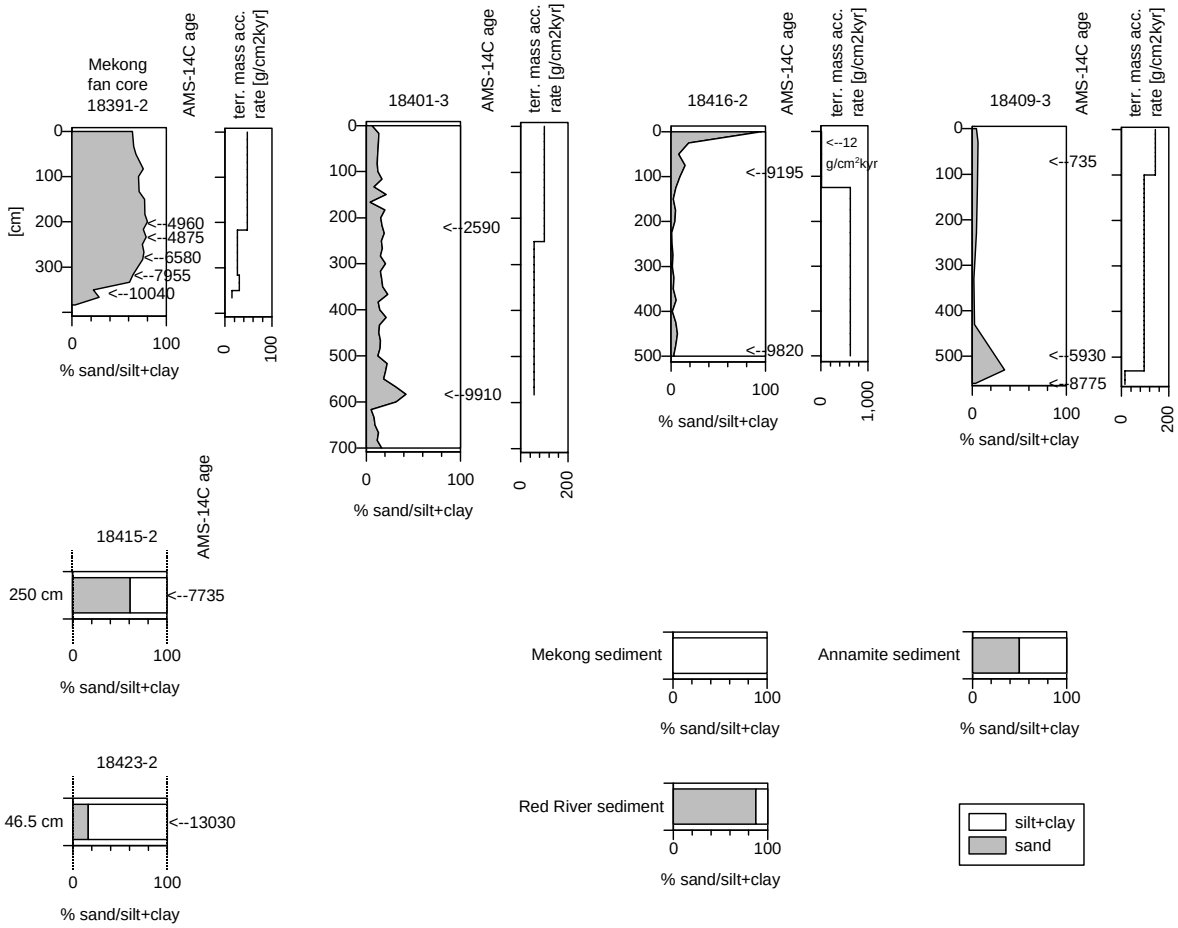

Fig. 29: *Content of sand and silt + clay with AMS-^{14}C ages and terrigenous mass accumulation rates of the sediment cores. Note that Mekong sediment consists of the manually separated silt and clay fraction*

Core 18401-3 has a relatively constant granulometric distribution of 20 to 40 % sand and a MAR of ca. 60 g/cm²kyr in the lower part and ca 100 g/cm²kyr in the upper part of the core. The core is dated by two AMS-^{14}C measurements.

The sand content of core 18416-2, which was dated on two samples with AMS-^{14}C, shows an extremely high variability between 1 % in the lower and 95 % in the uppermost part of the core. For the lower part a MAR of ca. 600 g/cm²kyr has been determined while the upper part barely returns 12 g/cm²kyr, probably due to sediment resuspension.

In core 18409-3 the granulometric distribution is dominated by silt and clay with ca 5 % sand content on the average and one single data point of ca 30 % in the lower part. Three AMS-^{14}C datings support the stratigraphic concept and the MAR lies in the range of 100 g/cm²kyr in the lower and 140 g/cm²kyr in the upper part of the core. The low values in the lowermost core section are attributable to a hiatus between the the two datings.

The two samples of core 18415-2 and 18423-2 are plotted separately. They show a dominance of 60 % sand and ca. 80 % silt + clay, respectively and have both been dated by AMS-^{14}C. The river samples show 100% silt + clay for the Mekong samples. Here the fraction $< 63\ \mu$m was separated manually prior to further processing due to a high sand content to ensure measurement of a signal from more distant regions. Red River and Annamite sediments contain about 87 % and 50 % sand.

The granulometric composition is reflected by the ratios of Fe_2O_3/SiO_2 and Al_2O_3/SiO_2 plotted in Fig. 30 with increasing ratios in the finer samples.

5.5 Results

5.5.1 Major Element Results

Results of the major elements analyses are listed in Tab. 11. Loss on ignition varies between 11 and 26 %. Samples with a high concentration in CaO are typically those with a high carbonate content. Furthermore, the highest Al_2O_3 concentrations occur in clay rich samples and correspondingly the highest SiO_2 concentrations in the coarser-grained siliciclastic samples.

Tab. 11: *Chemical composition of investigated samples*

Sample	Endmember Mekong sediment	Endmember Annamite sediment	Endmember Red River sediment	Mekong core 18391 surface	18391 220 cm	18391 290 cm	18391 332 cm	18391 360 cm
SiO_2	61.41	75.46	84.41	64.99	75	71.63	68.03	65.7
Al_2O_3	18.23	10.3	7.32	9.08	7.49	7.79	8.91	13.55
CaO	0.5	1.89	0.88	6.88	5.05	5.39	7.05	6.93
$Fe_2O_{3(tot)}$	6.99	3.79	3.62	3.6	3.06	3.2	3.61	5.15
K_2O	2.55	2.87	1.79	2.42	2.16	2.1	2.28	2.94
MgO	1.75	1.62	1.02	1.75	1.42	1.63	1.69	2.47
$Mn_3O_{4(tot)}$	0.172	0.085	0.066	0.106	0.05	0.052	0.056	0.08
Na_2O	2.03	5.35	2.83	5.79	3.43	4.35	4.69	5.5
TiO_2	0.93	0.58	0.71	0.51	0.53	0.56	0.59	0.75
P_2O_5	0.144	0.089	0.081	0.088	0.067	0.08	0.083	0.112
Total	94.71	102.03	102.73	95.21	98.26	96.78	96.99	103.18
LOI (%)	28.4	11.03	22.5	17.98	13.93	14.78	16.83	18.30
Sc 45	30.4	16.0	20.6	17.9	17.1	19.6	18.5	24.3
Co 59	8.40	4.26	4.57	5.15	4.30	4.36	5.41	7.25
Rb 85	171	136	97	145	117	115	130	173
Sr 86	79.4	113.8	80.9	73.7	79.4	79.5	83.0	84.4
Y 89	24.3	17.3	18.9	16.0	17.1	17.4	19.1	19.5
Zr 91	187	150	121	142	187	182	179	167
Nb 93	15.3	9.9	14.8	11.6	11.2	13.6	5.7	16.1
Cs 133	16.6	4.7	4.1	7.3	4.9	5.1	6.2	10.6
Ba 135	405	587	326	402	379	366	385	427
La 139	41.2	37.0	44.0	33.0	30.8	31.7	30.9	34.7
Ce 140	75.2	70.2	85.7	63.2	58.1	60.6	57.8	62.8
Pr 141	7.57	7.00	8.40	6.52	5.75	6.04	5.85	6.43
Nd 146	27.7	26.5	30.9	24.7	21.5	22.9	21.8	23.9
Sm 147	4.26	4.35	5.09	4.02	3.62	3.90	3.83	4.16
Eu 151	0.91	0.75	0.85	0.76	0.63	0.67	0.71	0.75
Gd 157	3.50	3.63	3.71	2.80	2.62	2.90	2.71	2.95
Tb 159	0.57	0.54	0.53	0.45	0.46	0.47	0.48	0.49
Dy 163	3.80	2.92	3.11	2.64	2.59	2.62	2.85	2.86
Ho 165	0.70	0.50	0.55	0.48	0.51	0.54	0.59	0.61
Er 167	2.45	1.60	1.80	1.58	1.62	1.68	1.81	1.89
Tm 169	0.35	0.20	0.24	0.21	0.21	0.23	0.25	0.26
Yb 174	2.49	1.53	1.69	1.61	1.66	1.67	1.96	1.97
Lu 175	0.33	0.20	0.20	0.21	0.21	0.22	0.25	0.26
Hf 178	4.80	4.13	3.16	3.72	4.88	4.62	4.72	4.29
Ta 181	4.42	3.66	4.73	3.83	3.72	3.71	1.63	5.57
Pb 208	12.0	13.1	9.63	10.8	9.92	9.74	9.38	10.4
Th 232	14.6	17.5	11.9	12.3	11.7	9.3	11.3	13.6
U 238	2.82	2.95	1.95	2.09	2.14	1.88	2.31	2.37
La/Th	2.83	2.11	3.70	2.68	2.63	3.42	2.74	2.56
Nd/Yb	11.1	17.3	18.3	15.4	13.0	13.8	11.2	12.1
Th/Nd	0.53	0.66	0.38	0.50	0.54	0.40	0.52	0.57
Eu/Eu*	1.11	0.89	0.92	1.07	0.97	0.93	1.04	1.01

Tab. 11 *(cont.)*

Sample	southern core		central cores			northern cores		
	18401 surface	18401 591 cm	18416 surface	18416 490 cm	18415 250 cm	18409 surface	18409 560 cm	18423 46.5 cm
SiO_2	61.33	61.05	62.09	68.13	77.22	61.58	68.32	59.59
Al_2O_3	16.55	10.4	2.92	12.9	9.08	14.45	13.4	16.77
CaO	4.91	9.13	16.39	2.3	1.64	1.62	1.24	2.46
$Fe_2O_{3(tot)}$	5.94	4.3	1.67	4.66	4	5.58	4.98	6.21
K_2O	2.93	2.22	1.18	2.71	2.22	2.69	2.72	3.28
MgO	2.69	1.98	1.43	2.04	1.35	2.23	1.8	2.31
$Mn_3O_{4(tot)}$	0.169	0.072	0.067	0.087	0.054	0.148	0.083	0.075
Na_2O	7.26	3.28	3.85	5.37	3.88	6.1	7.73	3.17
TiO_2	0.82	0.6	0.17	0.77	0.55	0.78	0.83	0.8
P_2O_5	0.139	0.092	0.064	0.11	0.062	0.114	0.084	0.091
Total	102.74	93.12	89.83	99.08	100.06	95.29	101.19	94.76
LOI (%)	18.43	19.88	23.45	14.23	12.68	16.70	15.08	16.40
Sc 45	28.1	22.6	5.39	26.1	17.6	27.7	24.9	28.1
Co 59	7.90	5.93	1.29	5.24	4.23	6.76	4.72	8.80
Rb 85	199	144	69	142	114	189	147	197
Sr 86	77.9	77.0	46.5	92.5	58.9	65.9	67.0	71.2
Y 89	22.4	18.7	4.22	20.8	12.9	24.5	22.5	23.8
Zr 91	175	181	40	177	126	184	193	186
Nb 93	17.7	13.9	3.2	15.5	11.2	17.3	15.2	17.4
Cs 133	13.2	8.3	2.0	8.7	5.8	12.4	10.0	14.8
Ba 135	466	384	306	416	374	446	390	469
La 139	39.9	31.6	7.3	32.1	22.6	42.6	37.0	36.6
Ce 140	69.9	57.5	12.7	59.8	42.1	76.4	67.7	65.5
Pr 141	7.34	5.86	1.37	6.04	4.29	7.84	6.87	6.67
Nd 146	28.2	22.5	5.3	23.8	16.2	30.5	26.9	25.4
Sm 147	4.65	3.76	0.84	3.94	2.82	4.99	4.30	4.23
Eu 151	0.83	0.64	0.21	0.72	0.49	0.80	0.72	0.78
Gd 157	3.37	2.98	0.69	3.24	2.10	3.90	3.52	3.22
Tb 159	0.56	0.49	0.11	0.52	0.36	0.63	0.57	0.59
Dy 163	3.29	2.85	0.64	3.09	2.01	3.70	3.34	3.42
Ho 165	0.73	0.63	0.15	0.66	0.43	0.78	0.72	0.78
Er 167	2.21	1.81	0.41	1.97	1.25	2.32	2.20	2.35
Tm 169	0.31	0.25	0.06	0.28	0.17	0.32	0.31	0.32
Yb 174	2.25	1.86	0.43	1.97	1.30	2.34	2.15	2.44
Lu 175	0.33	0.27	0.06	0.31	0.18	0.37	0.35	0.34
Hf 178	4.43	4.60	1.06	4.30	3.27	4.51	4.75	4.57
Ta 181	6.01	4.11	1.90	4.64	3.78	5.81	4.93	5.60
Pb 208	13.9	10.5	7.54	9.32	9.95	14.3	9.80	12.2
Th 232	17.2	12.9	3.6	10.5	8.5	17.3	12.8	15.6
U 238	3.07	2.21	0.58	2.04	1.60	3.11	2.50	2.66
La/Th	2.32	2.45	1.99	3.05	2.66	2.46	2.88	2.35
Nd/Yb	12.5	12.1	12.3	12.0	12.5	13.0	12.5	10.4
Th/Nd	0.61	0.57	0.69	0.44	0.53	0.57	0.48	0.61
Eu/Eu*	0.99	0.90	1.32	0.95	0.95	0.86	0.87	0.99

A linear plot of Fe_2O_3/SiO_2 versus Al_2O_3/SiO_2 shows the effect of mineralogical sorting (Fig. 30). The distribution pattern of sediment samples shows that finer sediments are enriched in Al and Fe and depleted in Si while the coarser sediments show contrasting compositions (Fig. 31). This systematic relationship corresponds to sorting of minerals during transport with clays in the fine grained fraction and quartz in the coarse grain fraction.

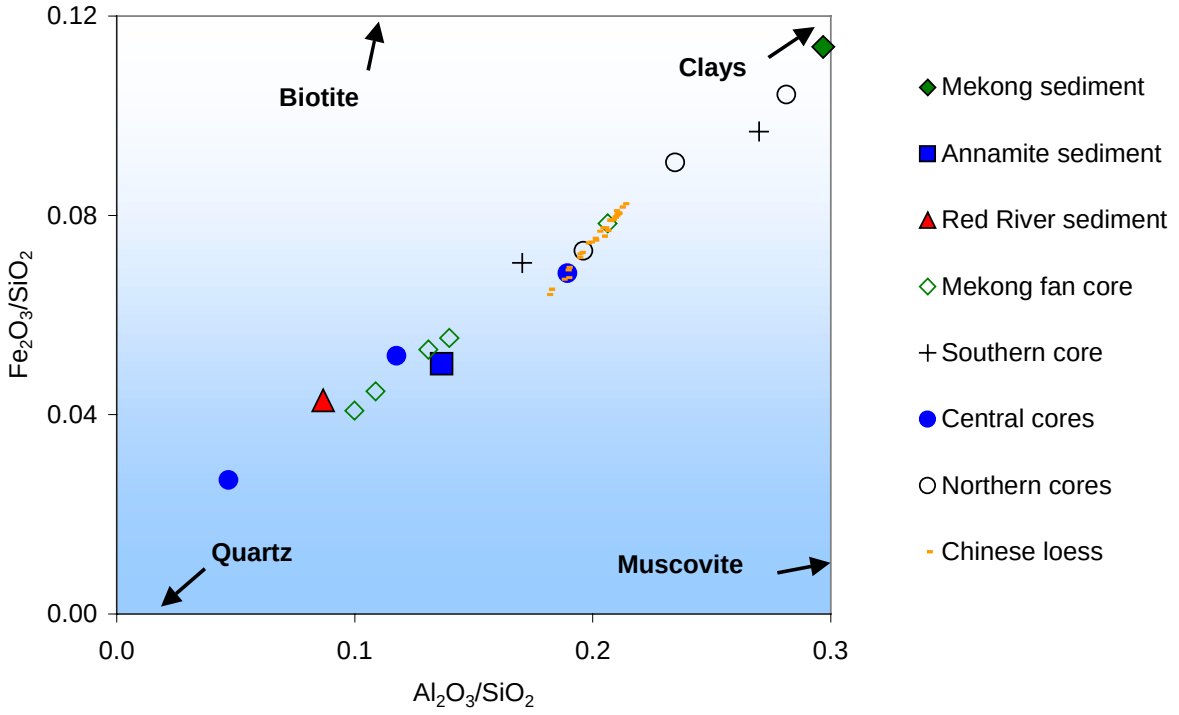

Fig. 30: *Mineralogical sorting indicated by Fe_2O_3/SiO_2 versus Al_2O_3/SiO_2. Chinese loess is shown for comparison*

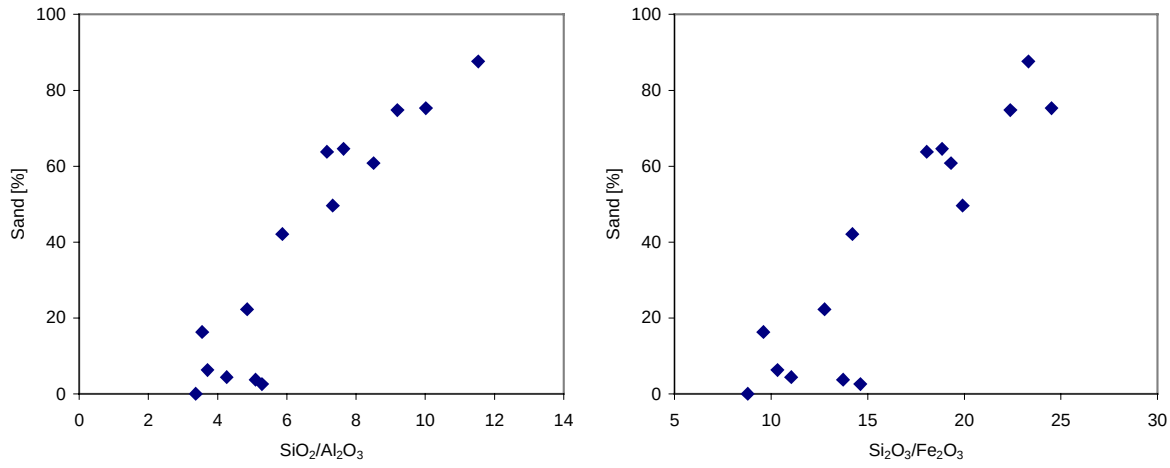

Fig. 31: *Enrichment of finer sediments in Al_2O_3 and Fe_2O_3 and depletion in SiO_2*

5.5.2 Trace Element Results

The concentrations of trace elements of the investigated samples can be found in (Tab. 11). The provenance of a clastic sediment is reflected by the composition of the rare earth elements (Fleet, 1984; McLennan, 1989). A plot of the REE normalized by post Archaean

average Australian shale (PAAS; McLennan, 1989) shows significant differences between the three river sediments (Fig. 32a). While Red River sediment is strongly enriched in light rare earth elements (LREE), Annamite chain sediment shows a slight enrichment of LREE and Mekong sediment shows a flat pattern for heavy rare earth elements (HREE). REE paterns of surface sediments from the South China Sea are presented in Fig. 32. All surface samples are enriched in LREE, whereas the northern surface sample shows the highest enrichment. Additionally a negative Eu anomaly is present in this sample. The surface sample of station 18416 has very low concentrations of REE and plots below the limits of the plotting area.

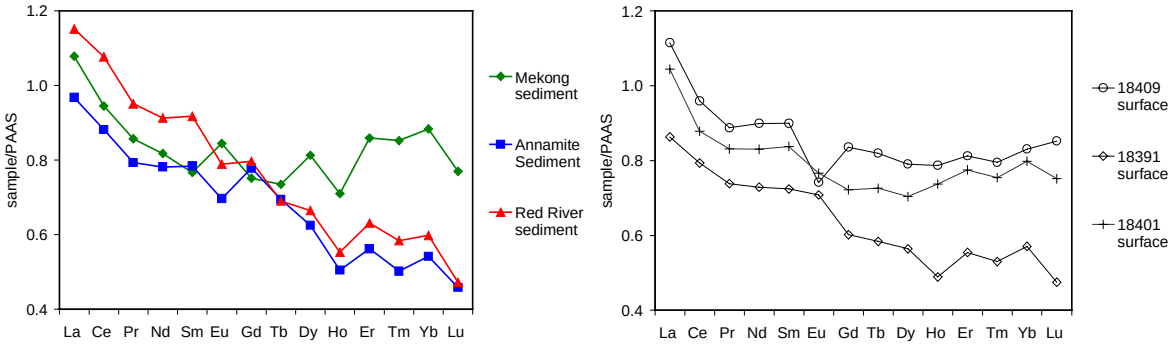

Fig. 32: *(a) Sample/PAAS of rare earth elements of the endmembers Red River sediment (red), Annamite sediment (blue) and Mekong sediment (green), (b) Sample/PAAS of rare earth elements of surface sediments. Normalizing values from McLennan (1989)*

5.5.3 Isotopic Results

Strontium and Nd isotopic data of bulk sediments, treated as described in the analytical section, are presented in Tab. 10 and Fig. 33. The samples from the rivers show clear differences in isotopic composition. The Mekong and Red River detritus have ε_{Nd} values of -10.7 and -11.3, respectively, whereas Annamite sediment shows a value of -13.1. $^{87}Sr/^{86}Sr$ ratios of the Red River sediment are with 0.720 lower than those from the Mekong and the Annamite chain with 0.723. Nd isotopic data of the sediment stations on the shelf generally lie between the river values with ε_{Nd} ranging from -10.5 to -12.5. $^{87}Sr/^{86}Sr$ ratios show larger variations with values between 0.720 and 0.730, where the higher values are confined to the *northern cores* 18409-3 and 18423-2.

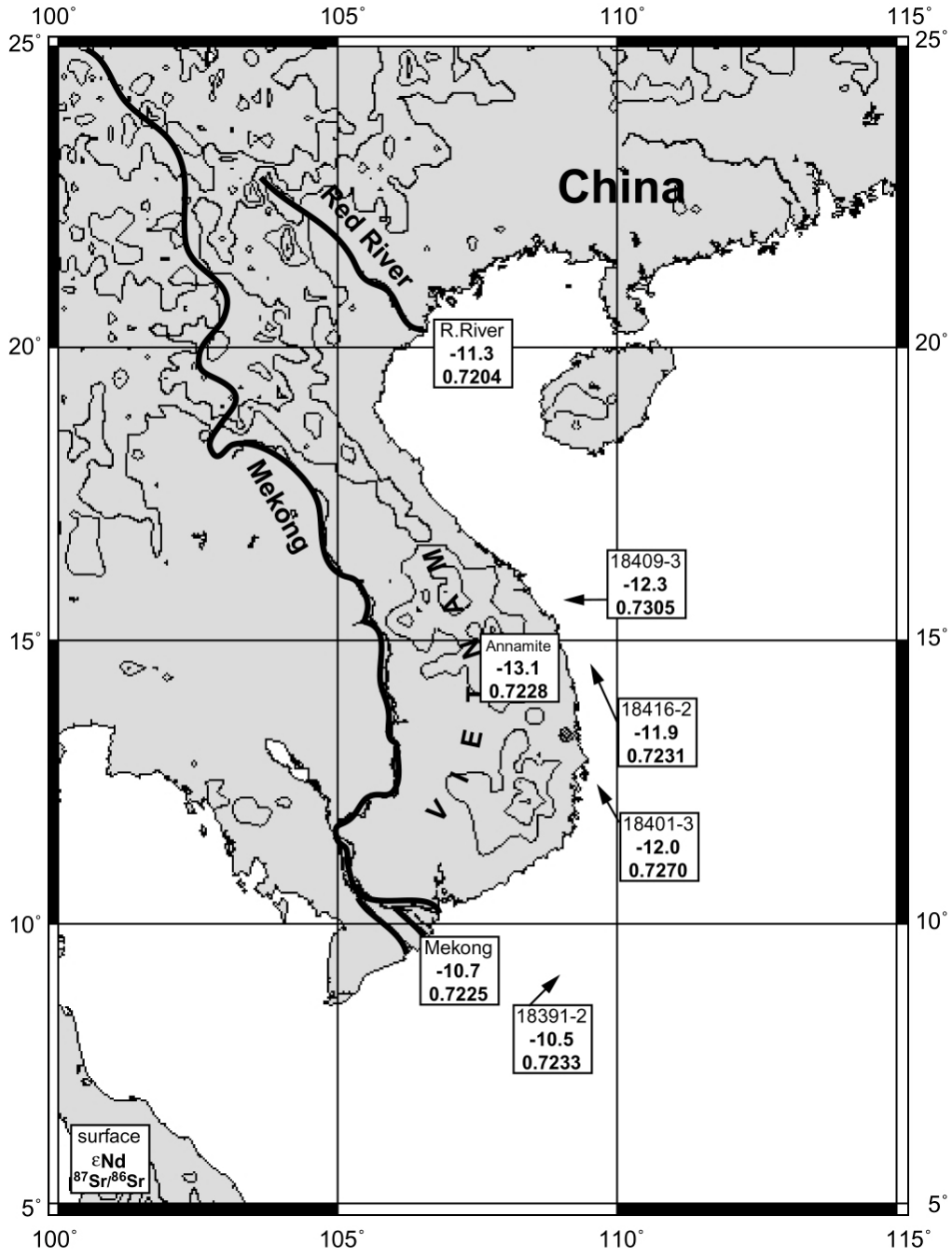

Fig. 33: *Sample locations with ε_{Nd} values and $^{87}Sr/^{86}Sr$ isotopic ratios for surface samples*

5.5.3.1 Lateral variations

The Nd isotopic value of the surface sample from the *Mekong core* with an ε_{Nd} of -10.5 plots close to the Mekong sediment (ε_{Nd} -10.3). *Southern* and *central cores* display values around -12.0 lying between the possible endmember values of Mekong and Annamite sediment. With -12.5 *northern cores* show the lowest core values, lying between those of Annamite and Red River endmembers. The $^{87}Sr/^{86}Sr$ ratios generally confirm the results from the core data, whereas some values are higher than any measured for the possible endmember sediments.

5.5.3.2 Downcore Variations

For *northern* and *central cores* a trend towards more negative ε_{Nd} values downcore is observable (Tab. 10). Samples of early Holocene age have ε_{Nd} values which are -0.2 and -0.3 ε-units lower than the corresponding surface samples of *northern* and *central cores*, respectively.

The *Mekong core* shows a decrease from -10.5 in the surface sample to -12.2 at 290 cm with an age of 6500 AMS-^{14}C years BP. This is followed by a subsequent increase to -11.5 at 7955 AMS-^{14}C years BP and a further decrease to -12.1 at 10040 AMS-^{14}C years BP.

In contrast to the general decrease of ε_{Nd} values in the latter cores, the *southern core* shows no changes. The measured values are, with -12.0 determined for the surface sample and -11.9 for sediment from 590 cm (dated to 9910 AMS-^{14}C years BP), within the error range.

^{87}Sr/^{86}Sr ratios are disperse and a correlation with the results of the Nd isotopic analyses can only be observed in the *southern core*. Grain size dependence of the samples is obvious from Fig. 31. Fine grained samples show a more radiogenic ^{87}Sr/^{86}Sr ratio than the coarse grained ones.

5.5.4 Clay Mineralogy Results

5.5.4.1 Lateral Variations

The clay mineralogical composition shows variations from north to south (Fig. 34). Considering the large uncertainty of the analytical method, results have been rounded to 5 % intervals (Tab. 12). The most abundant clay mineral in all samples is illite with percentages between 40 an 75 %. While illite content is highest in the Red River sample with 75 %, all other samples show values lower than 55 %. The lowest illite content (40 %) was observed in core 18416-2, which lies in the direct influence of the Annamite chain. Smectite contents vary between 0 and 20 % with the lowest value in Red River sediment and the highest value in core 18416-2. Kaolinite content shows not much variation with values between 20 and 30 % (Annamite sediment 30 %) and one lower value of 10 % measured on Red River sediment. Chlorite content ranges from 15 to 25 % with the lowest value in Red River sediment and the highest in Mekong fan sediment. Due to insufficient sample material, a Mekong River sample could not be measured and a value for the Mekong area from the literature (Chen, 1978) is presented for reference.

Tab. 12: *Clay mineral composition and smectite/(illite+chlorite) ratio of Vietnamese Shelf sediments*

Core No	Depth in core [cm]	Smectite [%]	Illite [%]	Kaolinite [%]	Chlorite [%]	Smectite/(Illite+Chlorite) [%]
Mekong area*	surface	10	47	20	23	0.14
18414-0	0	4	46	30	20	0.05
RRB	surface	1	75	8	16	0.01
18391-2	0	2	50	24	25	0.02
18391-2	220	7	48	24	20	0.10
18391-2	290	9	48	22	21	0.14
18391-2	332	21	38	20	21	0.35
18391-2	360	9	51	21	20	0.13
18401-3	591	13	44	21	23	0.20
18404-3	0	8	46	24	22	0.12
18416-2	0	20	38	25	18	0.35
18416-2	490	10	51	21	18	0.14
18409-3	0	5	56	22	17	0.07
18409-3	560	8	51	27	14	0.12
18423-2	46.5	10	50	21	19	0.14
18426-2	0	4	46	26	23	0.06

all samples glycolated, *Mekong area composition taken from Chen (1978)

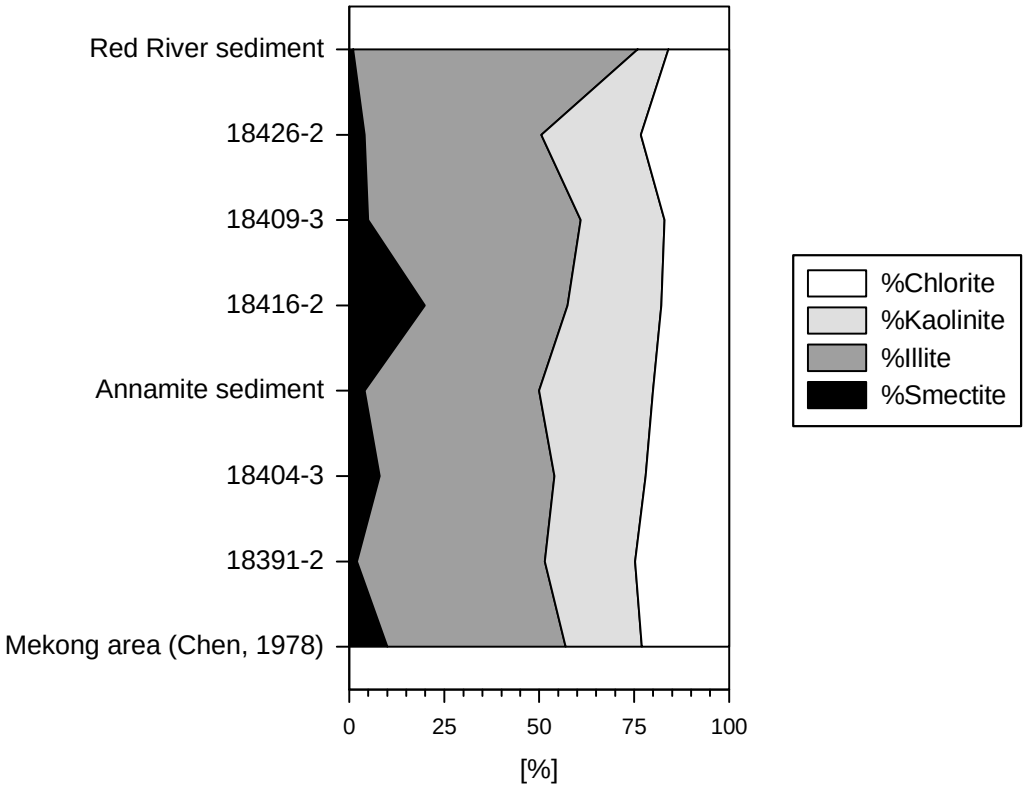

Fig. 34: *Clay mineral distribution in surface sediments from the Vietnamese Shelf from north to south*

5.5.4.2 Downcore Variations

Variations in clay mineralogy in core 18391-2 are confined to a higher smectite value in a core depth of 332 cm. All other clay minerals show no changes in distribution (Fig. 35). Illite, kaolinite and chlorite contents are in the range of 50 %, 20 % and 20 %, respectively. Smectite content is lower than 10 % with one outlier of 20 %. The smectite/(illite+chlorite)

ratio, which is used as a proxy of the intensity of chemical weathering, shows an increase downcore, with the highest value in core depth of 332 cm.

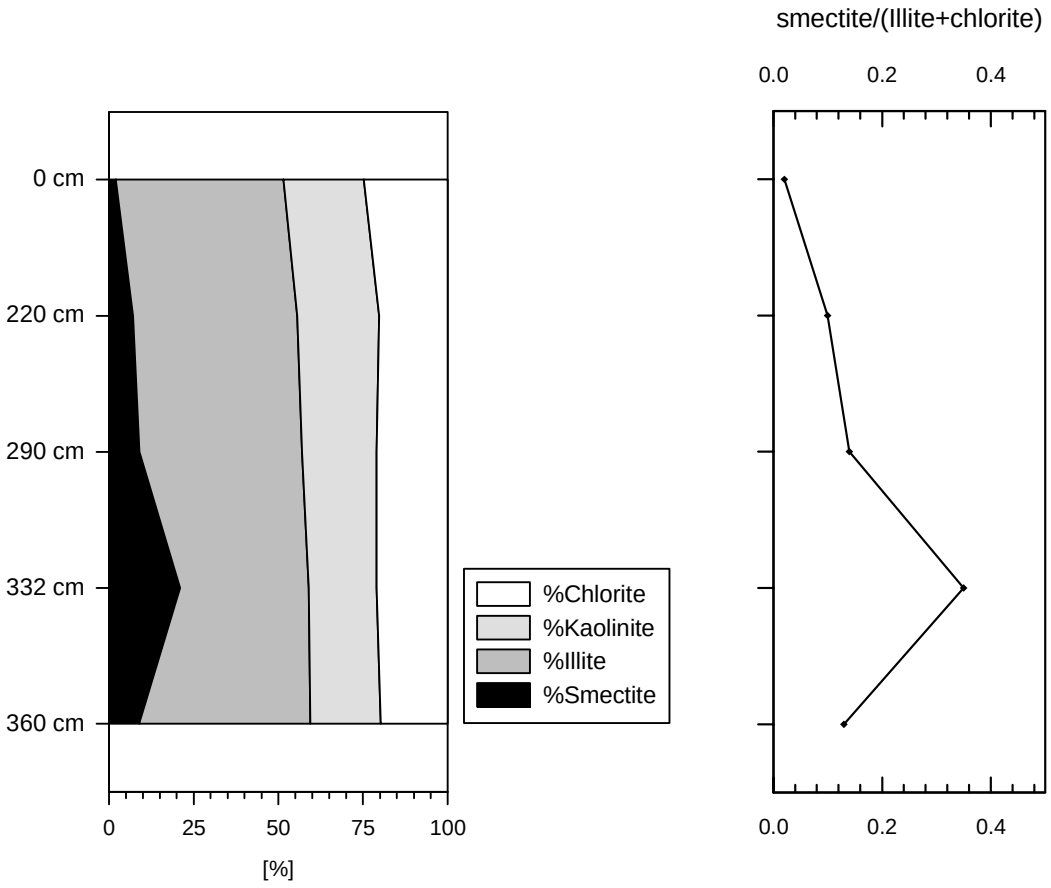

Fig. 35: *Clay mineral distribution in core 18391-2 and smectite/(illite + chlorite) ratio*

5.6 Discussion

5.6.1 Potential Sources of Terrigenous Sediment on the Vietnamese Shelf

Source regions for terrigenous sediment on the Vietnamese Shelf are the drainage basins of the rivers draining into the South China Sea along the Vietnamese coast, namely the Mekong, the Red River, and the numerous small mountainous rivers. While Mekong and Red River drain predominantly regions of Mesozoic to Cenozoic age formed in the course of the Himalayan Orogeny, the small mountainous rivers drain the Annamite chain, which contains crustal elements of Precambrian age (Fontaine and Workman, 1997; Lan et al., 2000; Nagy et al., 2001). Aeolian supply is a further potential source for detrital sediment as well as small rivers north of the Annamite chain, partly draining areas with higher differentiated rocks. The isotopic results of $^{87}Sr/^{86}Sr$ versus ε_{Nd} are presented in Fig. 36. ε_{Nd} values of Vietnamese Shelf sediments plot between the values of the possible endmember river sediments, while $^{87}Sr/^{86}Sr$

isotopic data are in part higher than those of river sediments. As shown in Fig. 37, the grain size dependence of Sr isotopes may be responsible for this and high $^{87}Sr/^{86}Sr$ ratios may be due to high clay contents of the samples. Fig. 37 shows a positive correlation of Al_2O_3/SiO_2 with $^{87}Sr/^{86}Sr$, whereas the Al_2O_3/SiO_2 ratio represents the grain size of the sample with high values for clays (high Al_2O_3, low SiO_2) and low values for sand (low Al_2O_3, high SiO_2). Sample 18416-2 (0 cm) shows unusual values (lowest Al_2O_3/SiO_2) due to a very high sand content. Various amounts of marine carbonate in the samples which have possibly not been removed completely during sample preparation may be responsible for unusual results. But regarding high $^{87}Sr/^{86}Sr$ ratios of the samples ($^{87}Sr/^{86}Sr$ = 0.720 - 0.730) compared to the seawater value ($^{87}Sr/^{86}Sr$ = 0.709), an influence of other sources seems more probable.

Another possible source for higher $^{87}Sr/^{86}Sr$ ratios than the three possible endmember sediments are gneisses and leucogranites from northern Vietnam (Zhang and Schärer, 1999) or Chinese loess (Jahn et al., 2001). The 'country gneisses' described by Zhang and Schärer (1999) as higher differentiated rocks, are abundant along the Ailao Shan - Red River shear belt in northern Vietnam and possibly influenced the samples of the northern cores. The REE pattern of the sediments from the northern cores supports higher differentiated rocks as source because the LREE are enriched (Fig. 32b) and the northern core 18409-3 shows a negative Eu anomaly with values of 0.86 and 0.87 (Tab. 11).

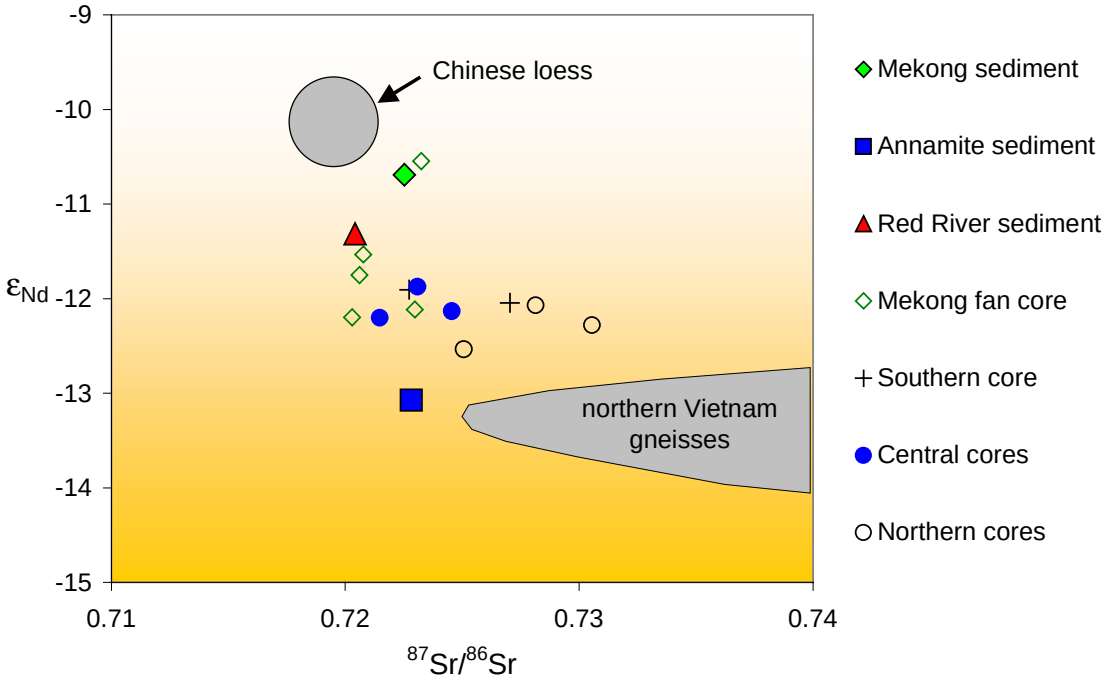

Fig. 36: *Sr and Nd isotopic composition of the investigated sediments*

Eu anomalies are also present in gneisses and leucogranites from northern Vietnam. Further sources could be granites and granodiorites of central Vietnam (Nagy et al., 2000) which show similar REE patters. The relatively flat REE pattern, observed in Mekong sediment (Fig. 32) and the Mekong fan core can be explained by sampling of a very large drainage basin area with many different potential sources, resulting in such a flat REE pattern similar to average continental crust (cp. Goldstein and Jacobsen, 1988). Furthermore, ε_{Nd}-values and $^{87}Sr/^{86}Sr$ of Mekong sediment plots close to the average signature of chinese loess (Fig. 36), which should as well possess an average continental crust signal. The influence of chinese loess with an average $^{87}Sr/^{86}Sr$ of ca. 0.715 to 0.718 and ε_{Nd} ranging around -10 could bias the isotopic signal of the investigated sediment towards the upper left corner of Fig. 36 (Jahn et. al, 2001).

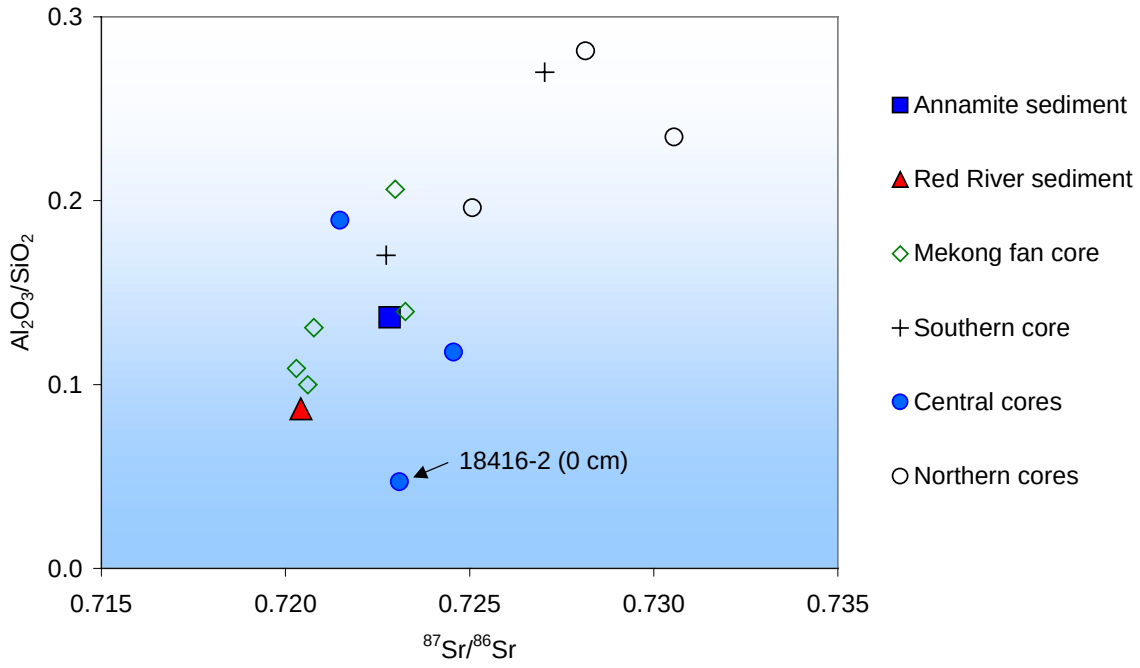

Fig. 37: *Positive trend of Al_2O_3/SiO_2 versus $^{87}Sr/^{86}Sr$, indicating grain size dependence of Sr isotopic composition*

Aeolian sediments may contribute a considerable amount of the material in SCS deposits (Wiesner et al, 1996). A dust flux (mineral aerosols) of 1 g/cm^{2}kyr has been estimated by Duce et al. (1991). For the study area the most probable source of aeolian sediment is eastern Asia with the Chinese loess plateau (Duce et al., 1991; Rea, 1994; Asahara et al.; 1999; Jahn et. al, 2001). The geochemical signature of Chinese loess (Jahn et. al, 2001) as a representative source for aeolian sediment is shown in Fig. 36 and Fig. 38. In both diagrams loess plots in the vicinity of the Mekong endmember and would bias the geochemical signal

of the analyzed samples towards this value. Due to the relative coarseness and low clay content of some samples (Fig. 29) the influence of aeolian dust in these samples is low.
Compared to the mass accumulation rates determined for the samples of this study, which are in the range of 20 to 600 g/cm^{2}kyr the influence of the quantity given by Duce et al. (2001) seems negligible. However, sediment stations on the Vietnamese Shelf with minimum MAR of 6 to 12 g/cm^{2}kyr (cp. chapter 4) could contain up to 16 % of aeolian dust.
In a Nd/Yb versus La/Th diagram most sediment samples from the shelf lie close to a mixing line between Mekong and Annamite sediments (Fig. 38), suggesting mixing of sediment from the two possible endmembers. The Red River sediment lies aside the general trend and has only minor influence on the sediments in the study area. Mixing calculations indicate that up to 40 % of the investigated deposits were delivered from the Annamite mountains. While surface samples of northern, central and southern cores indicate a strong influence of Annamite sediment, the surface sample of the Mekong fan core lies nearly congruent with the Mekong river sediment.

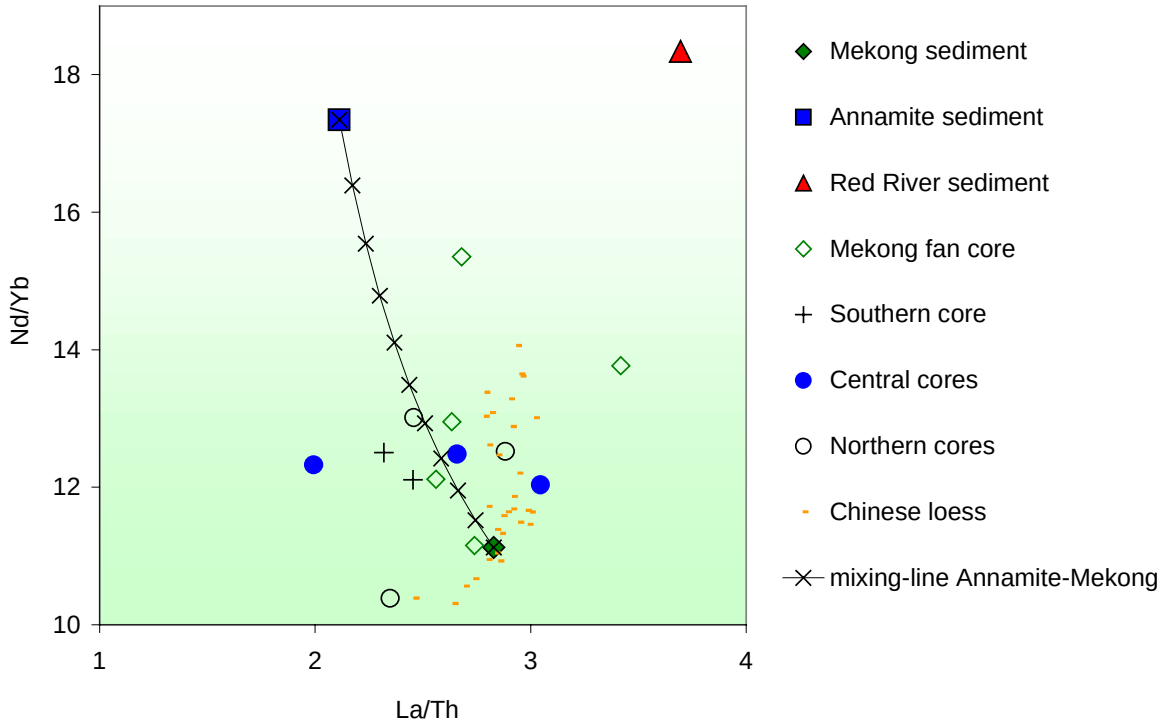

Fig. 38: *Discrimination diagram for Vietnamese Shelf sediments using Nd/Yb versus La/Th. Note that the Red River endmember lies far away from the composition of the other sediments. Tick marks show 10 % increments*

However, looking at potential mixing of sediments on the basis of Nd isotopes, a Th/Nd versus ε_{Nd} diagram shows a stronger influence of the Annamite endmember in the sediments from the study area (Fig. 40). Surface sediments of the northern, central and southern cores

contain up to 60 % of sediment with Annamite signal. Again the surface sample of the Mekong fan core plots very close to the Mekong endmember, implying a composition similar to present-day Mekong sediment, while older sediments indicate a stronger influence of Annamite sediment.

Sediments of the Annamite chain are not only transported in eastward direction directly into the South China Sea, but also in westward direction into the Mekong (Fig. 26). Sediment of the Mekong mouth should thus be partly composed of sediment with Annamite signature. Fig. 39 indicates mixing of upper Mekong sediment with Annamite sediment resulting in a signal for Mekong 'mouth' sediment (Mekong river sediment) between the two latter compositions. The mixing line indicates that Mekong 'mouth' sediment contains between 30 and 40 % of Annamite sediment. The slight deviation of Mekong mouth sediment from the ideal mixing line between upper Mekong sediment and Annamite sediment could be attributed to the influence of other sources in the lower course of the Mekong.

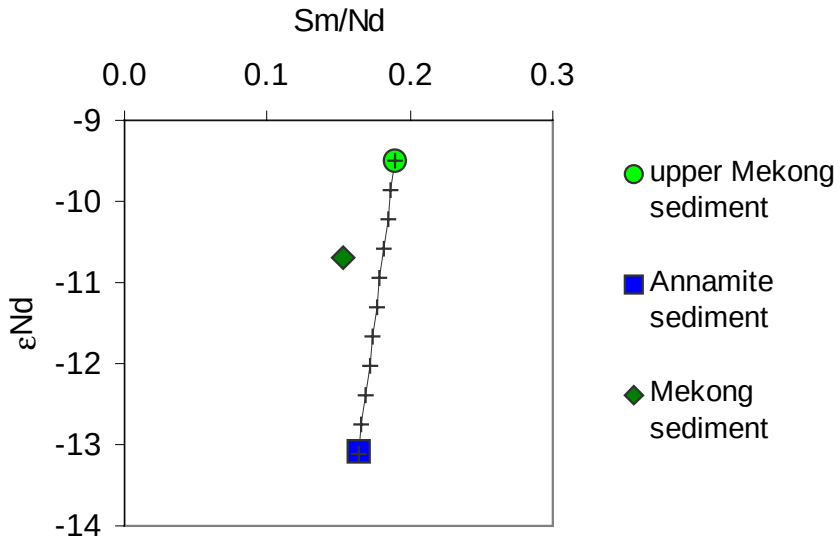

Fig. 39: *ε_{Nd} versus Sm/Nd diagram, indicating mixing of Annamite sediment with upper Mekong sediment. Tick marks indicate 10 % increments*

The composition of clay minerals generally supports the above stated provenance indications. Illite, the main product of physical weathering, represents the largest part of the clay minerals. The highest illite content of 75 % in Red River sediment is attributable to a short transport path and thus, with limited soil residence time little subsequent chemical weathering of illite, mirrored in almost non-existent smectite content. The Red River sample is the only sample with an illite content higher than 55 %. The lower illite content of the Mekong area sample (taken from Chen, 1978) and the Mekong fan core (18391-2), could be

explained by the much longer transport ways and thus enhanced weathering from Himalayan minerals and illite to kaolinite and smectite.

Core 18416-2, which is neighbouring the Annamite sediment sample and in direct influence of the Annamite chain, shows with 25 % the highest smectite values in the study area. Probably, weathering of granodioritic and basaltic formations within the Annamite mountains is responsible for this. Degradation from illite seems unlikely since soil residence times are too short due to the high gradient of the hinterland.

Generally, the high illite content of Vietnamese Shelf samples can be interpreted as a result of primarily physical weathering, either in the Himalayan or in the Annamite mountains.

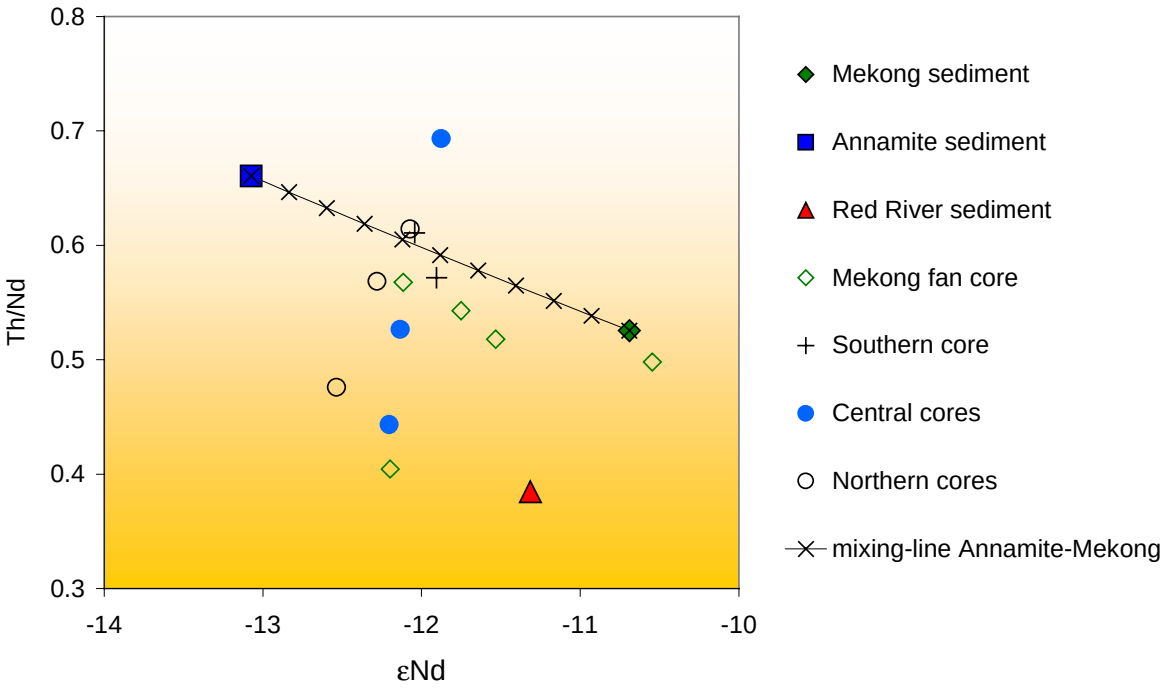

Fig. 40: *Discrimination diagram for Vietnamese Shelf sediments using Th/Nd versus* ε_{Nd}.

5.6.2 Composition of Mekong Sediment

Approximately 13 % (100 000 km^2) of the catchment area of the Mekong River lie in the area of the Annamite chain. With high precipitation rates on the western side of the Annamite mountains, this area contributes about 25 % of the total annual water flow of the Mekong River (Pantulu, 1986; Fedra et al., 1991). The steep rising mountains of the Annamite chain with a catchment area contributing to the Mekong River have an annual sediment yield of about 1000 t/km^2 (minimum value; Sharma, 2000). Thus, they provide large amounts of Annamite sediment to the Mekong River, which could bias the geochemical signal towards the Annamite endmember signal. Calculating the sediment load for Annamite rivers with a

catchment area of 100 000 km^2 and a sediment yield of 1000 t/km^{2}yr results in a value of 100 x 10^6 t/yr. This amount of sediment is contributed by the Annamite rivers draining in westward direction into the Mekong. The Mekong with a total catchment area of ca. 790 000 km^2 and a total sediment yield of 200 t/km^2/yr delivers approximately 160 x 10^6 t/yr of sediment to the SCS (Milliman and Meade, 1983). Thus the amount of sediment delivered to the South China Sea by the Mekong is strongly influenced by sediment from the Annamite mountains. Of course deposition of sediment in flooding areas along the course of the Mekong has to be assumed, so that the real influence of Annamite sediment on the Mekong budget is probably lower.

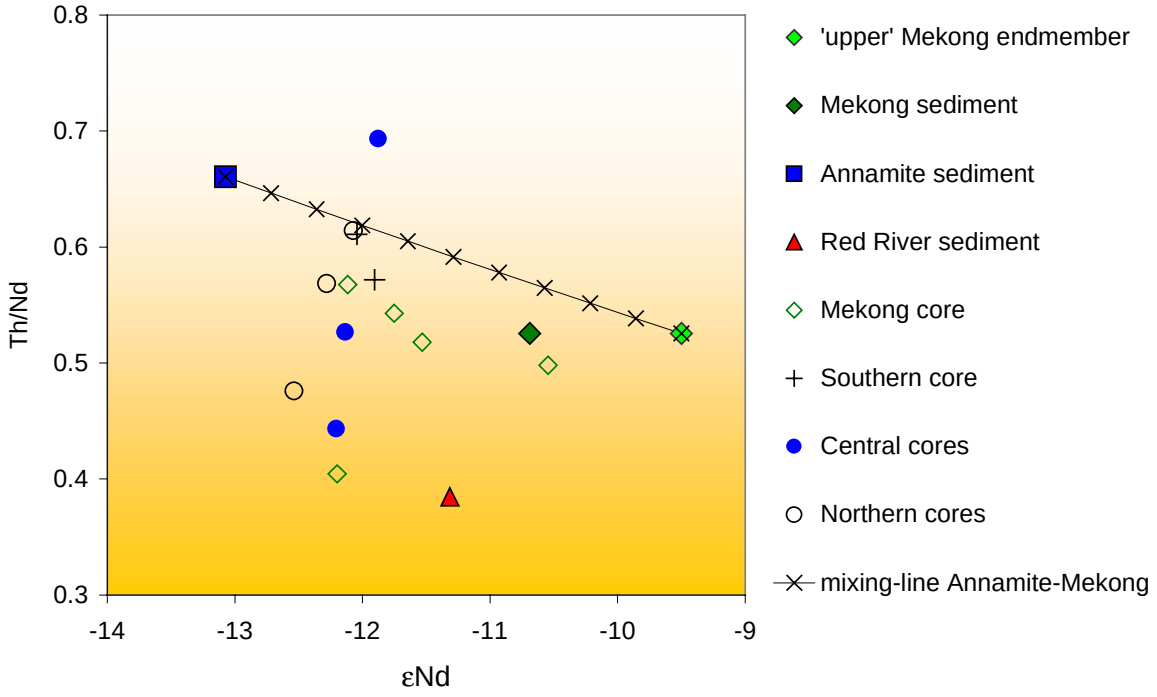

Fig. 41: *Modified mixing line between Annamite endmember sediment and upper Mekong endmember sediment using the ε_{Nd}-value of Goldstein et al. (1984). Tick marks are 10 % increments*

ε_{Nd} values for Mekong sediment from Cambodia show a value of - 9.5 (Goldstein et al., 1984) referred here as upper Mekong endmember. The ε_{Nd} for Mekong river mouth sediment determined in this study is -10.7. The negative shift of 1.2 ε-units could be explained by an influence of Annamite Rivers with an endmember ε_{Nd}-value of -13.1. Assuming only 35 % (compared to more than 50 % on the base of the calculations above) of Annamite sediment as contributor for the total Mekong sediment load, would result in an ε_{Nd}-value of -10.7, as it was measured for Mekong delta sediment. As shown in Fig. 39, mixing of upper Mekong

sediment with Annamite sediment can be assumed and thus it can be concluded that about one third of the total Mekong sediment load is composed of Annamite sediments.

Assuming the upper Mekong sediment with an ε_{Nd} of -9.5 (Goldstein et al., 1984) as the 'true' Mekong endmember leads to a new mixing line in Fig. 40 and the sedimentary composition of the samples between the Annamite and the Mekong endmember would shift relatively towards the Annamite endmember (Fig. 41). Due to a lack of data the Th/Nd ratio has been adopted from the Mekong 'mouth' sediment and mixing of 'upper' Mekong sediment with Annamite sediment has been shown in a Sm/Nd versus ε_{Nd} plot in (Fig. 39). On the average the sediments from the northern, central and southern cores are composed of at least 70 % Annamite sediment, based the above calculations. Sediments from the Mekong fan core show a stronger Mekong influence and will be discussed in the following part.

5.6.3 Temporal Variations and Possible Climatic Fluctuations during the Holocene

As can be seen in Fig. 38 and Fig. 40, the Nd/Yb ratio and the ε_{Nd} value of downcore samples of the Mekong "fan" core vary notably. These temporal variations are emphasized in Fig. 42. These variations could be due to either changing volumes of sediment from the Mekong or a variation of Mekong sediment composition. Climatic changes in the source region would imply changes in sediment yield, either for the total Mekong catchment area or on a regional scale. The endmember values of representative sediments from various source regions (Mekong mouth endmember, Annamite endmember and 'upper' Mekong endmember) are shown at the core top in Fig. 42. The Mekong endmember characterizes detritus from the entire Mekong basin, while the Annamite endmember reflects sediment originating from the Annamite chain and 'upper' Mekong sediment represents detritus from the Mekong basin excluding a large part (ca. 30 %) of Annamite derived sediments as shown before.

The ε_{Nd} data of Mekong endmember and and recent sediments from the Mekong fan core show similar values around -10.5. Downcore samples dated to ca. 4900 and 6580 AMS-^{14}C years BP, respectively, favor an increased influence of Annamite sediments on the location of the Mekong fan core. This could be explained by increased SW-monsoon in the source area, which was also observed by Maxwell (2001), who found monsoon intensification in lake sediments from northeastern Cambodia close to the Annamite mountains for the time span from 8400 - 5300 ^{14}C years BP.

A monsoon intensification would have resulted in higher precipitation in the Annamite mountains and would have resulted in a higher sediment yield of this source area. Core 18416-2 (cp. chapter 4) from the narrow shelf in front of the Annamite chain shows high (~600 g/cm²yr) mass accumulation rates between 9820 and 9195 ^{14}C years BP, which could have been caused by intensified SW-monsoon as well. Intensified summer monsoon in SE-Asia and the eastern Arabian sea has been reported by numerous authors (Sirocko et al., 1993; Sirocko et al., 1996; Feng et al., 1999; L. Wang et al., 1999; Goodbred and Kuehl, 2000; Sarkar et al., 2000) for the early Holocene (10000 - 7000 years BP).

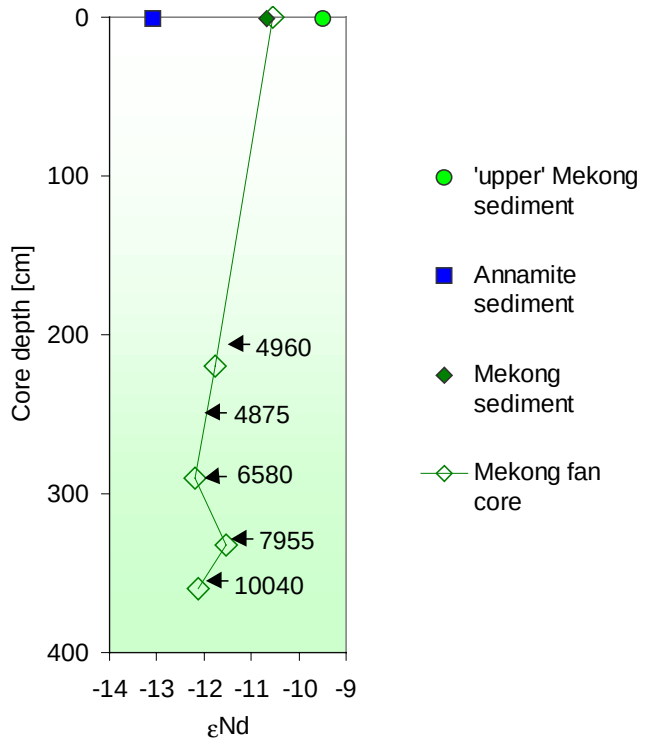

Fig. 42: *Downcore variations in Mekong fan core 18391-2: ε_{Nd} versus depth with AMS-^{14}C ages. At the core top, potential endmember values (Annamite sediment, Mekong sediment and 'upper' Mekong sediment (Goldstein et al., 1984) are given for comparison*

A Mekong fan core sample further downcore dated to 7955 ^{14}C years BP returns a higher ε_{Nd}-value indicating reduced Annamite sediment deposition or increased influence of 'upper' Mekong sediment on the core location. The deepest sample of the core, again, yields a more negative ε_{Nd} favouring the Annamite mountains as an important source for Mekong sediment. This change could probably be caused by monsoonal variations in the source areas of the Annamite chain and the Tibetan Plateau.

Although there is not much variation, the composition of clay minerals in core 18391-2 possibly supports the theory of intensified SW-monsoon over the Annamite region. The elevated smectite content in the lower part of the core could be attributed to intensified chemical weathering of granodiorites and young basalts which are present in the southern part of the Annamite chain (Fig. 27). A further possibility is the weathering of illite, as primary mineral derived from physical weathering, to smectite. With a sufficient soil residence time

(Singer, 1984) in the flood plains of the Mekong river. The unchanged abundance of chlorite in 332 cm core depth weakens this theory, since chlorite usually weathers before illite. The smectite/(illite + chlorite) ratio of clays in core 18391-2 speaks for increased chemical weathering in early Holocene times which could have been caused by intensified SW-monsoon in the region.

5.7 Conclusions

The provenance and distribution of recent sediments on the Vietnamese Shelf have been investigated on the basis of geochemical and isotopic variations of river sediments and a representative core-set from the shelf along a traverse from north to south.

Furthermore the geochemical evolution of sediments from an AMS-^{14}C dated core in front of the Mekong river has been investigated to reveal variations in the source area during the Holocene

(1) Endmember sediments from the Red River, Mekong and the Annamite mountains, show different geochemical and Sr- and Nd-isotopic compositions, which allow the discrimination of the source areas contributing sediment to the sampling locations investigated in this study.

(2) The data of the investigated samples lie between the values of the three defined endmember river sediments. ε_{Nd} values of the endmembers corner the values of the core samples while the $^{87}Sr/^{86}Sr$ ratio shows a higher variability.

(3) The $^{87}Sr/^{86}Sr$ ratio is grain size dependent with more radiogenic values in fine grained samples, but an influence of other sources which probably bias the Sr isotopic signal towards extreme values, cannot be excluded. Those potential sources are higher differentiated rocks like gneisses and granites from northern Vietnam or Chinese loess.

(4) Discrimination diagrams using trace elements show that Red River sediment is an unlikely source for sediments on the Vietnamese Shelf. The main feeders for sediments on the Vietnamese Shelf are the Mekong and the small mountainous rivers draining the Annamite mountains.

(5) Assuming an influence of Annamite sediments on the composition of Mekong sediment (30 %), and thus a 'contamination' of Mekong sediment, the sediments on the Vietnamese Shelf are mainly delivered by the small mountainous rivers of the Annamite chain. They provide at ca. 70 % of the total sediment deposited.

(6) Aeolian sediment input is negligible due to high mass accumulation rates caused by riverine input.

(7) Nd- isotopic variations during the Holocene in Mekong core 18391-2 suggest stronger erosion in the Annamite mountains during the early Holocenen probably due to an intensified SW-Monsoon.

(8) The clay mineral composition supports the results from the geochemical investigations concerning provenance. A high Illite content in all samples probably reflects physical weathering of rocks from the Himalayas and the Annamite mountains. The Red River sample has very high illite content due to short transport paths.

6 A Conceptual Sediment Budget for the Vietnamese Shelf: Mekong and Red River versus Small Mountainous Rivers

6.1 Introduction

Worldwide, rivers contribute ca. 20 x 10^9 tons per year of sediment to the oceans. About 70 % of this sediment origins from southern Asia and islands in the Pacific and Indian Oceans (Milliman and Syvitzki, 1992). High precipitation due to the Monsoon and steep gradients result in extremely high sediment yields in this region.

Along the Vietnamese Coast two of the major world rivers flow into the South China Sea (SCS). In the North, the Red River with a sediment load of 130 x 10^6 t/yr and building up a huge delta system, drains onto the wide shelf of the Gulf of Tonkin.

In the South, the Mekong builds up a large delta complex and discharges annually 160 x 10^6 t of sediment onto the wide vietnamese part of the Sunda Shelf (Fig. 43).

Between the two major rivers hundreds of small mountainous rivers drain into the SCS, contributing large amounts of sediment onto the narrow shelf (Wiesner et al., 1999; Schimanski and Stattegger, 2001, cp. previous chapters of this work). Other authors fortify the importance of small mountainous rivers in the tropics as major contributors of sediment to the world's oceans (Milliman and Syvitzki, 1992). Up to now, detailed studies concerning sediment flux from small mountainous rivers in the southeast Asian region do not exist. The fact that mountainous rivers draining South Asia and Oceania have much greater sediment yields (2-3 fold) than rivers draining other mountainous areas and the assumption that rivers of Asia and Oceania contribute up to 70 % of the total sediment discharged by rivers to the worlds oceans (Milliman and Meade, 1983; Milliman and Syvitzki, 1992) makes a study in this region even more appealing.

Core data from 25 sediment cores from the Vietnamese Shelf and more than 1000 miles of shallow seismic profiling, provide a profound database for the characterization of the shelf as sediment sink.

A limited number of publications on the Mekong as sediment source exists (Carbonnel and Meybeck, 1975; Milliman and Meade, 1983; Pantulu, 1986; Milliman and Syvitzki, 1992; Wolanski et al. 1998; Nguyen et al., 2000; Ta et al. in press), whereas publications on the Red River are sparse (Milliman and Meade, 1983; Milliman and Syvitzki, 1992; Mathers and Zalasiewicz, 1999). Published river data on the sediment discharge of the small mountainous rivers along the vietnamese coast do not exist.

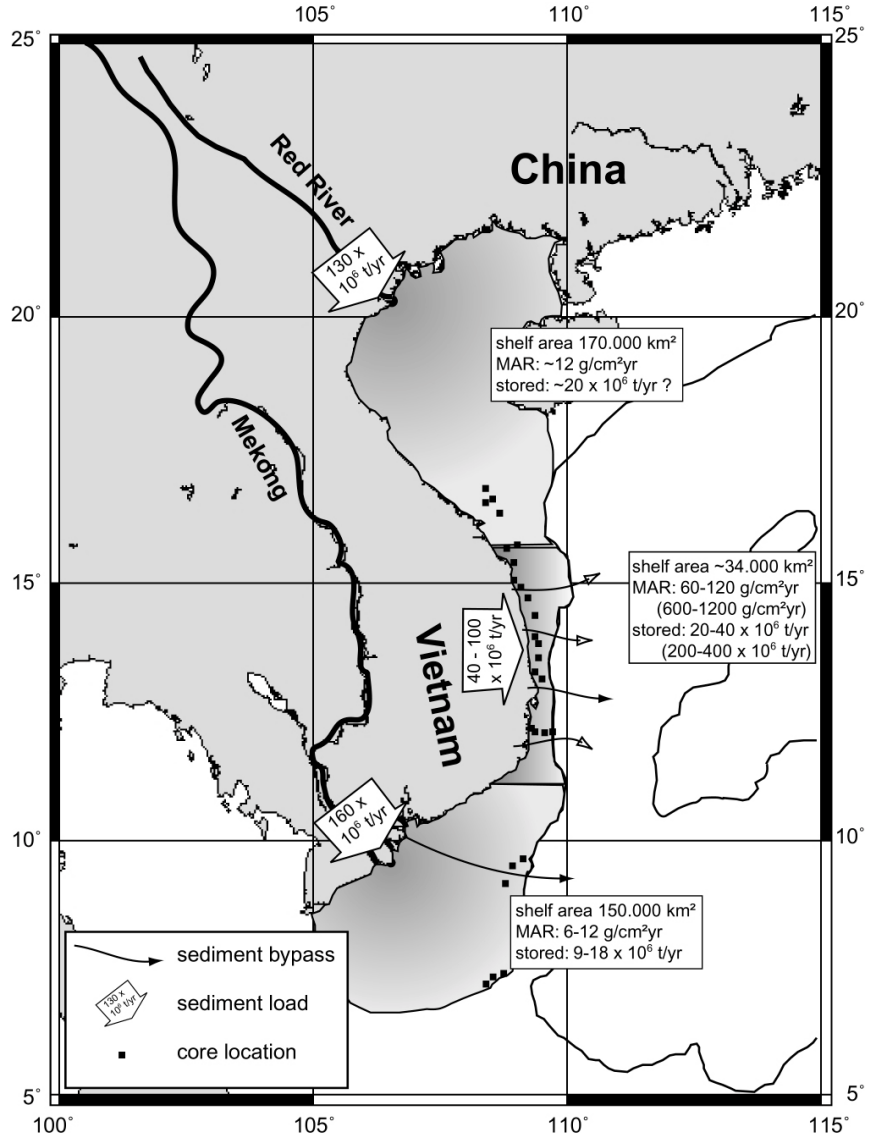

Fig. 43: *Study area with core locations, sediment sources and sediment sinks*

In the previous chapter, sediment sources (Mekong, Red River and small mountainous rivers) have been characterized and their influence on the sedimentation along the shelf has been quantified.

Here, a conceptual sediment budget for the Vietnamese Shelf will be established, opposing sediment sources and sediment sinks.

6.2 Sediment Sources

6.2.1 Denudation Rates and Sediment Discharge

Denudation rates in the catchment area of the Rivers contributing their load to the investigated area have sparsely been studied. Carter et al. (2000) calculated denudation rates

for the mountainous region of central Vietnam for the upper Miocene from apatite fission tracks. Their denudation rates range between 390 and 500 m/Myr. Although factors influencing denudation, like precipitation, plant cover and sea level have certainly not been constant since the upper Miocene, their denudation rates give a guess of how much is possible.

More recent mechanical denudation rates compiled by Einsele (2000) are in the range of 500 - 1000 m/Myr for tropical rivers draining areas of very high relief, and 200 - 500 m/Myr for tropical mountain rivers. For the Mekong River basin Einsele gives a mechanical denudation rate of 80 m/Myr. The chemical denudation rate, cited by Einsele as 30 m/Myr, is neglected in this study since the determination of mass accumulation rates (MAR) on the shelf can only account for suspended sediments which are produced by mechanical denudation. Furthermore the ratio between totally suspended sediment (TSS) and totally dissolved sediment (TDS) which is about 3.5 in the oceans (Einsele, 2000) tends to be higher in tropical regions with steep gradients. For the Ganges/Brahmaputra River system Einsele (2000) reports a TSS/TDS ratio of 11 while in tropical mountainous regions like the Annamite chain the TSS/TDS ratio ranges between 10 and 30. This strengthens the importance of mechanical denudation in relation to chemical denudation.

Some authors reported an increase of denudation rates in historic times due to anthropogenic influences like deforestation and agriculturization (Toy, 1982, Milliman et al., 1987). The sediment input from the Yellow River to the South China Sea increased dramatically (by a factor of 10) since agricultural use (Milliman et al., 1987; Saito et al., 2001). Ta et al. (in press) showed, that such an increase in sediment discharge did not occur for the Mekong River. Contrarily, for the area of the Annamite chain, Pantulu (1986) reports severe soil depletion due to agriculturization.

However, small drainage basins in mountainous regions have much higher sediment yields than large river systems due to a higher relief and steep stream channel gradients. In the previous chapter possible sediment discharge fluctuations of the Mekong River were explained with increased precipitation in the Annamite region and subsequent increase in erosion. These findings correlate with published results supporting strengthened SW-monsoon in the early Holocene (Sirocko et al., 1996; Feng et al., 1999; Wang et al., 1999; Goodbred and Kuehl, 2000; Sarkar et al., 2000; Maxwell, 2001).

Tab. 13 shows a compilation of denudation rates and sediment flux for the Red River, the Mekong River, the small mountainous rivers contributing to the Mekong and the small mountainous rivers draining eastward into the SCS. The data are taken from the literature or calculated according to published values and equations.

The conversion from denudation rate to sediment flux and vice versa occurred on the assumption of a rock density of 2.5 g/cm³ after the formula:

sediment flux [t/yr] = denudation rate [m/10^6yr] x rock density [t/m³] x area [10^4m²]

Tab. 13: *Compilation of denudation rates and sediment flux for Vietnam and vietnamese rivers*

	Catchment area [km²]	Denudation rate [m/Myr]	Sediment yield [x 10^6 t/km²y]	Sediment flux (load) [x 10^6 t/y]
Mekong				
Milliman and Syvitzki (1992)	790000	**80**	200	~160
Einsele (2000)	"	80	**200**	~160
Pinet and Souriou (1988)	"	**~120**	**~300**	**~237**
Annamite part of Mekong*				
Carter et al. (2000)	100000	390-500	**975-1250**	**97.5-125**
Einsele (2000)	"	200-500	**500-1250**	**50-125**
Pinet and Souridu (1988)	"	**~90**	**~225**	**~22.5**
Small mountainous rivers to SCS⁺				
Carter et al. (2000)	80000	390-500	**975-1250**	**78-100**
Einsele (2000)	"	200-500	**500-1250**	**40-100**
Pinet and Souridu (1988)	"	**~90**	**~225**	**~18**
Red River				
Milliman and Syvitzki (1992)	120000	**440**	1100	~130
Einsele (2000)	"	200-500	**500-1250**	**60-150**
Pinet and Souridu (1988)	"	**~170**	**~425**	**~51**

calculated results are **bold**
*calculated with data from Pantulu (1986) and Fedra et al. (1991)
⁺compiled and estimated from Vietnam Hydrometeorological Atlas, UNEP (1994)
conversion from denudation rate to sediment flux and vice versa occurred on the assumption of a rock density of 2.5 t/m³ and the equation:
sediment flux [t/yr] = denudation rate [m/10^6yr] x rock density [t/m³] x area [10^4m²]
Denudation rates calculated after Pinet and Souriau (1988):
D = (419 x 10^{-6} Elev - 0.245) x 1000 (for rocks younger than 250 My)
whereas D = denudation rate in m/Myr, and Elev = mean basin elevation

6.2.2 Mekong

Generally accepted values for sediment load of the Mekong are the ones published by Milliman and Syvitzki (1992). They assume a sediment load of 160 x 10^6 t/yr which is consistent with the data from Einsele (2000).

In a recent publication Ta et al. (in press) give a value of 144 ± 36 x 10^6 t/yr.

Furthermore sediment was calculated load after Pinet and Souriau (1988) whose model takes the mean basin elevation and the crustal age into account, resulting in a sediment load of ~237 x 10^6 t/yr.

6.2.3 Red River

The Red River influences the sediments investigated in this work only to a minor degree (cp. chapter 5). Therefore, only very limited calculations can be made concerning the sediment budget of this river and data will be presented in a few words.

The sediment load of the Red River is 130 x 10^6 t/yr (Milliman and Syvitzki, 1992). Calculations using the denudation rate given by Einsele (2000) confirm this value returning 60 – 150 x 10^6 t/yr. A calculation using the equation of Pinet and Souriau (1988) results in a much lower value of ca. 51 x 10^6 t/yr.

6.2.4 Small Mountainous Rivers

The small mountainous rivers of the Annamite chain contribute ca. 30 % of the total Mekong sediment (cp. chapter 5). The Annamite tributaries of the Mekong have a more gentle profile than the streams draining into the South China Sea (Fedra et al., 1991) which results in stronger erosion of the eastward Annamite mountains, contributing their sediment onto the narrow central part of the Vietnamese Shelf.

Estimating the load of those rivers with the denudation rates of Carter et al. (2000) results in a sediment load of 78 - 100 t/yr. The calculation with the values provided by Einsele (2000) returns a sediment load between 40 and 100 t/yr. Sediment load calculated with the denudation rate determined with the equation of Pinet and Souriau (1988) is relatively low with a value of ~18 t/yr. This results from their somewhat simple minded model which disregards important factors like precipitation rate and relief. The crustal age of the Annamite region is older than the one for the Mekong basin which implies that after Pinet and Souriau (1988) a modified equation should be used to calculate the denudation rate, resulting in a lower denudation rate compared to the Mekong basin. Since only parts of the Annamite chain are older than 250 Ma, the equation for rocks younger than 250 Ma was used for the Annamite source region as well. The average basin elevation for the Annamite region has been estimated to 800 m. Pinet and Souriaus modeled values stand in contrast to the much higher denudation rates calculated from Carter et al. (2000) and Einsele (2000), probably due to non-observance of both, precipitation and steep stream channel gradients, of their model. Both factors are very high and probably of extreme importance for denudation rates in the Annamite region.

6.3 Sediment Sinks

The sediment sinks for material delivered by vietnamese rivers are the deltas of the two major rivers Mekong and Red River, the wide shelf off the deltas, and the narrow shelf off central Vietnam. Tab. 14 shows an overview over sediment sinks for suspended river sediment.

Tab. 14: *Sinks for sediment delivered by vietnamese Rivers*

	area [km²]	MAR_{terr} [g/cm²kyr]	av. sediment thickness [cm]	sediment stored calc. from MAR_{terr} [10^9 t/kyr]	sediment stored calc. from thickness [10^6 t/yr]
Mekong delta*	18000		20000±500	*144±36*	**144±36**
Southern Shelf (Mekong influenced)	~150000	6-12 (30-45)		**9-18**	*9-18*
Central Shelf	~34000	60-120 600-1200		**20.4-40.8** **204-408**	*20.4-40.8* *204-408*
			430	*~20*$^+$	**~20**$^+$
Northern Shelf (Gulf of Tonkin)	170000$^{\#}$	~12		**~20**	*~20*

calculated results are **bold,** equivalent values *italic*
*data from Ta et al. (in press)
+average thickness of Holocene deposits from 10 sediment stations from modern water depths between 21 m and 169 m on the *Central Shelf*. Calculation assuming an average dry bulk density of 1.15 g/cm³
$^{\#}$data from Niino and Emery (1961)

6.3.1 Mekong Delta

The total area of the Mekong delta ranges between 62,520 and 93,781 km^2 (Orton and Reading, 1993; Nguyen et al., 2000). Ta et al. (in press) calculated the amount of sediment deposited in the Mekong delta for the last 3 kyr to 144 $\pm$ 36 x 10^6 tons per year, based on sediment volume analysis (20 $\pm$ 5 m in thickness, 18 x 10^3 km² in area, bulk density of 1.2 $\pm$ 0.1 g/cm³). Their value is in good accordance with the data from Milliman and Syvitzki (1992) who calculated the annual sediment load of the Mekong to 160 x 10^6 tons. However, this implies that the major part of the sediment transported by the Mekong is deposited in the Mekong delta and does not reach the outer shelf.

6.3.2 Southern Shelf

The area of the vietnamese part of the Sunda Shelf influenced by the Mekong is not known. The total area of the Sundashelf is ca. 1.8 x 10^6 km². We found modern sediments delivered by the Mekong at stations 18376, 18389, 18391 and 18393, up to 60 km off the coast (cp. chapter 4). From the distance of those locations we estimate a minimum area influenced by the Mekong in modern times which has an extension of ca.150,000 km².

The average MAR for sediments from this area is in the range of 6 - 12 g/cm²kyr (cp. chapter 4). Higher MAR have been found at station 18391 and 18393 (Fig. 44) with 30 - 45 g/cm²kyr. Calculating the amount of sediment stored on the Southern Shelf with the minimum MAR of 6 - 12 g/cm²kyr and an average dry bulk density of 1.15 g/cm³ results in a value of 9 - 18 x 10^6 t/yr.

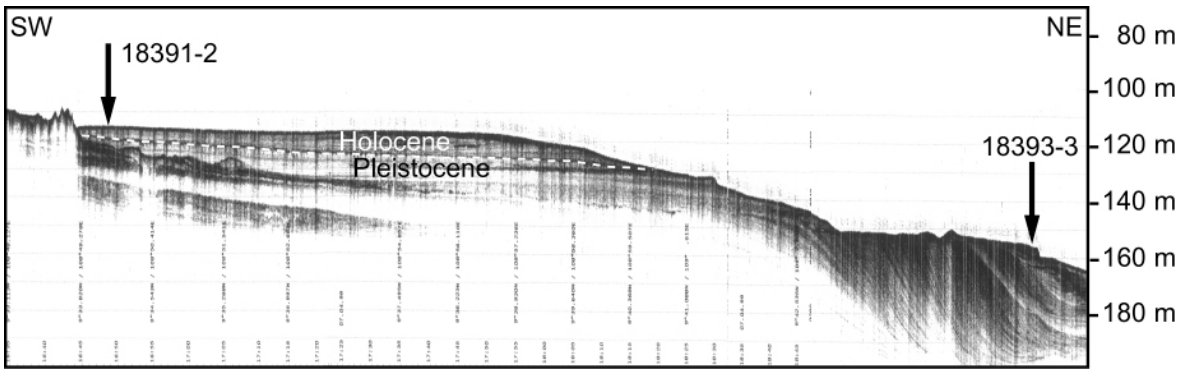

Fig. 44: *High resolution seismic profile of stations 18391 and 18393*

6.3.3 Central Shelf

Compared to the wide shelf in the Gulf of Tonkin and the wide Sundashelf, the expansion of the narrow shelf between 16° N and 11° N off Vietnam is very limited with ca. 34000 km², determined with geometric methods taking the 200 m isobath as seaward limitation of the shelf.

The amount of sediment stored on the central Vietnamese Shelf calculated from terrigenous MAR and the depositional area, is in the range of 20.4 - 40.8 x 10^6 t/yr for average MAR of 60 - 120 g/cm²kyr. Assuming a higher average MAR like calcultated from cores 18415-2 and 18416-2 (cp. chapter 4) results in a sediment storage ten times higher (204 - 408 x 10^6 t/yr). Calculations from the average sediment thickness (430 cm) of the Holocene sediments studied here, return a value of ca. 20 x 10^6 t/yr. Probably this value underestimates the importance of *delta-like* sediment bodies in front of the small mountainous rivers and other nearshore deposits, which have been found in Nha Trang Bay (stations 18397 – 18401, Fig.

45a). The age of this wedge-like sediment body is not clear: A dating from core 18397-2, which penetrated the transgressional surface, shows an age of 4800 ^{14}C years BP.

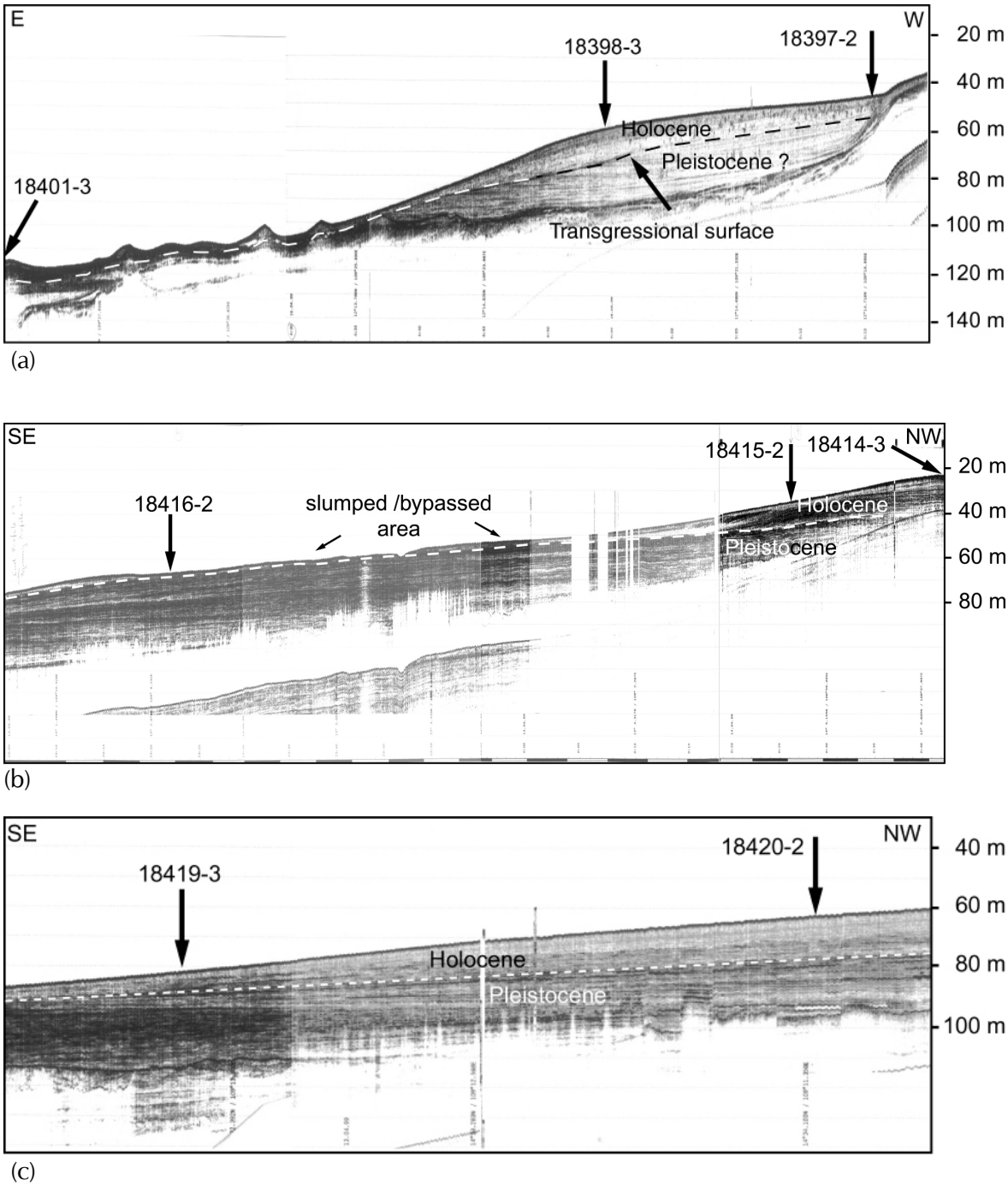

Fig. 45: *High resolution seismic profiles across the narrow central part of the Vietnamese Shelf a) station 18397 – 18401, b) station 18414 – 18416 and c) stations 18419 - 18420*

An episodic slump-like transport of accumulated sediment from the shelf to deeper parts of the SCS is very probable. Transect 18414-18417 shows very high mass accumulation rates in the lower part of cores 18415-2 and 18416-2 during the early Holocene (Fig. 45b). In

contrast the upper part of core 18416-2 lacks high MAR while core 18415-2 shows slump-like structures in the X-ray radiographies (cp. chapter 4) which could be the remainder of slumps that went off over the shelf break. Furthermore X-ray radiographies of stations 18419-3 and 18420-2 from a more gently inclined transect on the *Central Shelf* indicate a higher sediment thickness in landward direction (Fig. 45c), which after oversteepening would probably result in slumping of the accumulated material.

High denudation rates and the calculated sediment load from the small mountainous rivers draining onto the narrow *Central Shelf* suggest a higher value for the storage of sediment and indicate that sediment bypassing across the shelf to the deeper parts of the SCS is very probable. Sediment bypass was also found by Szczucínski and Stattegger (2001) for the central part of the Vietnamese Shelf.

6.3.4 Northern Shelf

On the Northern Shelf, Holocene sediments are limited to a thin blanket (Fig. 46). The calculated amount of sediment stored on the *Northern Shelf* (Gulf of Tonkin) from MAR for the southernmost part of the Gulf of Tonkin area is around 20 x 10^6 t/yr. This value must be regarded as highly speculative since it is based on the assumption of a constant modern MAR throughout the entire Gulf of Tonkin from a very limited dataset. Niino and Emery (1961) found areas with no modern sediments but sandstone bedrock cropping out in the central area of the Gulf of Tonkin.

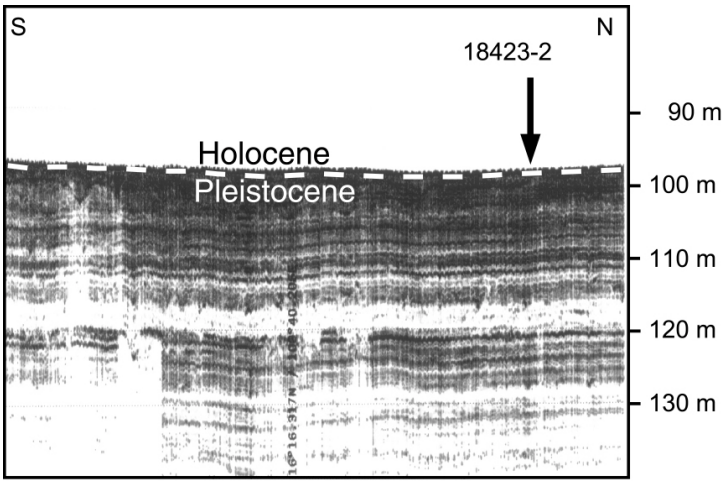

Fig. 46: *High resolution seismic profile of station 18423*

The occurrence of relic sediments, attested by large amounts of glaucony in core 18426-2 (cp. chapter 4), nearly excludes modern sedimentation in this area.

The amount of sediment stored in the Red River delta is not known, but it has become an area of interest in the last few years (Mathers and Zalasiewicz, 1999). It extends from the Vietnamese City Tri, ca. 150 km inland, to the coast, where it measures approximately 130 km across. Holocene delta sediments are up to 30 m thick (Mathers and Zalasiewicz, 1999).

6.4 Conclusions

A conceptual sediment budget for the Vietnamese Shelf, with special focus on the *Central Shelf* which receives sediments from the small mountainous rivers along the coast, was presented.

Denudation rates of the rivers draining into the study area (Mekong, small mountainous rivers and Red River) were estimated from literature resources. Accumulation rates for the areas acting as sediment sinks were calculated from detailed sediment core data and high resolution seismic records.

For the three source-sink systems the following was found:

(1) The biggest part of sediment transported by the Mekong River is deposited in the Mekong delta. 160 x 10^6 t/yr are delivered by the Mekong. 144 $\pm$ 36 x 10^6 t/yr are stored in the Mekong delta (Ta et al. in press) and only 9 - 18 x 10^6 t/yr are stored on the shelf off the Mekong. The amount of sediment transported to the deeper parts of the SCS is not known.

(2) The sediment delivered by the small mountainous rivers is with 40 - 100 x 10^6 t/yr about half of the amount transported by the Mekong. About 20 - 40 x 10^6 t/yr of sediment are stored on the *Central Shelf*. The remaining part bypasses the shelf or is transported towards the deeper parts of the SCS by slumps.

(3) The sparse database for the Red River and Gulf of Tonkin area does not allow the calculation of a sediment budget. The Red River transports about 130 x 10^6 t/yr of sediment. The major part of this sediment is deposited in the Red River delta (Mathers and Zalasiewicz, 1999). Conservative estimates of sediment accumulation for the Gulf of Tonkin results in a value of ca. 20 x 10^6 t/yr.

7 Comprehensive Conclusions

Sediment samples from northern, central and southern parts of the Vietnamese Shelf and the Mekong and Red River have been investigated with sedimentological, geochemical, micropaleontological and geophysical methods. This investigation is the first detailed and comprehensive characterization of deposits from the Vietnamese Shelf with a stratigraphy based on 45 AMS-^{14}C dates. On the basis of those investigations, the Vietnamese Shelf could be divided into three areas with depositional processes differing from each other: The *Northern Shelf* in the southern Gulf of Tonkin, the narrow *Central Shelf* in front of the high-rising Annamite mountain chain and the *Southern Shelf* in the area of the paleo-Mekong. For the three shelf areas the following was concluded:

- The *Northern Shelf* is characterized by a low sedimentation rate of ca. 10 cm/kyr. The *Central Shelf* shows high sedimentation rates of 50 - 100 cm/kyr (500 - 1000 cm/kyr over short periods of time). Sedimentation rates on the *Southern Shelf* are in the range of 5 - 10 cm/kyr (25 - 40 cm/kyr in sheltered areas).
- Although Mekong and Red River are among the ten largest rivers of the world concerning sediment discharge, mass accumulation rates are highest on the *Central Shelf* in front of the small mountainous rivers, which thus deliver large quantities of sediment. 60 - 120 g/cm^{2}kyr (600 - 1200 g/cm^{2}kyr over short periods of time) are the highest mass accumulation rates observed in the South China Sea so far. These values exceed mass accumulation rates of other shelves from the South China Sea at least by a factor of 2 to 4.
- The high mass accumulation rates of 600 - 1200 g/cm²yr occurred in early Holocene times and are probably caused by enhanced erosion in the Annamite mountains due to intensified SW-monsoon.
- The facies variability of deposits from the sediment cores is highest in cores from the *Northern Shelf* and *Southern Shelf,* where numerous facies have been preserved in incised valley systems. The central shelf shows a low facies variability due to lack of incised valley systems.
- On the Northern Shelf, a condensed section/marine flooding surface, indicated by the abundance of glaucony, occurs. Due to low sedimentation rates on the *Northern Shelf* and *Southern Shelf,* relict sediments are common. Here, an equilibrium between deposition and erosion could not be established, yet. Due to high terrigenous input from the small mountainous rivers the depositional equilibrium on the *Central Shelf* was established quickly.

- Comparison of tentative sea-level indications with the sea-level curve of Hanebuth et al. (2000) shows agreement for *Southern Shelf* deposits. Data points from *Central Shelf* deposits plot below the Hanebuth-curve and may be caused by subsidence due to a high mass accumulation rate. In contrast data points from *Northern Shelf* deposits, plotting above the Hanebuth-curve, are probably caused by tectonic uplift in this region.

To explain the high mass accumulation rates on the *Central Shelf* and to understand the provenance and distribution of sediments on the Vietnamese Shelf, the shelf deposits and river sediments have been investigated for geochemical and isotopic variations. Furthermore, the geochemical evolution of sediments from a core covering the Holocene time interval has been investigated to reveal variations in the source area during the Holocene. The Red River in the North, the Mekong in the South, and numerous small mountainous rivers draining the Annamite chain in Central Vietnam are the contributors of terrestrial sediments on the Vietnamese Shelf.

- Sediments of the potential endmembers (i.e. Red River, Mekong, small mountainous rivers) show different geochemical and Sr- and Nd-isotopic compositions and allow the discrimination of source areas.
- The data of the shelf sediments generally lie between the values of the endmembers. ε_{Nd}-values of shelf sediments are limited by those of the endmember river sediments, whereas the $^{87}Sr/^{86}Sr$ ratio shows a higher variability.
- The $^{87}Sr/^{86}Sr$ ratio is grain size dependent with more radiogenic values in fine grained samples. An influence of other sources biasing the Sr isotopic signal towards extreme values, cannot be excluded. Potential sources are higher differentiated rocks like gneisses and granites from northern Vietnam or Chinese loess.
- Discrimination diagrams using trace elements show that Red River sediment is an unlikely source for sediments on the Vietnamese Shelf. The main feeders for sediments on the Vietnamese Shelf are the Mekong and the small mountainous rivers draining the Annamite mountains.
- Assuming an influence of Annamite sediment on the composition of Mekong sediment of 30 % fortified by a Sm/Nd versus ε_{Nd} mixing diagram, the sediments on the Vietnamese Shelf are mainly delivered by the small mountainous rivers of the Annamite chain. They provide about 70 % of the total sediment deposited.
- The percentage of aeolian input is negligible due high mass accumulation caused by riverine input.

- Nd- isotopic variations during the Holocene in Mekong core 18391-2 suggest stronger erosion in the Annamite mountains during the early Holocene probably due to an intensified SW-Monsoon. The probability of intensified SW-monsoon has as well been suggested by high mass accumulation rates on the *Central Shelf*.
- The clay mineral composition supports the results from the geochemical investigations concerning provenance. A high Illite content in all samples probably reflects physical weathering of rocks from the Himalayas and the Annamite mountains. The Red River sample shows a very high illite content due to short transport paths.

With the knowledge of mass accumulation rates and provenance of the sediments it was possible to compile a conceptual sediment budget for the Vietnamese Shelf. Denudation rates from rivers draining into the study area (Mekong, small mountainous rivers and Red River) were estimated from the literature. Accumulation rates for the *Southern, Central* and *Northern Shelves,* acting as sediment sinks, were calculated from detailed sediment core data and high resolution seismic records:

- The Mekong River deposits the major part of his load in the Mekong delta. 160 x 10^6 t/yr are delivered by the Mekong but only 9 - 18 x 10^6 t/yr are stored on the shelf off the Mekong. 144 $\pm$ 36 x 10^6 t/yr are stored in the Mekong delta (Ta et al. in press). The amount of sediment transported to the deeper parts of the SCS is not known.
- The sediment delivered by the small mountainous rivers is with 40 - 100 x 10^6 t/yr about half of the amount transported by the Mekong. About 20 - 40 x 10^6 t/yr of sediment are stored on the *Central Shelf*. The remaining part bypasses the shelf or is transported towards the deeper parts of the SCS by slumps.
- The sparse database for the Red River and Gulf of Tonkin area (*Northern Shelf*) does not allow the calculation of a sediment budget. The Red River transports about 130 x 10^6 t/yr of sediment. The major part of this sediment is deposited in the Red River delta. Conservative estimates of sediment accumulation for the *Northern Shelf* result in a value of ca. 20 x 10^6 t/yr.

8 References

Amorosi, A., 1995. Glaucony and sequence stratigraphy; a conceptual framework of distribution in siliciclastic sequences. Journal of Sedimentary Research, Section B: Stratigraphy and Global Studies, 65(4): 419-425.

An, Z. et al., 2000. Asynchronous Holocene optimum of the East Asian monsoon. Quaternary Science Reviews, 19(8): 743-762.

Asahara, Y., Tanaka, T., Kamioka, H., Nishimura, A. and Yamazaki, T., 1999. Provenance of the North Pacific sediments and process of source material transport as derived from Rb-Sr isotopic systematics. Chemical Geology, 158(3-4): 271-291.

Barrat, J.A. and Nesbitt, R.W., 1996. Geochemistry of the Tertiary volcanism of Northern Ireland. Chemical Geology, 129(1-2): 15-38.

Bayon, G. et al., in press. An improved method for extracting marine sediment fractions and its application to Sr and Nd isotopic analysis. Chemical Geology.

Biscaye, P.E., 1964. Distinction between kaolinite and chlorite in recent sediments by X-ray diffraction. The American Mineralogist, 49: 1281-1289.

Biscaye, P.E., 1965. Mineralogy and Sedimentation of recent Deep-Sea Clay in the Atlantic Ocean and Adjacent Seas and Oceans. Geological Society of America Bulletin, 76: 803-832.

Bodet, F. and Schaerer, U., 2000. Evolution of the SE-Asian continent from U-Pb and Hf isotopes in single grains of zircon and baddeleyite from large rivers. Geochimica et Cosmochimica Acta, 64(12): 2067-2091.

Broecker, W.S. et al., 1988. New evidence from the South China Sea for an abrupt termination of the last glacial period. Nature (London), 333(6169): 156-158.

Bühring, C., 2001. Asian monsoon variability on orbital- and millennial-to-sub-decadel time scales. Doctoral Thesis, Universität Kiel, Kiel, 164 pp.

Calvert, S.E., Cousens, B.L. and Soon, M.Y.S., 1985. An X-ray fluorescence spectrometric method for the determination of major and minor elements in ferromanganese nodules. Chemical Geology, 51(1-2): 9-18.

Carbonnel, J.P. and Meybeck, M., 1975. Quality variations of the Mekong River at Phnom Penh, Cambodia, and chemical transport in the Mekong Basin. Journal of Hydrology, 27(3-4): 249-265.

Carpenter, R., Peterson, M.L. and Bennett, J.T., 1982. (super 210) Pb-derived sediment accumulation and mixing rates for the Washington continental slope. Marine Geology, 48(1-2): 135-164.

Carpenter, R., Peterson, M.L. and Bennett, J.T., 1985. (super 210) Pb-derived sediment accumulation and mixing rates for the Greater Puget Sound region. Marine Geology, 64(3-4): 291-312.

Carter, A., Roques, D. and Bristow, C.S., 2000. Denudation history of onshore central Vietnam; constraints on the Cenozoic evolution of the western margin of the South China Sea. Tectonophysics, 322(3-4): 265-277.

Chen, P.Y., 1978. Minerals in bottom sediments of the South China Sea. Geological Society of America Bulletin, 89(2): 211-222.

Colin, C., Turpin, L., Bertaux, J., Desprairies, A. and Kissel, C., 1999. Erosional history of the Himalayan and Burman ranges during the last two glacial-interglacial cycles. Earth and Planetary Science Letters, 171(4): 647-660.

Cushman, J.A., 1922. Shallow-water foraminifera of the Tortugas Region. Department of Marine Biology Papers, 311(17): 1-85.

Cushman, J.A., 1924. Samoan foraminifera. Department of Marine Biology Papers, 342(21): 1-75.

Dasch, E.J., 1969. Strontium isotopes in weathering profiles, deep-sea sediments, and sedimentary rocks. Geochimica et Cosmochimica Acta, 33(12): 1521-1552.

Defense-Mapping-Agency, 1972. Joint Operations Graphic. Defense Mapping Agency, Topographic Center, Washington, D.C.

Duce, R.A. et al., 1991. The atmospheric input of trace species to the world ocean. Global Biogeochemical Cycles, 5(3): 193-259.

Einsele, G., 2000. Sedimentary Basins: Evolution, Facies, and Sediment Budget. Springer-Verlag, Berlin, Heidelberg, New York, London, Paris, Tokyo, Hong Kong, Barcelona, Budapest, 792 pp.

Eisenhauer, A. et al., 1999. Grain size separation and sediment mixing in Arctic Ocean sediments; evidence from the strontium isotope systematic. Chemical Geology, 158(3-4): 173-188.

Emery, K.O., 1968. Relict sediments on continental shelves of world. The American Association of Petroleum Geologists Bulletin, 52(3): 445-464.

Fairbanks, R.G., 1989. A 17,000-year glacio-eustatic sea level record; influence of glacial melting rates on the Younger Dryas event and deep-ocean circulation. Nature (London), 342(6250): 637-642.

FAO, 1998. Integrated coastal area management and agriculture, forestry and fisheries: FAO guidelines, Environment and Natural Resources Service, Rome.

Fedra, K., Winkelbauer, L. and Pantulu, V.R., 1991. Expert Systems for Environmental Screening**:** An Application in the Lower Mekong Basin. RR-91-19, International Institute for Applied Systems Analysis, A-236l Laxenburg, Austria.

Feng, X., Cui, H., Tang, K. and Conkey, L.E., 1999. Tree-ring delta D as an indicator of Asian monsoon intensity. Quaternary Research (New York), 51(3): 262-266.

Fleet, A.J., 1984. Aqueous and sedimentary geochemistry of the rare earth elements. In: P. Henderson (Editor), Rare earth element geochemistry. Elsevier Sci. Publ. Co., Amsterdam, Netherlands, pp. 343-373.

Fontaine, H. and Delibrias, G., 1974. Niveaux marins pendant le Quaternaire au Vietnam. Arch Geol. Viet-Nam, 17: 35-44.

Fontaine, H. and Workman, D.R., 1997. Vietnam. In: E.M. Moores and R.W. Fairbridge (Editors), Encyclopedia of European and Asian regional geology. Chapman & Hall, London, United Kingdom, pp. 774-782.

Gingele, F.X., De, D.P. and Hillenbrand, C.D., 2001. Clay mineral distribution in surface sediments between Indonesia and NW Australia; source and transport by ocean currents. Marine Geology, 179(3-4): 135-146.

Goldstein, S.J. and Jacobsen, S.B., 1988. Rare earth elements in river waters. Earth and Planetary Science Letters, 89(1): 35-47.

Goldstein, S.L., O'Nions, R.K. and Hamilton, P.J., 1984. A Sm-Nd isotopic study of atmospheric dusts and particulates from major river systems. Earth and Planetary Science Letters, 70(2): 221-236.

Goodbred, Jr.S.L. and Kuehl, S.A., 2000. Enormous Ganges-Brahmaputra sediment discharge during strengthened early Holocene monsoon. Geology(Boulder), 28(12): 1083-1086.

Grousset, F.E., Biscaye, P.E., Zindler, A., Prospero, J. and Chester, R., 1988. Neodymium isotopes as tracers in marine sediments and aerosols; North Atlantic. Earth and Planetary Science Letters, 87(4): 367-378.

Grousset, F.E. et al., 1998. Saharan wind regimes traced by the Sr-Nd isotopic composition of subtropical Atlantic sediments; last glacial maximum vs today. Quaternary Science Reviews, 17(4-5): 395-409.

Hall, R., 1996. Reconstructing Cenozoic SE Asia. In: R. Hall and D.J. Blundell (Editors), Tectonic evolution of Southeast Asia. Geological Society Special Publications. Geological Society of London, London, United Kingdom, pp. 153-184.

Hanebuth, T., 2000. Sea-Level Changes on the Sunda Shelf during the last 50,000 years. 12, Institut für Geowissenschaften, Kiel.

Hanebuth, T., Stattegger, K. and Grootes, P., 2000. Rapid flooding of the Sunda Shelf; a late-glacial sea-level record. Science, 288(5468): 1033-1035.

Hanebuth, T.J.J., 2002. The Stratigraphic Evolution of the Sunda Shelf during the past fifty thousand years. In: F.H. Sidi, D. Nummedal, H.W. Posamentier, H. Darman and P. Imbert (Editors), Deltas of Southeast Asia and Vicinity Sedimentology, Stratigraphy, and Petroleum Geology. SEPM Special Publication, pp. XX-XX.

Hanebuth, T.J.J., Schimanski, A. and Stattegger, K., submitted. Late Pleistocene forced regression deposits on the Sunda Shelf (SE Asia). Marine Geology.

Hemming, S.R. et al., 1998. Provenance change coupled with increased clay flux during deglacial times in the western Equatorial Atlantic. Palaeogeography, Palaeoclimatology, Palaeoecology, 142(3-4): 217-230.

Holtzapffel, T., 1985. Les minéraux argileux. Préparation, analyse diffractométrique et détermination, Publication de la Société géologique du Nord, Villeneuve.

Jacobsen, S.B. and Wasserburg, G.J., 1980. Sm-Nd isotopic evolution of chondrites. Earth and Planetary Science Letters, 50(1): 139-155.

Jahn, B.m., Gallet, S. and Han, J., 2001. Geochemistry of the Xining, Xifeng and Jixian sections, Loess Plateau of China; eolian dust provenance and Paleosol evolution during the last 140 ka. Chemical Geology, 178(1-4): 71-94.

Jolivet, L. et al., 1999. Oligocene-Miocene Bu Khang extensional gneiss dome in Vietnam; geodynamic implications. Geology (Boulder), 27(1): 67-70.

Lan, C.Y. et al., 2001. First evidence for Archean continental crust in northern Vietnam and its implications for crustal and tectonic evolution in Southeast Asia. Geology (Boulder), 29(3): 219-222.

Lan, C.Y. et al., 2000. Geochemical and Sr-Nd isotopic characteristics of granitic rocks from northern Vietnam. In: C.H. Lo and U. Knittel (Editors), Lithosphere dynamics and natural resources in Indochina and adjacent areas. Pergamon. Oxford, United Kingdom. 2000.

Leloup, P.H. et al., 1995. The Ailao Shan-Red River shear zone (Yunnan, China), Tertiary transform boundary of Indochina. In: T.W.C. Hilde and M.F.J. Flower (Editors), Southeast Asia structure and tectonics. Tectonophysics. Elsevier, Amsterdam, Netherlands, pp. 3-84.

Lepvrier, C. et al., 1997. Indosinian NW-trending shear zones within the Truong Son Belt (Vietnam); (super 40) Ar- (super 39) Ar Triassic ages and Cretaceous to Cenozoic overprints. Tectonophysics, 283(1-4): 105-127.

Loutit, T.S., Hardenbol, J., Vail, P.R. and Baum, G.R., 1988. Condensed sections; the key to age determination and correlation of continental margin sequences. In: C.K. Wilgus et al. (Editors), Sea-level changes; an integrated approach. Special Publication - Society of Economic Paleontologists and Mineralogists. SEPM (Society for Sedimentary Geology), Tulsa, OK, United States, pp. 183-213.

Mathers, S. and Zalasiewicz, J., 1999. Holocene Sedimentary Architecture of the Red River Delta, Vietnam. Journal of Coastal Research, 15(2): 314-325.

Maxwell, A.L., 2001. Holocene Monsoon Changes Inferred from Lake Sediment Pollen and Carbonate Records, Northeastern Cambodia. Quaternary Research, 56(3): 390-400.

McLennan, S.M., 1989. Rare earth elements in sedimentary rocks; influence of provenance and sedimentary processes. In: B.R. Lipin and G.A. McKay (Editors), Geochemistry and mineralogy of rare earth elements. Reviews in Mineralogy. Mineralogical Society of America, Washington, DC, United States, pp. 169-200.

Milliman, J.D. and Meade, R.H., 1983. World-wide delivery of river sediment to the oceans. Journal of Geology, 91(1): 1-21.

Milliman, J.D., Qin, Y.S., Ren, M.E. and Saito, Y., 1987. Man's influence on the erosion and transport of sediment by Asian rivers; the Yellow River (Huanghe) example. Journal of Geology, 95(6): 751-762.

Milliman, J.D. and Syvitski, J.P.M., 1992. Geomorphic/Tectonic control of sediment discharge to the ocean; the importance of small mountainous rivers. Journal of Geology, 100(5): 525-544.

Moore, D.M. and Reynolds, R.C.J., 1989. X-ray Diffraction and the Identification and Analysis of Clay Minerals. Oxford University Press, Oxford, New York.

Nadeau, M.J. et al., 1998. Sample throughput and data quality at the Leibniz-Labor AMS facility. Radiocarbon, 40(1): 239-245.

Nadeau, M.J. et al., 1997. The Leibniz Labor AMS facility at the Christian-Albrechts University, Kiel, Germany. Nuclear Instruments and Methods in Physics Research B, 123: 22-30.

Nagy, E.A. et al., 2001. Geodynamic Significance of the Kontum Massif in Central Vietnam: Composite $^{40}Ar/^{39}Ar$ and U-Pb Ages from Paleozoic to Triassic. The Lournal of Geology, 109: 755-770.

Nagy, E.A., Schärer, U. and Minh, N.T., 2000. Oligo-Miocene granitic magmatism in central Vietnam and implications for continental deformation in Indochina. Terra Nova, 12: 67-76.

Nakai, S.i., Halliday, A.N. and Rea, D.K., 1993. Provenance of dust in the Pacific Ocean. Earth and Planetary Science Letters, 119(1-2): 143-157.

Nguyen, H., Flower, M.F.J. and Carlson, R.W., 1996. Major, trace element, and isotopic compositions of Vietnamese basalts; interaction of hydrous EM1-rich asthenosphere with thinned Eurasian lithosphere. Geochimica et Cosmochimica Acta, 60(22): 4329-4351.

Nguyen, V.L., Thi, K.O.T. and Tateishi, M., 2000. Late Holocene depositional environments and coastal evolution of the Mekong River Delta, southern Vietnam. In: C.D. Woodroffe and K. Berryman (Editors), Late Quaternary coastal dynamics and sea-level changes in the Asian and Pacific region. Pergamon. Oxford, United Kingdom. 2000.

Niino, H. and Emery, K.O., 1961. Sediments of shallow portions of East China Sea and South China Sea. Geological Society of America Bulletin, 72(5): 731-762.

Orton, G.J. and Reading, H.G., 1993. Variability of deltaic processes in terms of sediment supply, with particular emphasis on grain size. Sedimentology, 40(3): 475-512.

Pantulu, V.R., 1986. The Mekong River system. In: D.B. R and W.K. F (Editors), The ecology of river systems. Dr W. Junk Publishers, Dordrecht.

Petschik, R., 2000. MacDiff 4.2.5 Bedienungsanleitung.

Pinet, P. and Souriau, M., 1988. Continental erosion and large-scale relief. Tectonics, 7(3): 563-582.

Plas, L.v.d. and Tobi, A.C., 1965. A chart for judging the reliability of point counting results. American Journal of Science, 263(1): 87-90.

PONAGA, 1993. (Huchon, P., Phan Truong, T. and Le Pichon, X). Campagne Poanaga (N/O L'Atalante). Rapport de bord, fait à Nha Trang le 31 may 1993.

Rangin, C. et al., 1995. Cenozoic deformation of central and South Vietnam. In: T.W.C. Hilde and M.F.J. Flower (Editors), Southeast Asia structure and tectonics. Tectonophysics. Elsevier, Amsterdam, Netherlands, pp. 179-196.

Rea, D.K., 1994. The paleoclimatic record provided by eolian deposition in the deep sea; the geologic history of wind. Reviews of Geophysics, 32(2): 159-195.

Richter, A., 1998. Die Auswirkungen des spätpleistozänen Meeresspiegelanstiegs auf Sedimentationsprozesse im Paläo-Mekong Delta. Diplomarbeit, Universität Kiel, Kiel, 133 pp.

Roques, D., Matthews, S.J. and Rangin, C., 1997. Constraints on strike-slip motion from seismic and gravity data along the Vietnam margin offshore Da Nang; implications for hydrocarbon prospectivity and opening of the East Vietnam Sea. In: A.J. Fraser, S.J. Matthews and R.W. Murphy (Editors), Petroleum geology of Southeast Asia. Geological Society Special Publications. Geological Society of London, London, United Kingdom, pp. 341-353.

Saito, Y., 1991. Sequence stratigraphy on the shelf and upper slope in response to the latest Pleistocene-Holocene sea-level changes off Sendai, Northeast Japan. In: D.I.M. Macdonald (Editor), Sedimentation, tectonics and eustasy; sea-level changes at active margins. Special Publication of the International Association of Sedimentologists. Blackwell, Oxford, International, pp. 133-150.

Saito, Y., Yang, Z. and Hori, K., 2001. The Huanghe (Yellow River) and Changjiang (Yangtze River) delta: a review on their characteristics, evolution and sediment discharge during the Holocene. Geomorphology, 41(219-231).

Sarkar, A. et al., 2000. High resolution Holocene monsoon record from the eastern Arabian Sea. Earth and Planetary Science Letters, 177(3-4): 209-218.

Schimanski, A., 1999. Diversität und Entwicklung von Faziesräumen auf dem Sunda-Schelf im Verlauf der Postpleistozänen Transgression. Diplomarbeit, Universität Kiel, Kiel, 65 pp.

Schimanski, A., Haase, K., Stattegger, K. and Grootes, P.M., 2001. Provenance of Holocene and Recent Sediments on the Vietnamese Shelf Revealed by Sr and Nd Isotopes and Trace Elements. In: E. Transactions (Editor), AGU Fall Meeting, San Francisco, pp. 654.

Schimanski, A. and Stattegger, K., 2001. Deca-Meter-Scale Holocene Sedimentation on the Vietnamese Shelf. In: Anonymous (Editor), European Union of Geosciences conference abstracts; EUG 11. Journal of Conference Abstracts. Cambridge Publications, Cambridge, United Kingdom, pp. 182.

Schoenfeld, J. and Kudrass, H.R., 1993. Hemipelagic sediment accumulation rates in the South China Sea related to late Quaternary sea-level changes. Quaternary Research (New York), 40(3): 368-379.

Shackleton, N.J., 1977. The oxygen isotope stratigraphic record of the late Pleistocene. Philosophical Transactions of the Royal Society of London, Series B: Biological Sciences, 280(972): 169-182.

Shackleton, N.J., 1987. Oxygen isotopes, ice volume and sea level. Quaternary Science Reviews, 6(3-4): 183-190.

Shackleton, N.J. et al., 1988. Radiocarbon age of last glacial Pacific deep water. Nature (London), 335(6192): 708-711.

Sharma, K.P., 2000. Modelling oceanward sediment flux of the South and South-East Asian rivers. REGIONAL TRAINING WORKSHOP ON BIO-GEOCHEMICAL BUDGETING AND SOCIO-ECONOMIC MODELLING, 18-22 September, 2000, Colombo.

Singer, A., 1984. The paleoclimatic interpretation of clay minerals in sediments; a review. Earth-Science Reviews, 21(4): 251-293.

Sirocko, F., Garbe, S.D., McIntyre, A. and Molfino, B., 1996. Teleconnections between the subtropical monsoons and high-latitude climates during the last deglaciation. Science, 272(5261): 526-529.

Sirocko, F. et al., 1993. Century-scale events in monsoonal climate over the past 24,000 years. Nature (London), 364(6435): 322-324.

Southon, J., Kashgarian, M., Fontugne, M., Metivier, B. and W.-S., Y.W., in press. Marine reservoir corrections for the Indian Ocean and Southeast Asia. Radiocarbon.

Southon, J.E., Nelson, D.E. and Vogel, J.S., 1992. The determination of past ocean-atmopshere radiocarbon differences. In: E. Bard and W.D. Broecker (Editors), The Last Deglaciation: absolute and radiocarbon chronologies. Springer-Verlag, Berlin, pp. 219-227.

Southon, J.R., Rodman, A.O. and True, D., 1995. A comparison of marine and terrestrial radiocarbon ages from northern Chile. In: G.T. Cook, D.D. Harkness, B.F. Miller and E.M. Scott (Editors), Proceedings of the 15th international radiocarbon conference. Radiocarbon. American Journal of Science, New Haven, CT, United States, pp. 389-393.

Spieß, V., 1993. Digitale Sedimentechographie - Neue Wege zu einer hochauflösenden Akustostratigraphie. 35, Fachbereich Geowissenschaften Universität Bremen.

Steinke, S., 2001. Sedimentological and climatic changes during the last deglaciation recorded in cores from the Sunda Shelf margin and continental slope (southern South China Sea). Doctoral Thesis, Universität Kiel, Kiel, 84 pp.

Stuiver, M. and Braziunas, T.F., 1993. Modeling atmospheric (super 14) C influences and (super 14) C ages of marine samples to 10,000 BC. In: M. Stuiver and A. Long (Editors), Calibration 1993. Radiocarbon. American Journal of Science, New Haven, CT, United States, pp. 137-189.

Stuiver, M. and Reimer, P.J., 1993. Extended (super 14) C data base and revised CALIB 3.0 (super 14) C age calibration program. In: M. Stuiver and A. Long (Editors), Calibration 1993. Radiocarbon. American Journal of Science, New Haven, CT, United States, pp. 215-230.

Stuiver, M. et al., 1998. INTCAL98 radiocarbon age calibration, 24,000-0 cal BP. Radiocarbon, 40(3): 1041-1083.

Szarek, R., 2001. Biodiversity and biogeography of recent benthic foraminiferal assemblages in the south-western South China Sea (Sunda Shelf). Doctoral Thesis, Universität Kiel, Kiel, 273 pp.

Szczucínski, W. and Stattegger, K., 2001. Stayle and rate of shelf sedimentation offshore Nha Trang, Vietnam, South China Sea. Meyniana, 53: 143-162.

Ta, T.K.O., Nguyen, V.L., Tateishi, M., Kobayashi, I. and Saito, Y., 2002. Holocene delta evolution and sediment discharge of the Mekong River, southern Vietnam. Quaternary Science Reviews, in press.

Tapponnier, R., Peltzer, G., Le, D.A.Y., Armijo, R. and Cobbold, P., 1982. Propagating extrusion tectonics in Asia; new insights from simple experiments with plasticine. Geology (Boulder), 10(12): 611-616.

Toy, T.J., 1982. Accelerated erosion; process, problems, and prognosis. Geology (Boulder), 10(10): 524-529.

UNEP, I.H.P., 1994. Vietnam Hydrometeorological Atlas. Vietnam National Commitee, Hanoi.

Vail, P.R., Audemard, F., Bowman, S.A., Eisner, P.N. and Perez, C.G., 1991. The stratigraphic signatures of tectonics, eustacy and sedimentology; an overview. In: G. Einsele, W. Ricken and A. Seilacher (Editors), Cycles and events in stratigraphy. Springer Verlag, Berlin, Federal Republic of Germany, pp. 617-659.

Vail, P.R., Hardenbol, J. and Todd, R.G., 1984. Jurassic unconformities, chronostratigraphy, and sea-level changes from seismic stratigraphy and biostratigraphy. In: J.S. Schlee (Editor), Interregional unconformities and hydrocarbon accumulation. AAPG Memoir. American Association of Petroleum Geologists, Tulsa, OK, United States, pp. 129-144.

Van, W.J.C., 1988. Sequences and parasequences in siliciclastic rocks. In: D.P. James and D.A. Leckie (Editors), Sequences, stratigraphy, sedimentology; surface and subsurface. Memoir - Canadian Society of Petroleum Geologists. Canadian Society of Petroleum Geologists, Calgary, AB, Canada, pp. 572-573.

Voelker, A.H.L. et al., 1998. Correlation of marine (super 14) C ages from the Nordic Seas with the GISP2 isotope record; implications for (super 14) C calibration beyond 25 ka BP. In: W.G. Mook and d.P.J. van (Editors), Proceedings of the 16th international radiocarbon conference; Part 1. Radiocarbon. University of Arizona, Department of Geosciences, Tucson, AZ, United States, pp. 517-534.

Walter, H.J., Hegner, E., Diekmann, B., Kuhn, G. and Rutgers, v.d.L.M.M., 2000. Provenance and transport of terrigenous sediment in the South Atlantic Ocean and their relations to glacial and interglacial cycles; Nd and Sr isotopic evidence. Geochimica et Cosmochimica Acta, 64(22): 3813-3827.

Wang, L. et al., 1999. East Asian monsoon climate during the late Pleistocene; high-resolution sediment records from the South China Sea. In: M. Sarnthein and P. Wang (Editors), Response of West Pacific marginal seas to global climate change. Marine Geology. Elsevier, Amsterdam, Netherlands, pp. 245-284.

Wang, L. and Wang, P., 1990. Late Quaternary paleoceanography of the South China Sea; glacial-interglacial contrasts in an enclosed basin. Paleoceanography, 5(1): 77-90.

Wang, P., 1999. Response of Western Pacific marginal seas to glacial cycles; paleoceanographic and sedimentological features. In: M. Sarnthein and P. Wang (Editors), Response of West Pacific marginal seas to global climate change. Marine Geology. Elsevier, Amsterdam, Netherlands, pp. 5-39.

Wang, P., Wang, L., Bian, Y. and Jian, Z., 1995. Late Quaternary paleoceanography of the South China Sea; surface circulation and carbonate cycles. In: H. Tokuyama, A. Taira and S.i. Kuramoto (Editors), Asian marine geology. Marine Geology. Elsevier, Amsterdam, Netherlands, pp. 145-165.

Wang, P.L., Lo, C.H., Lee, T.Y., Chung, S.L. and Yem, N.T., 1998. Thermochronological evidence for the movement of the Ailao Shan-Red River shear zone: a perspective from Vietnam. Geology, 26(10): 887-890.

Wiesner, M., Stattegger, K. and Kuhnt, W.e.a., 1999. Cruise Report SONNE 140 SÜDMEER III. 7, Institut für Geowissenschaften, Kiel.

Wiesner, M.G., Zheng, L., Wong, H.W., Wang, Y. and Chen, W., 1996. Fluxes of particulate matter in the South China Sea. In: V. Ittekkot, P. Schäfer, S. Honjo and P.J. Depetris (Editors), Particle Flux in the Ocean. Wiley and Sons Ltd., New York, pp. 293-312.

Willkomm, H., 1986. Anomalous high (super 14) C activity found in Recent corals from the Philippines. In: M. Stuiver and R. Kra (Editors), Twelfth international radiocarbon conference. Radiocarbon. American Journal of Science, New Haven, CT, United States, pp. 486-494.

Wolanski, E., Nguyen, H.N. and Spagnol, S., 1998. Sediment dynamics during low flow conditions in the Mekong River estuary, Vietnam. Journal of Coastal Research, 14(2): 472-482.

Wyrtki, K., 1961. Physical Oceanography of the Southeast Asian water, Scripps Institution of Oceanography.

Zhang, L.S. and Schaerer, U., 1999. Age and origin of magmatism along the Cenozoic Red River shear belt, China. Contributions to Mineralogy and Petrology, 134(1): 67-85.

APPENDIX

FIGURES

Basic sedimentological data containing core logs of sand content, carbonate content, organic carbon content, C/N ratio, magnetic susceptibility, coarse grain analyses and X-ray logs of the investigated cores

PLATES

Photographs of dated material

TABLES

Table A: Sedimentological Parameters

Table B: Coarse Grain Analyses

Table C: Oxygen Isotopes

ADDITIONAL CONTRIBUTIONS

Journal Publications:

"LATE PLEISTOCENE FORCED REGRESSION DEPOSITS ON THE SUNDA SHELF (SE ASIA)"
Till J.J. Hanebuth, **Alexander Schimanski** and Karl Stattegger
submitted to MARINE GEOLOGY

Conference Abstracts:

Alexander Schimanski and Karl Stattegger (2001) Deca-Meter-Scale Holocene Sedimentation on the Vietnamese Shelf. *European Union of Geosciences XI, Strasbourg 2001, J. Conf. Abs.* ***6*** *(1) : 68*

Alexander Schimanski, Karl Stattegger and Pieter M. Grootes (2001) Holocene Sedimentation on the Vietnamese Shelf. *Schriftenreihe Deutsche Geol. Ges.,* ***14****: 182-184 (Roth, S. & Rüggeberg, A. /Ed.s.: 2001 Margins Meeting, 2.- 6.10.2001, Kiel; Abstracts).*

Alexander Schimanski, Karsten Haase, Karl Stattegger and Pieter M. Grootes (2001) Provenance of Holocene and Recent Sediments on the Vietnamese Shelf Revealed by Sr and Nd Isotopes and Trace Elements. *EOS, Transactions of the American Geophysical Union* ***82*** (47) : 654

FIGURES

Basic sedimentological data containing core logs of sand content, carbonate content, organic carbon content, C/N ratio, magnetic susceptibility, coarse grain analyses and X-ray analyses/core descriptions of cores:

18375-2, 18376-2

18377-2, 18389-3

18391-2, 18393-3

18396-3, 18397-2

18398-3, 18401-3

18404-3, 18405-3

18408-3, 18409-3

18414-3, 18415-2

18416-2, 18417-3

18419-3, 18420-2

18422-3, 18423-2

18424-2, 18425-2

18426-2

Legend for X-ray Logs

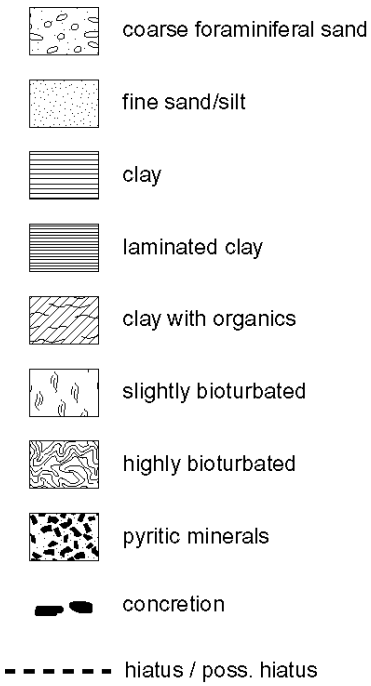

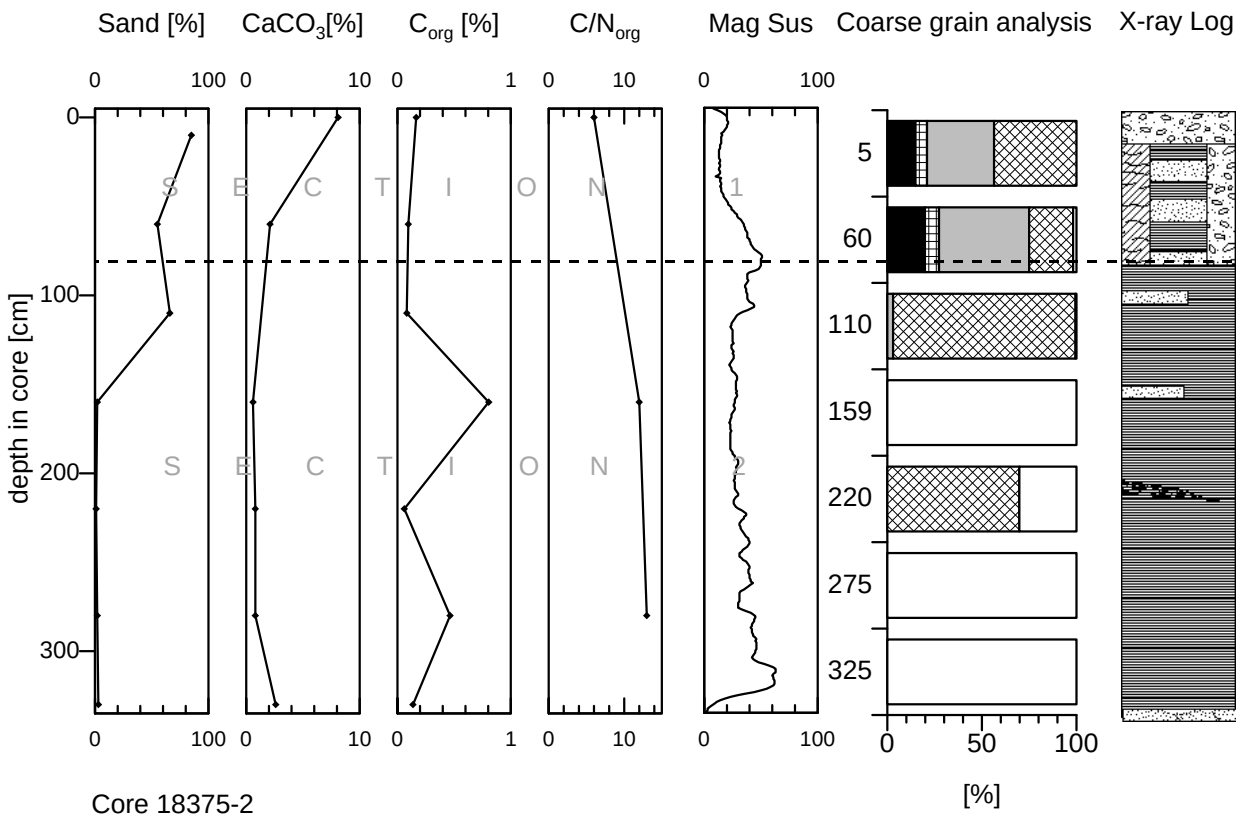
Sand [%]
CaCO3[%]
Corg [%]
C/Norg
Mag Sus
Coarse grain analysis
X-ray Log
depth in core [cm]
SECTION 1
SECTION 2
5
60
110
159
220
275
325
[%]
Core 18375-2

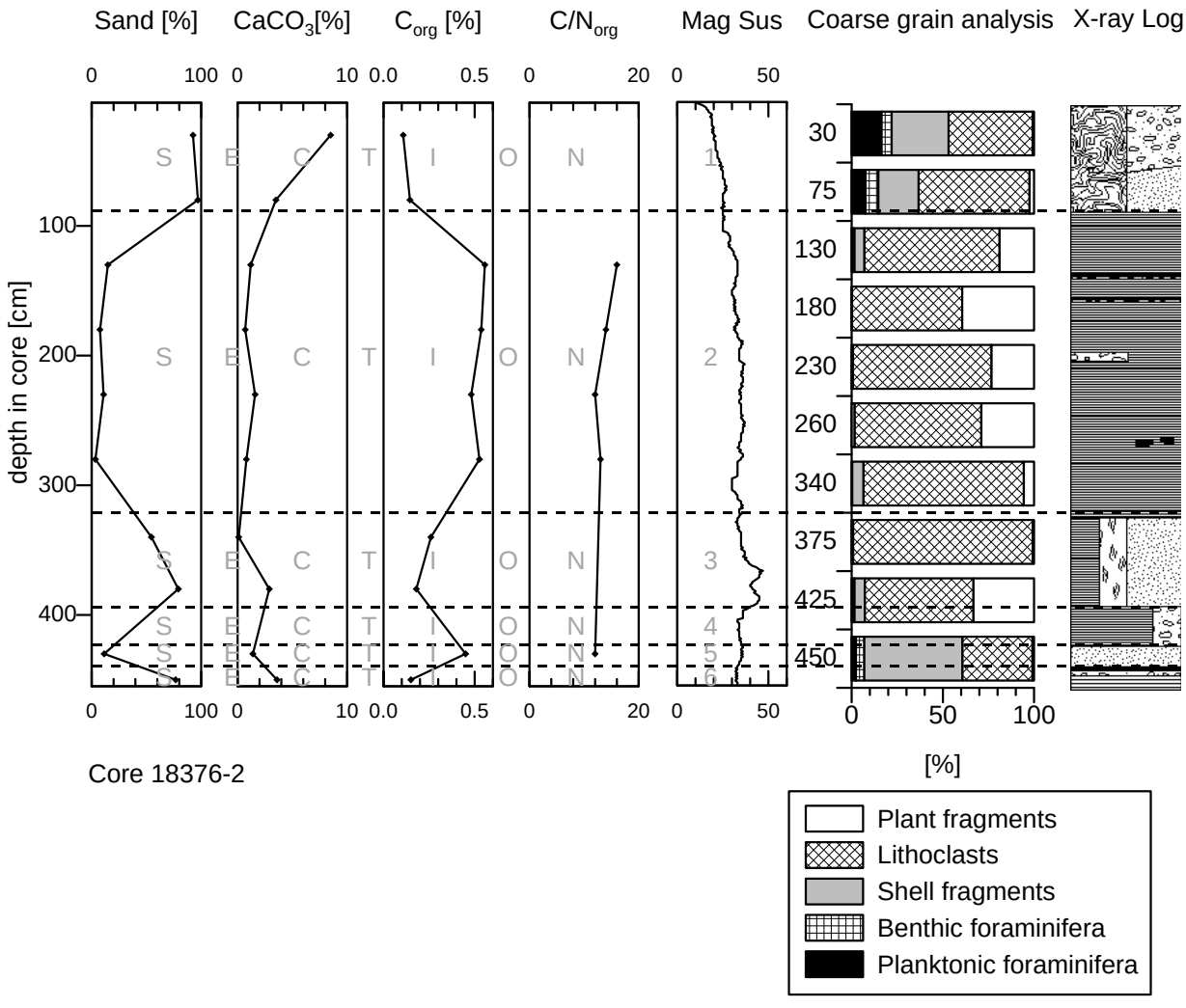
Sand [%]
CaCO3[%]
Corg [%]
C/Norg
Mag Sus
Coarse grain analysis
X-ray Log
depth in core [cm]
SECTION 1
SECTION 2
SECTION 3
SECTION 4
SECTION 5
SECTION 6
30
75
130
180
230
260
340
375
425
450
[%]
Core 18376-2
Plant fragments
Lithoclasts
Shell fragments
Benthic foraminifera
Planktonic foraminifera

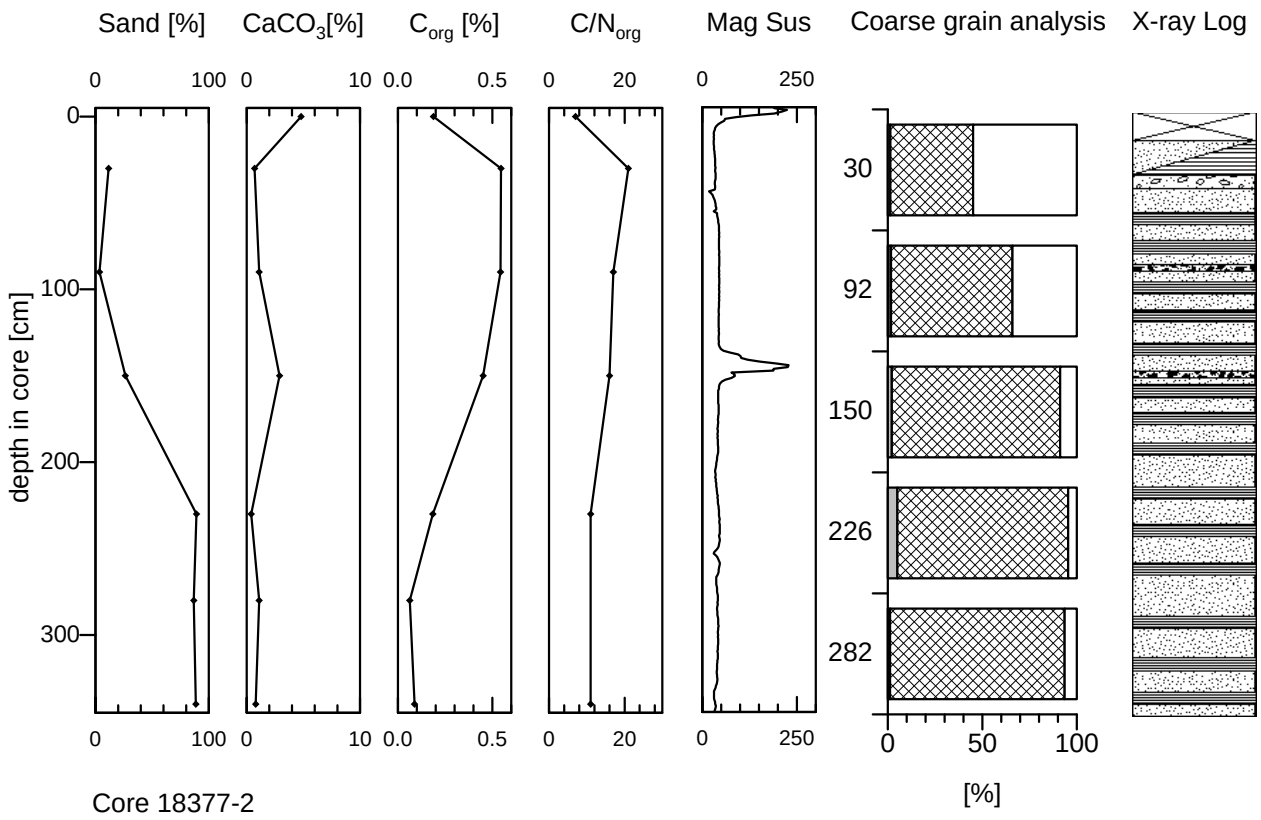
Sand [%]
CaCO3[%]
Corg [%]
C/Norg
Mag Sus
Coarse grain analysis
X-ray Log
depth in core [cm]
0
100
200
300
30
92
150
226
282
0
50
100
[%]
Core 18377-2

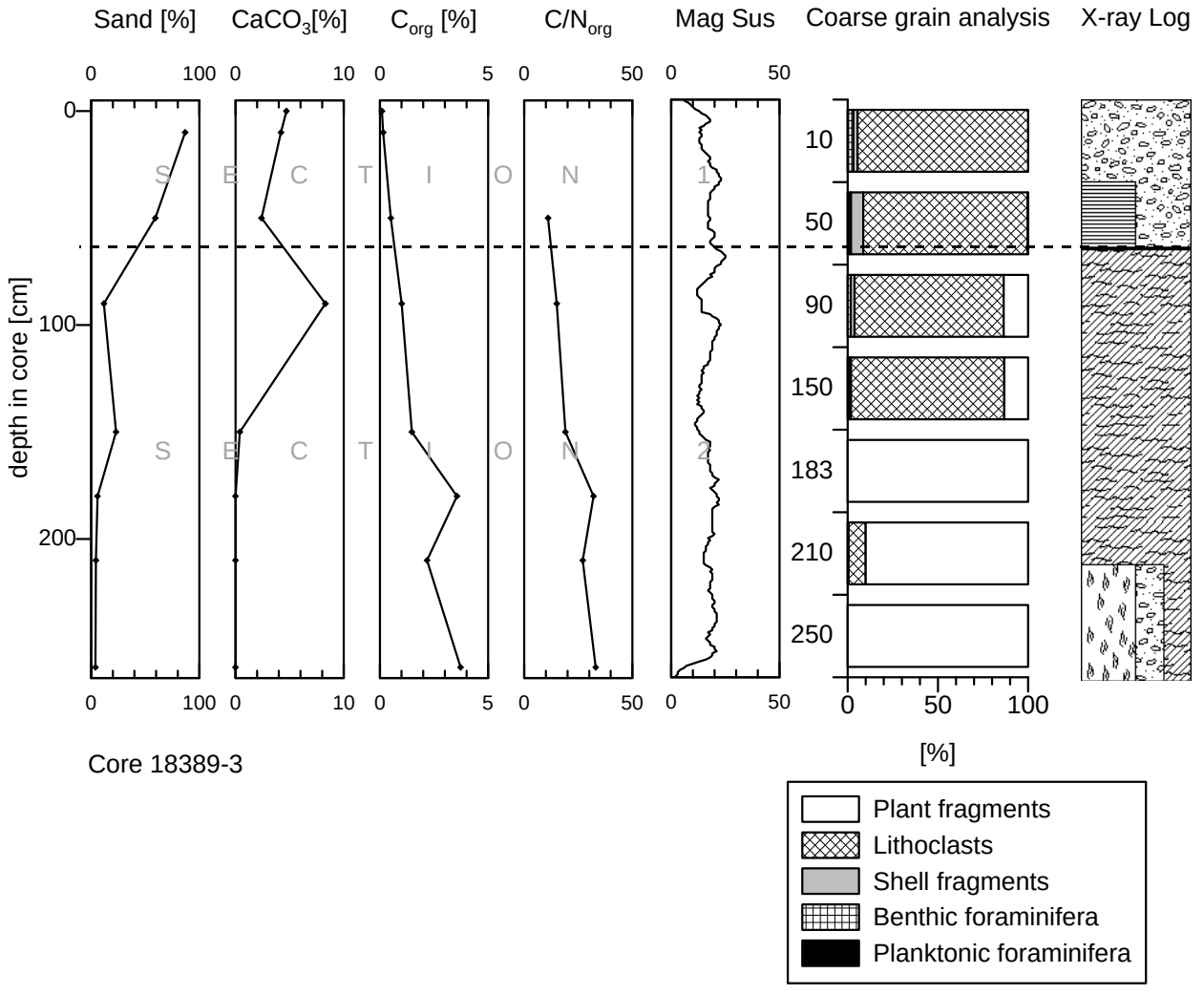
Sand [%]
CaCO3[%]
Corg [%]
C/Norg
Mag Sus
Coarse grain analysis
X-ray Log
depth in core [cm]
SECTION 1
SECTION 2
10
50
90
150
183
210
250
0
50
100
[%]
Core 18389-3
Plant fragments
Lithoclasts
Shell fragments
Benthic foraminifera
Planktonic foraminifera

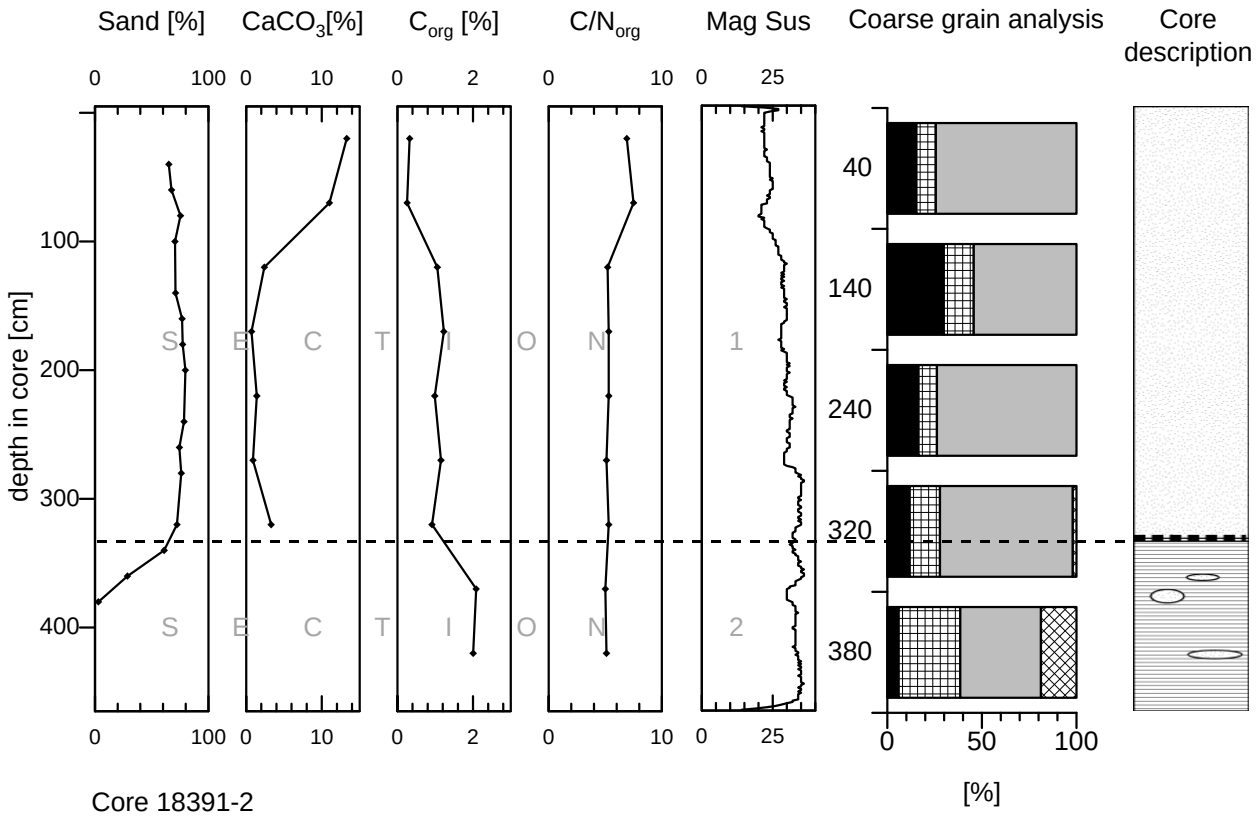
Sand [%]
CaCO3[%]
Corg [%]
C/Norg
Mag Sus
Coarse grain analysis
Core description
depth in core [cm]
SECTION 1
SECTION 2
40
140
240
320
380
[%]
Core 18391-2

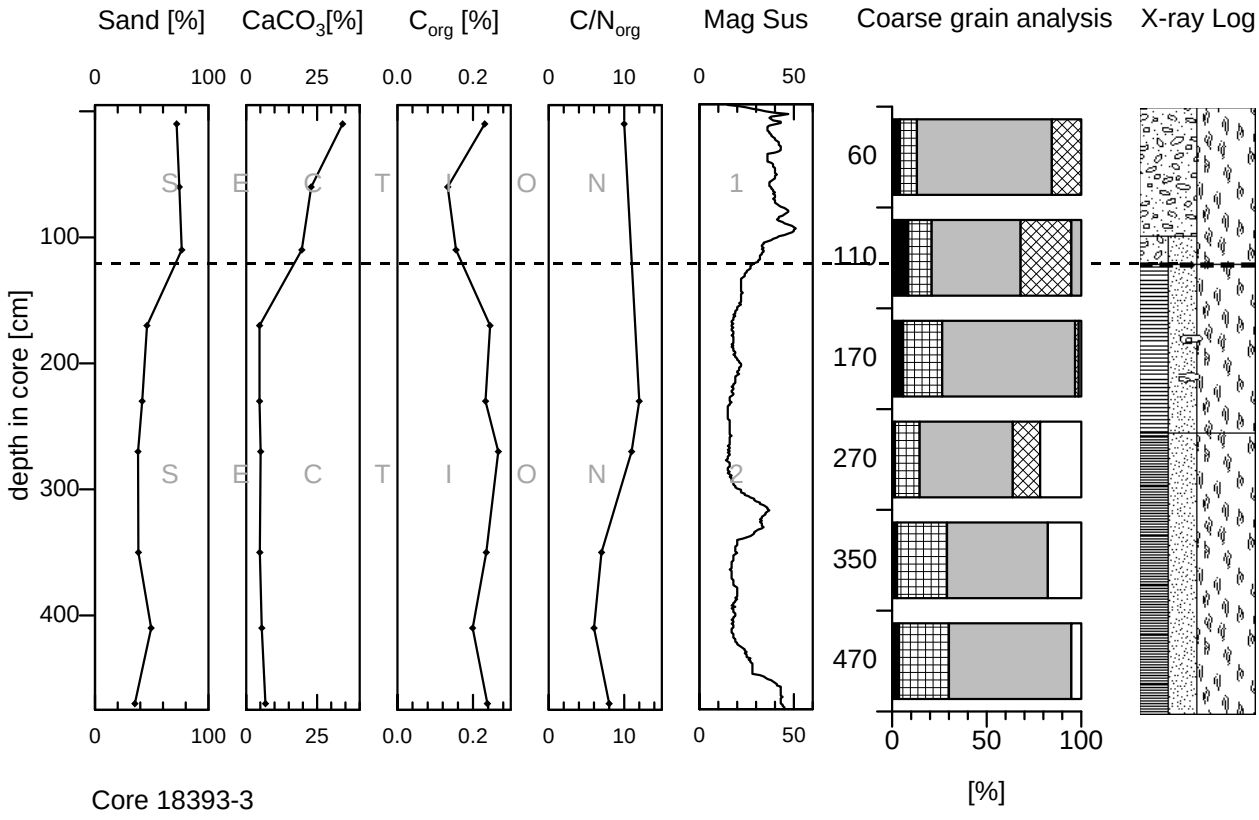
Sand [%]
CaCO3[%]
Corg [%]
C/Norg
Mag Sus
Coarse grain analysis
X-ray Log
depth in core [cm]
SECTION 1
SECTION 2
60
110
170
270
350
470
[%]
Core 18393-3
Glaucony
Plant fragments
Lithoclasts
Shell fragments
Benthic foraminifera
Planktonic foraminifera

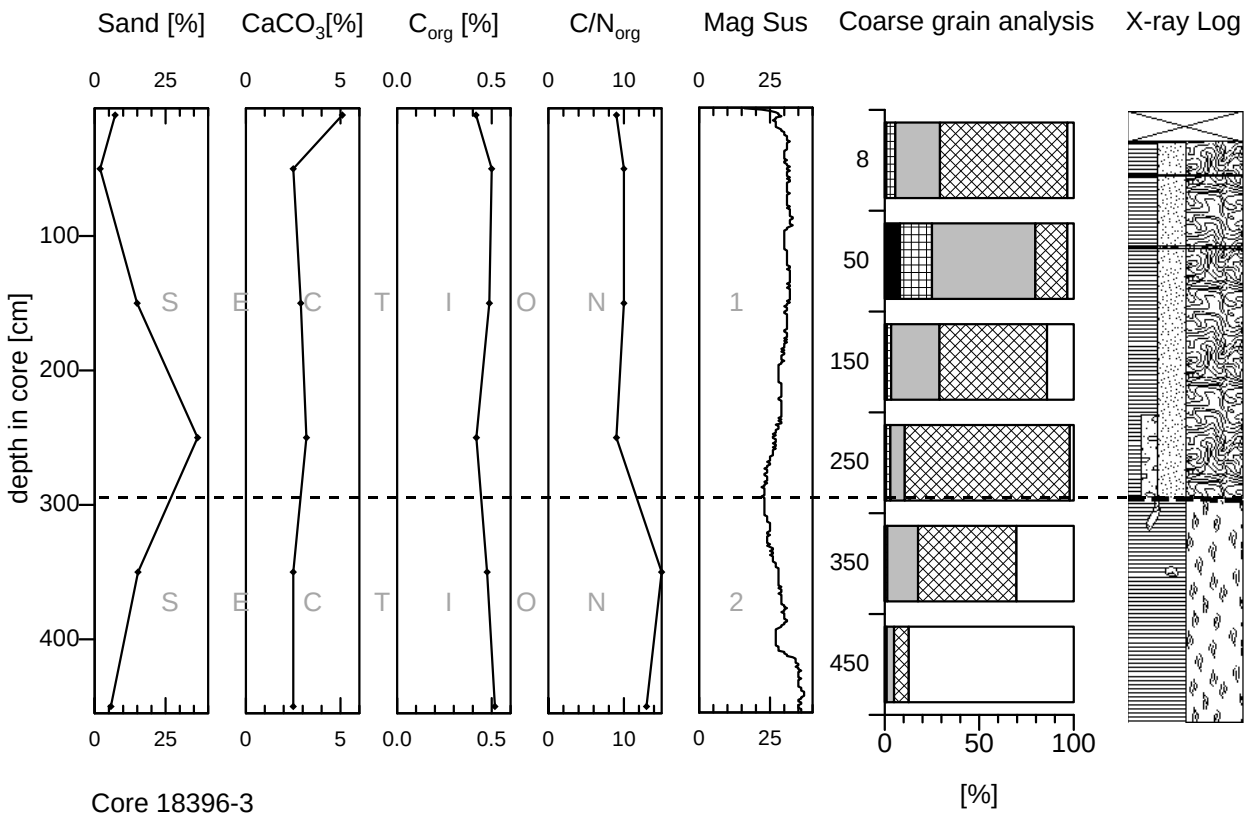
Sand [%]
CaCO3[%]
Corg [%]
C/Norg
Mag Sus
Coarse grain analysis
X-ray Log
depth in core [cm]
SECTION 1
SECTION 2
[%]
Core 18396-3

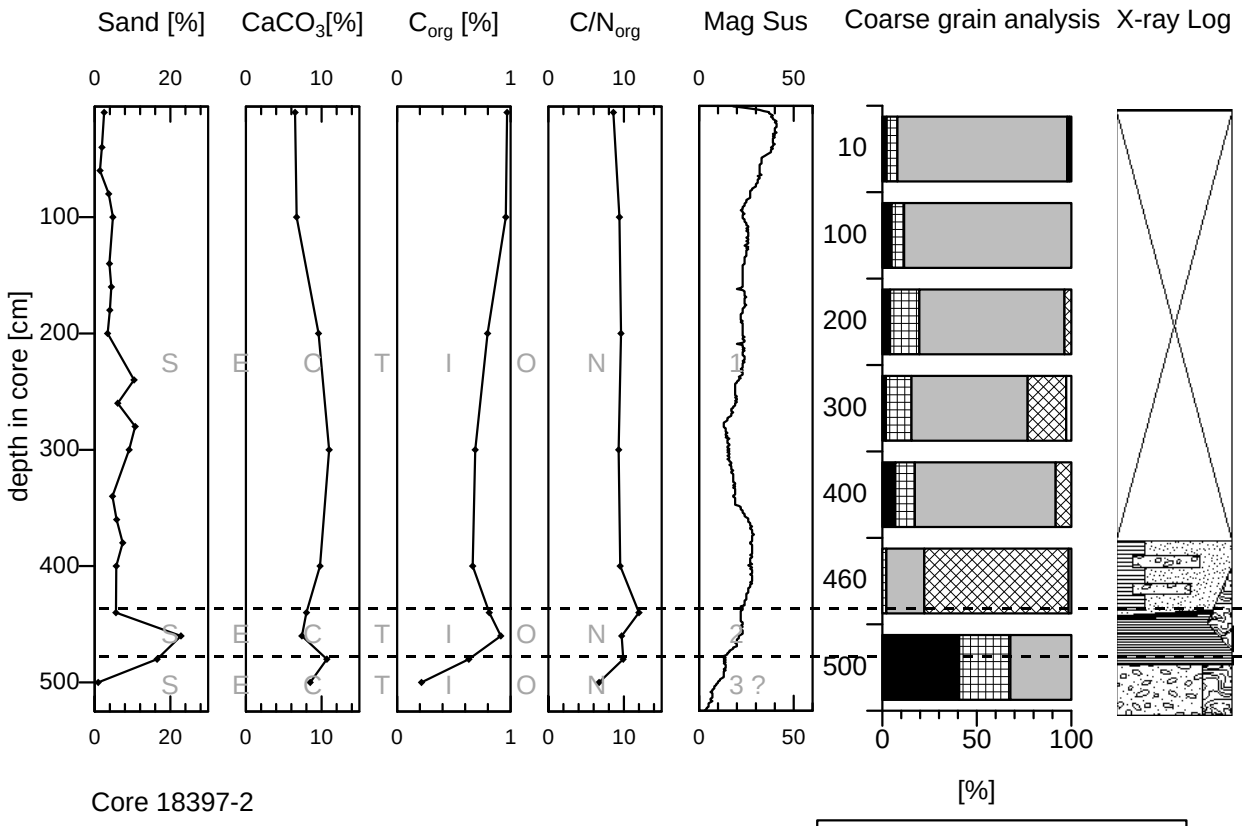
Sand [%]
CaCO3[%]
Corg [%]
C/Norg
Mag Sus
Coarse grain analysis
X-ray Log
depth in core [cm]
SECTION 1
SECTION 2
SECTION 3 ?
[%]
Core 18397-2
Plant fragments
Lithoclasts
Shell fragments
Benthic foraminifera
Planktonic foraminfera

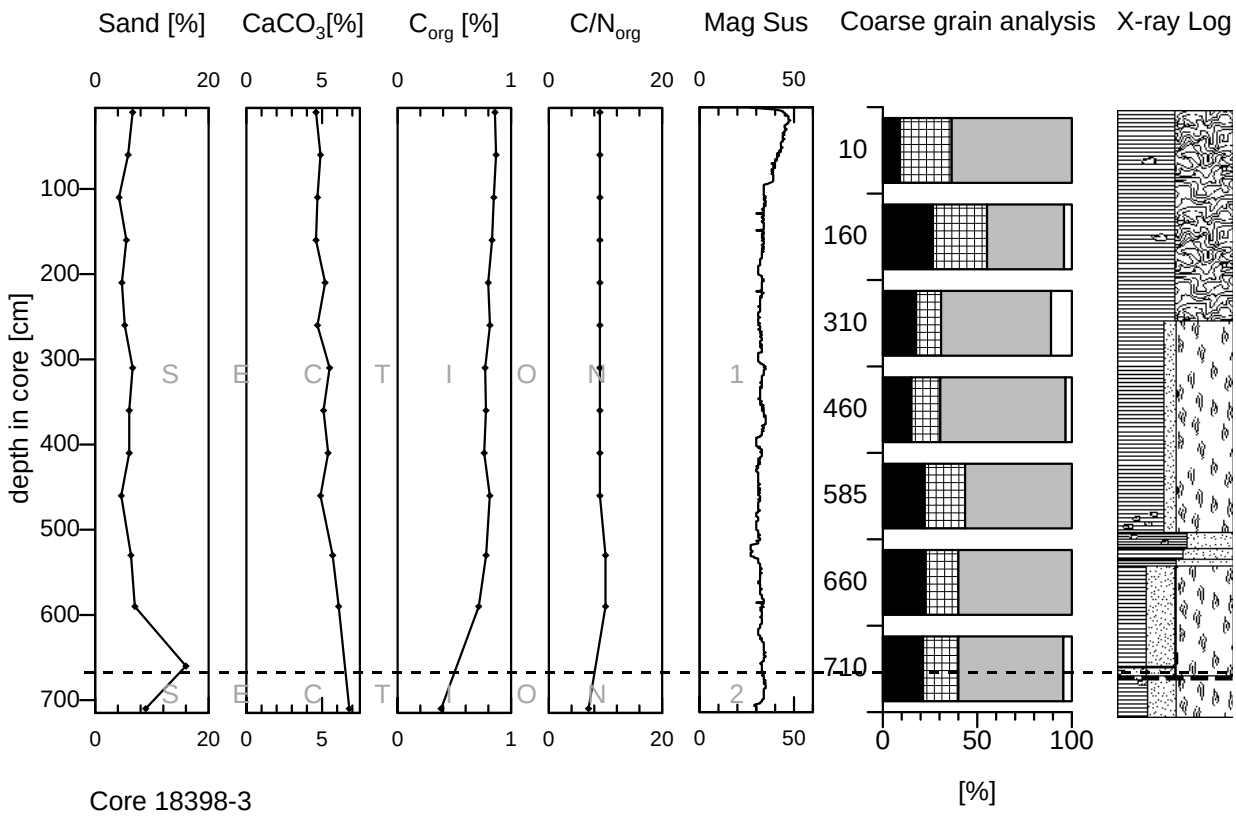
Sand [%]
CaCO3[%]
Corg [%]
C/Norg
Mag Sus
Coarse grain analysis
X-ray Log
depth in core [cm]
SECTION 1
SECTION 2
[%]
Core 18398-3

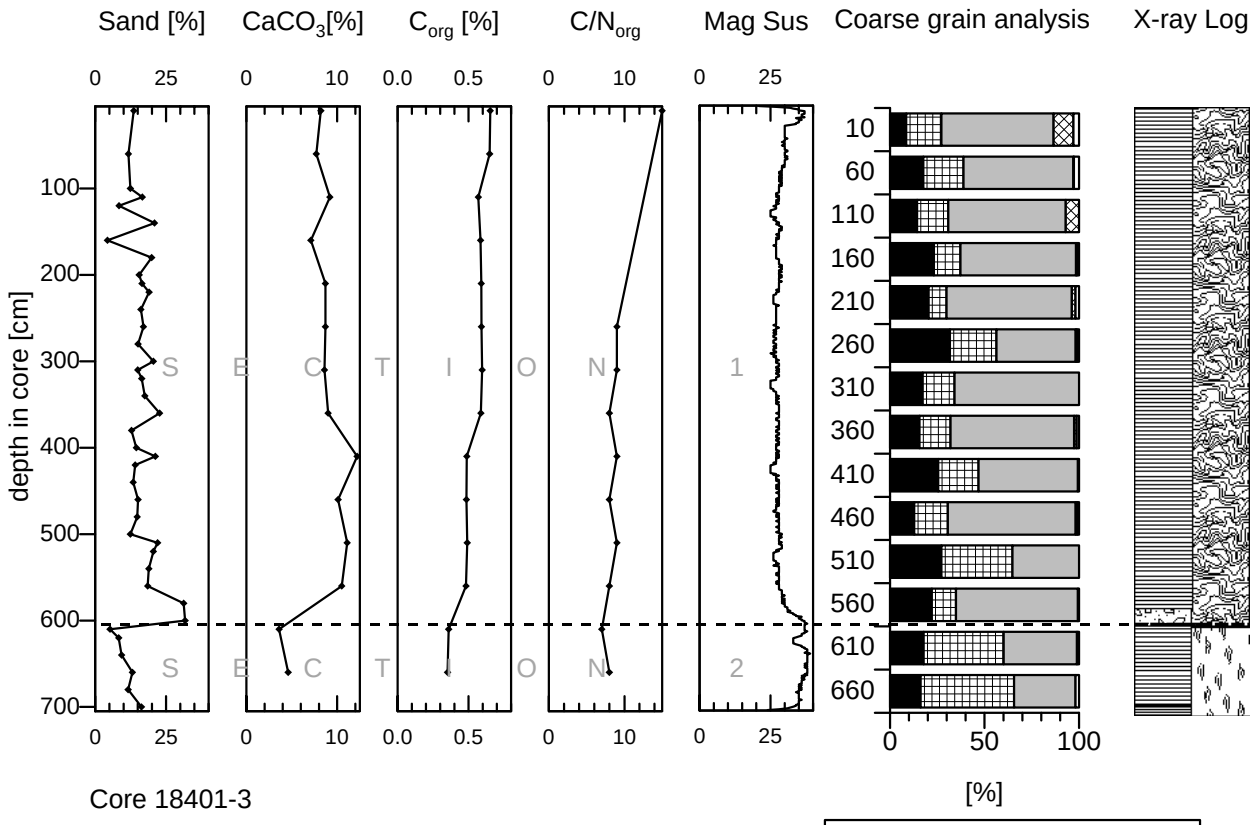
Sand [%]
CaCO3[%]
Corg [%]
C/Norg
Mag Sus
Coarse grain analysis
X-ray Log
depth in core [cm]
SECTION 1
SECTION 2
[%]
Core 18401-3
Plant fragments
Lithoclasts
Shell fragments
Benthic foraminifera
Planktonic foraminifera

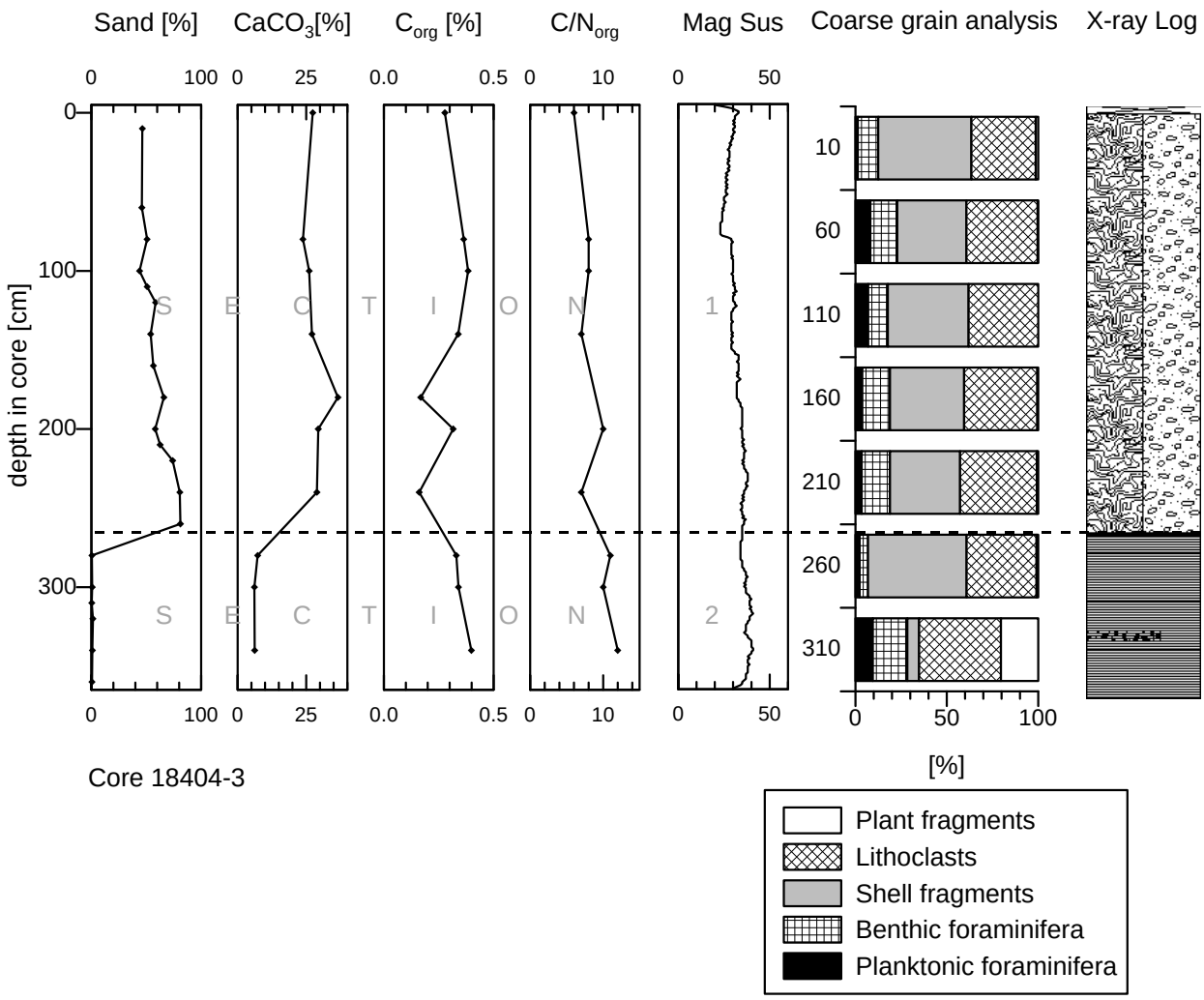

Core 18404-3

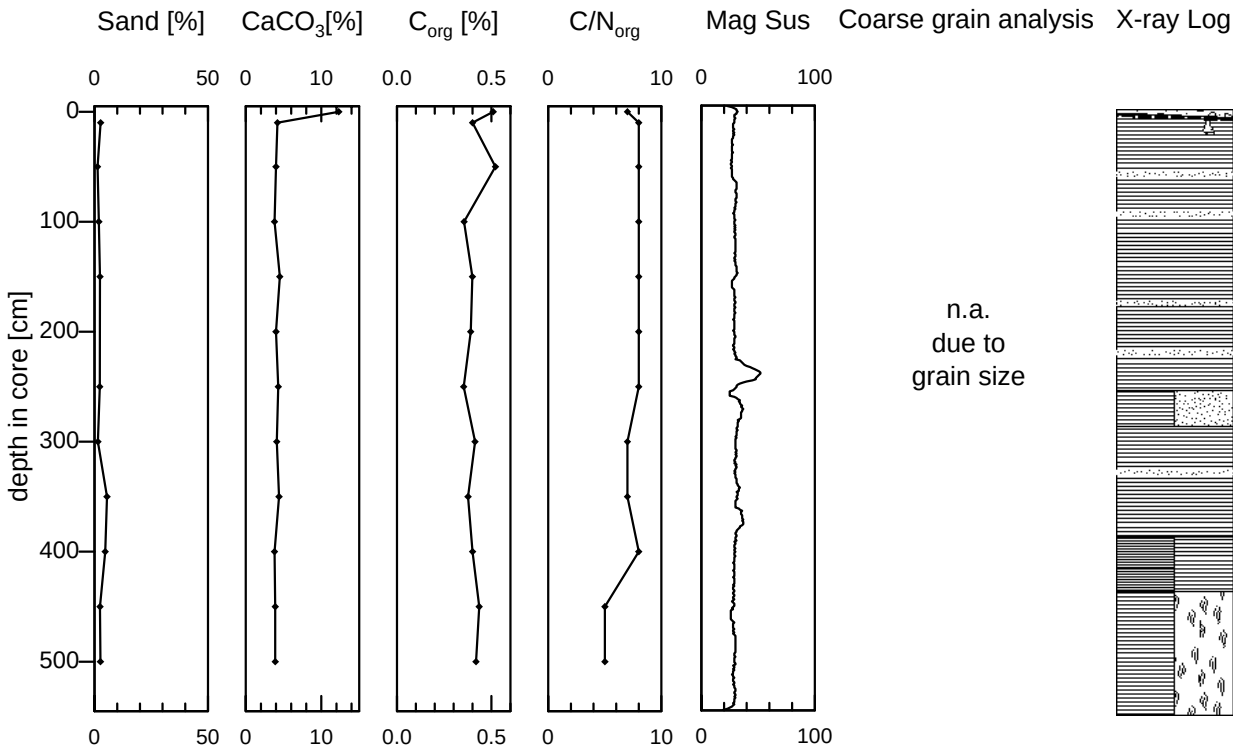

Core 18405-3

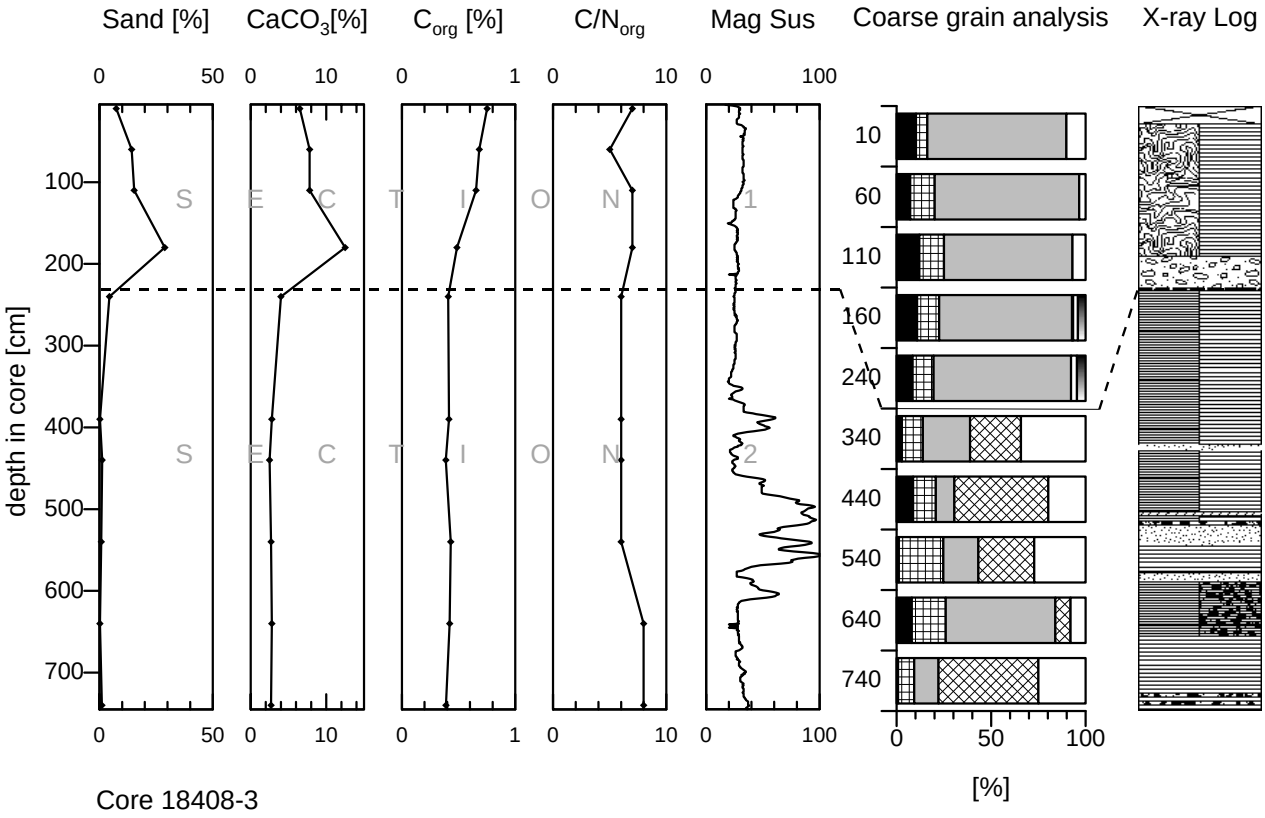
Sand [%]
CaCO3[%]
Corg [%]
C/Norg
Mag Sus
Coarse grain analysis
X-ray Log
depth in core [cm]
SECTION 1
SECTION 2
[%]
Core 18408-3

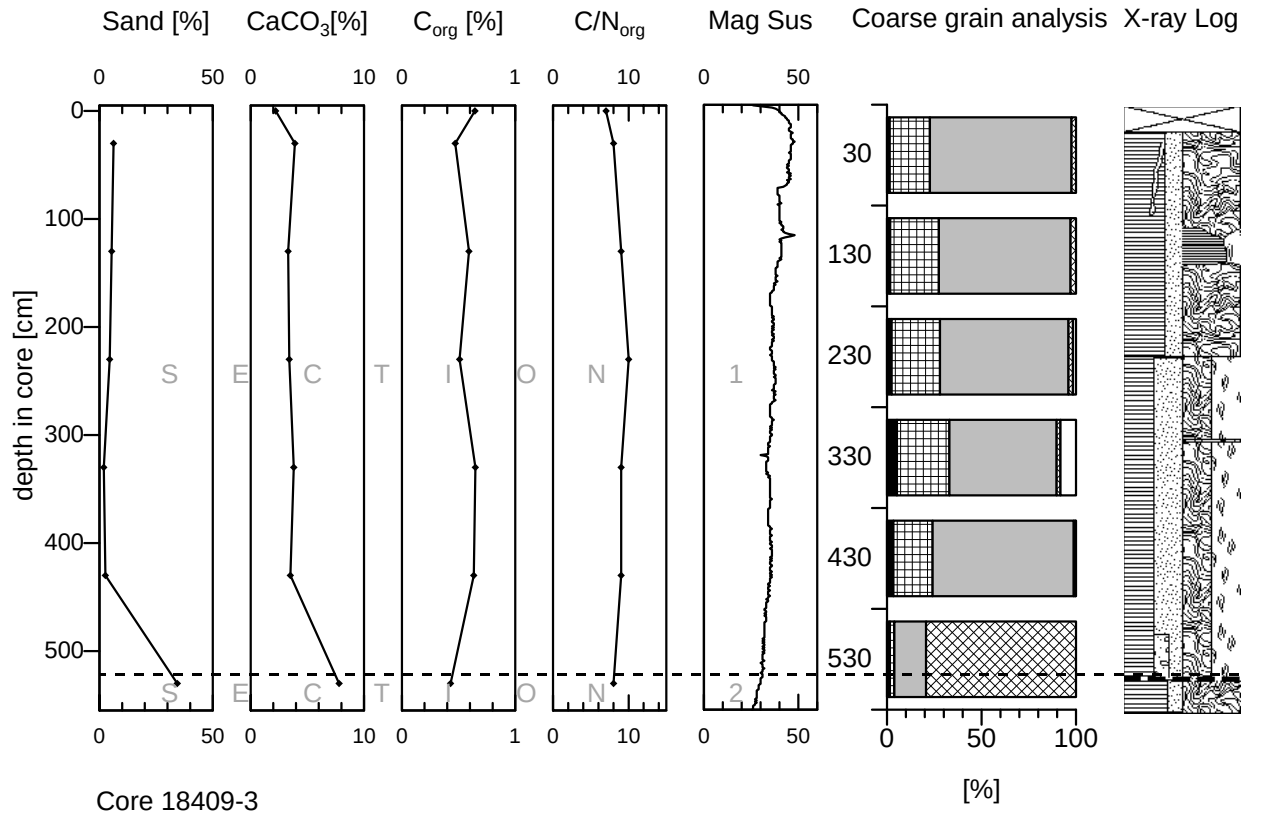
Sand [%]
CaCO3[%]
Corg [%]
C/Norg
Mag Sus
Coarse grain analysis
X-ray Log
depth in core [cm]
SECTION 1
SECTION 2
[%]
Core 18409-3

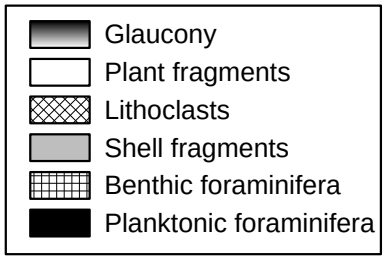
Glaucony
Plant fragments
Lithoclasts
Shell fragments
Benthic foraminifera
Planktonic foraminifera

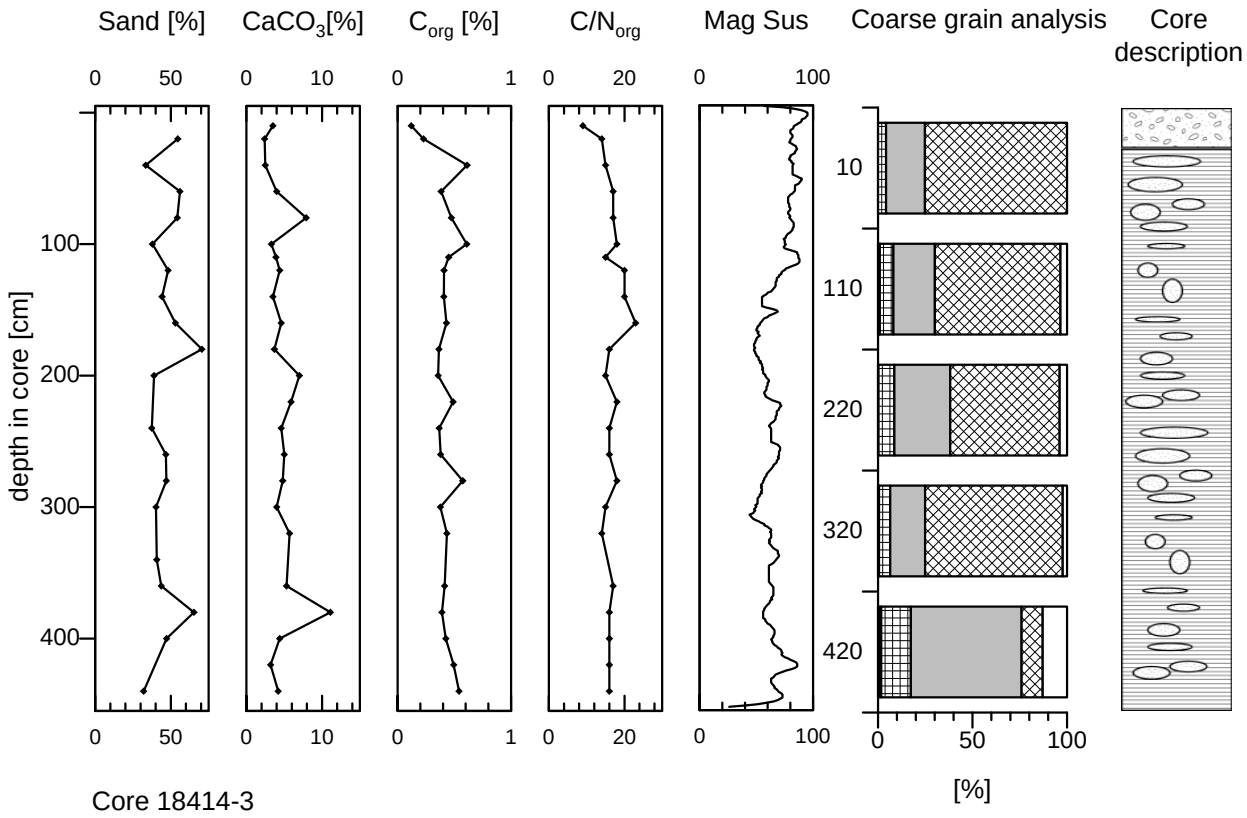
Sand [%]
CaCO3[%]
Corg [%]
C/Norg
Mag Sus
Coarse grain analysis
Core description
depth in core [cm]
[%]
Core 18414-3

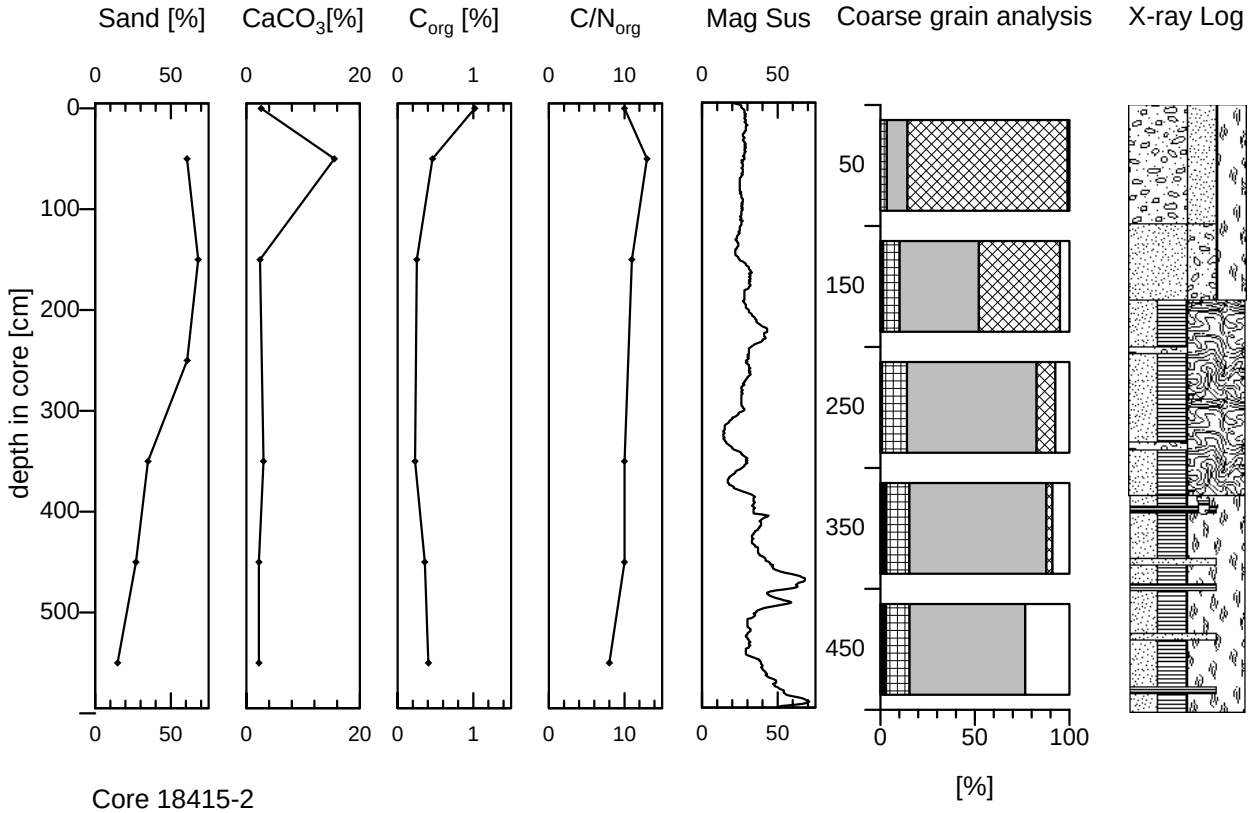
Sand [%]
CaCO3[%]
Corg [%]
C/Norg
Mag Sus
Coarse grain analysis
X-ray Log
depth in core [cm]
[%]
Core 18415-2
Plant fragments
Lithoclasts
Shell fragments
Benthic foraminifera
Planktonic foraminifera

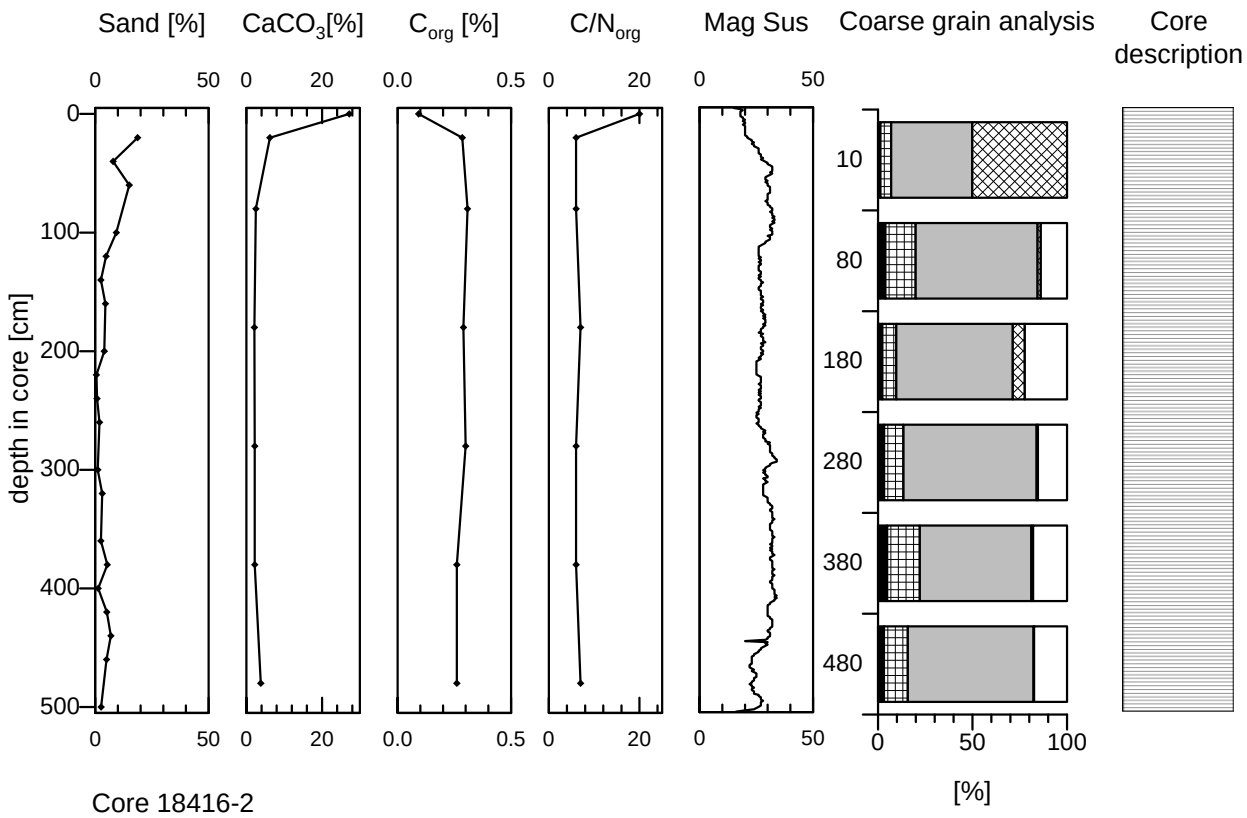
Sand [%]
CaCO3[%]
Corg [%]
C/Norg
Mag Sus
Coarse grain analysis
Core description
depth in core [cm]
[%]
Core 18416-2

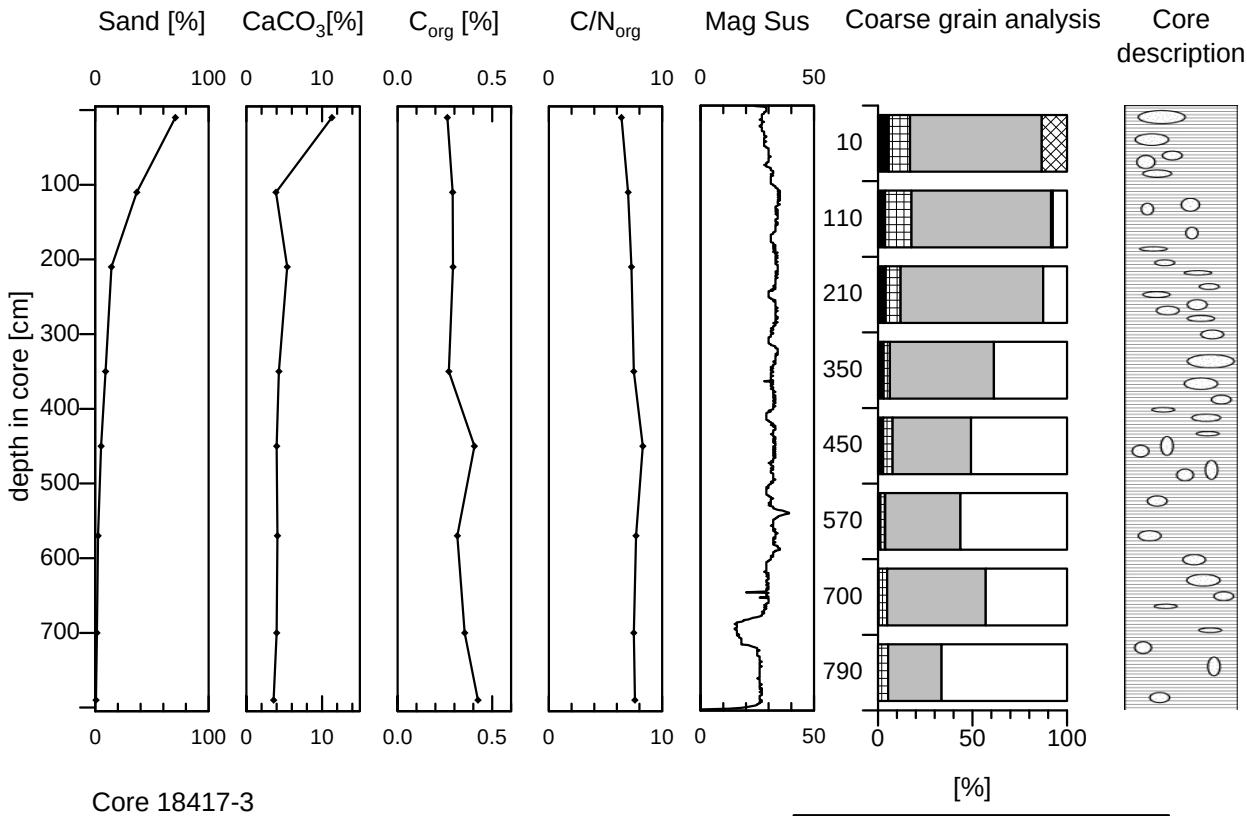
Sand [%]
CaCO3[%]
Corg [%]
C/Norg
Mag Sus
Coarse grain analysis
Core description
depth in core [cm]
[%]
Core 18417-3
Plant fragments
Lithoclasts
Shell fragments
Benthic foraminifera
Planktonic foraminifera

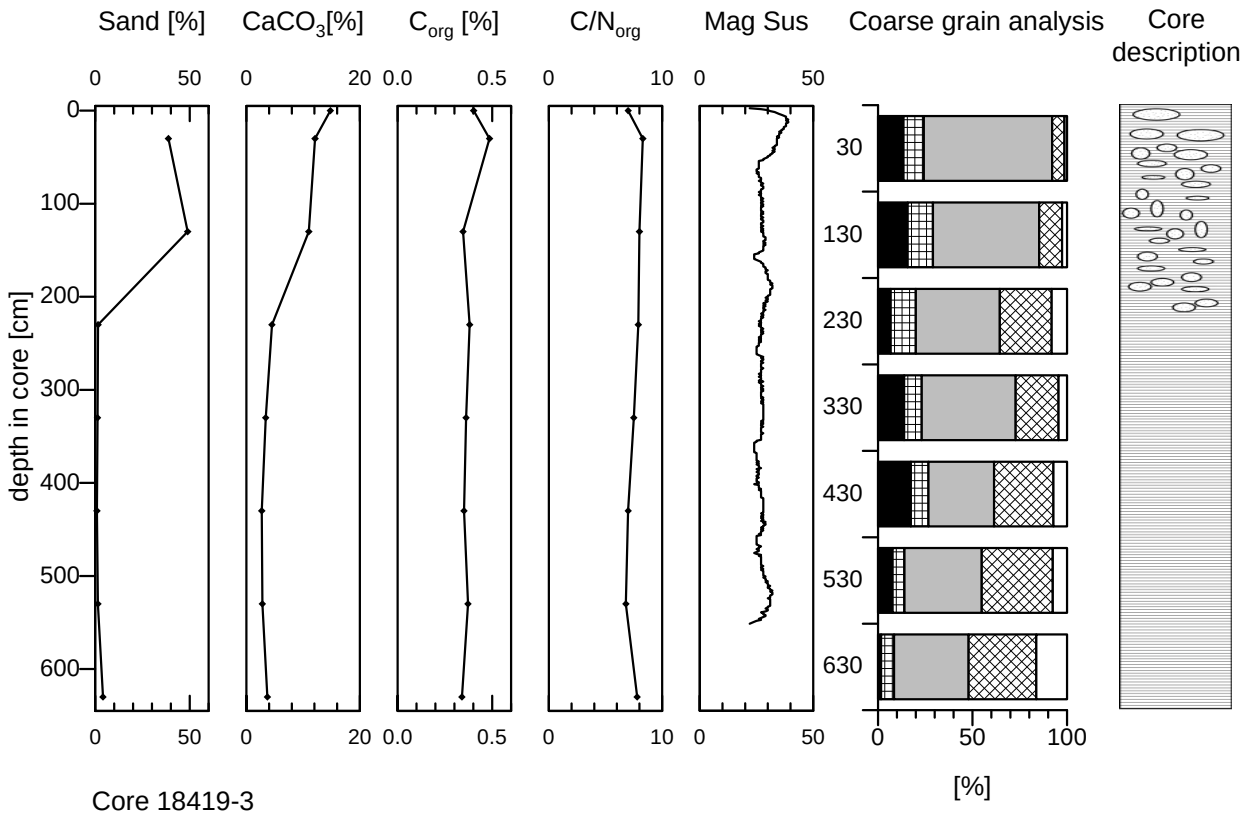
Sand [%]
CaCO3[%]
Corg [%]
C/Norg
Mag Sus
Coarse grain analysis
Core description
depth in core [cm]
[%]
Core 18419-3

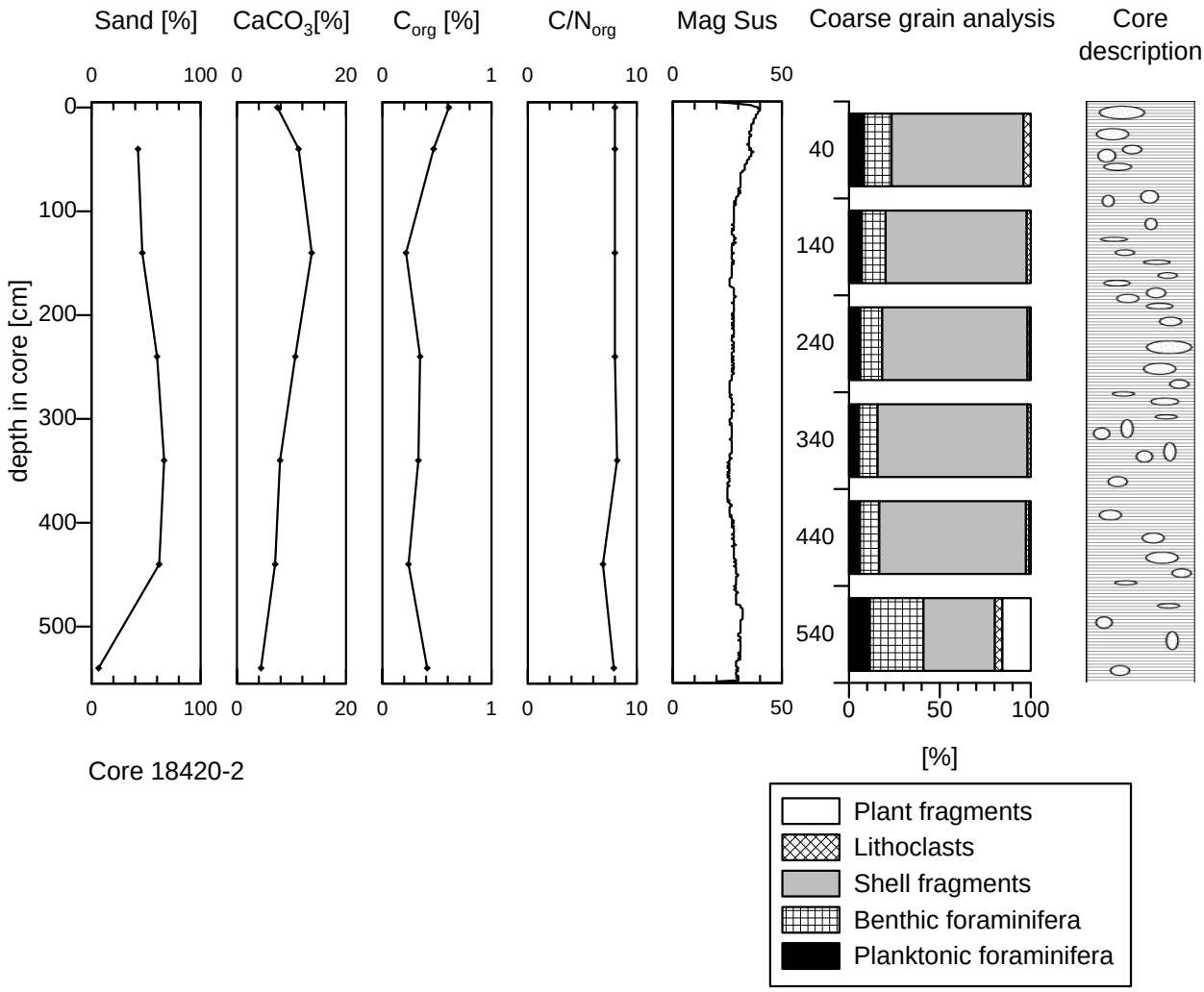
Sand [%]
CaCO3[%]
Corg [%]
C/Norg
Mag Sus
Coarse grain analysis
Core description
depth in core [cm]
[%]
Core 18420-2
Plant fragments
Lithoclasts
Shell fragments
Benthic foraminifera
Planktonic foraminifera

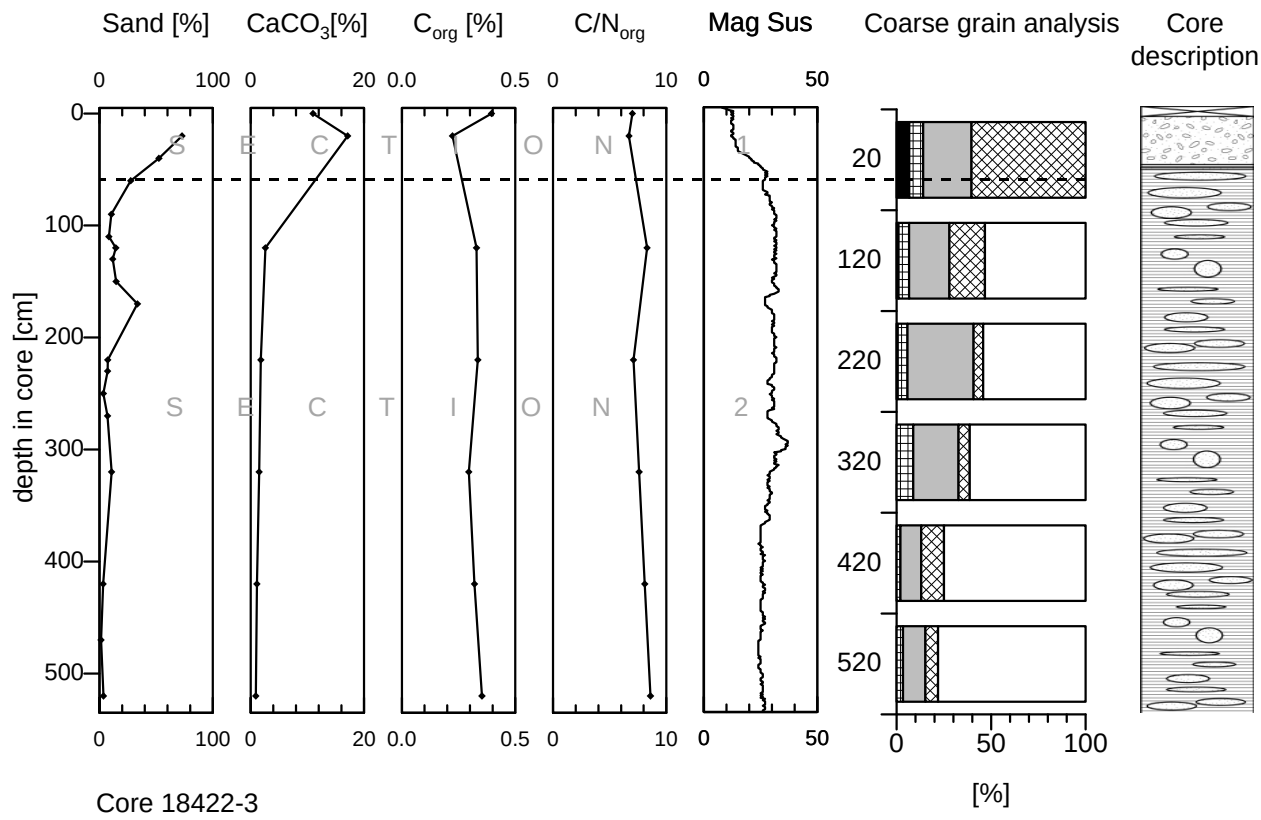
Sand [%]
CaCO3[%]
Corg [%]
C/Norg
Mag Sus
Coarse grain analysis
Core description
depth in core [cm]
SECTION 1
SECTION 2
20
120
220
320
420
520
[%]
Core 18422-3

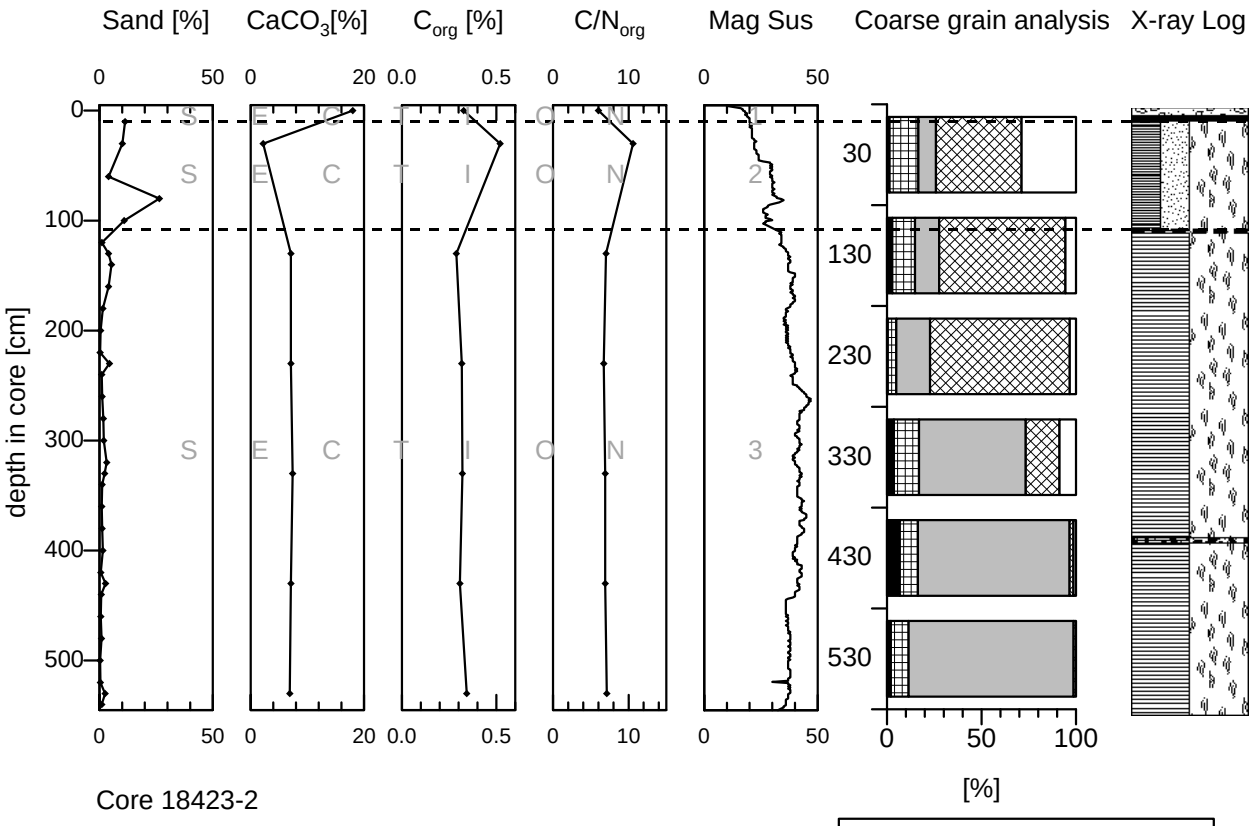
Sand [%]
CaCO3[%]
Corg [%]
C/Norg
Mag Sus
Coarse grain analysis
X-ray Log
depth in core [cm]
SECTION 1
SECTION 2
SECTION 3
30
130
230
330
430
530
[%]
Core 18423-2
Plant fragments
Lithoclasts
Shell fragments
Benthic foraminifera
Planktonic foraminifera

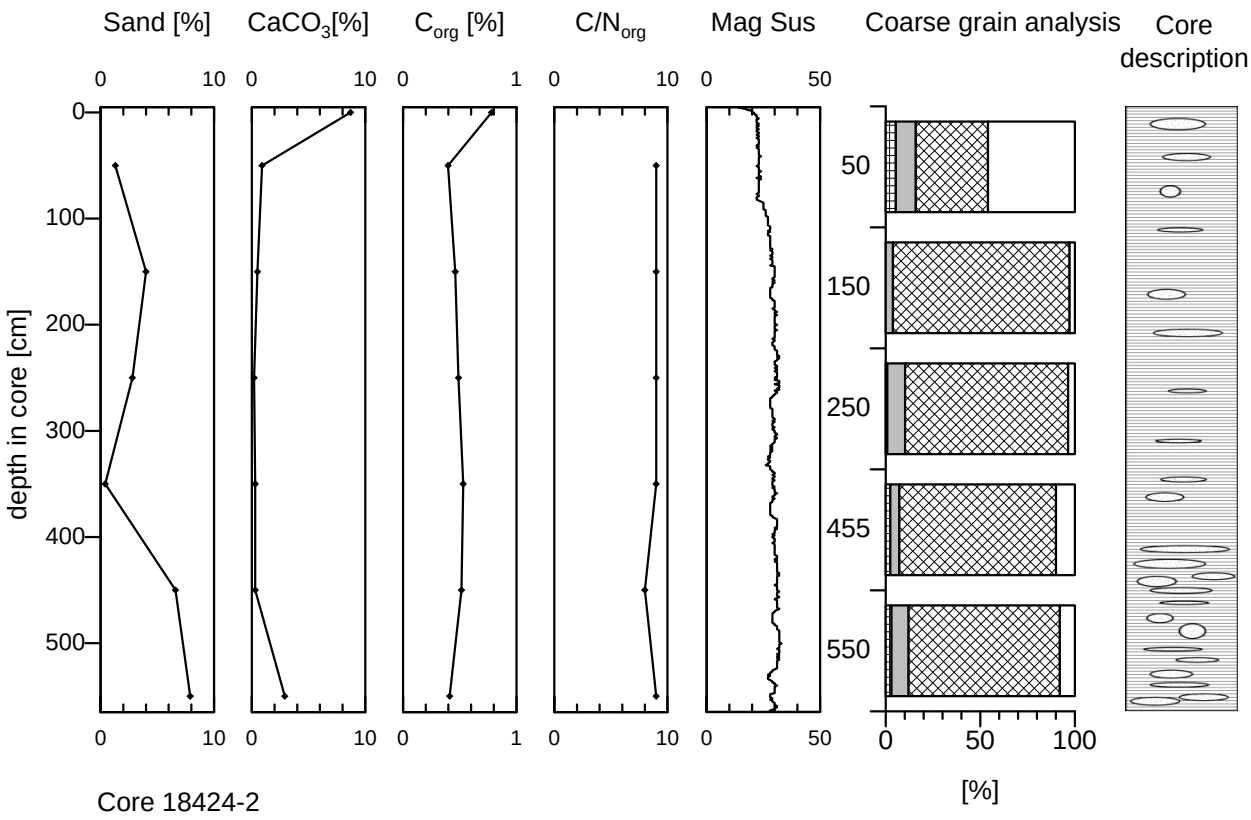
Sand [%]
CaCO3[%]
Corg [%]
C/Norg
Mag Sus
Coarse grain analysis
Core description
depth in core [cm]
0
100
200
300
400
500
0 10
0 10
0 1
0 10
0 50
50
150
250
455
550
0 50 100
[%]
Core 18424-2

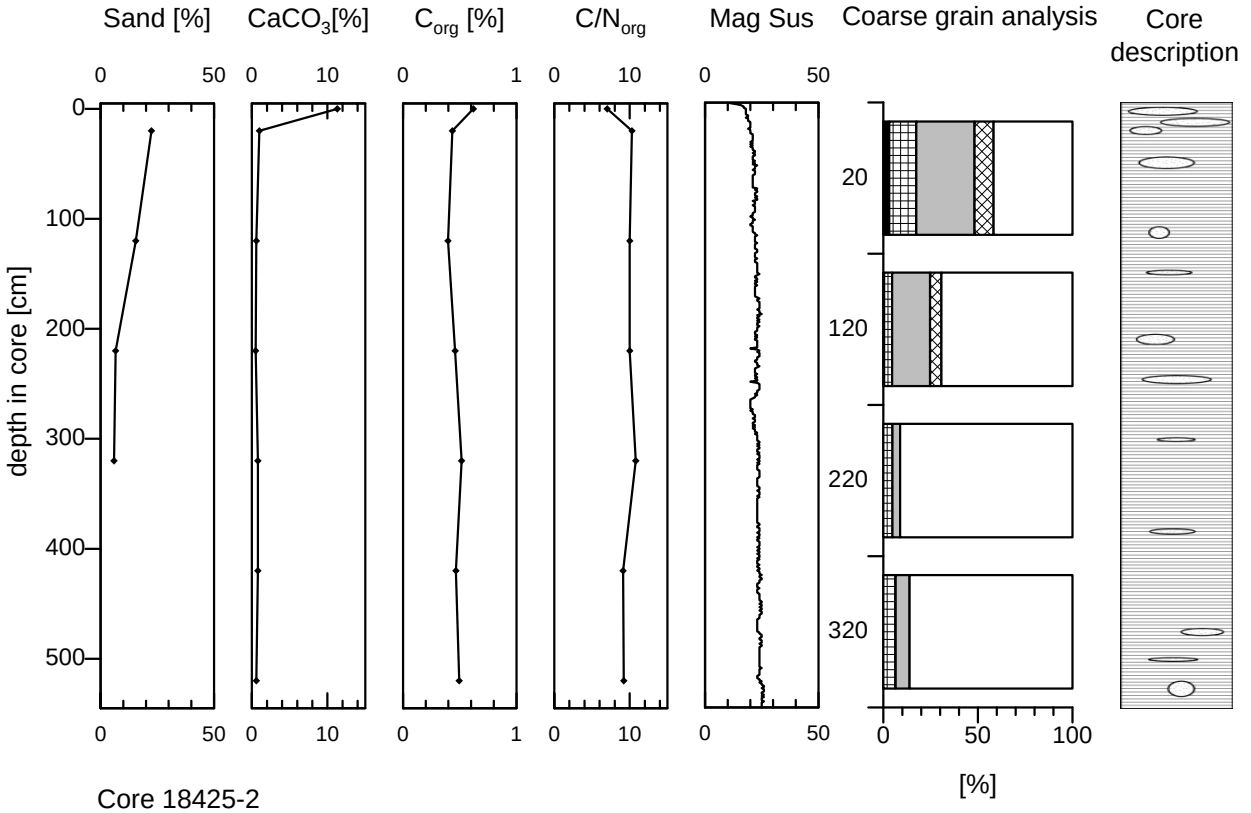
Sand [%]
CaCO3[%]
Corg [%]
C/Norg
Mag Sus
Coarse grain analysis
Core description
depth in core [cm]
0
100
200
300
400
500
0 50
0 10
0 1
0 10
0 50
20
120
220
320
0 50 100
[%]
Core 18425-2
Plant fragments
Lithoclasts
Shell fragments
Benthic foraminifera
Planktonic foraminifera

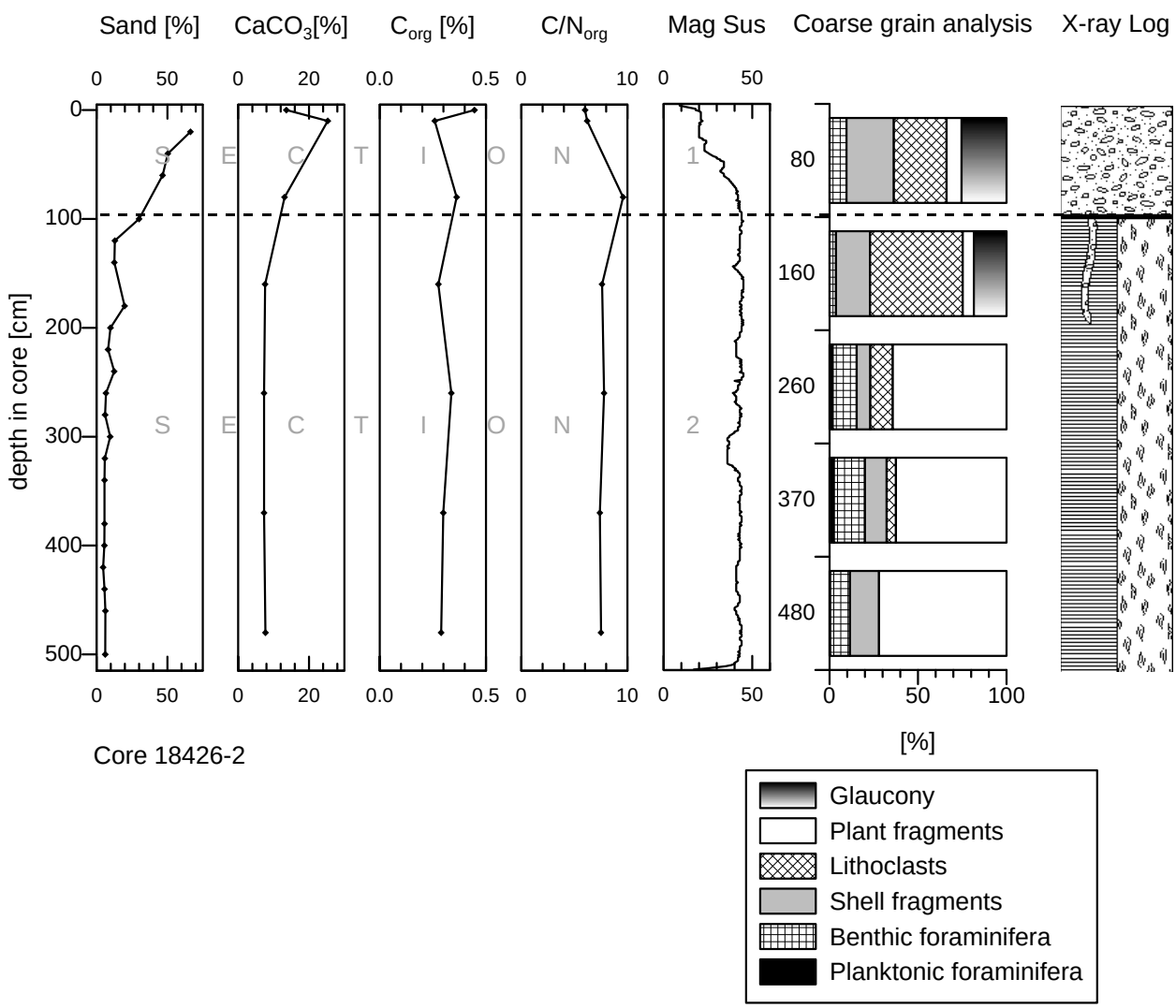
Sand [%]
CaCO3[%]
Corg [%]
C/Norg
Mag Sus
Coarse grain analysis
X-ray Log
depth in core [cm]
SECTION 1
SECTION 2
Core 18426-2
[%]
Glaucony
Plant fragments
Lithoclasts
Shell fragments
Benthic foraminifera
Planktonic foraminifera

PLATE

a) Wood fragment of core 18389-3 from 99 cm depth in core. Photograph ~1.3 cm across.

b) Wood fragment of core 18389-3 from186 cm depth in core. Photograph ~1.4 cm across.

c) Sand dollar of core 18391-2 from 332 cm depth in core. Photograph ~4 cm across.

d) Gastropod of core 18404-3 from 225 cm depth in core. Photograph ~3 cm across.

e) Sand dollar of core 18409-3 from 559 cm depth in core. Photograph ~1.3 cm across.

f) Bivalve shell (*Cardium sp.*) of core 18414-3 from 267 cm depth in core. Photograph ~4 cm across.

g) Benthic foraminifera (*Rotalia sp.*) of core 18417-3 from 450 cm depth in core. Photograph ~1.2 cm across.

h) Pteropods of core 18415-2 from 250 cm depth in core. Photographs ~0.5 cm (upper) and ~1.2 cm (lower) across.

i) Bivalve shell (*Paphia sp.*) 18416-2 from 98 cm depth in core. Photograph ~6 cm across.

j) Gastropod of core 18422-3 from 51 cm depth in core. Photograph ~4 cm across.

k) Sea urchin of core 18423-3-2 from 46.5 cm depth in core. Photograph ~3.3 cm across.

Plate

a)

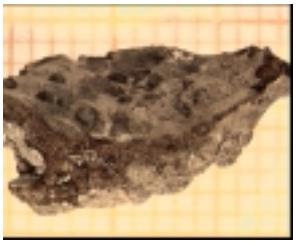

b)

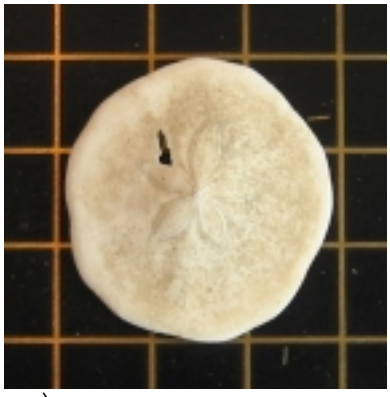

c)

d)

e)

f)

g)

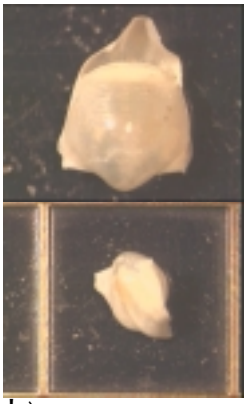

h)

i)

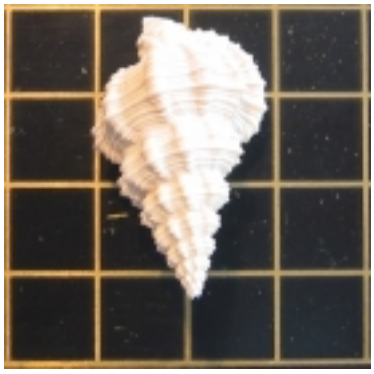

j)

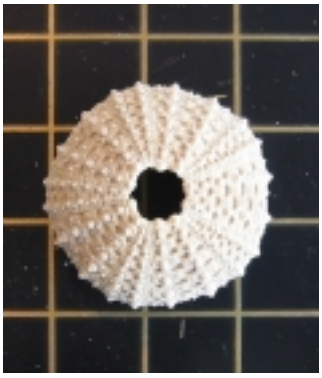

k)

Table A: Sedimentological Parameters

Depth [cm]	Watercontent [%] corr.	Sandcontent [%]	TC [%]	TOC [%]	$CaCO_3$ [%]	N [%]	C/N
Core 18375-2							
0			1.144	0.166	8.1	0.027	6
5	15.7	84.9					
60	25.3	55.1	0.346	0.096	2.1		
110	15.1	66.1	0.083				
159	36.5	2.1	0.882	0.805	0.6	0.068	12
220	22.9	1.3	0.158	0.061	0.8		
275	32.1	1.6	0.566	0.464	0.8	0.037	13
325	29.7	3.2	0.445	0.137	2.6		
Core 18376-2							
0			0.920	0.122	6.6		
30	20.6	92.6	1.132	0.108	8.5		
75	31.3	97.1	0.562	0.145	3.5		
130	44.4	14.8	0.703	0.556	1.2	0.035	16
180	25.1	7.6	0.617	0.536	0.7	0.039	14
230	44.1	10.9	0.672	0.481	1.6	0.041	12
280	41.2	3.4	0.618	0.526	0.8	0.042	13
340	25.8	54.6	0.267	0.260	0.1		
375	17.8	79.2	0.534	0.180	2.9		
425	44.2	11.4	0.619	0.450	1.4	0.037	12
450	28.8	76.7	0.585	0.150	3.6		
Core 18377-2							
30	46.1	11.6	0.631	0.546	0.7	0.026	21
92	45.9	3.6	0.679	0.543	1.1	0.033	17
150	36.2	26.3	0.796	0.451	2.9	0.028	16
226	15.2	89.1	0.235	0.185	0.4	0.017	11
282	25.6	86.7	0.192	0.063	1.1		
345	26.0	88.5	0.185	0.088	0.8	0.008	11
Core 18389-3							
0			0.665	0.096	4.7		
10	25.1	86.8	0.654	0.152	4.2		
50	30.6	59.3	0.791	0.506	2.4	0.046	11
90	75.6	11.8	2.009	1.007	8.3	0.067	15
150	69.5	23.0	1.528	1.477	0.4	0.077	19
183	65.4	5.9	3.210	3.560	-2.9	0.111	32
210	53.7	4.4	1.916	2.179	-2.2	0.081	27
260	66.7	4.0	3.404	3.726	-2.7	0.113	33
Core 18391-2							
0		63.8	1.758	0.407	11.3	0.060	7
20	43.3		1.922	0.324	13.3	0.047	7
40	45.8	65.1					
60	44.6	67.5					
70			1.581	0.257	11.0	0.034	7
80	35.1	75.4					
100	42.5	70.5					
120	36.1		1.339	1.055	2.4	0.201	5
140	34.1	71.0					
160	32.0	76.8					
170			1.311	1.227	0.7	0.231	5
180	30.9	77.3					
200	29.7	79.7					
220	31.6		1.149	0.987	1.4	0.187	5
240	29.6	78.5					
260	31.9	74.4					
270			1.257	1.152	0.9	0.226	5
280	31.1	76.1					
320	33.0	72.3	1.305	0.914	3.3	0.172	5
340	37.4	61.0					
360	50.2	28.6					
370			1.171	2.082		0.416	5
380	82.9	3.0					
420	62.1		1.026	2.003		0.390	5
Core 18393-3							
0			3.380	0.295	25.7	0.045	7
10	11.2	72.0	4.314	0.231	34.0	0.023	10
60	17.5	74.3	2.880	0.133	22.9		
110	22.1	76.5	2.503	0.155	19.6		
170	23.5	45.8	0.812	0.245	4.7		
230	20.9	41.6	0.800	0.233	4.7	0.020	12
270	32.5	37.9	0.884	0.267	5.1	0.025	11
350	18.7	38.3	0.812	0.235	4.8	0.033	7
410	19.5	49.5	0.856	0.199	5.5	0.031	6
470	23.6	35.2	1.054	0.238	6.8	0.032	8
Core 18396-3							
0			1.189	0.703	4.1	0.090	8
8	56.8	7.2	1.027	0.417	5.1	0.045	9
50	48.5	1.9	0.797	0.500	2.5	0.049	10
150	44.7	15.0	0.833	0.488	2.9	0.048	10
250	34.5	36.3	0.803	0.419	3.2	0.046	9
350	37.7	15.3	0.775	0.476	2.5	0.032	15
450	40.3	5.7	0.811	0.517	2.5	0.040	13

Table A: Sedimentological Parameters (cont.)

Depth [cm]	Watercontent [%] corr.	Sandcontent [%]	TC [%]	TOC [%]	$CaCO_3$ [%]	N [%]	C/N
Core 18397-2							
0			1.660	0.902	6.3	0.109	8
10	100.1	2.5	1.75	0.969	6.5	0.112	9
40	86.2	1.9					
60	89.4	1.4					
80	87.2	3.7					
100	109.7	4.8	1.763	0.958	6.7	0.102	9
140	76.5	3.9					
160	75.9	4.4					
180	83.8	4.0					
200	82.4	3.4	1.954	0.797	9.6	0.083	10
240	79.2	10.4					
260	72.0	6.1					
280	67.9	10.7					
300	68.2	9.1	2.007	0.688	11.0	0.074	9
340	70.9	4.7					
360	72.6	5.8					
380	67.5	7.4					
400	69.3	5.7	1.842	0.666	9.8	0.070	9
440	86.0	5.6	1.767	0.812	8.0	0.067	12
460	65.0	22.8	1.802	0.914	7.4	0.095	10
480	68.1	16.5	1.913	0.632	10.7	0.064	10
500	26.7	0.9	1.231	0.215	8.5	0.032	7
Core 18398-3							
0			1.480	1.016	3.9	0.124	8
10	87.4	6.6	1.407	0.858	4.6	0.096	9
60	65.2	5.8	1.454	0.868	4.9	0.096	9
110	71.5	4.2	1.411	0.848	4.7	0.094	9
160	80.0	5.5	1.389	0.833	4.6	0.092	9
210	76.3	4.7	1.425	0.799	5.2	0.086	9
260	73.3	5.2	1.373	0.814	4.7	0.088	9
310	67.5	6.6	1.433	0.771	5.5	0.081	9
360	68.5	6.0	1.386	0.779	5.1	0.084	9
410	68.6	6.0	1.416	0.763	5.4	0.085	9
460	68.8	4.6	1.407	0.813	4.9	0.089	9
535	61.4	6.3	1.465	0.780	5.7	0.081	10
585	52.7	7.0	1.446	0.715	6.1	0.074	10
660	47.1	16.0					
710	45.6	8.9	1.200	0.383	6.8	0.051	7
Core 18401-3							
0		6.3	1.634	0.769	7.2	0.105	7
10	77.2	13.6	1.634	0.653	8.2	0.044	15
20	71.6						
40	74.6						
60	68.5	11.7	1.577	0.649	7.7		
80	72.0						
100	68.7	12.4					
110	64.5	16.6	1.675	0.569	9.2		
120	76.0	8.4					
140	68.1	20.9					
160	65.5	4.3	1.436	0.585	7.1		
180	65.4	19.9					
200	66.2	15.5					
210	66.5	16.5	1.630	0.590	8.7		
220	67.4	19.0					
240	63.1	16.1					
260	61.3	17.0	1.630	0.591	8.7	0.068	9
280	63.8	15.1					
300	59.6	20.5					
310	62.6	15.0	1.633	0.596	8.6	0.068	9
320	63.2	16.4					
340	62.8	17.5					
360	62.4	22.7	1.672	0.587	9.0	0.070	8
380	66.0	12.8					
400	64.2	14.5					
410	58.4	21.2	1.946	0.488	12.2	0.056	9
420	64.8	14.1					
440	66.3	13.4					
460	55.9	15.1	1.699	0.485	10.1	0.059	8
480	62.8	14.8					
500	63.7	12.4					
510	57.1	22.0	1.820	0.491	11.1	0.057	9
520	56.2	20.5					
540	60.8	18.9					
560	52.0	18.5	1.738	0.482	10.5	0.057	8
580	47.2	31.2					
591geochem		42.1					
600	56.4	31.7					
610	50.9	5.2	0.792	0.360	3.6	0.050	7
620	56.3	8.3					
640	54.2	9.3					
660	48.7	13.1	0.904	0.352	4.6	0.047	8
680	50.4	11.6					
700	46.5	16.3					

Table A: Sedimentological Parameters (cont.)

Depth [cm]	Watercontent [%] corr.	Sandcontent [%]	TC [%]	TOC [%]	$CaCO_3$ [%]	N [%]	C/N
Core 18404-3							
0			3.570	0.278	27.4	0.045	6
10	50.9	46.5					
60	49.8	46.0					
80	41.9	50.7	3.221	0.364	23.8	0.048	8
100	48.1	43.9	3.519	0.384	26.1	0.049	8
110	42.7	50.8					
120	36.3	58.5					
140	39.4	54.0	3.593	0.339	27.1	0.046	7
160	36.5	56.5					
180	32.8	66.1	4.559	0.168	36.6	0.025	7
200	34.2	58.2	3.850	0.316	29.4	0.031	10
210	35.0	62.6					
220	30.5	74.1					
240	31.5	80.6	3.630	0.161	28.9	0.014	
260	18.2	81.1					
280	36.9	0.5	1.202	0.330	7.3	0.031	11
300	34.9	0.7	1.071	0.340	6.1	0.033	10
310	34.0	0.3					
320	33.4	1.3					
340	35.0	0.9	1.141	0.399	6.2	0.033	12
360	33.1	0.5					
Core 18405-3							
0			1.991	0.509	12.3	0.074	7
10	52.7	2.7	0.899	0.400	4.2	0.049	8
20	45.5	0.5					
50	60.4	1.3	1.005	0.521	4.0	0.062	8
100	45.3	1.9	0.817	0.355	3.8	0.044	8
150	49.6	2.4	0.938	0.399	4.5	0.052	8
250	42.8	2.3	0.864	0.353	4.3	0.045	8
300	47.3	1.5	0.907	0.413	4.1	0.057	7
350	43.8	5.5	0.901	0.376	4.4	0.051	7
400	44.1	4.7	0.852	0.400	3.8	0.053	8
450	44.4	2.4	0.907	0.435	3.9	0.087	5
500	44.7	2.6	0.892	0.418	3.9	0.083	5
Core 18408-3							
0			1.810	0.675	9.5	0.089	8
10	90.7	7.4	1.528	0.751	6.5	0.114	7
60	80.2	14.2	1.618	0.683	7.8	0.126	5
110	69.7	15.3	1.585	0.654	7.8	0.093	7
180	62.3	28.8	1.984	0.486	12.5	0.072	7
240	56.3	4.4	0.891	0.409	4.0	0.065	6
390	53.5	0.2	0.752	0.415	2.8	0.067	6
440	49.8	1.2	0.690	0.388	2.5	0.063	6
540	54.5	0.8	0.752	0.431	2.7	0.070	6
640	33.4	0.2	0.757	0.422	2.8	0.052	8
740	35.3	1.1	0.711	0.389	2.7	0.052	8
Core 18409-3							
0		4.4	0.907	0.644	2.2	0.089	7
30	67.8	6.2	0.942	0.470	3.9	0.057	8
130	64.1	5.4	0.990	0.591	3.3	0.065	9
230	54.4	4.5	0.914	0.509	3.4	0.052	10
330	58.1	1.9	1.104	0.648	3.8	0.071	9
430	55.4	2.6	1.058	0.634	3.5	0.068	9
530	39.8	34.3	1.363	0.429	7.8	0.054	8
560geochem		3.7					
Core 18414-3							
0			0.298	0.119	1.5		
10	35.3		0.536	0.120	3.5	0.014	9
20	29.3	54.6	0.513	0.228	2.4	0.016	14
40	41.5	33.4	0.918	0.612	2.5	0.040	15
60	29.6	56.0	0.858	0.383	4.0	0.023	17
80	33.3	54.3	1.426	0.474	7.9	0.028	17
100	43.3	37.8	1.004	0.610	3.3	0.034	18
110	36.5		0.914	0.450	3.9	0.030	15
120	36.0	48.2	0.934	0.409	4.4	0.021	20
140	37.2	44.2	0.825	0.407	3.5	0.020	20
160	39.3	53.0	0.986	0.430	4.6	0.019	23
180	30.6	70.5	0.805	0.364	3.7	0.023	16
200	44.2	38.9	1.194	0.357	7.0	0.024	15
220	32.9		1.193	0.489	5.9	0.027	18
240	43.7	37.4	0.916	0.366	4.6	0.024	16
260	39.3	46.7	0.977	0.379	5.0	0.024	16
280	37.8	47.0	1.147	0.574	4.8	0.032	18
300	34.0	40.2	0.862	0.377	4.0	0.025	15
320	39.5		1.017	0.434	4.9	0.031	14
340	41.0	40.7					
360	37.8	43.7	1.050	0.414	5.3	0.024	17
380	38.1	65.3	1.726	0.390	11.1	0.024	16
400	42.0	47.2	0.951	0.425	4.4	0.026	16
420	40.1		0.878	0.494	3.2	0.030	16
440	43.0	32.0	1.051	0.541	4.2	0.034	16
Core 18415-2							
0			1.330	1.020	2.6	0.103	10
50	31.3	60.7	2.319	0.462	15.5	0.034	13
150	33.7	68.1	0.538	0.253	2.4	0.023	11
250	34.7	60.8	0.480				
350	42.0	34.9	0.594	0.230	3.0	0.023	10
450	44.7	26.9	0.626	0.359	2.2	0.036	10
550	46.4	14.8	0.666	0.407	2.2	0.049	8

Table A: Sedimentological Parameters (cont.)

Depth [cm]	Watercontent [%] corr.	Sandcontent [%]	TC [%]	TOC [%]	$CaCO_3$ [%]	N [%]	C/N
Core 18416-2							
0		95.3	3.355	0.093	27.2	0.005	20
10	34.8		3.006				
20	59.1	18.7	1.029	0.285	6.2	0.045	6
40	60.7	7.9					
60	59.6	15.0					
80	59.4		0.610	0.308	2.5	0.048	6
100	47.5	9.3					
120	55.5	4.8					
140	55.7	2.5					
160	57.2	4.5					
180	56.4		0.544	0.290	2.1	0.044	7
200	59.8	4.0					
220	58.8	0.5					
240	65.9	0.8					
260	61.5	1.9					
280	55.7		0.567	0.300	2.2	0.047	6
300	64.8	1.1					
320	55.4	3.1					
340	48.7						
360	58.0	2.5					
380	49.8	5.3	0.523	0.261	2.2	0.041	6
400	56.7	1.3					
420	49.6	5.1					
440	48.9	6.9					
460	45.7	5.0					
480	41.4		0.715	0.261	3.8	0.036	7
490		1.3					
500	43.8	2.6					
Core 18417-3							
0			1.141	0.187	7.9	0.033	6
10	33.7	70.7	1.624	0.263	11.3	0.041	6
110	38.4	36.7	0.759	0.291	3.9	0.042	7
210	41.7	14.3	0.944	0.293	5.4	0.040	7
350	38.8	9.1	0.785	0.271	4.3	0.036	7
450	38.6	5.2	0.884	0.406	4.0	0.049	8
570	39.7	2.5	0.805	0.315	4.1	0.041	8
700	42.6	1.5	0.831	0.355	4.0	0.047	8
790	47.4	0.7	0.863	0.425	3.6	0.056	8
Core 18419-3							
0			2.180	0.402	14.8	0.057	0
30	61.6	38.7	1.941	0.486	12.1	0.058	0
130	49.7	48.9	1.670	0.346	11.0	0.043	0
230	61.2	1.5	0.925	0.381	4.5	0.048	0
330	62.6	1.2	0.769	0.362	3.4	0.048	0
430	68.5	0.9	0.676	0.351	2.7	0.050	0
530	58.0	1.4	0.708	0.372	2.8	0.055	0
630	43.8	4.1	0.789	0.340	3.7	0.044	0
Core 18420-2							
0			1.497	0.610	7.4	0.076	8
40	69.4	42.6	1.830	0.470	11.3	0.060	8
140	60.0	46.5	1.860	0.217	13.7	0.028	8
240	47.3	60.0	1.634	0.346	10.7	0.043	8
340	43.0	66.5	1.279	0.330	7.9	0.040	8
440	37.1	62.0	1.082	0.239	7.0	0.034	7
540	50.9	6.5	0.938	0.411	4.4	0.052	8
Core 18422-3							
0			1.716	0.395	11.0	0.060	7
20	37.1	72.8	2.276	0.223	17.1	0.034	7
40	37.6	52.4					
60	73.5	27.6					
90	50.8	10.5					
110	47.7	8.3					
120	43.8	14.4	0.638	0.329	2.6	0.039	8
130	50.4	11.7					
150	43.3	14.7					
170	35.2	33.5					
190	45.6						
210	41.9						
220	55.1	7.3	0.553	0.335	1.8	0.047	7
230	34.4	7.2					
250	41.3	3.4					
270	45.4	7.1					
290	30.3						
310	49.0						
320	44.7	10.7	0.473	0.295	1.5	0.039	8
330	45.8						
350	46.3						
370	49.7						
390	36.0						
410	48.0	0.3					
420	45.3	3.2	0.450	0.320	1.1	0.039	8
430	46.5	0.2					
450	48.7	0.5					
470	40.4	1.4					
490	47.2						
510	45.9						
520	51.4	3.5	0.459	0.353	0.9	0.041	9
530	57.1						
550	47.1						

Table A: Sedimentological Parameters (cont.)

Depth [cm]	Watercontent [%] corr.	Sandcontent [%]	TC [%]	TOC [%]	$CaCO_3$ [%]	N [%]	C/N
Core 18423-2							
0			2.530	0.327	18.4	0.051	6
10	66.2	11.3					
30	59.2	10.1	0,7861	0.520	2.2	0.049	11
46.5geochem		87.6					
60	67.9	4.0					
80	54.0	26.4					
100	50.4	10.9					
120	38.6	1.1					
130	38.6	4.0	1,1394	0.288	7.1	0.041	7
140	38.2	5.3					
160	34.4	4.0					
180	36.7	1.5					
200	37.0	0.5					
220	36.2	0.3					
230	34.6	4.4	1,1688	0.317	7.1	0.048	7
240	36.1	1.0					
260	36.7	1.2					
280	48.2	1.7					
300	55.9	1.9					
320	56.1	3.2					
330	36.9	2.3	1,2051	0.320	7.4	0.046	7
340	36.0	1.2					
360	32.6	1.0					
380	34.8	1.2					
400	38.4	1.5					
420	38.5	0.6					
430	35.4	2.7	1,1595	0.307	7.1	0.045	7
440	35.7	0.8					
460	38.6	0.6					
480	37.7	0.9					
500	38.3	0.3					
520	37.2	0.4					
530	34.9	2.5	1,1745	0.343	6.9	0.049	7
540	36.0	1.0					
Core 18424-2							
0			1.820	0.780	8.7	0.113	
50	55.1	1.3	0.500	0.397	0.9	0.043	9
150	57.9	4.0	0.516	0.460	0.5	0.051	9
250	60.0	2.8	0.514	0.489	0.2	0.053	9
350	62.3	0.4	0.572	0.530	0.3	0.060	9
455	58.8	6.6	0.556	0.515	0.3	0.061	8
550	44.2	7.9	0.762	0.411	2.9	0.047	9
Core 18425-2							
0			1.974	0.620	11.3	0.091	7
20	50.3	22.4	0.557	0.435	1.0	0.042	10
120	51.2	15.5	0.470	0.396	0.6	0.040	10
220	52.2	6.6	0.517	0.459	0.5	0.046	10
320	52.3	5.9	0.616	0.516	0.8	0.048	11
420	60.1		0.562	0.466	0.8	0.051	9
520	58.5		0.572	0.495	0.6	0.054	9
Core 18426-2							
0			2.084	0.446	13.6	0.070	6
10	47.2		3.296	0.259	25.3	0.042	6
20	46.3	66.3					
40	47.6	50.3					
60	51.9	46.6					
80	39.7		1.937	0.362	13.1	0.038	10
100	35.6	30.0					
120	35.3	12.9					
140	37.5	12.5					
160	34.9		1.185	0.276	7.6	0.036	8
180	33.6	19.8					
200	35.0	9.8					
220	36.4	8.1					
240	36.1	12.4					
260	37.5		1.208	0.337	7.3	0.043	8
280	33.1	6.0					
300	38.8	9.6					
320	33.7	5.8					
340	37.8	5.6					
370	34.2		1.179	0.299	7.3	0.041	7
380	31.9	5.6					
400	33.5	5.5					
420	34.0	4.6					
440	35.9	5.6					
460	42.4	6.2					
480	32.9		1.219	0.289	7.7	0.039	7
500	33.1	6.1					

Table B: Coarse Grain Analyses

Core No	Depth in core [cm]	Planktonic foraminifera [%]	Benthic foraminifera [%]	Shell fragments [%]	Lithoclasts [%]	Plant fragments [%]	Glaucony [%]
18375-2	5	14.9	6.1	35.4	43.6	0	0
	60	19.9	7.4	47.7	23.3	1.7	0
	110	0	0	3	96.5	0.5	0
	159	0	0	0	0	100	0
	220	0	0	0	69.8	30.2	0
	275	0	0	0	0	100	0
	325	0	0	0	0	100	0
18376-2	30	16.4	5.5	31.3	46.1	0.8	0
	75	7.6	7	22.1	60.8	2.5	0
	130	1.1	0.5	5.4	74.1	18.9	0
	180	0	0	0.2	60.4	39.4	0
	230	0	0	0.7	76	23.3	0
	260	0	0	1.7	69.4	28.9	0
	340	0	0.3	6.2	87.9	5.6	0
	375	0	0	0.8	98.5	0.7	0
	425	0.8	0.8	5.7	59.5	33.3	0
	450	2.3	4.6	53.9	38.3	0.9	0
18377-2	30	0	0	1.3	43.8	54.9	0
	92	0	0.3	1.4	64.2	34.1	0
	150	0	0	2.1	89.1	8.8	0
	226	0	0	5.1	90.3	4.6	0
	282	0	0	1.2	92.4	6.5	0
18389-3	10	0.2	2.9	2.4	94.5	0	0
	50	0.6	1.2	6.8	91	0.3	0
	90	0	1.7	2.1	82.6	13.6	0
	150	0	0.6	1.2	85	13.2	0
	183	0	0	0	0	100	0
	210	0	0	0.5	9.5	90	0
	250	0	0	0	0	100	0
18391-2	40	15.4	10.2	74.4	0	0	0
	140	29.8	15.8	54.4	0	0	0
	240	16.5	9.7	73.8	0	0	0
	320	11.8	16.0	70.2	1.9	0	0
	380	6.0	32.6	42.7	18.7	0	0
18393-3	10	4.8	8.2	65.3	21.8	0	0
	60	4.1	9.0	71.3	15.6	0	0
	110	8.5	12.4	47.1	26.8	0	0
	170	5.8	20.6	70.3	1.9	1.3	0
	270	1.4	13.0	49.3	14.5	21.7	0
	350	2.6	26.4	53.4	0	17.6	0
	470	3.6	26.4	64.8	0	5.2	0
18396-3	8	0.9	4.7	23.6	67.4	3.4	0
	50	8.1	16.9	54.6	16.9	3.4	0
	150	1.1	2.3	25.6	56.9	14.1	0
	250	0.7	2.3	7.6	87.4	2.1	0
	350	0.1	1.3	16.2	52	30.3	0
	450	0.3	0.7	3.9	7.8	87.3	0
18397-2	10	2.3	5.7	89.8	1.1	1.1	0
	100	4.9	6.6	88.5	0	0	0
	200	4.1	15.5	76.8	3.6	0	0
	300	1.9	13.5	61.5	20.4	2.7	0
	400	6.9	10.3	74.5	8.3	0	0
	460	0	2.1	20.1	76.4	1.4	0
	500	40.7	27.1	32.2	0	0	0
18398-3	10	9.1	27.3	63.6	0	0	0
	160	26.5	28.6	40.8	0	4.1	0
	310	17.6	13.2	58.2	0	11	0
	460	15.2	15.2	66.3	0	3.3	0
	585	22.2	21.3	56.5	0	0	0
	660	22.7	17.3	60	0	0	0
	710	21.3	18.7	55.5	0	4.5	0
18401-3	10	8.6	18.6	59.3	10.5	3	0
	60	17.6	21.3	58.1	0.3	2.7	0
	110	14.3	16.5	62.2	7	0	0
	160	23.2	14.1	61.1	0.5	1.1	0
	210	20.4	9.5	66.4	1.9	1.9	0
	260	31.7	24.6	41.9	0.6	1.2	0
	310	17.3	16.8	65.9	0	0	0
	360	15.6	16.4	65.3	1.3	1.3	0
	410	25.5	21.3	52.6	0	0.6	0
	460	12.8	17.8	67.6	0.9	0.9	0
	510	27.2	37.6	35.2	0	0	0
	560	22.1	12.8	64.5	0	0.6	0
	610	17.8	42.3	38.8	0	1.1	0
	660	16.2	49.4	32.5	0	1.9	0

Table B: Coarse Grain Analyses (cont.)

Core No	Depth in core [cm]	Planktonic foraminifera [%]	Benthic foraminifera [%]	Shell fragments [%]	Lithoclasts [%]	Plant fragments [%]	Glaucony [%]
18404-3	10	1.3	11.2	51	35.3	1.3	0
	60	8.2	14.7	37.9	39	0.3	0
	110	7	10.7	44.2	38.1	0	0
	160	3.8	15.1	40.6	40.1	0.5	0
	210	3.4	15.5	38.4	42	0.7	0
	260	2.3	4.6	53.9	38.3	0.9	0
	310	9.5	18.9	6.5	44.8	20.4	0
18408-3	10	10.2	6	73.6	0	10.2	0
	60	7.2	12.9	76.4	0	3.4	0
	110	12	13	67.9	0	7	0
	160	10.8	11.7	70.3	0.6	2.5	4.1
	240	8.4	11.1	72.8	0	3.1	4.6
	340	2.8	11.1	25	26.9	34.3	0
	440	8.7	12	9.8	49.7	19.7	0
	540	1.2	23.5	18.5	29.6	27.2	0
	640	8	18	58	8	8	0
	740	0.7	8.6	12.9	52.9	25	0
18409-3	30	1.4	21.3	74.9	2.4	0	0
	130	1.7	25.7	69.7	2.9	0	0
	230	2.4	25.6	68	2.4	1.6	0
	330	5.2	27.8	56.7	2.1	8.2	0
	430	3.4	20.7	74.7	0.8	0.4	0
	530	1.5	2.4	16.7	79.4	0	0
18414-3	10	5.7	11.3	69.7	13.4	0	0
	110	3.7	14	73.8	1	7.5	0
	210	4.1	7.9	75.4	0	12.6	0
	350	3	3.3	55	0	38.7	0
	450	2.8	5	41.4	0	50.8	0
	570	1.3	2.6	39.7	0	56.4	0
	700	0.4	4.4	52.2	0	43	0
	790	0	5.4	28.3	0	66.4	0
18415-2	50	0	3.4	10.9	84.8	0.9	0
	150	1.4	8.7	42.0	42.9	5.0	0
	250	0.8	13.2	68.6	9.9	7.4	0
	350	3.2	12.2	72.5	3.2	9.0	0
	450	3.0	12.4	61.2	0	23.4	0
18416-2	10	1.3	5.7	43.0	50.1	0	0
	80	3.9	16.0	64.5	1.7	13.9	0
	180	2.3	7.3	61.7	6.3	22.3	0
	280	3.2	10.3	70.4	0.6	15.4	0
	380	4.8	17.3	59.0	1.0	18.0	0
	480	3.2	12.6	66.6	0.2	17.4	0
18417-3	10	5.7	11.3	69.7	13.4	0	0
	110	3.7	14.0	73.8	1	7.5	0
	210	4.1	7.9	75.4	0	12.6	0
	350	3.0	3.4	55.0	0	38.7	0
	450	2.8	5.0	41.4	0	50.8	0
	570	1.3	2.6	39.7	0	56.4	0
	700	0.4	4.4	52.2	0	43.0	0
	790	0	5.4	28.3	0	66.4	0
18419-3	30	13.5	10.7	67.9	6.6	1.3	0
	130	15.7	13.4	56.2	12.1	2.6	0
	230	6.7	13.3	44.4	27.4	8.1	0
	330	13.8	9.3	49.7	22.6	4.5	0
	430	17.4	9.3	34.7	31.4	7.2	0
	530	7.7	6.3	40.8	37.6	7.5	0
	630	1.6	6.9	39.5	35.8	16.3	0
18420-2	40	8.3	15.2	72.5	4	0	0
	140	7.1	13.1	77.6	2.2	0	0
	240	6.3	12	79.9	1.5	0.3	0
	340	5.6	10.2	82.4	1.8	0	0
	440	6.1	10.6	80.7	1.8	0.8	0
	540	11.5	29.5	39.3	4.1	15.6	0
18422-3	20	6.7	7.3	25.6	60.4	0	0
	120	1	5.6	21.3	18.8	53.3	0
	220	0.6	5.1	35	5.1	54.2	0
	320	0	8.8	23.9	6	61.3	0
	420	0	2	11	12	75	0
	520	0	3.4	11.8	6.7	78.2	0

Table B: Coarse Grain Analyses (cont.)

Core No	Depth in core [cm]	Planktonic foraminifera [%]	Benthic foraminifera [%]	Shell fragments [%]	Lithoclasts [%]	Plant fragments [%]	Glaucony [%]
18423-2	30	1.3	15.3	9.3	45.3	28.8	0
	130	2.8	12	12.8	66.8	5.6	0
	230	0.4	4.5	17.9	74	3.3	0
	330	3.6	13.3	56.4	17.9	8.7	0
	430	6.8	9.5	80.4	2	1.4	0
	530	2	9.4	87.2	1.3	0	0
18424-2	50	0	5.3	10.6	38.2	45.9	0
	150	0	0	3.8	93.4	2.8	0
	250	0	0.8	9.4	86.2	3.5	0
	455	0	2.4	4.8	82.9	10	0
	550	0	3	9.1	80	7.9	0
18425-2	20	3.1	14.3	30.8	10.1	41.7	0
	120	0.4	4.2	20.1	6	69.3	0
	220	0	4.8	4.1	0	91.2	0
	320	0	6.5	7.3	0	86.1	0
18426-2	80	0	9.6	26.8	29.9	8.5	25.4
	160	0	3.7	19.2	52.4	6.3	18.4
	260	1.8	13.6	7.7	12.7	64.3	0
	370	2.5	17.5	12.3	5.3	62.5	0
	480	0.4	11.1	16.4	0	72	0

Table C: Oxygen isotopic composition of benthic foraminifera of cores 18414-3 and 18416-2

Core 18414-3 Fraction 250-500µm	depth in core [cm]	$\delta^{18}O$ Nonion sp. [‰]	$\delta^{18}O$ Elphidium sp. [‰]
	20	-1.78	-1.78
	40	-1.69	-1.94
	60	-1.57	-2.35
	80	-1.86	-1.77
	100	-1.53	-1.87
	120	-1.43	-1.60
	140	-1.57	-1.56
	160	-1.39	-1.69
	180	-1.65	-1.62
	200	-1.47	-1.70
	240	-1.46	-1.49
	260	-1.52	-1.40
	280	-1.40	-1.51
	300	-1.39	-1.66
	320	-1.38	-1.40
	360	-1.54	-1.54
	380	-1.63	-1.69
	400	-1.48	-1.39
	440	-1.29	-1.71

Core 18416-2 Fraction 250-500µm	depth in core [cm]	$\delta^{18}O$ Nonion sp. [‰]	$\delta^{18}O$ Elphidium sp. [‰]
	20		-1.15
	60		-1.48
	100	-1.76	
	100	-1.34	
	120	-1.38	-0.65
	120		
	160	-0.64	-1.11
	200	-1.28	-1.47
	200		-0.89
	220		-0.83
	260	-1.18	-1.79
	260		-1.37
	300		-1.49
	360	-1.60	-0.82
	360		-2.37
	380		-1.12
	400		-0.81
	500	-1.22	-0.83
	500	-0.96	-1.24

T. J.J. Hanebuth, A. Schimanski, K. Stattegger

Late Pleistocene forced regression deposits on the Sunda Shelf (SE Asia)

Abstract Regressive deposits from the central Sunda Shelf (SE Asia) were investigated by seismic surveying and on sediment cores. The stratigraphic resolution is favoured by the low shelf gradient and featured by a strong focused sediment supply during periods of lower sea level. Three types of regressive deposits have formed over the past fifty thousand years: (i) Thick lens-shaped foresetting sediment 'bodies' up to 30 km wide which fill slight depressions; (ii) Thin horizontally bedded deposits between the 'bodies'; (iii) A thick sediment wedge on the outer shelf and at its margin, showing progradation (to aggradation). The sediment cores reached the upper parts of the regressive deposits and contain a regressive-transgressive succession comprising terrestrial, tidal and shallow-marine facies.

The sediment 'bodies' are interpreted as detached regressive deposits due to the interplay of low gradient and minor sea-level fluctuations, which resulted in the reduction of accumulation space and local stacking deposits.

By dating plant remnants, a sea-level envelope was determined, showing differences to established sea-level records: (i) sea level was slightly lower during 50 to 40 kyr; (ii) the rapid drop leading to the last glacial maximum lowstand appeared a few kyr earlier; (iii) the low-stand was not deeper than –120 m.

Keywords Forced regression · siliciclastic shelf deposits · sea-level changes · Late Pleistocene · Sunda Shelf · facies analysis · seismic survey

Introduction

When significant fluvial sediment supply continuously reaches the coastline over a long period, the changes in water level of the recipient water body (e.g., ocean) are the main factor in determining whether and how prograding deposits build up. If sea level remains stable, the sedimentary system progrades with clinoforms basinward and forms an extended delta system including submarine (pro-) delta fans. In contrast, sea-level lowering reduces the available *accommodation space*, forcing the depositional system to shift basinward with downward stepping tendency (Fig. 1). It also causes a massive lowering in baselevel. In areas which subsequently become exposed, the erosion of the upper parts of older, more proximal foresets and valley incision take place (cf. Field and Trincardi 1991; Tesson et al. 2000; Zaitlin et al. 1994). In this case, the active river delta is restricted to a relatively narrow zone within the coastal area. Waves, tidal and longshore currents may additionally perturb the construction of a delta and lead to a wider distribution of the sediments, thus expanding the lateral extent of the foresets.

Till Hanebuth* (✉), Alexander Schimanski
Graduiertenkolleg "Dynamik globaler Kreisläufe im System Erde"
GEOMAR Forschungszentrum, Wischhofstr. 1-3, 24148 Kiel, Germany

* Current address (✉):
AIST, Geological Survey of Japan, MRE
Higashi 1-1-1, Tsukuba, Ibaraki, 305-8567, Japan
Email: till.hanebuth@aist.go.jp

Karl Stattegger
Institut für Geowissenschaften, Universität Kiel
Olshausenstr. 40-60, 24118 Kiel, Germany

The effect of sea-level lowering to a responding depositional system which builds up prograding foreset packages is known as *forced regression* (Posamentier et al. 1992). Forced regression deposits appear on numerous shelves worldwide as a response of fluvial deposystems to past sea-level fall. A complete succession is never preserved, since erosion during subaerial and submarine exposure and during the subsequent transgression mostly removes major parts of these deposits (Field and Trincardi 1991; Sydow and Roberts 1994; Hunt and Tucker 1995). Thus, the relict-like preservation of sediments in bodies isolated from each other is common, and the existence of former morphologic depressions obviously favours this distribution pattern (Trincardi and Field 1991).

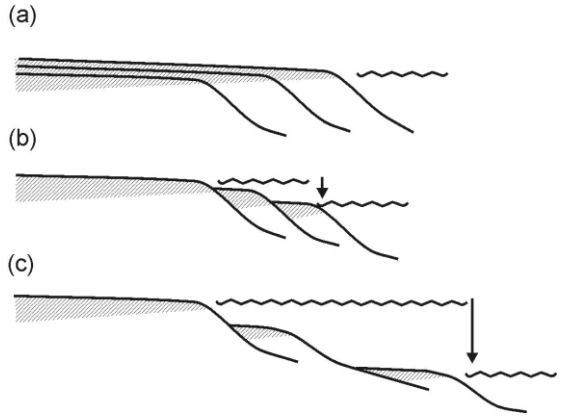

Fig. 1: Schematic progradational succession of a siliciclastic delta system ramp, according to Hunt and Tucker (1995) and Posamentier and Morris (2000). (a) Progradation and subordinate aggradation during relative sea-level stability (*normal regression*). (b) *Attached* and (c) *detached* stepwise progradation in response to sea-level lowering (*forced regression*). Dotted area: shoreline deposition. The deposits of forced regression systems are subsequently affected by soil formation and erosion due to exposure. The succession is further diminished by several phases of ravinement during the following transgression.

The sea-level curve of the last deglacial transgression (Fig. 2a), which is derived from siliciclastic shoreline-related deposits from the Sunda Shelf (for references see figure), shows that the rate of sea-level rise varied repeatedly within time intervals lasting thousands or only hundreds of years. Prior to the Last Glacial Maximum (LGM; ~ 21 calibrated thousands of years before present = *kyr* in the following), the accuracy of the generally assumed sea-level curves strongly decreases, since the methods employed cannot deliver the same precision as for the time interval after the LGM (cf. Clark et al. 2001) The oxygen isotope curves of global validity (e.g., Imbrie et al. 1984; Shackleton 1987) indicate several sea-level fluctuations during the past glacial cycle (Fig. 2b), but they do not resolve shorter variations and also show discrepancies of up to tens of meters during distinct time intervals. The record presented by Shackleton (1987) describes additional peaks in sea level lasting several thousands of years in length and tens of meters in amplitude (Fig. 2b). Records deduced from coral reefs (Bard 1996; Chappell et al. 1996), on the other hand, are limited by the fact that reef growth is strongly suppressed during phases of rapidly accelerated rates of sea-level fall or rise. They also preferably indicate phases of relative highstands in sea level (Fig. 2b). The past major regression after the Eemian sea-level highstand performed stepwise: during marine isotope stage (MIS) 5 at a relatively high level, with fluctuations around –20 to –50 m below modern water depth, during MIS 4 at a level around –80 m and during MIS 3 at a relatively low level with fluctuations around –50 to –90 m. MIS 2 is characterized by a sharp drop leading to the glacial lowstand around –120 m or deeper and a comparably sharp rise afterward (Fig. 2b).

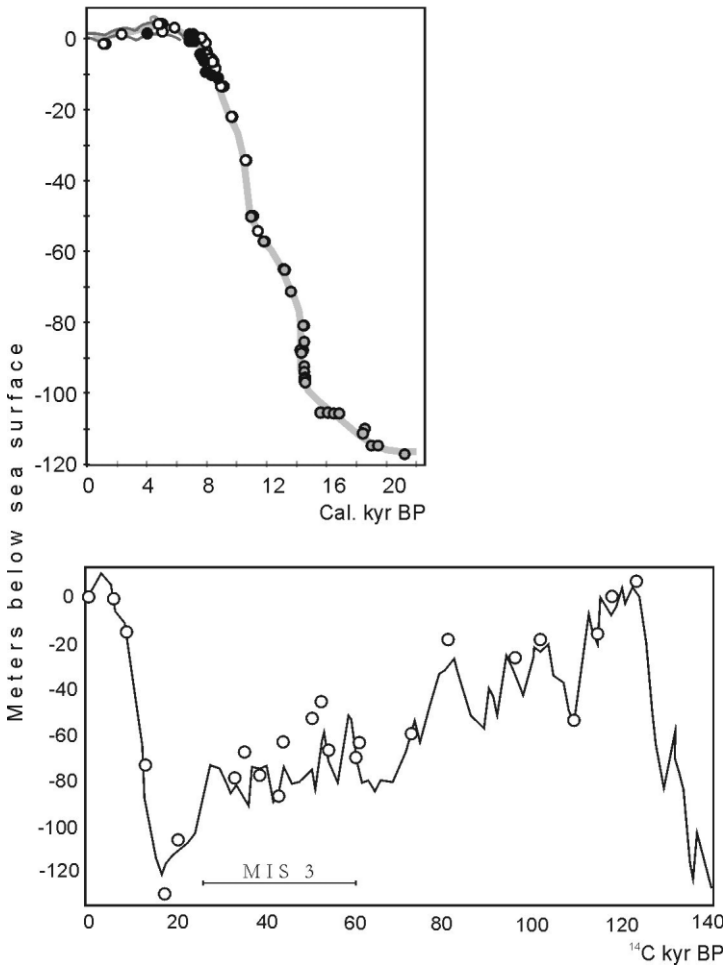

Fig. 2: Sea-level curves. (a) Composed sea-level curve from the siliciclastic Sunda Shelf for the deglacial time interval (data from Geyh et al. 1979 [white circles]; Tjia and Fuji 1992 [ranges between black lines]; Hesp et al. 1998 [black circles]; Hanebuth et al. 2000 [grey circles]). Sea level rose at varying rates since the lowstand of the Last Glacial Maximum at about –120 m. (b) Sea-level estimations based on oxygen isotope (Shackleton 1987) and coral reef records (Chappell et al. 1996). Note the numerous minor fluctuations and also the gap between the records. Other oxygen isotope records also show remarkable biases from each other.

High sediment supply and a low coastal plain/shelf gradient in interaction with varying rates in sea-level fall or rise provide a potential high resolution of the depositional succession. The analysis of a *regressive* sedimentary system using a set of numerous sediment cores should enable a reconstruction of:

(1) the detailed shelf architecture, which has been rarely cored worldwide since the material is situated offshore, is poorly preserved and is often covered by younger deposits;

(2) a sea-level curve spanning MIS 3 using tidally influenced deposits which contain organic macro-remnants.

The *Sunda Shelf* represents the southwestern margin of the South China Sea in Southeast Asia (Fig. 3a). This area provides particularly well-suited conditions for studying sedimentary stratigraphy. Indeed, the two most important counterparts to fluctuations in sea level which control the evolution of depositional strata were of extreme dimension: (1) flat shelf physiography as the shelf extends over 800 km and is very gently inclined, and (2) high sediment supply due to the huge paleo-catchment area and the high tropical precipitation ratio canalised by paleo-rivers (e.g., Molengraaff 1921; Tjia 1980; Hanebuth and Stattegger 2001). The Sunda Shelf was tectonically stable during the Quaternary (Tjia 1996). Down-lifting effects, such as compaction, subsidence, and hydro-isostatic compensation, were lacking or occurred only very subordinately during the relatively short time interval of the past tens of thousands of years (Lambeck et al. 2001). The South China Sea basin was much more isolated from the world's ocean during the last glacial interval by the disappearance of several ocean passages during past interglacial times. This should have led to a reduction of the tidal range, which spans about 2 m in average nowadays. The paleo-Sunda

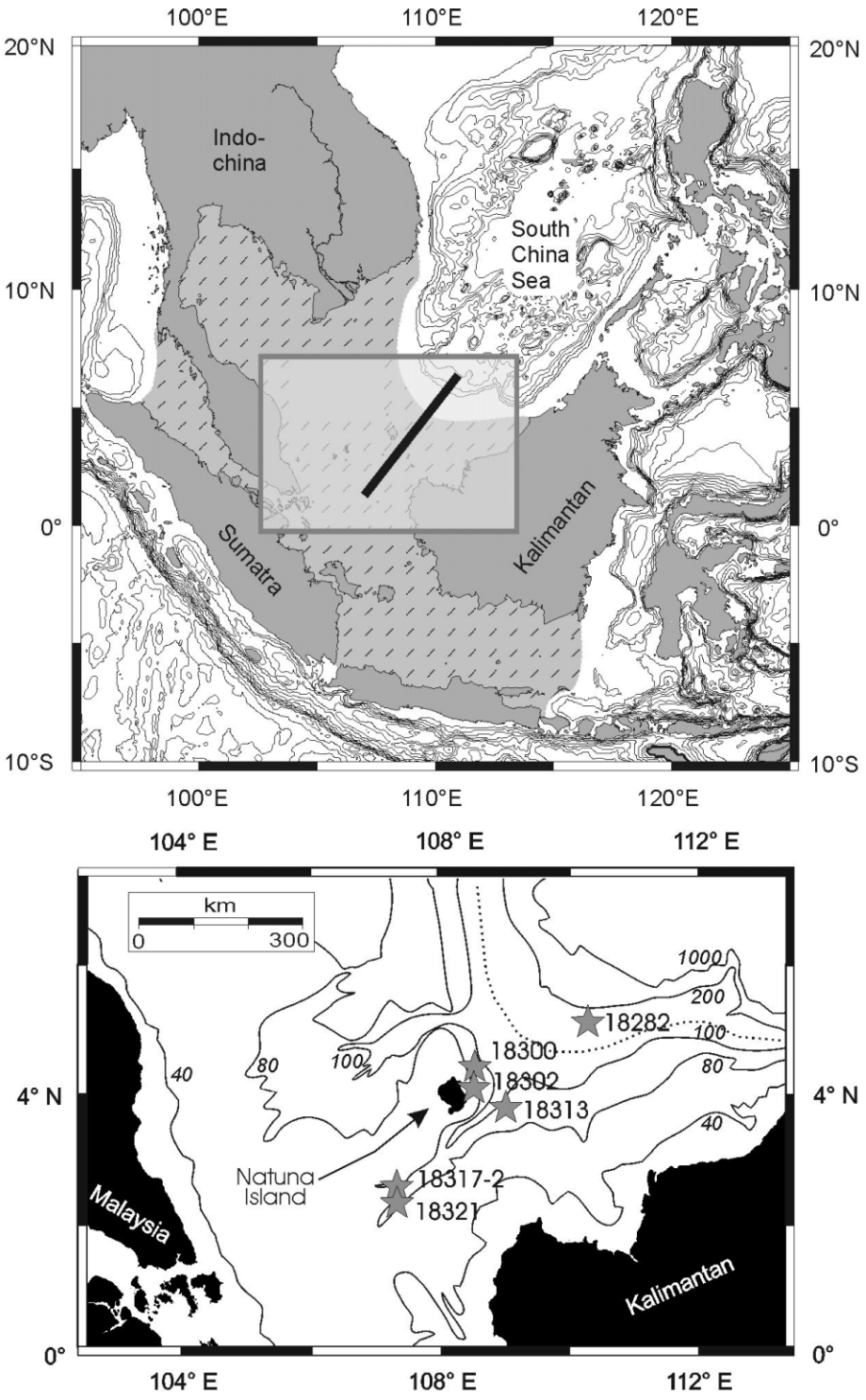

Fig. 3: Regional overview of the Sunda Shelf in Southeast Asia. (a) Borders of paleo-Sundaland. The greyish, hatched area roughly indicates the extension of subaerial exposure during the LGM. The black line shows the position of the SO-115 transect. (b) Bathymetric map of the study area. Stars display the cores which are specifically mentioned.

plain was drained by a large river system during exposure in latest Pleistocene times and flowed into the southern part of the semi-enclosed basin of the South China Sea. The run of one of these fluvial systems, the *North Sunda River* ("Molengraaff River"), intersected the central part of the Sunda plain. This paleo-river valley and the directly adjacent part of the Sunda plain is the objective of our studies. The valley cut into basinward-directed clinoforms and made the preservation of regressive and subsequent transgressive deposits possible. The transgressive deposits were formed mainly within the direct influence of the paleo-coastline (cf. Biswas 1973; Hanebuth and Stattegger 2001). The shallow-seismic (*Parasound*) survey generally shows prograding clinoforms below the transgressive cover crossing the entire Sunda Shelf down to the shelf break into a north-eastern direction (Wong et al. 2001).

Core number	Latitude	Longitude	Water depth	Recovery
18269-2	4°46'013 N	109°26'321 E	113 m	881.5 cm
18273-2	4°37'289 N	109°33'931 E	126 m	348 cm
18276-2	4°44'897 N	109°44'837 E	116 m	721 cm
18300-2	4°21'778 N	108°39'215 E	91 m	885 cm
18302-2	4°09'585 N	108°34'535 E	83 m	598 cm
18303-2	4°26'425 N	108°55'491 E	107 m	736 cm
18305-2	4°17'318 N	109°04'599 E	109 m	514 cm
18313-2	3°52'194 N	108°52'226 E	98 m	620 cm
18314-2	3°59'469 N	108°59'473 E	100 m	370 cm
18315-2	2°01'669 N	107°02'041 E	69 m	583 cm
18316-2	2°29'263 N	107°27'522 E	71 m	597 cm
18317-3	2°36'596 N	107°22'517 E	95 m	197 cm
18318-3	2°36'609 N	107°22'508 E	87 m	406 cm
18320-2	2°36'726 N	107°22'491 E	76 m	492 cm
18321-2	2°18'453 N	107°25'326 E	109 m	569 cm
18323-2	2°47'030 N	107°53'200 E	92 m	540 cm
18282-2 $	5°14'687 N	110°14'605 E	151 m	634 cm

Tab. 1: Coordinates of the SO-115 cores relevant for this study. $ from Steinke (2001).

Material and Methods

During research cruise SO-115 (Stattegger et al. 1997), 38 gravity and vibro cores were taken along a transect from the shallow part of the central Sunda Shelf basinward, following the major incised valley structure of the ancient North Sunda River in a SE-NW direction (–70 to –150 m below modern sea surface). The penetration depth of the cores was up to 14 m below the seafloor with an average recovery of about 7 m. 16 of these cores are of relevance for this study (Tab. 1, Fig. 3b) as the others remained bogged in transgressive deposits.

The sediments recovered were investigated using various sedimentological and geochemical methods to characterise and classify the different types of sedimentary facies. The application of several analytic methods was required because the paleo-environment beyond and in front of the coastline and the river mouth generally shows complex patterns of facies association (cf. Reading 1996). Measurements of magnetic susceptibility on each core and X-ray radiographs of 5-mm-thick slabs made fine-scale changes in sediment composition and texture visible. The coarse-grain analysis of the dry-sieved fractions (63-125, 125-250, and > 250 mm) is an effective method for specifying the quantity and quality of the material by counting at least 300 specimens. In general, the composition reflects both the conditions of the depositional environment and of the source from which the material was delivered. Methods such as the measurement of physical and geochemical sediment properties and pollen analysis give additional information to determine the paleo-environment as precisely as possible. Physical properties (water content, sand content, shear strength, etc.) indicate changes in the quality of supplied sediments and in the hydrographical and post-depositional process *loco* deposition. Stable carbon isotopes measured on carbonate tests are

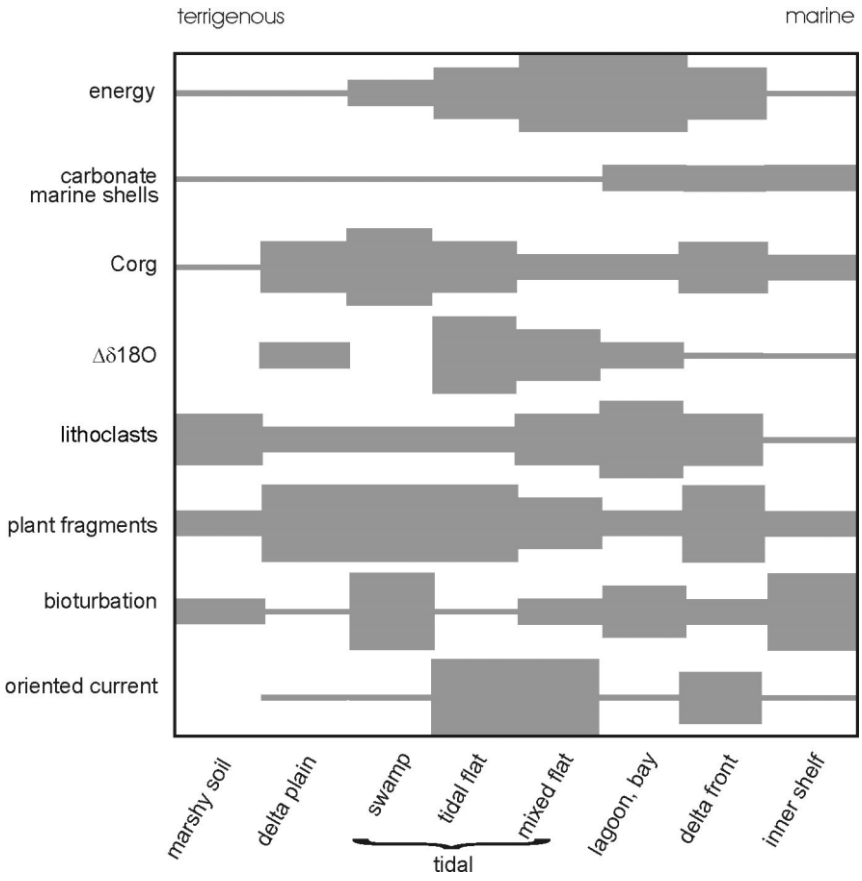

Fig. 4: '*Proxy-facies-chart***'** (Schimanski et al. in prep.). The six facies used in this study are defined by geochemical and sedimentological parameters. The thickness of beams indicates the relative frequency/appearance of a parameter.

strongly influenced by the variability of freshwater input in the nearshore environment as found on the Sunda Shelf. Stable carbon isotopes of organic plant material generally reflect the various plant associations that potentially occur in the wide coastal spectrum from

tropical forest to marsh and mangrove to freshwater and marine algae. Isotopic values become heavier with increasing distance to the paleo-shoreline. Terrestrial vegetation is also reflected by the composition of pollen: the closer the environment of deposition to the paleo-coastline was, the higher the content of mangrove pollen. The larger the distance to the paleo-shoreline, the broader the pollen spectrum, indicating increasing mixture of pollen from different vegetational sources during transport.
Total organic carbon content and carbonate content give evidence for the accumulation of organic matter and the intensity of marine influence, respectively (Hanebuth 2000).
The combination of these methods led to a schematic "proxy-facies chart" (Fig. 4), presented in detail by Schimanski et al. (in prep.), who have investigated facies successions of the *transgressive* system on the Sunda Shelf.
Siliciclastic sediments, especially from nearshore environments, contain a mixture of both (a) fresh organic material of terrestrial and marine origin and (b) older reworked organic-rich terrigenous and carbonate-rich marine material (cf. Stanley and Hait 2000). Therefore, the generation of meaningful dates requires the selection of material whose pathway from origin to burial is more or less understood. For age determination of the deposits, we used large (cm-sized), manually selected plant remnants and large benthic foraminifers (*Ammonia/Rotalia* sp.). We preferentially chose facies which formed within an assessable relation to the paleo-shoreline. Residues of an acid-alkali-acid extraction were isolated to obtain better evidence of the true age of deposition. Hanebuth (2000) has dated separately leached humic acids and acid-resistant material (residue) in comparison. Humic acids always show a different age than the residual material due to their capability for unhampered migration through the sediment strata. In a next analytical step, the residue material was split into different grain-sizes before ages were determined. The results provide a general rule: the coarser the organic pieces are, the younger the date is. This, in turn, implies that the detritic microfibres which were concentrated to organic "peaty" layers contain the highest amount of older reworked material. In contrast, single woody pieces of several centimetres in size reflect the most realistic age of deposition. As a consequence, we avoided dating using fine plant-fibre detritus or bulk sediment samples whenever possible. An estimation of the degree of contamination can also be used to provide information concerning the paleo-environment (i.e. distance to shoreline, position relative to river supply, hydrographical conditions, etc.).
The AMS-^{14}C ages were measured at the Leibniz-Labor for Radiometric Dating and Isotope Research at the University of Kiel, Germany, to a precision (counting statistics and machine statistics) of 0.3 % for modern samples (Nadeau et al. 1997). The applicability of the AMS-^{14}C method is limited by the half-life period of ^{14}C to ~ 50 thousand years for organic carbon samples. Ages were calibrated using the latest version of CALIB (Stuiver et al. 1998). Dates prior the LGM were not calibrated ('^{14}C kyr') in this study, because the calibration aspect is poorly defined before 12.5 ^{14}C kyr BP (equiv. 14.7 cal. kyr BP; Stuiver et al. 1998). Fluctuations in atmospheric ^{14}C content (Stuiver et al. 1991) have certainly shifted the ages of some thousands of years towards older ages (Bard et al. 1998; Völker et al. 1998), which can be roughly estimated but not yet reliably corrected.
Shallow-seismic records were obtained along all profiles of the cruise using the *Parasound* shipboard system aboard the German R/V *Sonne* with a significant impedance contrast within the uppermost 80 m at a maximum.
We principally use the "proxy-facies chart" mentioned above (Fig. 4) to determine the facies types of the *regressive* deposits. The resulting *facies mosaicing* process includes all appropriate cores in combination with AMS-^{14}C datings (cf. Hanebuth and Stattegger 2001). This term points to the effort to correlate the diverse numerous facies sections into a stratigraphic concept. The characteristic paleo-facies successions are scattered by short-lasting

event-like sedimentation, erosion resulting in hiatuses which comprise long-term intervals and general rapid lateral shifts in the paleo-environment through time. This caused the necessity of their mosaic-like combination. The procedure led finally to the general stratigraphic concept of the regressive unit on the Sunda Shelf.

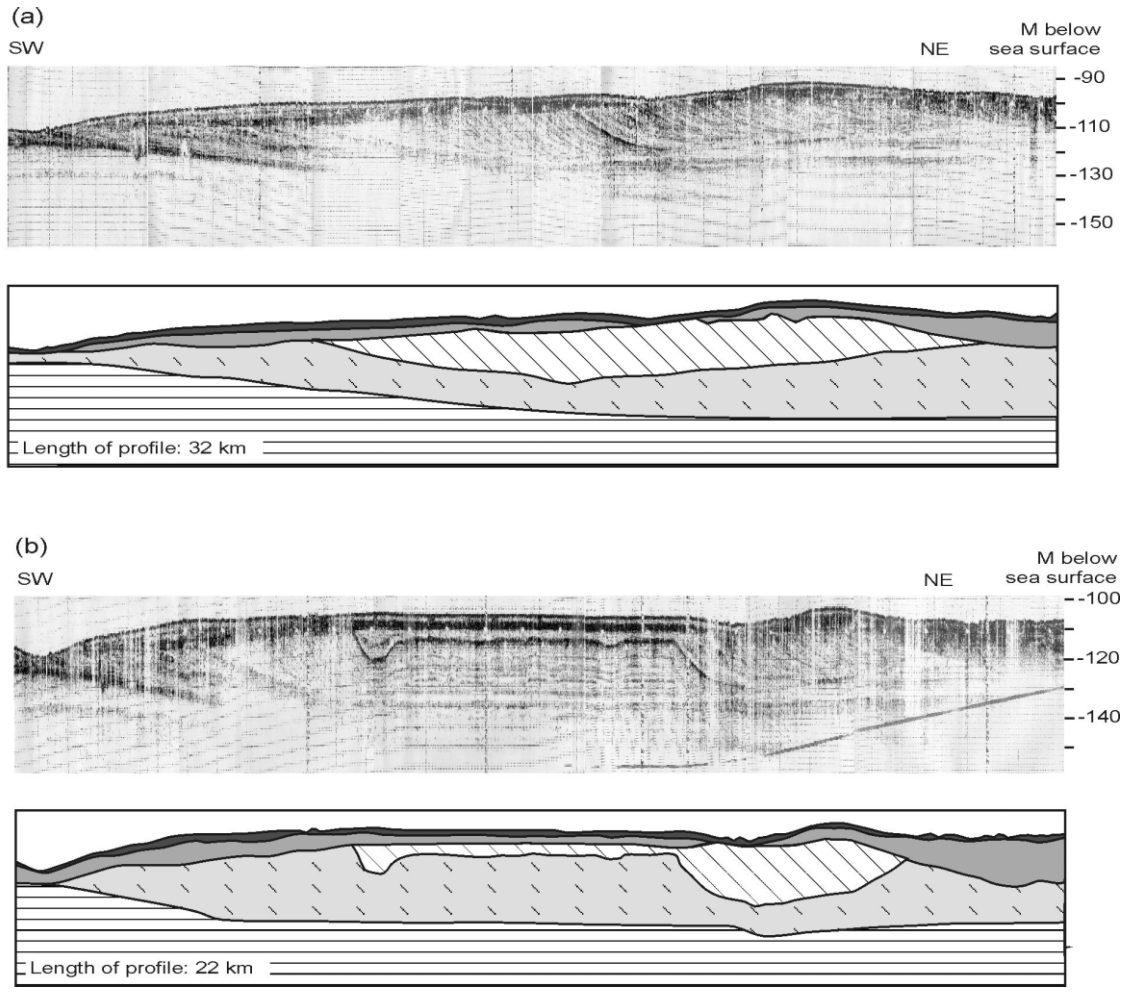

Fig. 5: Shallow-seismic surveys (*Parasound*). (a) Profile from the innermost part of the SO-115 transect. (b) Profile from the middle part. The regressive unit (grey, dashed and white, hatched) rests in wide depressions of underlain units (vertically lined) and is bordered upwards by the Late Pleistocene exposure surface [strong seismic reflector], subsequent transgressive deposits (darkish grey), and a thin Holocene blanket (black). The regressive unit is subdivided by an (probably fluvially) incised surface into a lower and an upper part.

Results

Seismic Profiles

A number of laterally succeeding sediment bodies with basinward dipping foreset structures was detected by the shallow-seismic survey within the paleo-river valley, which expands up to 50 km in width and several decametres in depth nowadays. These bodies, up to 30 m in

thickness and 20 km in lateral basinward extension, fill moderate depressions in the underlying paleo-relief. The sediment bodies surmount the adjacencies level for some meters (Fig. 5). Outside the slight paleo-depressions, the regressive sediments thin out, covering an older progradational unit. Commonly, the regressive units are overlain by a transparent, bedded, or chaotically structured cover of younger sediments (post-LGM to Holocene in age) with additional internal reflectors (cf. Hanebuth and Stattegger, 2001). A continuous rigid soil horizon (see below) is indicated by a prominent reflector separating the regressive from the younger units.

The regressive bodies between the underlain older progradational unit and the transgressive deposits can be subdivided into a lower and an upper part (Fig. 5). The *lower* part rests on the gentle depression and shows slightly inclined internal surfaces. Its upper surface is sharply truncated by channel-like concavities. Steeper dipping foresets and an obvious lateral thinning-away at the fringes of the incised structure characterize the *upper* part. The internal beddings within the regressive bodies dip at partly steep as well as partly more gentle angles and also downlap unconformably on the bottom. The top part is almost always sharply truncated; the *onlap* (or *offlap sensu* Plint and Nummedal 2000) segments have been eroded if they ever have been deposited (Fig. 6). Nevertheless, two cores (*18314* and *18315)*, as demonstrated below, contain sedimentary facies which formed in a tidal and in a terrestrial environment, respectively. There is possibly evidence that sediments of the upper *onlap* segment (Fig. 6), which extends landward of the inflection zone to the part of steeper inclination, has preservation potential.

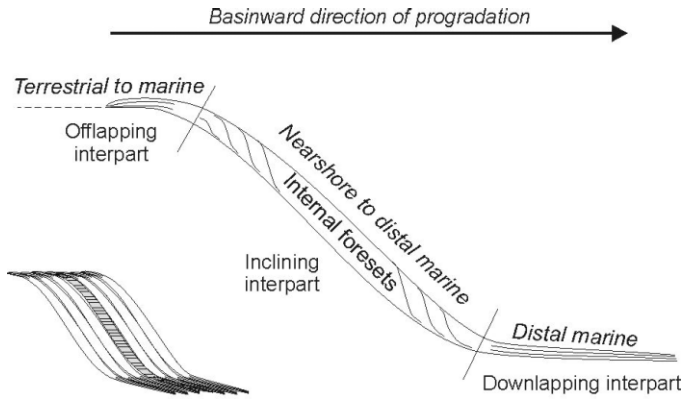

Fig. 6: Schematic section through a clinoform foreset. The size of the structure can be small-scale as well as of wide extension. The landward-directed upper interpart develops as *onlap* or, in the case of forced regression, often as *offlap* (Plint and Nummedal 2000) and is most affected by ensuing erosion. The lower interpart of the foreset arises as *downlap*. The deposits of the upper interpart, especially the *offlap* deposits, form in proximity to or within the shoreline.

On the outer shelf in modern water depths exceeding –110 m, the regressive deposits thicken continuously basinward, regardless of the former topography at their base, and obtain thicknesses of more than 80 m at the shelf margin (in about –180 to –220 m water depth). The top is continuously and intensively capped above a modern water depth of –125 m. Foreset progradation as known from more proximal parts of the shelf platform is, moreover, replaced by large-scale progradational (to aggradational) patterns. The only evidence of vertical movement on the entire Sunda Shelf comes from parallel vertical faults at the shelf margin probably caused by gravity movements due to sediment instability along the shelf break (Wong et al. 2001).

Selection of Sites Based on Seismic Survey

Generally, deposits cover the regressive unit that belong to three younger successive stages. From today's mainland down to a modern water depth of –110 m, the stiff (soil) horizon (1) seals the underlain regressive beds. This horizon appears as a strong reflector in the shallow-seismic images of the exemplarily cores presented here (Fig. 8a to c). A transgressive unit (2) builds up the second younger package. The thickness is highly variable up to more than 10 m: it is preferably preserved in paleo-depressions such as those found in the widespread channel network (Fig. 8a) or as a thin but continuous blanket on plain areas (Fig. 8c). It is completely lacking on the former plains of the inner shelf (Fig. 8d). Here, the soil horizon is exposed to the sea bottom (only covered by a thin blanket of Holocene mud). The transgressive succession is indicated by a transparent to slightly chaotic horizon between the sea-bottom reflector and the reflecting soil surface. In channel fills, it also shows internal horizontal subreflectors (8a). A full-marine cover (3), which does not exceed a few decimetres in thickness, can be found in all parts of the shelf, and its thickness is just sufficient to be resolved by the *Parasound* method.

Types of Facies

The types of facies occurring in the Sunda Shelf cores can be attached to three genetic groups due to a general division into *terrestrial*, *shoreline*, and *marine* paleo-environments. All facies types are clearly dominated by terrigenous material, with the exception of the most distal deeper-marine deposits beyond the break of the respective pro-delta. The majority of the facies originated in nearshore environments. Table 1 shows 16 of the 38 cores taken along the transect which contain a facies that was deposited during the phase of sea-level lowering preceding the LGM (compiled in Fig. 7). Three other cores, not presented here, reached the stiff soil horizon without deeper penetration and five further cores, also not presented here, stopped right at the top of this horizon during coring due to its rigidity.

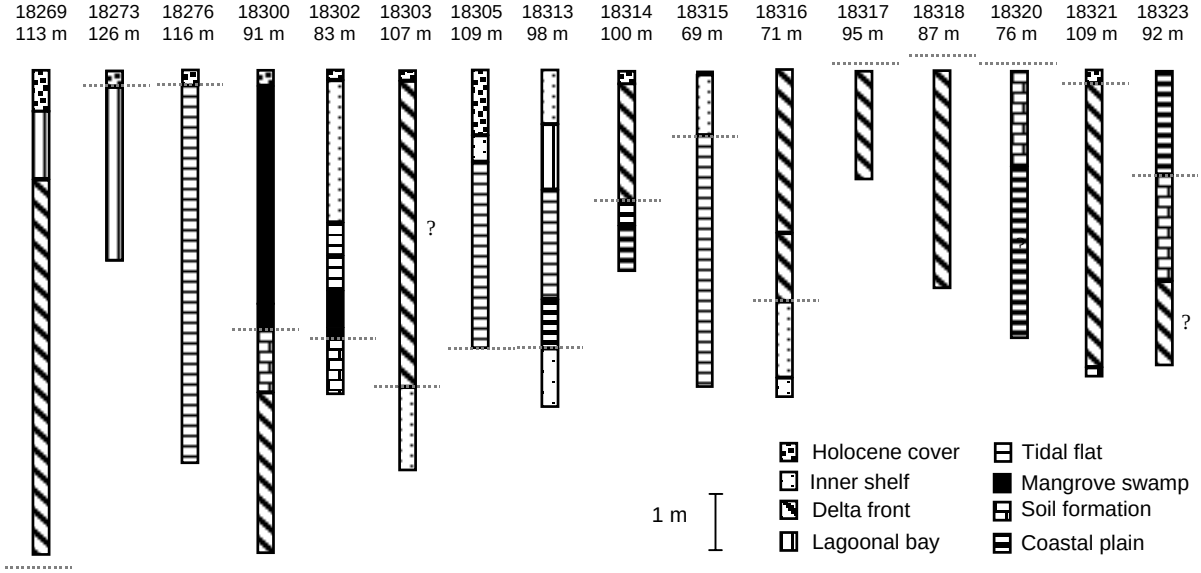

Fig. 7: Facies determination of the cores listed in Table 1. Horizontal lines: boundary of regressive to transgressive deposits. Facies of unsure classification indicated with "?".

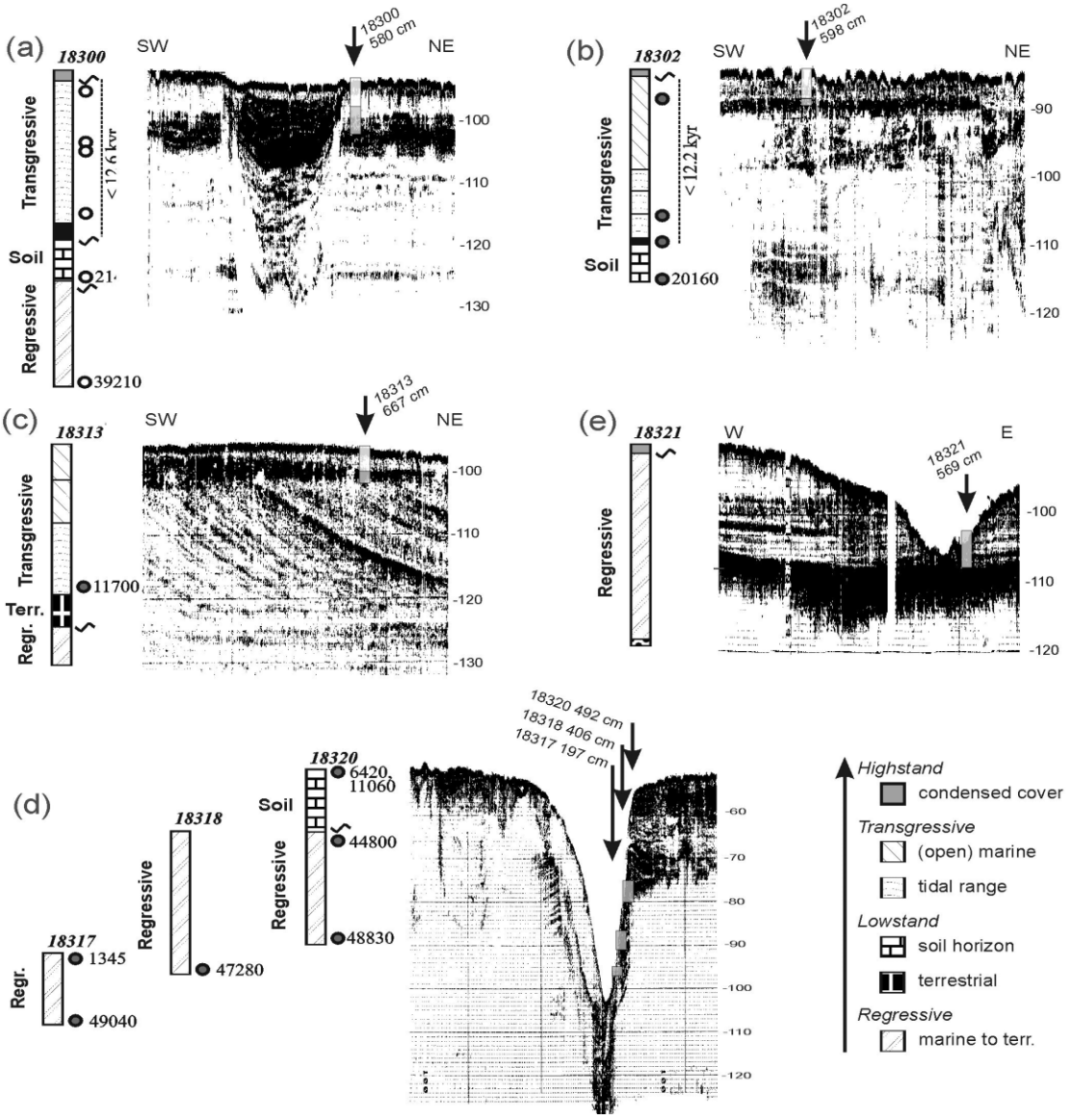

Fig. 8: Exemplarily presented cores and the corresponding seismic section. Facies interpretation and AMS-^{14}C dates are shown in the first column, the relation to sea-level phases in the right. AMS-^{14}C datings are given as uncalibrated ^{14}C ages (circles). Arrows in *Parasound* profiles indicate core position and the length of core-recovery. Width of all profiles: approx. 3 km. For details see text.

For interpretation purposes, six different types of facies were defined, each of them enclosing closely related paleo-(sub)environments. This schematisation was made to obtain an effective tool using reliably determined facies types.

One terrestrial facies type (*coastal plain*) comprises the deposits which formed on the delta/coastal plain with episodic or rhythmic lamination probably caused by overbanking processes. Thicker oxidised sand layers additionally document the general exposition and may also indicate the existence of paleo-beach sand cheniers.

Another land facies (*marshy soil*) (Fig. 9b, right column), already mentioned above, with a noticeable greyish orange-flamed colour represents the only strongly consolidated deposit of the Sunda Shelf deposits at all. The plural changes of reducing and oxidising conditions

underline the formation in a marshy paleo-environment directly after emergence during sea-level fall. This horizon probably protected the underlying and nearly unconsolidated regressive deposits against any subsequent remobilisation during regressive shoreline and foreshore ravinement as well as subaerial and transgressive erosion. It should be mentioned that this facies mainly incorporated the underlain deposits but also contains obviously aerially supplied material, which is concentrated in bands or has been distributed dispersely. Authigenic concretions in the form of crusts, orange-brownish patches and "sideritic spherulites" attest laterisation. This marshy soil formation was distributed over large distances of the Sunda Shelf and the adjacent regions (cf. Biswas 1973; Sinsakul 2000).

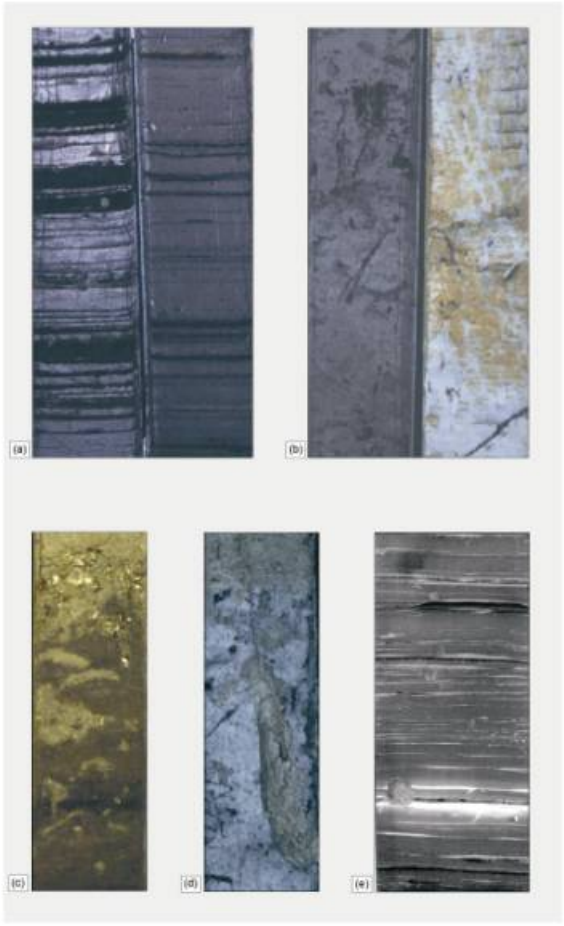

Fig. 9: Photographs emphasising the contrast between different facies types and common discontinuities. (a) *Delta front* mud intercalated by numerous thick peaty layers and thin sand layers. (b) Transgressive facies succession. Right section: underlain *soil* horizon with oxidized mottles and secondary root penetration; left section: *coastal swamp* intensively penetrated by mangrove roots. (c) *Shelf* sediments covering the Late Pleistocene surface. Injection of shelf sediments into the underlain beds by abundant macro-bioturbation. (d) Large burrows in the *mangrove swamp* deposits filled by younger sediments. (e) X-ray radiography showing fine rhythmic laminations in a *delta front* facies with crossbedding, small vertical and large horizontal burrows, and material separation: sandy layers (dark), peaty layers (light), muddy 'background' sedimentation (grey).

Both terrestrial facies are related to the paleo-shoreline and originated some meters above the corresponding sea level.
The shoreline environment (*tidal flat*) was situated within a micro-tidal span of approximately 2 m at maximum. Cross-lamination, ripples, and high organic content characterise the sediments. As the pollen record and root remnants preserved *in situ* have shown (Hanebuth 2000), mangrove (Fig. 9b, left column) covered the paleo-shorelines at ecologically suitable locations and contributed a high amount of organic matter to coastal *drift-and-concentrate* processes.
The *delta front* facies (Fig. 9a, e) is finely laminated with tidally induced rhythmic intercalations of organic debris and sand layers, respectively. This facies generally occurs in a range of ≤ 20 m water depth in which terrigenous input continuously predominates. An extremely high but episodic sedimentation rate characterizes this environment.
A shallow-water environment of hydrographically calm conditions (*lagoonal bay*) exists apart from strong terrigenous riverine input. High bioturbation efficiency destroyed the original beddings. Organic patches are abundant but shells of marine organisms also occur frequently.
Open-shelf conditions under a full-marine sedimentation regime (*inner shelf*) were found beyond the distal limit of strong terrigenous input. Marine tests of foraminifers and the shells of molluscs and echinoderms dominate the sand fraction, as reflected by high carbonate contents. Due to relatively low sedimentation rates, ventilation is good and bioturbating organisms are very active.
The facies variety presented above can also be discovered in the subsequently deposited transgressive unit (Hanebuth and Stattegger 2001). One further type of facies should be introduced here though it does not belong to the unit of regressive deposits. The *Holocene cover* facies (Fig. 9c, d) sheets the underlain units as a thin blanket of fully marine foraminiferal mud-starved terrigenous supply, which formerly dominated the sedimentary processes over a long period.

Age Control
The AMS-^{14}C age series measured on the regressive deposits shows remarkable discrepancies between insoluble residue material and relatively mobile humic acids. The general bias of the ages of humic acids tends towards younger ages with increasing sample age.
Coarser-sized organic material is quite rare in regressive deposits compared to the content of transgressive sediments (Hanebuth et al. 2000). Therefore, the age difference between single wood fragments and 'bulk sediment' plant remnants could be determined only in one case (Core 18315-2). A slightly younger age of the fragment to the 'bulk sediment' appears to be subordinate compared to the noticeably bigger age bias between insoluble residue material and the associated humic acid. These results may confirm the relative credibility of the residue material used for age assignment, although Yim (1999) advised the interpretation of radiocarbon ages from siliciclastic deposits prior to the LGM (21 kyr) with caution.
We observed a tendentious rejuvenation of the depositional ages of the regressive unit basinward (Tab. 2; Fig. 7). The intercepts of AMS-^{14}C measurements return ages around 50 (to 45) ^{14}C kyr in the proximal, i.e., southwestern part of the transect. One date from the middle section plots around 40 ^{14}C kyr (Core *18300*) and determinations of a core from the outer shelf range between 34 and 31 ^{14}C kyr in age (Core *18282*; Steinke 2001). The overlying transgressive unit dates between 19 and 13 kyr, the Holocene veneer age varies between 10 and 2 kyr. This illuminates the long time gaps between regressive and post-LGM deposits.

Core number	Sample depth [cm]	Water depth [m]	Type of facies dated	Material sampled	Wood macro insolub.	Dev. +/-	Wood macro humic	Dev. +/-	Bulk sediment insolub.	Dev. +/-	Bulk sediment humic	Dev. +/-	KIA
Facies during latest lowering to lowstand													
18269-2	226	113	delta front	organic					17200	70	15670	70	5975
18269-2	805	113	delta front	organic					17060	100	15580	70	5976
18276-2	60	116	tidal flat	organic					17680	80	16220	80	5980
18276-2	60	116	tidal flat	organic							16110 #	160	5980
18300-2	590-592	91	mangrove	organic					21490	330/320			3528
18302-2	590	83	marshy soil	organic					20160	330/310	19400	230	3531
18314-2	343	100	coastal plain	organic	26850 *	170	23310 *	310/290	27110	150	24790	220	5988
18323-2	380-382	92	marshy soil	organic					23460	160/150	23270	330/320	3544
18323-2	534-536	92	delta front ?	organic					22810	120	21980	190/180	3545
Facies during lowering													
18273-2	273	126	lagoonal bay	organic					39870	10707950	42810	1680/1390	5977
18273-2	273	126	lagoonal bay	organic							36370	2400/1840	5977
18300-2	879-881	91	marshy soil	organic					39210 #	3190/2280			3529
18315-2	40-42	69	tidal flat	organic					47670	2090/1660	37330	1600/1340	5618
18317-3	190-192	95	delta front	organic					49040	3080/2220			3538
18318-3	390-392	87	delta front	organic					47280	2180/1710			3539
18320-2	200-202	76	delta front	peaty					44800	1850/1500	40400	3100/2230	3541
18320-2 =	484-486	76	delta front	peaty					48830	25001910	45140	2650/1990	3542
Facies during lowering, age determination not sufficient													
18273-2	273	126	lagoonal bay	organic					> 47740				5977
18300-2	879-881	91	delta front	organic					> 33210 #				3529
18300-2	879-881	91	delta front	organic					> 41510				3529
18305-2	510-512	109	tidal flat	resin	> 52850								3533
18317-3	190-192	95	delta front	organic							> 36820		3538
18317-3	190-192	95	delta front	organic							44240	1170/4540	3538
18318-3	390-392	87	delta front	organic							> 39720		3539
18320-2	200-202	76	delta front	peaty	> 46670						40400	3100/2230	3541
18320-2	200-202	76	delta front	charcoal	> 54360								3541
Foraminifera dates													
18303-2	575	107		*Rotalia*	>43770								4191
18303-2	722	107	inner shelf	*Rotalia*	>47520								4192
18316-2	597	71	inner shelf	*Rotalia*	>50370								2479
18282-2 §	49-50	151	inner shelf	*G. ruber*	32640	660							
18282-2 §	139-141	151	inner shelf	*G. ruber*	31400	560							
18282-2 §	260	151	inner shelf	*G. ruber*	31680	580							
18282-2 §	377-379	151	inner shelf	*G. ruber*	34020	780							

Tab. 2: AMS-^{14}C datings relevant for the regressive post-Eemian phase of sea-level changes. Ages measured at the Leibniz-Labor, Kiel (KIA). * Organic material but not woody macro-pieces; # samples of less than 1 mg carbon. The high organic content and the accumulation of plant remnants to peaty layers provide a good source for AMS-^{14}C determination. Nevertheless in approximation to the limitation of the AMS-^{14}C method, some dates are accompanied by immoderate 2σ errors of several thousands of years. As a consequence, only a minimum age is given. Data partly from Hanebuth et al. (2000) and Hanebuth and Stattegger (2001). § from Steinke (2001).

Selected Cores

In this chapter, selected cores are presented to exemplify how the subsurface deposits are characterized and are transferable to other sites on the wide Sunda Shelf.

Core 18300-2 (Fig. 8a) is located at the south-eastern margin of an incised-channel fill. The core penetrated the filling sediment body and also reached the older horizontally bedded deposits. The latter have been truncated by incision; the former filled it, subsequently build-

ing up concavely inflected horizons. The stiff soil horizon (125 cm thick; in the upper part of the lower half of the core) separates a lower section from an upper section in the core. The *lower* one (115 cm thick) is of marine origin and continuously laminated. Rhythmically intercalating thin sand layers and high siliciclast contents indicated the proximity of the environment to the paleo-coastline/fluvial system, as well a high accumulation rate. This facies is interpreted as *delta front*. An AMS-^{14}C age (39 ^{14}C kyr) affiliates this section to the progressed phase of sea-level regression. The *upper* section (445 cm thick) is composed of highly bioturbated *mangrove swamp* facies and with mangrove root remnants preserved *in situ*. This has been multiple-dated at different depths delivering ages between 12.65 and 12.44 ^{14}C kyr (Hanebuth et al. 2000). The full-marine *Holocene cover* caps this core with a minor thickness of a few decimetres. The datings, supported by X-ray radiographs, give evidence that unconformities of several thousands of years exit between the sections of different facies.

Core 18313-2 represents a noteworthy example, since this core vertically spans three succeeding seismic reflectors as shown by the shallow-seismic profile (Fig. 8c). This core is sedimentologically subdivided into three facies sections. The *lower* section (120 cm thick) is constructed by basinward directed clinoforms. The top of these clinoforms is lopped, resulting in a loss of the formerly *onlap* segment (cf. Fig. 6). This *lower* section consists of two facies. The basal facies is made up of laminated silty clay with high shell content and is interpreted as marine environment (*inner shelf*). The facies on the top of the lower section originated under terrestrial conditions, since it lacks shells and is interpreted as *coastal plain* deposit. It appears as a black massive horizon in the seismic profile but is not overconsolidated, such as is the marshy soil horizon developed in other cores. The material of the *middle* section (65 cm) is marine-influenced. Flaser bedding and a high sand content occur in the lower part, increasing bioturbation and organic patches in the middle and well-established marine conditions in the upper part. The deposits of this section formed closely to the paleo-shoreline during the transgressive phase with a tendency of increasing water depth upcore from a *tidal flat* facies to *lagoonal* and *inner shelf* deposits. The *upper* section (30 cm) formed under fully marine *quasi*-modern shelf conditions (*Holocene cover* facies). Although the lower section is not dated, the capping terrestrial facies and overlying transgressive deposits dated at around 11.7 ^{14}C kyr infer it as regression deposits in consideration of its stratigraphic position and the modern water depth of –101 m.

A special opportunity arose at Sites 18317, 18318, and 18320 (Fig. 8d) by a remarkable morphological feature. A recently unfilled channel structure of more than 50 m in depth and 800 m in width allowed deeper parts of older deposits to be sampled through a series of cores from near the bottom of the channel up to its margin close to the general level of the seafloor. The reason why this morphological structure remained unfilled is speculative but may be related to the modern current regime in the Karimata Strait. The facies development in all three cores is quite similar, indicating a continuous deposition process. The deposits contain a high amount of siliciclasts of terrigenous origin and a subordinate presence of organic and thin sandy layers. This composition leads to the conclusion that it formed in an environment close to the mainland delivering the coarse-grained material. Whereas a rudimentary quota of foraminifera occurs in the deepest core, these marine organisms are absent in both shallower cores. This fact indicates an approximation trend towards terrestrial conditions upcore and may be ascribed to a drop in sea level or to strong sediment discharge leading to delta progradation, respectively. Seismic survey made clinoforms in the deeper part and rather chaotic structures in the upper part visible. Seismic penetration was generally low, however, suggesting high sand contents in the sediments beneath the sea bottom. The rigid soil horizon occurs in the uppermost core. The AMS-^{14}C dates (49 to 45 ^{14}C kyr) give evidence that this unit was deposited over a period of several

thousand years. An age "*reversal*" is certainly ascribed to strong material mixing during sediment supply, as is possible for the other dates in a subordinate quantum as well.
The channel structures disappear on the outer shelf. The sediments from this area, as typically shown in Core *18282* (–152 m water depth) by Steinke (2001), are relatively homogeneous without plural facies changes as found in those which, in contrast, are continuously observed on the central and inner shelf. The deposits are marine but formed under a strong terrestrial influence. They date between 34 and 31.5 ^{14}C kyr, showing an age shift which indicates moderate and continuous accumulation rates. Only one major hiatus occurs, separating the lower regressive deposits (600 cm) from the thin fully marine sediment cover of deglacial to Holocene age (35 cm). This discontinuity spans a long time interval of more than 20 kyr, potentially allowing extended erosion activity.
Additionally, two further cores are briefly introduced here which illustrate the stratigraphic and physiographic patterns of the regressive system in the study area, although the first did not interpenetrate the stiff soil horizon and the second is not dated.
The corer bogged within the rigid soil horizon at Site *18302* (Fig. 8b). This horizon is clearly documented by the shallow-seismic survey. Several other cores of the transect probably did not break through this widespread paleo-surface but stopped at its top and only a few cores interpenetrated it. The facies section, which overlies the horizon of soil formation in this core (~ 20 ^{14}C kyr), consists of a gradual and typically transgressive succession (490 cm): *mangrove swamp* (bearing root remnants) overlies a horizon of organic accumulation, *tidal flat* deposits (current marks, occurrence of marine organisms) lead over to marine conditions, and open-*marine shelf* deposits (decreasing terrigenous influence) complete the series. The Holocene cover is only 20 cm thick.
Core 18321-2 was taken from another unfilled paleo-channel (Fig. 8e). The shallow-seismic image shows three different seismic units. The *lower* unit has no visible internal structures and is topped by a strong black and sharp reflector. The *middle* unit is characterized by horizontal bedding and a less sharp surface reflector. The *upper* unit appears as a transparent body. The channel completely truncates the upper and middle sections and its erosive base coincides with the surface of the top reflector of the lower unit. A thick yellowish oxidized sand layer at the base of the core substantiates the terrestrial origin of the *lower* core section (20 cm). The overlying beddings of the *middle* section (525 cm) contain only traces of marine influence and thick sandy layers, indicating a nearshore environment in the direct range of fluvial input. The *upper* section was obviously not reached by coring, and a possible relation to the deglacial phase of transgression may be speculative. A thin *marine cover* blankets the older deposits (25 cm), and its Holocene age can be supposed compared to the other cores. As other results from the Sunda Shelf have shown (Hanebuth and Stattegger 2001), all fluvial valleys and channels were incised either after exposure of an area during sea-level lowering (major valleys) or synchronously with sea-level rise (channel network), respectively, but in the latter case they always cut into the regressive unit before transgressive deposits built up. This, in turn, should lead to the assumption that the sediment preserved in the core belongs to the regressive sequence.

Discussion

Seismic Architecture and Stratigraphic Organisation
The regressive strata on the Sunda Shelf can be divided into three different morphogenetic types as inferable from seismic investigations. The *first* is a horizontally layered seismic facies in the subbottom. It seems to extend over the whole shelf, although limited *Parasound* penetration depth prevents an uninterrupted correlation. The upper boundary is irregular and covered by younger deposits.

The *second* type is mainly restricted to large lens-shaped 'bodies' of about 20 km in width and up to 40 m in thickness. The upper boundary forms a slightly convex hill-like structure (Fig. 5). These sedimentary 'bodies' fill in depressions in the bottom. At the landward edge, they build up a very thin bed or disappear completely, a fact which is interpreted to be a result of *offlap* or erosion. The strata extend basinward of the 'lens' but with continuously decreasing thickness (*downlap*). We interpret this type as *detached* deposits during *forced regression*. Sea level dropped by several minor but rapid steps during the past regression. *Accommodation space* was, thereby, reduced stepwise, and the gentle gradient of the wide shelf favoured rapid lateral shifts when sea level lowered at accelerated rates. During these shifts, sediment bypass probably dominated the areas between a former and the new (detached) depocenter. Three reasons are assumable why the deposits (bodies) of exceeded thickness formed: either (1) they were sheltered within previously existing depressions; or (2) they built up during phases of stabilizing or even a slight rise in sea level which would mean a temporary trend from *forced* to *normal* regression (i.e. an additional aggradational trend); or (3) the riverine sediment input was not continuous through time but pulsating due to changes in (monsoonal) precipitation. A form of bottom depression was detected in the seismic records (Fig. 5), but the second point additionally provides an explanation for the convex surface of the bodies as deposits close to the paleo-shoreline. In this context, the existence of fluvial but probably submarine incisions and fills, such as the second element (*upper* part) of the bodies, is remarkable. The steep inclination of these internal clinoforms decreases basinward (NE) and the foresets climb slightly upwards, resulting in a seawards declination of the 'lens'. In our study area, generally low sea level of around –80 to –100 with intermediate minor highstands of a few tens of meters would have been required for development of these depositional structures. The depth is at the lower limit of assumed sea-level fluctuations during the second half of MIS 3 (Fig. 2b). The internal surfaces (of at least partly fluvial origin) inside the bodies give evidence for a relative stability in sea level during distinct time intervals (Fig. 5). There is no evidence from the shelf margin and slope that minor pulsating fluctuations in the fluvial input (Steinke 2001) took place beside the general glacial/interglacial contrast in sediment supply. Therefore, it is difficult to ascribe scattered deposition to changes of the atmospheric system (Point 3). A further aspect masking eventual climatic influence is that, with increasing sediment yield during progressing exposure, river sediment discharge generally increases but, as well, the content of coarse-grained material decreases due to extending low-lying plains. Beside these facts, a two-dimensional transect is, of course, not able to detect lateral shifts of deltaic structures.

The *third* type of regressive deposits is restricted to the outer shelf (below ca. –120 m) and to the margin as a thick prograding wedge (Wong et al. 2001). Increasing thickness towards the shelf edge can be ascribed to the permanent submarine conditions, which were not affected by the general reduction of *accommodation space* on the shallower shelf. Moreover, strong sediment bypass delivered a high amount of sediments through major river valleys crossing the exposed shelf (Hanebuth and Stattegger 2001) and by increasing fluvial sediment discharge due to an extended catchment area during sea-level lowering. This led to the progradational but also aggradational formation of a sediment wedge during sea-level fall as well as during lowstand.

Discontinuities are of particular importance for the correlation of strata. They can be classified according to different orders on the basis of the regressive deposits of the Sunda Shelf. *Major* surfaces that are related to different phases in sea level separated the depositional units from each other change. *Minor* unconformities occur frequently as borders of clinoforms as well as within the individual sediment packages, except for wedge deposits on the outer shelf (Steinke 2001). Their existence attests that erosion led to a more or less con-

tinuous loss of deposited material and enhanced, thus, the typomorphic contrast between the successive sediment facies.

The regressive strata described here are bordered by an undulating relief at the base. At the top, the surface partly undulates over long distances (Fig. 5), partly erosionally pronounced or fluvially incised (Fig. 8a, d, e) as known from other broad shelves (e.g., Trincardi and Field 1991; Hunt and Gawthorpe 2000). An extended unconformity on the outer Sunda Shelf separates deposits of the thick regressive wedge from deglacial transgressive deposits. Similarly, Tesson et al. (2000) recently described strongly thickening deposits tending seaward from the outer shelf off the Rhône Delta with a hiatus of about 30 kyr until transgressive deposition started. They found that regressive sediments are lacking on the middle shelf in front of the Rhône Delta. In contrast, the depositional system on the middle Sunda Shelf was obviously able to build up *detached* sediment bodies with *stacking patterns*, prograding clinoforms of sufficient thickness (to resist complete remobilisation later) and riverine structures, since the Sunda Shelf area was characterised by a very gentle gradient and a continuous strong fluvial sediment supply during the relevant time interval.

The regressive sediments of the Sunda Shelf cover a broad spectrum of environments that mainly formed in close relation to the paleo-shoreline. Usually, the individual cores comprise a facies succession, which provides the reconstruction of a facies shift from regressive marine to terrestrial and, afterwards, from transgressive terrestrial to marine deposits. However, the facies record does not commonly report a continuous shift, but very well reports abrupt facies steps separated by unconformable surfaces. The distinct facies types are distributed over the shelf without a recognizable relation or zonation. These distribution patterns in both the local vertical and the wide lateral directions can be ascribed to four independent factors of different dimension in impact. (1) The combination of low gradient and sea-level fall led to thinning or detachment of depositional units over long lateral distances during regression. (2) The deposits that are within the reach of gravity coring can be attributed to the foreset scheme (Fig. 6). They either formed close to the *offlap* segment or the uppermost part of the dipping foreset if they occurred in *detached* bodies. Or they are part of the youngest of very gently inclined to subhorizontally stacking deposits. In both cases, the environments are attributed to a proximal position near the paleo-coastline, and progradation would have caused a repetition of these environments during the post-Eemian phase of *forced regression*. (3) The formation of deposits during basinward migration directly depends on local, particularly physiographic and sedimentary conditions (quantity of sediment input, processes in the coastline/river mouth, morphology, hydrography, etc.). The interactions within the coastal environment generally create complex local depositional structures and facies associations. Furthermore, sediment discharge delivered by the major river system must generally have increased during baselevel lowering due to sea-level fall. On the one hand, the drop in sea level led to an extension of the catchment area, while, on the other hand, an increasing number of lower-order rivers drained into the major valley with expanding shelf exposure, which thus focussed the sediment supply to the corresponding depocenter. (4) Erosion affected the area with locally varying intensity. A flat shelf area has a great potential for re-mobilisation and ravinement during regression and transgression that additionally border the long interval of shelf exposure. Intensive reworking during regressive times is underlined by an accessory but frequent content of polished dark yellowish tests of foraminifers among abundant 'fresh' (un-polished, white) tests and of glaucony which occurs only rarely in the comparable facies types of the transgressive unit. 'Cannibalism' of substratum was also inferred from an incised valley fill discovered at Station 18303. The sedimentary composition of this filling is identical to that of the host sediments from the surrounding area, which has been truncated. In contrast, some detritic peaty layers appear inside the filling. These layers date into the transgressive phase with an age of 13.43

^{14}C kyr, whereas foraminifer tests from the same sediment return an age of more than 43.4 ^{14}C kyr (Schimanski 1999). This proves that sediment was also re-deposited without sorting or separation processes, as is generally the case during transportation over wide distances.
The existence of these four factors that affect the depositional process synchronously and successively makes clear why shelf architecture based on an interpretative correlation of facies and units using only a few cores does often not reflect reality in a reliable or satisfactory way (cf. Tesson et al. 2000).
If the assumption is correct that the underlain horizontally bedded unit was cored at the deep unfilled channel (Fig. 8d), this would mean that the age of the uppermost beds of this unit dated between 49 and 45 kyr. Since the overlying unit (Fig. 5) is also *regressive* and partly embedded in depressions, it must not only have been deposited between 45 kyr and exposure then, and the incision, which divides the regressive 'lens' body, must also have formed in this time interval. This would circumstantiate a highly variable environment of plural changes of deposition and reworking processes, of drowning and exposure resulting in progradation and erosion. This, in turn, may also challenge the assumption that the main structure of the *North Sunda River* valley was already established before the Eemian interglacial stage and was only re-activated during the following exposure of the shelf area.

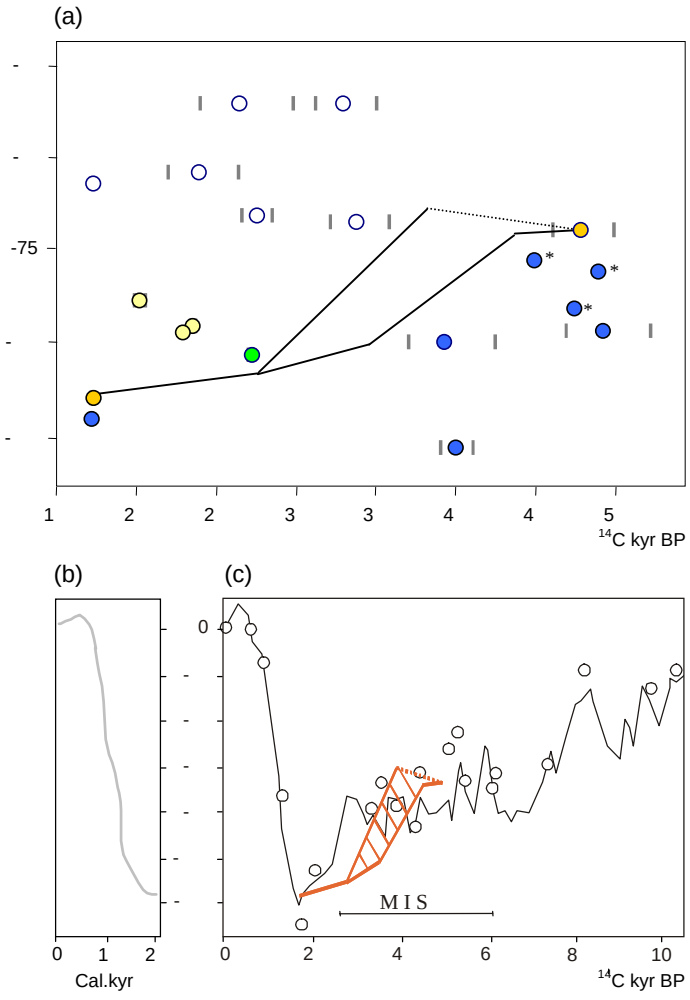

Fig. 10: AMS-^{14}C datings and sea-level estimation. (a) Tidal facies occur within, marginal-marine and in a distinct vertical range relative to, terrestrial facies above the contemporaneous paleo-sea level. Circles indicate the age intercepts, bars to the right and left the 1σ deviation. Blue: shallow-marine, orange: tidal, green: terrestrial [yellow: marshy soil]; white: terrestrial data from the Strait of Malacca (Geyh et al. 1979). * With approximation of the physical limitation of the AMS-^{14}C method, the uncertainty increases towards intolerable 2σ spans. Consequently, dates with inappropriate uncertainties are given as minimum ages. mbss = meters below modern sea surface. (b) Deglacial sea-level curve (see Fig. 2 a). (c) Sea-level estimation for the time prior to the LGM (cf. Fig. 2 b). Black line: Shackleton (1987), open circles: Chappell et al. (1996), red curve taken from (a).

Sea-Level

The idea of reconstructing a sea-level curve from organic-rich shoreline deposits of a siliciclastic shelf environment considers the advantages over established sea-level estimations using oxygen isotope curves from the deep sea or coral reef records. Isotope records (e.g., Imbrie et al. 1984; Shackleton 1987) can be affected by several partly local factors – such as surface temperature, salinity, local water masses and vital effects – biasing the oxygen isotope fractionation in addition to the global ice effect. The coral records are based on the growth of coral reefs within the first meters below sea surface and preferentially reflect sea-level highstands preserved as reef terraces (Gallup et al. 1994; Bard et al. 1996; Chappell et al. 1996). These reefs grow primarily around islands, and tectonic compensation may have been active at changing rates. Furthermore, sea-level changes at rapid rates, which seem to have occurred with high frequency during the entire past sea-level cycle, obviously exacerbate their growth potential (Fairbanks 1989; Colonna et al. 1996). The attempt of sea-level reconstruction from a siliciclastic environment also has disadvantages. Organic material must have originated in a *tidal* facies to directly indicate paleo-sea level and may potentially have been mixed with matter from older sources biasing the true age of deposition. Moreover, the study areas are covered by water nowadays, and a high number of cores is required, thus making a project a quite challenging enterprise. In addition, the hydro-isostatic compensation must be calculated at all core locations.

The dated facies of this study give some evidence for the evolution of the sea level during MIS 3. For this purpose, they are pooled into three genetic groups. The first group comprises deposits from *shallow-marine* environments, and dates are positioned below the paleo-sea level. These dates are comparable in age and depth to recently published data from 'brackish' to shallow-marine environments from the Bonaparte Gulf based on micropalaeontological analyses (Yokoyama et al. 2001). Moreover, the basinward-directed age shift towards younger ages between 48 and 31 kyr amounts, as a rough approximation, from 81 m to 153 m, which is equivalent to ~ 72 m during ~ 17 kyr, but sea level dropped from approximately half (our curve) to a quarter (Shackleton 1987) of this value on average during the same time interval. This deepening is consistent with the observed facies trend towards increasing water depths and additionally indicates an increase in subsequent erosion activity (and sediment bypass) on the outer parts of the shelf.

Dates of *tidal* facies (second group) are rare but should be considered as direct indicators of paleo-sea level.

The third group, composed of the *terrestrial* facies, appears above paleo-sea level. This group also includes samples from *marshy* environments, which were apparently deposited shortly after the exposure of the distinct part of the Sunda plain.

The dates of this study are enhanced by the only other existing set of offshore dates from the Sunda Shelf. Geyh et al. (1979) determined these ages from root remnants, wood fragments and peat material from terrestrial deposits in the Strait of Malacca. These sediments are overlain by marine mud, but a long-lasting hiatus between these different facies must be assumed. As shown in Figure 10a, a rough sea-level curve can be interpreted from *all* dated facies of the regressive sediments from the Sunda Shelf. The curve joins two points of tidal origin at 47.7 $\pm$ 2090/1660 and 17.7 $\pm$ 80 ^{14}C kyr and is restricted in its depth extension by marine and terrestrial facies spanning a range envelope. Here, uncertainty is defined in terms of several thousands of years and tens of meters.

The ages derived from the Sunda Shelf correspond closely to established sea-level curves (e.g., Shackleton 1987) and do not contradict the slightly scattering coral reef data from the Huon Peninsula (Chappell et al. 1996; Fig. 10b). The sea-level lowstand during the LGM is, as expected, not deeper than –120 m (Hanebuth et al. 2000). However, two discrepancies occur in comparison with the oxygen isotope curve. Around the time interval from 50 to 40

kyr, the data from the Sunda Shelf indicate a water depth of ca. –75 m, which is slightly (~ 10 m) above the isotope record. More remarkable is the excursion of the drop in sea level, which led to the LGM lowstand of –120 m. This lowering occurs in the record from the Sunda Shelf a few thousand years earlier. The minor fluctuations in sea level recorded by Shackleton (1987) shortly after 30 kyr cannot be reproduced either. No data points are available from the coral reef record for this time interval, and other oxygen isotope curves are partly smoothed and diverge from each other. Therefore, the reason why the Sunda record does not match generally suggested sea level remains debatable, particularly since it is generally believed that sea level dropped towards the lowstand later and more rapidly towards the LGM.

Regressive Deposits on the Sunda Shelf – Conclusions

Appearance

Three different types of regressive depositional units are deduced from shallow-seismic *Parasound* surveying and interpreted as having been formed during MIS 3. On the central part of the shelf, (1) laterally restricted lenticular-shaped sediment bodies in slight depressions were built up by sets of prograding foresets. The bodies extend over 20 to 30 km, have a convex upper surface and fluvial structures inside. (2) As a lateral continuation, horizontally stratified but thin deposits cover the shelf between the sediment bodies. In contrast, (3) a sediment wedge occurs on the outer shelf and at the shelf margin, gradually thickening basinward.

The sediment cores yield a regressive-transgressive facies succession. Six different types of sedimentary facies are distinguished and belong to terrestrial (*marshy soil*, *coastal plain*), tidal (*tidal flat* including mangrove), and shallow-marine (*delta front*, *lagoonal bay*, *open shelf*) paleo-environments.

Major discontinuities separate regressive subunits and mark the border to overlying deposits. They are accompanied by a truncation of the upper part of the foresets (*offlap*), probably fluvially induced incisions, and abundant minor erosional hiatuses, which are often associated with abrupt facies shifts.

Particularities

The progradational sediment 'bodies' are *detached* from each other. They reflect temporary rapid shifts in the paleo-coastline and in the *accommodation space* down the planed shelf towards the basin during intervals of sea-level lowering, but they may also give discussable evidence for an *interim* which interrupts relative stability or even for slight rises in sea level by an arching top and fluvial incisions inside. Prominent hiatuses, detached sediment bodies, and a thick marginal wedge appear concurrently but are laterally separated. This leads to the conclusion that erosion and sediment bypass were dominant processes on the shelf during shallow-marine and subaerial conditions and only the permanently submarine margin received a continuous sediment supply during lower sea level.

The facies show no systematic distribution or zonation over the shelf. This can be deduced from the interplay between low gradients and sea-level variations (basinward-shifting repetition of facies association), and the fact that only the upper part of the regressive deposits was cored (related to shoreline). Locally limited conditions such as morphological settings, hydrographical features and variable sediment supply were important factors during the formation of a complex paleo-environment.

Implications for Sea Level

During the time interval from 50 to 40 kyr, there is evidence that sea level was slightly higher (~ 10 m) than indicated by other sea-level estimations. After this time, a drop led to the LGM lowstand, when other records even show a last minor rise in sea level. The maximum lowstand was not deeper than –120 m and is, therefore, about 15 m shallower than recently assumed for some other regions. Short-term fluctuations of a few tens of meters at maximum may be responsible for the existence of the *detached* deposits and their internal und superficial characters.

Acknowledgements We wish to acknowledge PM Grootes and his team for their co-operation. We thank J Wolf-Welling, DJ Bellis and C Sharma for their kind support of this manuscript. Appreciation is also expressed to R Schneider and one anonymous reviewer for their helpful comments on the manuscript. The study was financed by BMBF (grant 03G0115A), DFG (grant Schm 250/47) and the State of Schleswig-Holstein.

References

Bard E, Jouannic C, Hamelin B, Pirazzoli P, Arnold M, Faure G, Sumosuastro P, Syaefudin (1996) Pleistocene sea levels and tectonic uplift based on dating of corals from Sumba Island, Indonesia. Geophys Res Lett 23: 1473-1476

Bard E, Arnold M, Hamelin B, Tisnerat-Laborde N, Cabioch G (1998) Radiocarbon calibration by means of mass spectrometric 230Th/234U and ^{14}C ages of corals: An updated database including samples from Barbados, Mururoa and Tahiti. Radiocarbon 40 (3): 1085-1092

Biswas B (1973) Quaternary changes in sea-level in the South China Sea. Geol Soc Malaysia, Bull 6: 229-256

Chappell J, Omura A, Esat T, McCulloch M, Pandolfi J, Ota Y, Pillans B (1996) Reconciliation of late Quaternary sea levels derived from coral terraces at Huon Peninsula with deep sea oxygen isotope records. Earth Planet Sci Lett 141: 227-236

Clark PU, Mix AC, Bard E (2001) Ice sheets and sea level of the Last Glacial Maximum. EOS 82 (22): 241-247

Colonna M, Casanova J, Dullo WC (1996) Sea-level changes and δ^{18}O record for the past 34,000 yr from Mayotte Reef, Indian Ocean. Quat Res 46: 335-339

Fairbanks RG (1989) A 17,000-year glacio-eustatic sea-level record: influence of glacial melting rates on the Younger Dryas event and deep-ocean circulation. Nature 342: 637-642

Field ME and Trincardi F (1991) Regressive coastal deposits on Quaternary continental shelves: preservation and legacy. In "From shoreline to abyss" (Osborne RH, ed), SEPM Spec Publ 46: 107-122

Gallup CD, Edwards, R L, Johnson RG (1994) The timing of high sea levels over the past 200,000 years. Science 263: 796-800

Geyh MA, Kudrass HR, Streif H (1979) Sea-level changes during the late Pleistocene and Holocene in the Strait of Malacca. Nature 278: 441-443

Hanebuth T, Stattegger K, Grootes, PM (2000) Rapid flooding of the Sunda Shelf - a late-glacial sea-level record. Science 288: 1033-1035

Hanebuth TJJ (2000). Sea-level changes on the Sunda Shelf during the last 50.000 years. Ber - Rep 12, Inst für Geowiss, Universität Kiel, pp. 104

Hanebuth TJJ, Stattegger K (2001) The stratigraphic evolution of the Sunda Shelf during the past fifty thousand Years. In "Deltas of Southeast Asia and vicinity - sedimentology, stratigraphy, and petroleum geology". (Sidi FH, Nummedal D, Posamentier HW, Darman H, and Imbert P, eds) SEPM Spec Publ XX: XX

Hesp PA, Hung CC, Hilton M, Ming CL, Turner IM (1998) A first tentative Holocene sea-level curve for Singapore. J Coastal Res 14: 308-314

Hunt D, Gawthorpe RL (eds) (2000) Sedimentary responses to forced regressions. Geol Soc London Spec Publ, 172, pp 1-383

Hunt D, Tucker ME (1995) Stranded parasequences and the forced regressive wedge systems tract: deposition during baselevel fall - reply. Sed Geol 95: 145-160

Imbrie J, Hays JD, Martinson DG, McIntyre A, Mix AC, Morley JJ, Pisias NG, Prell WL, Shackleton NJ (1984) The orbital theory of Pleistocene climate: support from a revised chronology of the marine δ^{18}O record. In "Milankovich and climate." (Berger AL et al., ed), D. Reidel, Norwell, Mass., pp. 269-305

Lambeck K, Yokoyama Y, Purcell T (2001) Into and out of the Last Glacial Maximum: sea-level change during oxygen isotope stages 3 and 2. Quat Sci Rev XX: XX

Molengraaff GAF, Weber, M (1921) On the relation between the Pleistocene glacial period and the origin of the Sunda Sea (Java- and South China Sea), and its influence on the distribution of coral reefs and on the land- and freshwater fauna. Proc Royal Acad 23: 395-439

Nadeau MJ, Schleicher M, Grootes PM, Erlenkeuser H, Gottdang A, Mous DJW, Sarnthein JM, Willkomm, H. (1997) The Leibniz Labororatory AMS facility at the Christian-Albrechts University, Kiel, Germany. Nuclear Instrum Meth Phys Res B 123: 22-30

Posamentier HW, Allen GP, James DP, Tesson M (1992) Forced regression in a sequence stratigraphic framework: concepts, examples, and exploitation significance. AAPG Bull 76: 1687-1709

Reading HG (ed) (1996) Sedimentary environments and facies. 3rd ed., Blackwell Science, Oxford, pp 1-688

Schimanski A (1999) Diversität und Entwicklung von Faziesräumen auf dem Sunda-Schelf im Verlauf der postpleistozänen Transgression. Unpublished Diploma thesis, University of Kiel

Schimanski A, Hanebuth TJJ, Stattegger K (in prep.) Recognition of detailed facies zonation on tropical siliciclastic shelves: Transgressive deposits from the Sunda and Vietnamese Shelves

Shackleton NJ (1987) Oxygen isotopes, ice volume and sea level. Quat Sci Rev 6, 183-190

Sinsakul S (2000) Late Quaternary geology of the Lower Central Plain, Thailand. J Asian Earth Sci 18: 415-426

Stanley DJ, Hait AK (2000) Deltas, radiocarbon dating, and measurements of sediment storage and subsidence. Geology 28: 295-298

Stattegger K, Kuhnt W, Wong HK et al. (1997) Cruise Report SONNE 115 SUNDAFLUT. Ber - Rep 86, Geol-Paläont Inst, Universität Kiel, pp. 211

Steinke S (2001) Sedimentological and climatic changes during the last deglaciation recorded in cores from the Sunda Shelf margin and continental slope (southern South China Sea). PhD thesis, University of Kiel

Stuiver M, Braziunas TF (1991) Climatic, solar, oceanic, and geomagnetic influences on late-glacial and Holocene atmospheric $^{14}C/^{12}C$ change. Quat Res 35: 1-24

Stuiver M, Reimer PJ, Bard E, Beck JW, Burr GS, Hughen KA, Kromer B, McCormac G, Van der Plicht J, Spurk M (1998) INTCAL98 radiocarbon age calibration, 24,000-0 cal BP. Radiocarbon 40: 1041-1084

Sydow J, Roberts HH (1994) Stratigraphic framework of a late Pleistocene shelf-edge delta, Northeast Gulf of Mexico. AAPG Bull 78: 1276-1312

Tesson M, Posamentier HW, Gensous B (2000) Stratigraphic organization of late Pleistocene deposits of the western part of the Golf du Lion Shelf (Languedoc Shelf), Western Mediterranean Sea, using high-resolution seismic and core data. AAPG Bull 84: 119-150

Tjia HD (1980) The Sunda Shelf, SE Asia. Z Geomorph, NF 24: 405-427

Tjia HD (1996) Sea-level changes in the tectonically stable Malay-Thai Peninsula. Quat Int 31: 95-101

Tjia HD, Fuji S (1992) Late Quaternary shorelines in the tectonically stable Malay-Thai Peninsula. In "The coastal zone of Peninsula Malaysia " (Tjia HD, Abdullah SMS, eds), pp. 28-41. Penerbit Universiti Kebangsaan Malaysia, Bangi.

Trincardi F and Field ME (1991) Geometry, lateral variation, and preservation of downlapping regressive shelf deposits: eastern Tyrrhenian Sea margin, Italy. J Sed Petr 61 (5): 775-790

Völker AHL, Sarnthein M, Grootes PM, Erlenkeuser H, Laj C, Mazaud A, Nadeau MJ, Schleicher M (1998) Correlation of marine ^{14}C ages from the Nordic seas with the GISP2 isotope record: implications for ^{14}C calibration beyond 25 ka BP. Radiocarbon 40: 517-534

Wong HK, Haft C, Paulsen A-M, Lüdmann T, Hübscher C, Geng J (2001) Late Quaternary sedimentation and sea-level fluctuations on the northern Sunda Shelf, southern South China Sea. In "Deltas of Southeast Asia and vicinity - sedimentology, stratigraphy, and petroleum geology". (Sidi FH, Nummedal D, Posamentier HW, Darman H, and Imbert P, eds) SEPM Spec Publ XX: XX

Yokoyama Y, Lambeck K, De Deckker P, Johnston P, Fifield LK (2000) Timing of the Last Glacial Maximum from observed sea-level minima. Nature 406: 713-715

Yim, WW-S (1999) Radiocarbon dating and the reconstruction of late Quaternary sea-level changes in Hong Kong. Quat International 55: 77-91

Zaitlin BA, Dalrymple RW, Boyd R (1994) In "Incised-valley system: origin and sedimentary sequences." (Dalrymple RW, Boyd R, Zaitlin BA, eds), SEPM Spec Publ 51: 45-60

Poster Presentation at the EUG XI Conference, Strasbourg; Abstract published in:
European Union of Geosciences XI, Strasbourg 2001, J. Conf. Abs. **6** (1) : 68

Deca-Meter-Scale Holocene Sedimentation on the Vietnamese Shelf

Alexander Schimanski and Karl Stattegger

Shallow seismic survey data aquired during a cruise with the German RV Sonne (Südmeer III) in April 1999 (Wiesner et al., 1999) shows a thick sediment cover on the shelf along the Vietnamese coast.

Four sediment cores (18414-3, 18415-2, 18416-2 and 18417-3) from waterdepths ranging between 21 and 97 m along a transect have been investigated by component analysis of the coarse fraction (250–500 μm) considering planktonic foraminifers, benthic foraminifers, shell fragments, lithoclasts and plant fragments.

The deepest core (18417-3, 97m waterdepth) shows a high percentage of plant fragments in the deeper parts of the core. This indicates a strong influence of terrigenous material, probably due to lower sea level, whereas in the shallower part of the core the amount of shell fragments prevails, indicating a strong marine influence.

Core 18416-2 (66 m waterdepth) has been dated by AMS ^{14}C yielding an age of 9820 ^{14}C years BP of *in situ* bivalve shells in his deepest portion, and an age of 9195 ^{14}C years BP one meter below the top. Above, the sediment composition changes from the dominance of shell fragments in the deeper part towards an increasing amount of lithoclasts in the upper part, corresponding to the coarse fraction in core 18415-2 (38 m waterdepth). The age control indicates a high sedimentation rate of 4 meters within less than 700 years.

The two shallowest cores show a high amount of shell fragments in their deeper parts passing into a high percentage of lithoclasts indicating a more nearshore position.
Core 18414-3 (21 m waterdepth) has an age of 6005 ^{14}C years BP from *in situ* bivalve shells in the lower middle part. Benthic foraminifers of this core have been investigated for their oxygen isotopic composition. The isotope curves of *Nonion subturgitum* and *Elphidium advenum* show a trend from heavier to lighter oxygen isotopes in the range of 0.5 ‰ from the deeper to the shallower parts in the core. This trend in the shallowest core could be the result of an increasing influence of riverine waters due to shoreline progradation following the slight sea level lowering after the last highstand at approx. 5500 years BP and/or due to more humid climatic conditions.

Component analysis as well as the seismic record suggests, together with high precision AMS ^{14}C age control, the possibility of teleskoping the cores to an extended section of more than 10 m of Holocene sediments.

Future investigations will aim at high resolution stratigraphy and paleoceanographic reconstruction of the Holocene in the coastal, tropical, siliciclastic environment of the Vietnamese shelf.

Oral Presentation at the 2001 MARGINS Meeting in Kiel, Abstract published in:
Schriftenreihe Deutsche Geol. Ges., **14**: 182-184 (Roth, S. & Rüggeberg, A. /Ed.s.: 2001 Margins Meeting, 2.- 6.10.2001, Kiel; Abstracts).

Holocene Sedimentation on the Vietnamese Shelf

Alexander Schimanski, Karl Stattegger and Pieter M. Grootes

We have studied 25 sediment cores from modern waterdephts between 21 m and 169 m taken during cruise SONNE 140 along the Vietnamese Coast between the Mekong River Delta and the Gulf of Tonkin. The flooding of the shelf off the Vietnamese Coast beginning after the Last Glacial Maximum did intensively influence the sedimentation in this region.

After the reconstuction of a sea-level curve for the time from 21 kyr BP to 11 kyr BP and a detailed sedimentation history resulting from studies on the Sunda Shelf (e.g. Hanebuth 2000), we focused on the sedimentological conditions on the Vietnamese Shelf during the Holocene. Here we found sediments covering the Holocene time interval which are nearly lacking or are reduced to a thin sediment cover of a few centimeters on the Sunda Shelf.

So far 22 AMS radiocarbon datings have been measured returning AMS ^{14}C-ages between 5 kyrs and 43 kyrs BP. 10 of the datings reveal ages younger than 10 AMS ^{14}C-kyrs BP. Most of the remaining datings reflect the age of the deeper parts of the cores and datings of the younger parts are in process.

As proved by four cores from a transect on the narrow central part of the Vietnamese Shelf high sedimentation rates are observable in this region (Schimanski and Stattegger 2001). We found sedimentation rates of up to four meters in less than 700 years for the early part of the Holocene in core 18416-2 from 66 m of modern waterdepth (mmwd). We expect continuous sedimentary sequences for extended parts of Holocene sediments. Core 18401-3 from 134 mmwd off Nha Trang Bay on the narrow part of the Vietnamese Shelf has been dated to 9900 AMS 14C years on benthic foraminifers in a core depth of 590 cm. X-ray radiographies show continuous sedimentation throughout the upper part of the core. Further datings are in progress.

Most of the cores have been investigated by X-ray radiography to locate hiatuses, possibly related to the late Pleistocene or Holocene transgression, depending on the waterdepth. Where possible we dated the material shortly above the hiatus which usually occurs as an abrupt change from clayey to much more sandy sediment. All datings in combination with the paleo-waterdepth are in accordance to the established sea leve curve by Hanebuth et al. 2000, although clear sea level indicators like mangrove roots or adequate paleoenvironments are absent. They probably have been eroded by the transgression itself or never formed on the steep and narrow central part of the Vietnamese Shelf.

Furthermore all cores have been examined for sand content, content of organic carbon and carbonate with a spacing of at least one meter (regarding the high sedimentation rates).

Component analyses considering planktonic foraminifers, benthic foraminifers, shell fragments, lithoclasts and plant fragments generally show an increasing marine influence in the shallower parts of the cores.

In contrast, the shallow core 18414-3 from 21 mmwd shows possible decreasing marine influence supported by oxygen isotope measurements. From 267 cm core depth, dated to

6000 AMS 14C years, the oxygen isotope analyses are showing an upwards trend to lighter values by approximately 0,5 ‰. This trend could be explained by increasing influence of riverine waters due to shoreline progradation following the slight sea level lowering after the last highstand at approximately 5500 years BP. A change to more humic climatic conditions could be involved as well.

Up to now we can draw the following conclusions concerning a north-center-south sedimentation pattern:

- in the N and S where the shelf is wide, the Holocene sediment cover is restricted to a few decimeters

- on the central part of the Vietnamese Shelf thick stacks of Holocene sediment (more than 10 m) are abundant

- the influence of the two large rivers, Mekong in the south of the study area and Red River (draining into the Gulf of Tonkin) in the north, seem to have a big influence on the sedimentation by means of dilution and transport of material in and off the delta regions. In contrast on the central part of the Vietnamese Shelf sedimentation occurs as a combination of marine shelf sedimentation and probably high seasonal input of terrigenous material due to the high gradient of the mountainous hinterland in central Vietnam. Thus, considerable amounts of planktonic foraminifers have only been found on the central part of the Vietnamese Shelf

- a continuous record of Holocene sedimentation is best preserved on the central part of the Vietnamese Shelf as shown by AMS datings, oxygen isotope analyses and component analyses

Poster Presentation at the AGU 2001 Fall Meeting, San Francisco; Abstract published in:
EOS, Transactions of the American Geophysical Union ***82*** (47) : 654

Provenance of Holocene and Recent Sediments on the Vietnamese Shelf Revealed by Sr and Nd Isotopes and Trace Elements

Alexander Schimanski, Karsten Haase, Karl Stattegger and Pieter M. Grootes

The erosion of the Himalayas and surrounding mountains supplies large volumes of sediment to the oceans. The sediment sources and mass balance can be determined using geochemical and isotopic data. This study aims to determine the provenance of terrigenous sediments on the Vietnamese shelf and to compare the recent sediment compositions with sediments deposited during the Holocene.

Terrigenous sediments on the Vietnamese Shelf are mainly derived from two large rivers, the Mekong in the south and the Red River in the north. The source of the Mekong lies in the eastern Tibetan Plateau while the Red River arises in the mountains of southwestern China. Numerous small rivers of the Annamite mountain chain seem to supply much of the sediment to the central part of the Vietnamese Shelf which was largely affected by the late Pleistocene Transgression starting after 21 kyrs BP. We determined very high sedimentation rates of up to 4 meters in less than 700 years for this part of the shelf during the Holocene.

We have studied 13 sediment samples from the Vietnamese Shelf between 7°N near the Mekong River mouth to 16°N in the southernmost part of the Gulf of Tonkin as well as sediments from the Annamite mountains, the Mekong and Red River. The Sr and Nd isotope and trace element compositions of surface (recent) bulk sediment samples as well as samples dated to approximately 8000 AMS ^{14}C years BP will be presented. We also focused on an AMS ^{14}C dated sediment core near the mouth of the Mekong river comprising the entire Holocene time interval. This core is used to reconstruct possible changes in erosion due to climatic changes (monsoon) in the source area over the past 10000 AMS ^{14}C years.

The possible endmembers show significantly different εNd values (-10.7 for Mekong River sediment, -13.1 for sediment from the Annamite chain and -11.3 for Red River sediment). Analyses of shelf sediments show relatively high εNd of -11 to -12 and low $^{87}Sr/^{86}Sr$ compared with published data from the Ganga-Brahmaputra delta. Preliminary low $^{87}Sr/^{86}Sr$ data of 0.712-0.718 in the shelf sediments favour young magmatic rocks such as from the Himalayan batholiths or the Cenozoic plutons of the Red River shear belt as main sources for the Vietnamese shelf sediments. The Red River sediments have significantly higher La/Th and Nd/Yb compared to the Mekong River and Annamite sediments while the Vietnamese shelf sediments mainly plot between the two latter endmembers. We conclude that the shelf sediments show mixing of sediments from three different sources, i.e. the Mekong, the Red River, and the Annamite chain.